Novel Double Stator Switched Flux Permanent Magnet Machines

Mr Chukwuemeka Chijioke Awah

A thesis submitted for the degree of Doctor of Philosophy (PhD)

Department of Electronic and Electrical Engineering,

University of Sheffield, United Kingdom

October 2016

ABSTRACT

The scarcity and high price of rare-earth magnets have always been a major concern in the design and analysis of permanent magnet (PM) machines. Thus, it is pertinent to develop high torque density PM machines with reduced magnet volume, which is the main purpose of this research.

In this thesis, novel topologies of switched flux permanent magnet machines having two separate stators as well as different stator and rotor pole number combinations are proposed. All machines are optimized by genetic algorithm technique under fixed copper loss condition with the goal to achieve maximum output torque. The electromagnetic performances of the machines are quantitatively compared, such as the open-circuit flux-linkage and back-EMF waveforms and spectra, cogging torque and static torque waveforms and spectra, winding inductances, average torque versus current/copper loss saturation curves, torque- and power-speed characteristics, flux-weakening performances, as well as PM utilization ratio, etc.

Moreover, the influence of winding configurations, i.e. all- and alternate-pole-wound, on the electromagnetic performances of the machines is also investigated. Furthermore, comprehensive study of the core and PM eddy current losses in these machines are also presented, together with their efficiency characteristics.

Finally, prototype machines are manufactured and tested to validate the analyses with good agreement.

The proposed machines are suitable for direct-drive applications which require high torque at low speed. They can also be applied to other applications such as aerospace, automobile industry, and wind power generation.

ACKNOWLEDGEMENTS

I would like to thank all those who have contributed to the success of this thesis. My first thanks go to my supervisor Prof. Z.Q. Zhu for his invaluable comments, advice, encouragement and instructions throughout my study period, without whom it would have been difficult to realise this dream. Permit me to say that my supervisor's strong criticisms during this research made significant positive impact on my technical knowledge and understanding about the field of electrical machines. I cannot thank him enough for the transferable research skills/knowledge he allowed me to grab, especially for the regular weekly meetings we had.

I would like to thank immensely my colleagues and all members of the Electrical Machines and Drives Research Group (EMD), at the University of Sheffield, UK for their useful discussions, comments and help during my stay with them, especially Dr. D. Evans, Dr. M.M.J. Al-Ani, Dr. D. Wu, Mr. Z.Z. Wu, Dr. P. Taras and Mr. H.L. Zhan. In particular, may I thank specially Mr. John Wilkinson, Mr. Lawrence Obodo and the technical team for making the prototypes.

My deepest gratitude is due to all members of my immediate and extended families, too numerous to mention for their love, support and encouragement, in particular my wife, Florence Awah, my son, Chukwuemeka Success Emmanuel Awah, my parents, Mr and Mrs Reuben Kalu and Ngozi Awah, Ugochukwu Awah and family, Ijeoma Awah, Victor Awah, Mrs. Oluchi Okoh, Mrs Christiana Onyishi and family, and every member of my maternal home where I grew up from childhood, especially the F.N.C. Nwanna's family.

May I use this opportunity to thank the Commonwealth Scholarship Commission, UK for the award and sponsorship to undertake this study.

I sincerely wish to thank my mentor, Prof. O.I. Okoro and his family who inspired me to undertake this venture of acquiring sound western education. I remain indebted to him and his family. Also, I will not forget to express my gratitude to Michael Okpara University of Agriculture Umudike for the granted study leave. In particular, the Vice-Chancellor, Prof. H.O. Edeoga, and the Director of Academic Planning, Prof. O. C. Ohaeri, for their high level of integrity/transparency during the scholarship nomination process.

Moreover, I wish to thank the following good friends and mentors: Dr. C.N. Okoye, Prof. I.I. Ezebuiro, Prof. Edward Chikuni, Prof. L.U. Anih, Prof. E.S. Obe, Dr. S.E. Oti, Miss J.O. Nebe, Engr. O.A. Nwaorgu, Engr. R.U. Obasi, Engr. Uduma Okoro and Engr. Ikechukwu Okigbo and their families.

Above all, I give glory to the ALMIGHTY GOD for HIS grace upon me.

To the memory of my beloved nephew, Master Emmanuel Chinemerem Awah

who departed in June, 2012, when I was in South Africa.

CONTENTS

NOMENCLATURE

2D-FEA	two-dimensional finite element analysis	
A_a	slot area	mm^2
ALL-W	all-pole-wound winding configuration	
ALT-W	alternate -pole-wound winding configuration	
B_m	maximum value of the magnetic flux density	T
C_T	goodness factor of cogging torque	
d-axis	direct-axis	
DS-SFPM	double-stator switched flux permanent magnet	
DSSRM	double stator switched reluctance machine	
EMF	electromagnetic force	V
f	frequency	Hz
F	force	N
FEM	finite element	
g	acceleration due to gravity	m/s^2
G_{ratio}	transmission gear ratio	
HCF	highest common factor	
HTS	high temperature superconducting	
I	rated current	A

$i_{d,}\, I_d$	direct-axis current	A
I_{max}	maximum input current	A
IPM	interior permanent magnet	
$i_{q,}\, I_q$	quadrature-axis current	A
j	integer	
k	integers	
K_c	eddy current loss coefficient	
K_e	excess loss coefficient	
k_{fw}	flux-weakening factor	
K_h	hysteresis loss coefficient	
k_{pf}	winding packing factor	Ωm
L_{aa}	self-inductance	H
L_{axial}	active stack length	mm
LCM	lowest common multiple of the stator/rotor pole	
L_d	direct-axis inductance	H
L_{end}	end winding length	mm
Lq	quadrature-axis inductance	H
m	number of phases	
M_{ab}	mutual-inductance	H

N	number of turns per phase	
n	number of coils per phase	
NdFeB	neodymium iron boron	
N_r	rotor pole number	
N_s	stator pole number	
N_{si}	inner stator poles	
N_{so}	outer stator slots or poles	
N_t	number of turns per coil	
P_{cu}	copper loss	W
P_{EM}	electromagnetic power	W
P_{in}	input power	W
P_{iron}	iron loss	W
PM	permanent magnet	
P_{mag}	permanent magnet eddy current loss	W
P_{out}	output power	W
P_s	no. of inner stator slots	
PS-SFPM	partitioned stator switched flux permanent magnet	
q-axis	quadrature-axis	
R_{load}	phase resistance	ohms

rpm	revolution per minute	rpm
SFPM	switched flux permanent magnet	
SPM	surface permanent magnet	
t	time	sec.
T	electromagnetic torque	Nm
T_{avg}	average torque	Nm
THD	total harmonic distortions	
T_{max},	maximum torque	Nm
T_{min},	minimum torque	Nm
T_{ripple}	torque ripple	Nm
UMF	unbalanced magnetic force	Nm
V_1	fundamental magnitude of the voltage	V
V_{dc}	dc-link voltage of the inverter	V
V_i	*rms* value of the *ith* harmonic of the voltage	V
V_{max}	maximum voltage of the inverter	V
Δ	change	
η	efficiency	
θ	rotor position	deg
$\theta_{d\text{-}q\ axis}$	mechanical angle between the *d*- and *q*-axes	deg

ρ_{cu}	resistivity of copper	
ϕ	phase flux	Wb
ψ	flux-linkage	Wb
ψ_{aa}	total excited flux-linkage in windings of phase A due the PMs and phase A current	Wb
ψ_{ab}	total excited flux-linkage in windings of phase A due to the PMs and phase B current	Wb
ψ_{PM}	open-circuit flux-linkage of phase A due to the magnets only	Wb
ω	angular speed of the machine.	rad/s
ω_r	rotational velocity of the rotor-PMs and	rad/s
ω_s	rotational velocity the stationary modulating ring	rad/s

CHAPTER 1
GENERAL INTRODUCTION

1.1 Introduction

There is a high demand for permanent magnet (PM) machines in most industrial and domestic applications due to their several potential advantages, such as high torque/power density, low-cost, improved efficiency and reliability [GAL13], as well as good fault-tolerant and flux-weakening capabilities, etc. However, a trade-off is usually made in order to achieve these potentials. Hence, in order to accomplish this target, exhaustive research activities have been carried out, resulting in a lot of different designs, concepts and techniques for PM machines. Furthermore, tremendous research is still on going in this area of discipline. Thus, more efficient and high performance PM machine topologies are still emerging. In addition, the concern about environmental emissions has also added to the quest for more efficient electric machine [BOL14]. Similarly, the associated issues such as noise, vibration and regular maintenance of mechanical gears have resulted in more viable research options such as development of magnetic gears [ATA01] and magnetically-geared machines. Fortunately, high energy density magnets such as Neodymium Iron Boron (NdFeB) could satisfy most of these needs when used appropriately in the design and analysis of electric machines. However, the availability of these rare-earth magnets is limited in addition to their high market price [LIU13]. Although the cost of permanent magnets is currently stable, it is worth noting that there could be fluctuations and high market prize of the rare earth magnets in the future due to the present monopoly of the product.

Therefore, there is a need to investigate the magnetless machines and/or machines with less magnet volume, which has necessitated this study. Hence, this research will investigate and analyse the electromagnetic performance of different novel topologies of switched flux permanent magnet (SFPM) machine having two airgaps with reduced magnet volume, without sacrificing the output electromagnetic torque.

1.2 State of the art of permanent magnet machines

As aforementioned, the recent growing research interests in the area of design and analysis of PM machines could be attributed to the emergence of high energy density rare-earth magnets as well as the recent advances in power electronics, design and control of PM machines. More importantly, due to their numerous advantages which include but not limited to high

torque density, good thermal management potential, and better efficiency as well as high reliability [TOD04], [CHO06] [LIU08], and [BEL10] compared to other electric machines of the same size. Due to the high price of magnets, induction and reluctance machines are promising candidates for low-cost applications. For example, a low-cost doubly salient machine free of PMs and capable of producing high output torque is proposed in [LEE14]. The high torque density of the machine was realized by adopting the principles of flux modulation. However, the torque density and efficiency of PM machines are considerably higher than of the magnetless machines such as induction and reluctance machines [CHE01], [HUA98], [PEL12] [GU15], [ZHU15a], [JAC96] and [BOL14]. However, a handful of literature is available on high torque/power density switched reluctance machines. In particular, the ones with double stator (DSSRM) [ABB10], and also double rotor configurations [CUI08] with high constant-power speed range.

The topologies of PM machines are too numerous to mention. In most PM machines, the permanent magnets are located in the rotating part of the machine. However, as will be shown later, PMs can also be housed in the stationary part of electric machines. Thus, based on the location of permanent magnets on the rotor or stator of the machine, PM machines could be classified as either rotor- or stator-PM machines, respectively. The rotor-PM machines have been researched extensively due to their high output torque and power capability. However, it has been shown that the rotor-PM machines are characterized by poor thermal management compared to their stator-PM counterparts [PYR12]. Therefore, the rotor-PM machines have higher demagnetization potential compared to their stator-PM counterparts [GRI13]. The common types of stator-PM machines are the doubly-salient [SAR94], flux reversal [DEO97] and switched flux [HOA97] PM machines as shown in Fig.1.1. Some of the attractive features of flux reversal PM machines include: simple and rugged rotor structure which is good for high speed operation and their low inductance, desirable for fault-tolerant applications [DEO97], [WAN99] and [KIM04]. However, one of the major disadvantages of the flux reversal PM machines is their high risk of demagnetization [KIM09], owing to the series combination effect of the magnetic flux of both the armature windings and the permanent magnets. They also have high leakage flux [BOL01] compared to other PM machines. In addition, flux reversal PM machines have high cogging torque/torque ripple characteristics [KIM05]. However, flux reversal PM machines capable of enhancing the overall performance of the machine which includes reduced

cogging torque and enhanced torque density by inserting PMs on the stator teeth is proposed in [KIM09].

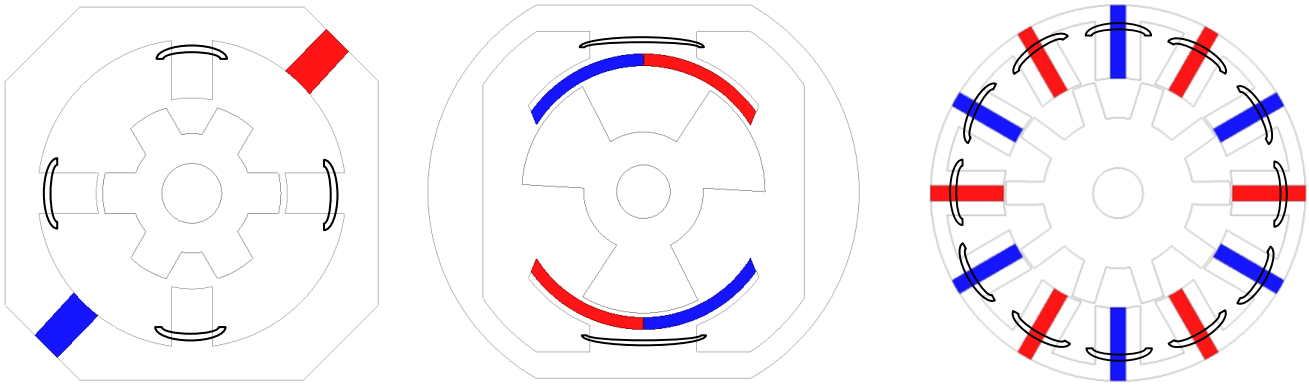

(a) Doubly-salient [SAR94] (b) Flux reversal [DEO97] (c) Switched flux [HOA97]

Fig.1.1 Cross sections of stator-PM machines.

It is worth mentioning that the flux linkage waveforms of the SFPM and flux reversal PM machines are bipolar unlike that of the doubly-salient PM machine whose flux linkage waveform is unipolar. Thus, the torque density of the doubly-salient PM machines is relatively low compared to that of flux reversal and SFPM machines of the same size. In addition, the flux-linkage and back-EMF waveforms of SFPM machines are typically sinusoidal. Thus, they have relatively low cogging torque compared to their output electromagnetic torque.

Since the introduction of 3-phase SFPM machine by [HOA97], extensive research has been investigated on this machine topology, for example, [ZHU05], [HOA07], [HUA08] [ZHU10] and [ZUL12], due to their numerous advantages which include but limited to: high torque/power density, robust rotor structure, better efficiency and good thermal capability. Further, as depicted in Fig.1.2, different machine topologies have been developed from the conventional SFPM machines which includes the E-core [CHE11], the C-core [ZHU10], the multi-tooth [ZHU08a], the hybrid [CHE11a], [GAU14], and the outer-rotor [FEI12] SFPM machines, to mention but a few. Moreover, a lot of literature is also currently available on multiphase SFPM machines [THO09], [LI11], [XUE13] and [SED15] due to their high fault-tolerant capabilities especially for critical applications where safety and reliability are of top priority, such as in the aircraft and military devices.

Further, the power density of SFPM machines could be enhanced by employing high-temperature superconducting material as presented in [WAN13]. Furthermore, it has been shown that the torque density of SFPM machines could be improved by complementing the stator of conventional C-core SFPM machine with Halbach array material [WAL13]. Also, two independent SFPM machines are integrated in [LI15] so as to mitigate the unbalanced back-EMF as well as the even order harmonics of a given 4-rotor pole SFPM machine. It should be noted that the SFPM machines would be very suitable for high speed applications, since it has a simple and rugged rotor structure free of PMs and windings.

Further, in terms of the direction of magnetic flux of PM machines, we could have the following types of machines: radial field, axial field, and transverse flux PM machines. Research have shown that small size radial field PM machines have larger torque density than their axial field counterparts in addition to the associated manufacturing complexity and high cost of axial field machines [GER12] [SIT01]. However, the axial field machines possess higher torque-weight-ratio as well as better heat dissipation. However, there is more flexibility to adjust the airgap of the axial field machines [POP13]. Moreover, the axial field PM machines have significant cogging torque compared to conventional PM machines [HAO14]. Further, it is worth noting that there are a lot of flexibilities in the choice of stator/rotor combinations in this kind of machine, i.e. single-stator single-rotor [STE12], single-stator double-rotor [LOP08], double-stator single-rotor [ZHA13], etc. This group of machines would be suitable for in-wheel applications.

The transverse flux PM machines are well suited for low speed, high torque applications such as in direct-drive. It is proven that the transverse flux PM machines could deliver very high torque compared to their counterparts of same size [CHA07], achieved by enhancing the airgap flux density through a flux concentration technique [SIA08] [CHE08]. Nevertheless, transverse flux PM machines is not only costly, but also exhibit low power factor [CHE08], [ATA01] as well as attendant manufacturing difficulties [WAN15] [LEI15].

Furthermore, the PM machines could be grouped based on the placement of PMs, i.e. interior permanent magnet (IPM) machine, when buried in either the rotor or the stator, and surface permanent magnet (SPM) machine, when mounted on the surface of the stator or rotor. According to research, it has been shown that the IPM machines exhibit higher torque density than their SPM equivalents of the same size [FAS14], [RED12], and [MUN08], as well as better efficiency. Moreover, the SPM machines suffer from poor PM retention as mentioned

in [ZHA15], higher demagnetization potential [CHE14], [ZHA15], as well as poor flux weakening capability compared to their IPM counterparts [SOO94]. Thus, IPM machines would be more suitable for high speed applications.

In terms of winding configuration, PM machines can be categorized into all- and alternate-pole-wound machines. It is worth noting that the alternate-pole wound machines exhibit higher fault-tolerant capability than their all-pole wound counterparts [ISH06], [CHE10a], [ELR08], [CHE11b], and [OWE10]. Basically, since the physical isolation between phases is higher in the alternate-pole wound machines, thus there would be minimum short circuit faults in these machines compared to the all-pole-wound machines [JAC96] [BIA08]. However, all-pole-wound PM machines have higher overload capability [WAN15] and lower eddy current loss values as well as better efficiency than their alternate-pole-wound counterparts due their lower armature reaction [MAG07]. Further, on PM machine classification based on winding topology, PM machines could be wound with distributed windings which are usually overlapping or concentrated windings, while the later could be either overlapping or non-overlapping. In general, PM machines having concentrated windings exhibit a lot of advantages relative to their distributed-wound counterparts of same size. It is worth mentioning that the machines with non-overlapping concentrated windings are naturally simple and compact than the distributed-wound PM machines [XUA13]. Further, they are relatively cheaper (since they uses less material), and exhibits higher inductance, with improved torque/power density [MAG04] as well better flux-weakening capability compared to their distributed-wound counterparts. However, the machines having non-overlapping concentrated windings are associated with higher MMF harmonics and eventually higher PM eddy current losses [GOS13], higher vibration [VAL15], as well as lower reluctance torque [WAN14]. In this study, non-overlapping concentrated windings are employed in the analyses of the proposed machines. Thus, there would be shorter end windings, reduced copper losses and hence improved motor efficiency, as noted in [CHE10b].

Double-stator PM and vernier PM machines are other kinds of permanent magnet machines with good performance. Many researchers have directed their attention towards the design and analysis of different double-stator PM machines, owing to their high performance characteristics. More importantly, it is noted that double-stator PM machines have larger torque density than their single-stator counterparts [NIU07] and [LIU12a]. Similarly, vernier PM machines have also been investigated extensively. Vernier PM machines work basically

on the principles of magnetic gearing by adopting the flux modulation concept. Although the vernier PM machines can produce high output torque, it is characterised by low power factor which will eventually affect their overall efficiency [SPO03] [LI14]. However, efforts have been made and are still on, in order to minimize this inherent low power factor problem. As result, flux-modulation technique is adopted in [ZHA14] in order to enhance the power factor and the torque density of the vernier PM machine. Moreover, there have been several other studies on the power factor improvement of vernier PM machines [LI14], [JAN14]. Also, vernier PM machines have high flux leakage around the airgap compared to other PM machines as noted in [LI11].

Recently, memory PM machines are also attracting considerably attention [OST03], [ZHU11] due to their ability to regulate the flux produced by the PMs especially in the constant-power operating region. This concept of flux regulation has also been extended to SFPM and magnetic-geared machines as shown in [LIU14], [WU15] and [LIU14]. However, there may be increased copper losses in the existing memory machines, owing to their field excitation windings.

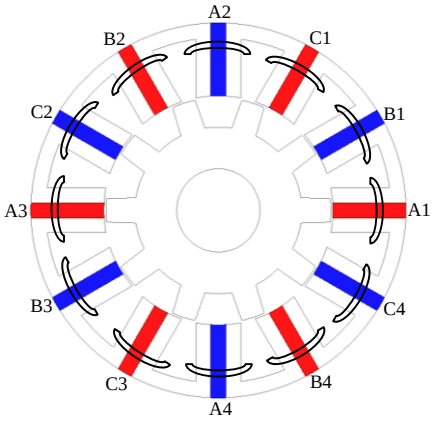

(a) Conventional SFPM

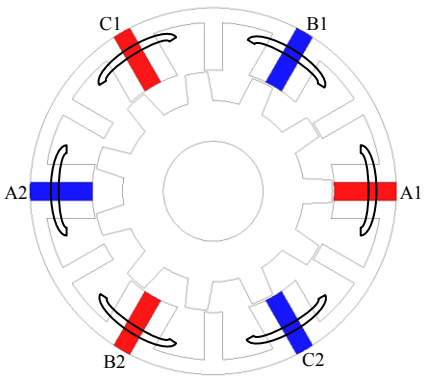

(b) E-core

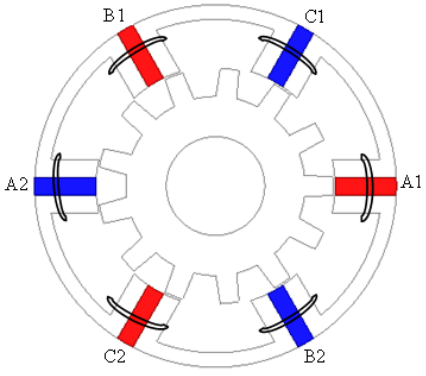

(c) C-core

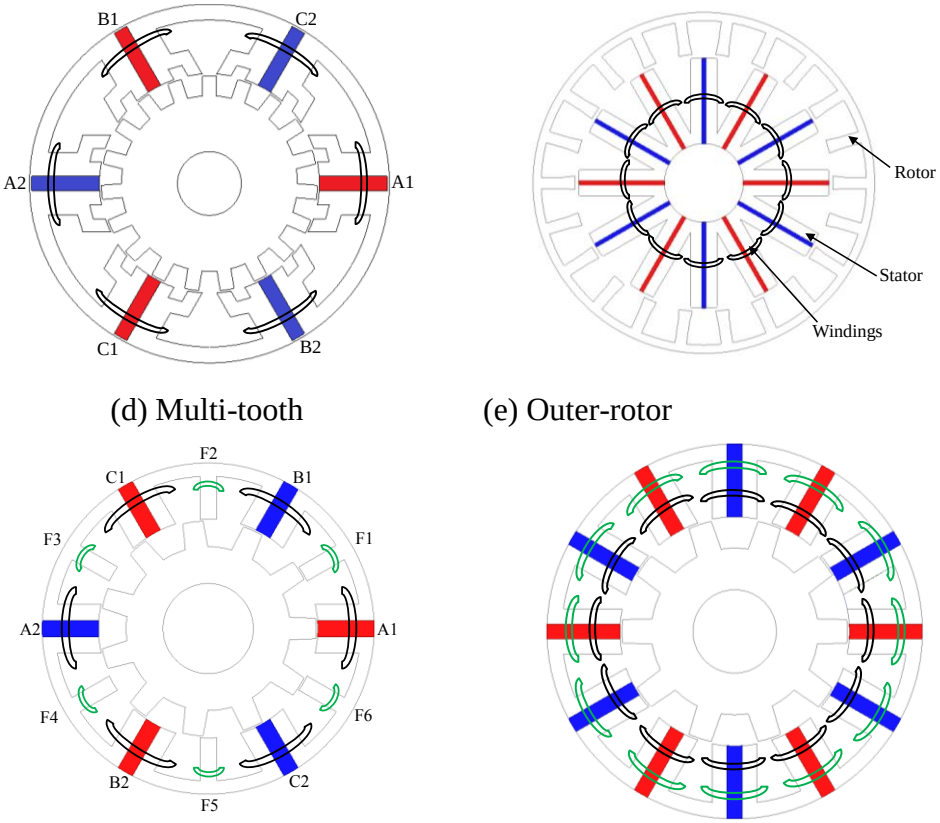

(d) Multi-tooth (e) Outer-rotor

(f) Hybrid

Fig.1.2 Different topologies of SFPM machines.

1.3 Topologies of magnetic gears and magnetic-geared machines

Magnetic gears are quite old machines, although they only received a lot of attention quite recently when it was introduced in [ATA01] by employing rare-earth magnets, which revealed its competitive high torque density potential comparable to conventional PM machine. The operation principle of the magnetic gear was also detailed in [ATA01] and subsequently its design concept and performance were described in [ATA04]. As pointed out in [ATA01], [RAS05], [WAN09] and [JIA09], magnetic gears are preferable to mechanical-geared machines since they require little or no maintenance, have low noise and vibration, as well as exhibit high efficiency and reliability. Moreover, since the bulky gear boxes are eliminated, the size and cost of the machine is reduced. However, it is still expensive to produce this type of machine due to their high utilization of PMs compared to conventional brushless PM machines. Also, there is manufacturing difficulty in the fabrication of magnetic gear machines owing to their multiple air-gap structures [LIU14].

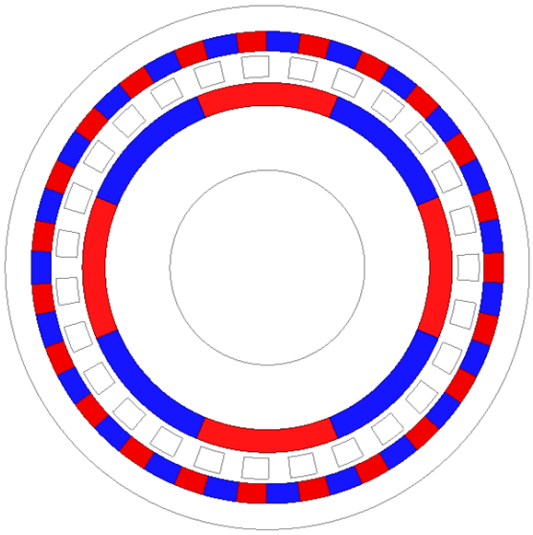

Fig.1.3 Common magnetic gear topology [ATA04].

Basically, the torque transmission of a magnetic gear is achieved by flux modulation between the stationary pieces and the PM rotors. The amplitude of this torque is a function of the machine's gear ratio, obtained from the appropriate combination of the rotor and stator pole pairs.

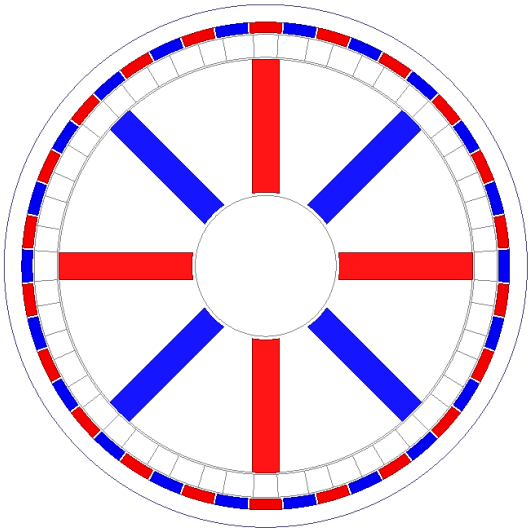

Fig.1.4 Coaxial magnetic gear with spoke PMs [RAS05].

The performance of a coaxial magnetic gear having sandwiched spoke PMs in the inner rotor is analysed in [RAS05] with particular reference to the end effect, the associated losses, and the system's efficiency. The proposed machine also utilizes the flux focusing advantage to enhance its torque density capability.

Further, [JIA09] showed that the torque density of a coaxial magnetic gear could be enhanced by employing the Halbach magnetized PMs arrays. Also, the core losses and torque ripples are significantly reduced compared to the non-Halbach array magnetic gear type.

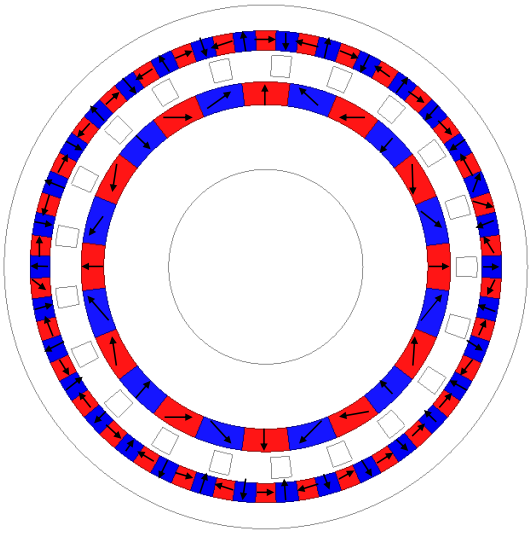

Fig.1.5 Coaxial magnetic gear with Halbach magnetized PMs [JIA09].

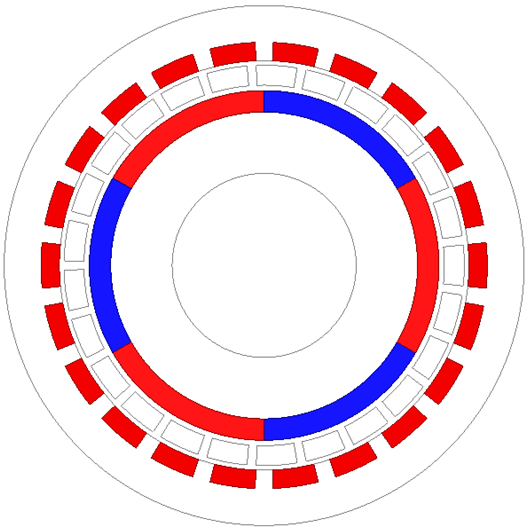

Fig.1.6 Concentric magnetic-geared machine [LIU09].

Similarly, a concentric magnetic gear was proposed in [LIU09] with an enhanced mechanical strength, by burying the outer rotor PMs inside the iron core. Moreover, a three-dimensional finite element (FEM) approach was employed to take care of the end-effect. The schematic diagram of the proposed magnetic gear machine is depicted in Fig.1.6.

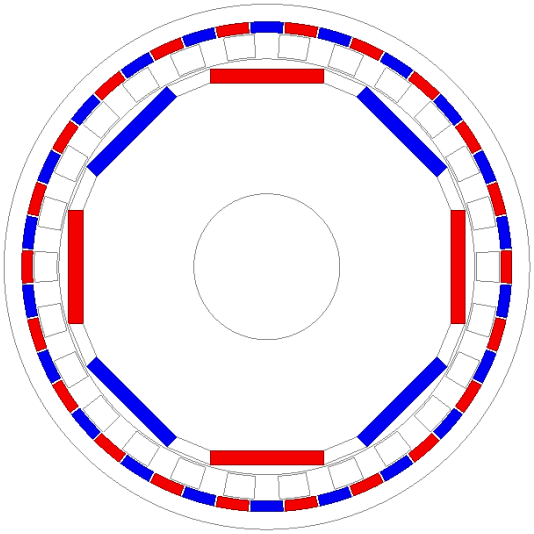

Fig.1.7 Magnetic gear IPM machine [FRA11].

Analytical technique was adopted in [FRA11] to model and simulate the performance of a given magnetic gear by employing the winding function approach. The proposed magnetic gear is an IPM type buried in the high speed rotor. However, it should be noted that the PMs were considered as wound coils in the analysis.

Magnetic-geared machines are basically integrated machines that combine the advantages of magnetic gear and electrical machine.

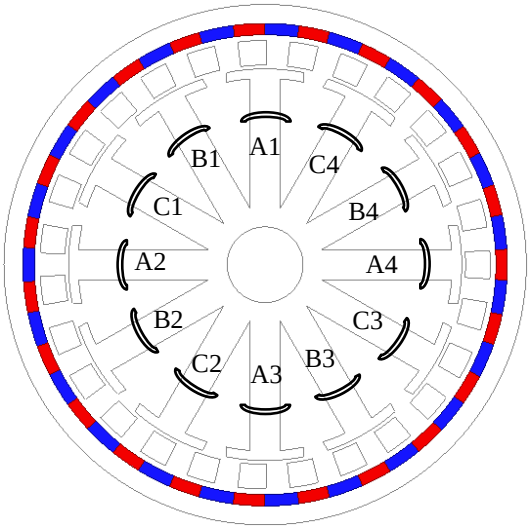

Fig.1.8 Magnetic-geared outer rotor machine [WAN09].

In [WAN09], a novel magnetically-geared machine that is suitable for direct drive applications and having an outer rotor is proposed together with a comparative study of the different stator combinations. Further, the proposed machine was optimized with different

inner stator teeth. It was observed that the machine with higher number of inner stator teeth produces the largest output torque. Similarly, in order to enhance the torque capability of a direct-drive machine, a high power factor integrated machine consisting of a magnetic gear and a brushless PM machine is proposed in [ATA08].

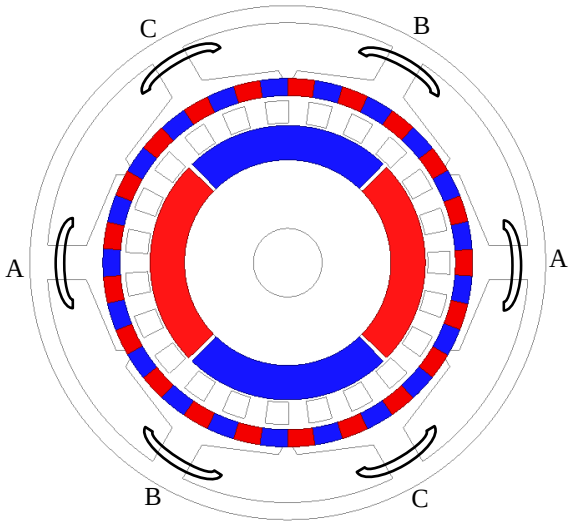

Fig.1.9 Pseudo direct-drive PM machine [ATA08].

High performance double-stator magnetically geared machines with different rotor arrangement are proposed in [LIU12b]. The cross sections of the machine are shown in Fig.1.10. The machine combines the merits of brushless PM machine and the principles of gear effect to produce a high torque at low speed. A comparative study between the different rotor arrangements is detailed as well.

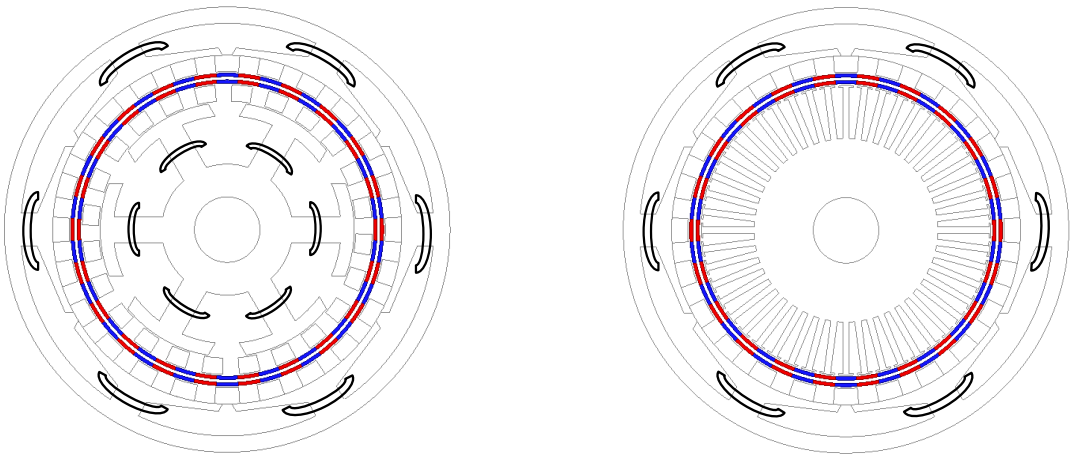

(a) Dual-ring (b) Single-ring

Fig.1.10 Double-stator magnetically-geared machine [LIU12b].

Furthermore, as shown in Fig.1.11, a more complicated compact design consisting of double-rotor and double-stator is developed in [LIU14], suitable for wind power generation. However, the developed machine is expensive due to its many mechanical parts.

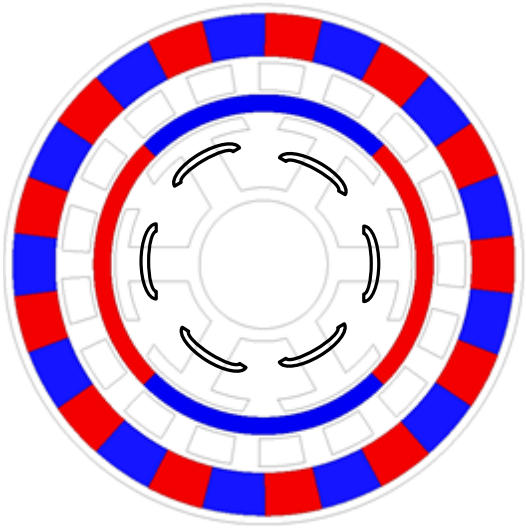

Fig.1.11 Double-rotor magnetically-geared machine [LIU14].

A dual-rotor single-stator magnetically-geared machine is proposed in [TLA16]. The predicted results show that the proposed dual-rotor single-stator machine could deliver higher output torque comparable to the traditional PM machines. The structure of this machine is shown in Fig.1.12.

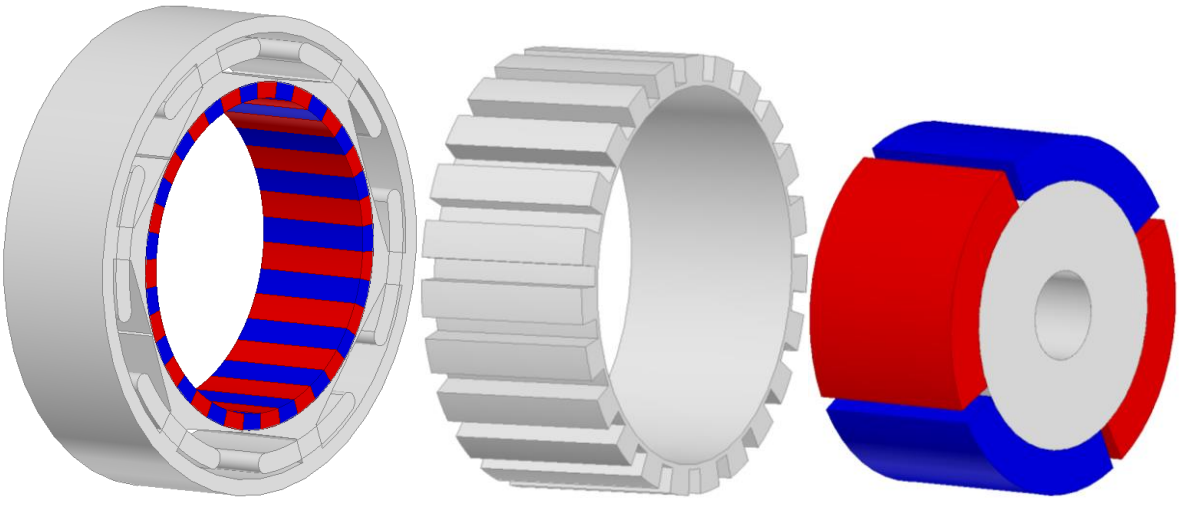

Fig.1.12 Outer stator magnetically geared machine [TLA16].

In order to enhance the torque capability of the magnetically-geared machine, different types of magnetic geared machines having different magnetic flux direction such as axial [NIG12], linear [NIU11], induction [MEZ15], and claw pole [UKA14], etc. have been developed.

Moreover, many new topologies are still emerging owing to their numerous potentials of combining the advantages of magnetic gears and permanent magnet machines.

1.4 Scope and contributions of research

Low-cost SFPM machines with reduced magnet volume and having two separate stators are proposed in this study. Firstly, the proposed machines are optimized by genetic algorithm technique in order to obtain the maximum output torque. Further, the effect of design parameters on the overall performance of the proposed machines is given. Similarly, the influence of winding configuration as well as the impact of different stator/pole number combinations on the electromagnetic performance of the proposed machines is also presented and quantitatively compared. The electromagnetic performance of the proposed machines which includes: the open-circuit and load characteristics, the winding inductances, the torque ripple and the unbalanced magnetic force (UMF), is investigated in this study. Moreover, a comprehensive account of losses and efficiency characteristics of the proposed machines is also given.

There is optimum utilization of space in the proposed machines since their inner stators are accommodated in the inner space of the machine. It is worth noting that the developed machines could be used as dual-three phase machine for fault-tolerant applications. Note also that the investigated machines have identical rotor structure with that of DSSRM machines [ABB10], Fig.1.13. However, the stator geometries of the two different machines are not the same.

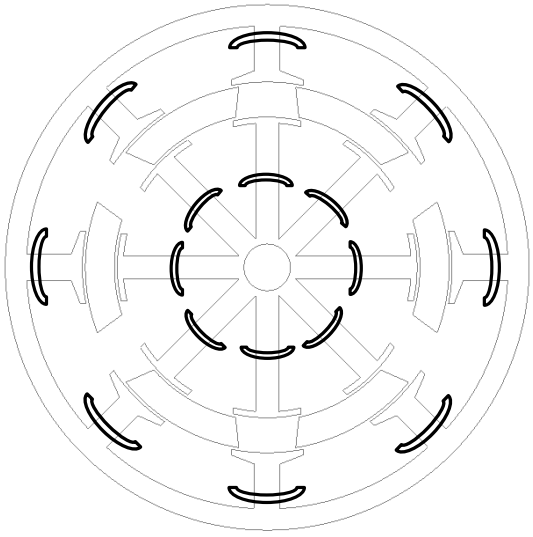

Fig.1.13 Double stator switched reluctance (DSSRM) machine [ABB10].

Moreover, the PMs of the developed machines are not easily demagnetized due the fact that the magnetic circuit of both the permanent magnets and the armature windings are in parallel, unlike the series magnetic circuit of flux reversal PM machines. Fig.1.3 shows the cross sections of the developed machine topologies.

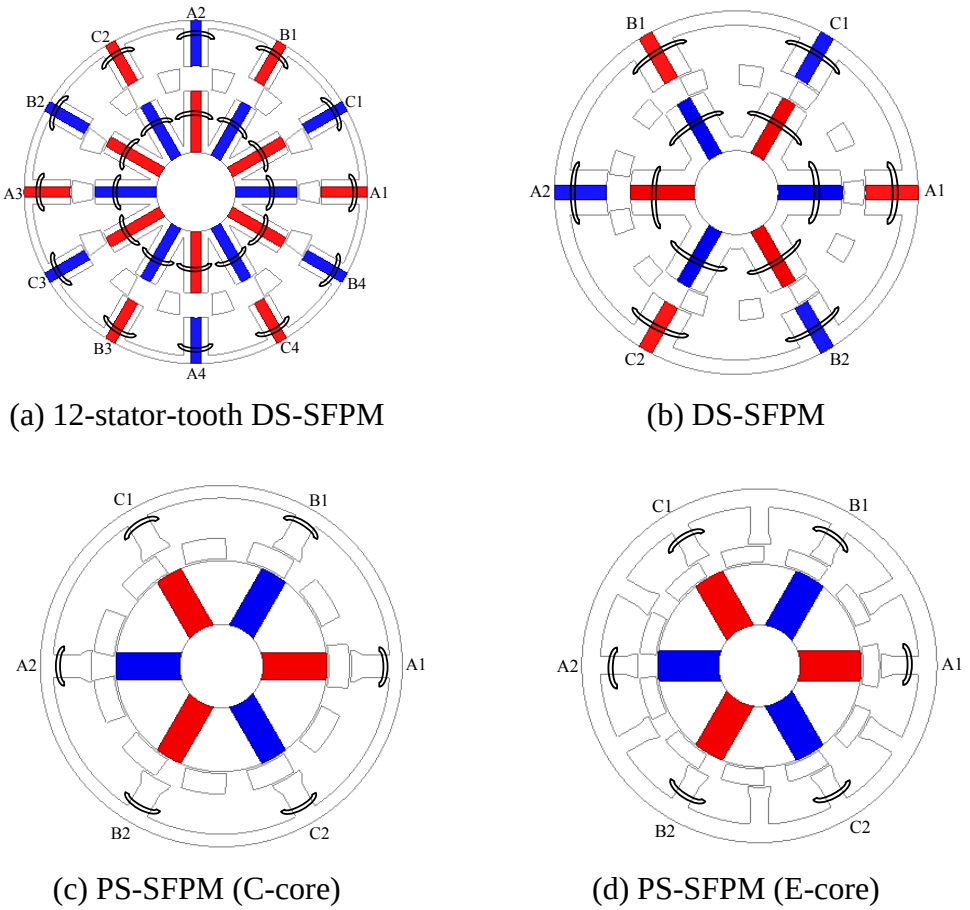

(a) 12-stator-tooth DS-SFPM (b) DS-SFPM

(c) PS-SFPM (C-core) (d) PS-SFPM (E-core)

Fig.1.14 Schematic diagrams of investigated machines.

This thesis is organized in seven chapters as follows.

Chapter 1:

This chapter gives a general introduction about the study with special reference to the update on permanent magnet, magnetic gear and magnetically-geared machines.

Chapter 2:

In this chapter, double-stator switched flux permanent magnet (DS-SFPM) machines having 12-separate stator slots are developed and analysed. Moreover, the influence of design parameters on the average torque of the developed machines is given. It is worth noting that

the design parameters of these machines are optimized globally at a set condition of fixed copper loss (30W). Further, a quantitative comparison of the electromagnetic performances of the machines having all- and alternate-pole-wound topologies is presented by 2-dimensional finite element analysis (2D-FEA). Furthermore, a comprehensive study of the core and PM eddy current losses in these machines are also presented, together with their efficiency characteristics. The torque- and power-speed characteristics as well as the winding inductances of the machines are also illustrated in this chapter. Moreover, the effects of load on the total harmonic distortion of the voltage and torque ripple of the analysed machines are also given in this chapter.

Chapter 3:

Double-stator SFPM (DS-SFPM) machine having 6-stator tooth is developed in this chapter. Also, the feasible stator and rotor pole number combinations (N_s and N_r) and the influence of rotor pole numbers on the overall performance of developed double-stator machines are quantitatively compared. Further, the influence of rotor pole number on the electromagnetic performance of double-stator SFPM machines is investigated. The analyses show that the developed DS-SFPM machines could deliver higher electromagnetic torque than their equivalent single-stator counterparts. The inductance, unbalanced magnetic force (UMF), loss and efficiency characteristics of the analysed machines are also presented. Finally, the FEA results are validated by experiments with good agreement.

Chapter 4:

A novel type of partitioned stator switched flux permanent magnet (PS-SFPM) machines with either all- or alternate-pole-wound are developed in this chapter. The proposed PS-SFPM machines have two stators which separately accommodate the armature windings and the PMs, between which is the rotor made of iron pieces, and/or the number of stator poles with PMs equal to half of that with armature windings. Their electromagnetic performances are compared, such as open-circuit flux-linkages and back-EMFs, cogging torque, static torque waveforms, average torque against current and PM utilization ratio, etc. A prototype machine is manufactured and tested to validate the analyses.

Chapter 5:

Firstly, double-stator SFPM machine having C-core outer stator structure is proposed. The proposed machines were optimized for maximum output torque using genetic algorithm

approach. The 2-dimensional finite element (FEA) analysis is employed in the performance prediction of the magnetically-geared SFPM machines. Then, the influence of main design parameters on the average electromagnetic torque is investigated. The selected design parameters include: the split ratio, the slot opening/slot pitch ratio, the rotor radial thickness, the rotor pole arc/pole pitch, the stator-tooth width, and the back-iron thickness. Further, the influence of stator and rotor pole combinations on the electromagnetic performances is investigated and quantitatively compared. Finally, a prototype is built and tested for validation of the predicted FEA results.

Chapter 6:

In this chapter, a comparative study of the electromagnetic performance of different machines which includes the double-stator SFPM (DS-SFPM) machine, the conventional SFPM machines and the partitioned stator SFPM (PS-SFPM) machines having C-core and E-core stator structures, is presented. The analyses include open circuit flux-linkage and back-EMF waveforms and spectra, torque-current and torque-copper loss characteristics, self- and mutual-inductance waveforms, and loss and efficiency maps.

Chapter 7:

General conclusions on the overall performance of the proposed machines are made in this chapter. Moreover, suggestions on further investigations are given.

Appendices:

The test procedures are described in appendix A.

Publications from the PhD research study is given in appendix B.

CHAPTER 2

DOUBLE-STATOR SWITCHED FLUX PM MACHINES WITH 12-STATOR TEETH/POLES HAVING ALL- AND ALTERNATE-POLES-WOUND

2.1 Introduction

The need for permanent magnet (PM) machines in various industrial/domestic applications ranging from aerospace, automobile, to wind energy generation cannot be overemphasized, apparently due to their high torque/power density capability, high efficiency, as well as rugged structure. Hence, permanent magnet machines are better substitute for induction and reluctance machines in most industrial applications. Nevertheless, it could be liable to irreversible demagnetization when subjected to high temperature and load. Consequently, there have been tremendous researches on permanent magnet machines especially the SFPM type [ZHU10], [NIU07], [CHE10a], [WAN12], and [HUA09]. A comparison of the electromagnetic performance of DS-SFPM machine is given in [ZAI14], which consists of a salient pole stator and salient pole rotor. However, the machine structure in [ZAI14] essentially consists of two independent SFPM machines, *i.e.* inner and outer SFPM machines respectively. The rotor of developed DS-SFPM machine is made of modulating iron segments. Similarly, a double-stator switched flux PM machine utilizing ferrite material and having twelve stator teeth is proposed in [KIM16]. The operating principle of the developed machines in this study is also similar to that of SFPM and magnetically-geared machines [ZHU10] and [AWA15]. In order to enhance the torque capability of magnetic gears and magnetically-geared machines, a lot of literature is available in recent years [LIU14], [RAS05], [ATA01], and [EVA11]. Since the machine dimensions have great impact on the electromagnetic performance, the influence of the rotor geometry on the output torque of double-stator switched reluctance machine is investigated in [WAN15]. Generally speaking, PM machines are characterized by magnet eddy current losses, and thus, a comprehensive account of losses and reduction of permanent magnet eddy current loss by means of magnet segmentation are detailed in [CHE10c] and [ZHU08b] respectively.

The electromagnetic performances of the developed machines are detailed in this chapter with particular reference to its quantitative comparisons. It includes the open-circuit waveforms, torque and inductance characteristics, torque-current and torque-copper loss curves. Furthermore, the losses and efficiency of the analysed machines are given in this study. The schematic diagram of the developed machines is shown in Fig.2.1. Moreover, the

influence of stator/rotor pole combination as well as the winding configurations (*i.e.* all- and alternate-pole wound topologies) on the overall electromagnetic performances of the machines is also investigated.

In this chapter, we developed and analysed double-stator switched flux PM machines with identical numbers of inner and outer stator structure/teeth. Basically, the developed machines have a simple arrangement comprising of the identical inner and outer stators, and the rotor made of modulating iron segments. In the analysed machine configurations, there is optimum utilization of inner stator space, and thus, the torque as well as the overload capability of the machines is enhanced. Similar to spoke type of PM machines [KIM13] and [ELR14], the flux focusing technique is adopted in order to enhance the torque production. The mechanical structure of the DS-SFPM machines is similar to that of a double-stator switched reluctance machine [WAN15], although with some differences. It should be noted that the developed machines are good candidates for fault-tolerant applications, since it could be designed and used as dual three-phase or multi-phase machines.

More importantly, its inner stator could be equipped with dc source for ease of flux control/regulation which is similar to the hybrid type of SFPM machines that have attracted unceasing attention in literature [CHE11a], [GAU14], and [WAN12]. In order to minimize control complexities, the inner and outer stator windings are connected in series and equipped with ac armature coils. The proposed machines have the working principles of both magnetic-gearing and switched-flux effect. Note that field excitation of the proposed machines is mainly due to the permanent magnet. The polarity and magnitude of the flux-linkages changes with respect to the rotation of the modulating ring. This periodic change of flux-linkage with the rotating modulating iron segments will induce an EMF in the machine and consequently torque production.

All the analysed machines are optimized using genetic algorithm technique with the goal to achieve maximum average torque at fixed copper loss (30W) condition. In a bid to maintain the same level of copper losses in the inner and outer stators, the number of turns per coil in both stators is allocated in proportion to the ratio of its slot areas. The machine size including the active length and the outer diameter as well as the total number of turns per phase is kept the same in the comparison in the whole analysis for fairness.

The cost of the rare-earth magnets and the manufacturing complexity of the cup-rotor are some drawbacks of this type of machine. Nevertheless, its numerous advantages outweigh

these demerits. Further, the cost issue could be overcome by replacing the NdFeB magnets with ferrite magnets [KIM16], although with a trade-off of some amount of average torque since the ferrite magnets are characterized by low residual magnetization property of ~ 0.4T.

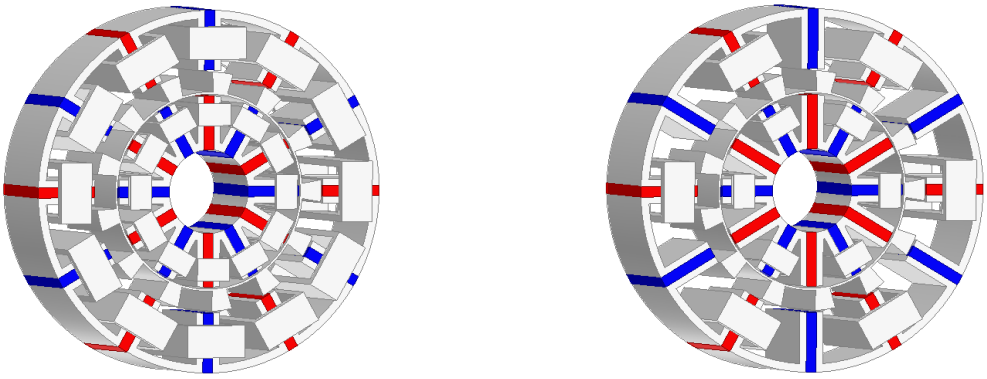

(a) All-pole wound DS-SFPM (b) Alternate-pole wound DS-SFPM

Fig.2.1 Schematic diagram of the developed DS-SFPM machine.

Henceforth, the analysed machines having all- and alternate-pole-wound configurations would be designated as ALL-W and ALT-W respectively, to ease discussions. The parameters of the analysed machines are listed in Table 2.1.

TABLE 2.1 PARAMETERS OF ANALYSED DS-SFPM MACHINES

Item	Value							
Machine topology	12/10 ALL-W	12/10 ALT-W	12/11 ALL-W	12/11 ALT-W	12/13 ALL-W	12/13 ALT-W	12/14 ALL-W	12/14 ALT-W
Stator pole number, N_s	12							
Number of phases, m	3							
No. turns/coil (inner-stator)	6	12	6	12	6	12	6	12
No. turns/coil (outer-stator)	12	24	12	24	12	24	12	24
Coils/phase	4	2	4	2	4	2	4	2
Outer stator diameter (mm)	90							
Active stack length (mm)	25							
Split ratio	0.58	0.60	0.61	0.62	0.66	0.63	0.64	0.66
Rotor radial thickness (mm)	5.49	5.48	5.38	5.45	5.46	5.27	5.44	5.46
PM thickness (mm)	2.83	2.91	2.88	2.68	2.63	2.73	2.67	2.78
Outer rotor iron width/pitch ratio	0.35	0.34	0.34	0.37	0.38	0.37	0.36	0.36
Inner rotor iron width/pitch ratio	0.41	0.39	0.37	0.34	0.31	0.32	0.31	0.28
Stator back-iron thickness (mm)	2.22	2.23	2.01	2.07	2.04	2.03	2.08	2.06
Max. torque (Nm), (I_{max}=15A)	1.06	1.07	1.14	1.18	1.31	1.34	1.38	1.35
Maximum power (W)	509.32	509.26	509.34	509.41	509.14	509.36	509.26	509.18
Torque density (kNm/m^3)	14.53	14.30	15.60	16.11	17.76	18.05	18.91	17.57
Efficiency (%)	91.01	90.00	91.07	90.75	91.07	90.69	91.15	89.37
Power factor	0.7	0.51	0.9	0.77	0.9	0.6	0.9	0.83

2.2 Machine optimization and influence of leading design parameters on the average torque

All the developed machines are optimized for maximum torque at fixed copper loss (30W) condition using the evolutionary technique. The influence of design parameters which includes the split ratio (Fig.2.2), the PM thickness (Fig.2.3), the rotor radial thickness (Fig.2.4), the rotor iron pole arc/pole pitch (Fig.2.5), and the back-iron thickness (Fig.2.6) are presented in this section. We could see that there is an optimum torque value in each of the varied design parameters due to the saturation effects of the electromagnetic circuit owing to the differing armature reactions. The compared results also show that the average torque of these machines are dependent on the machine configuration, *i.e.* all- and alternate-pole-wound which essentially is a function of their varying winding factors. The optimum values of the design parameters are listed in Table 2.1.

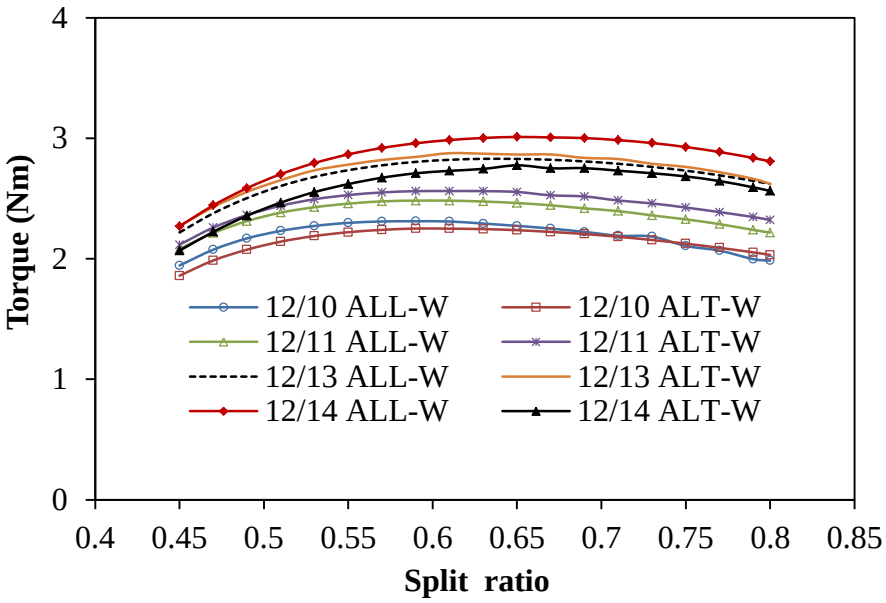

Fig.2.2 Variation of average torque with split ratio, i_d=0.

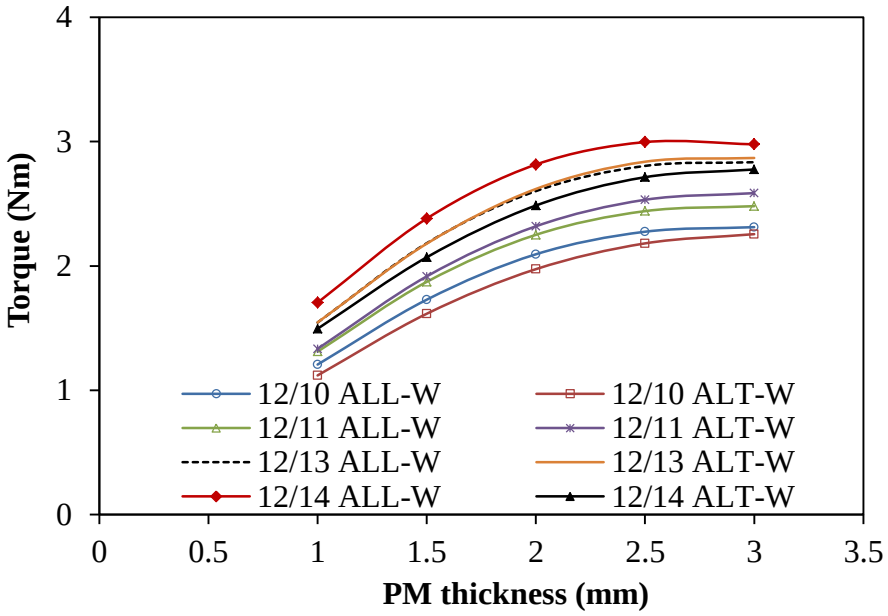

Fig.2.3 Variation of average torque with PM thickness, i_d=0.

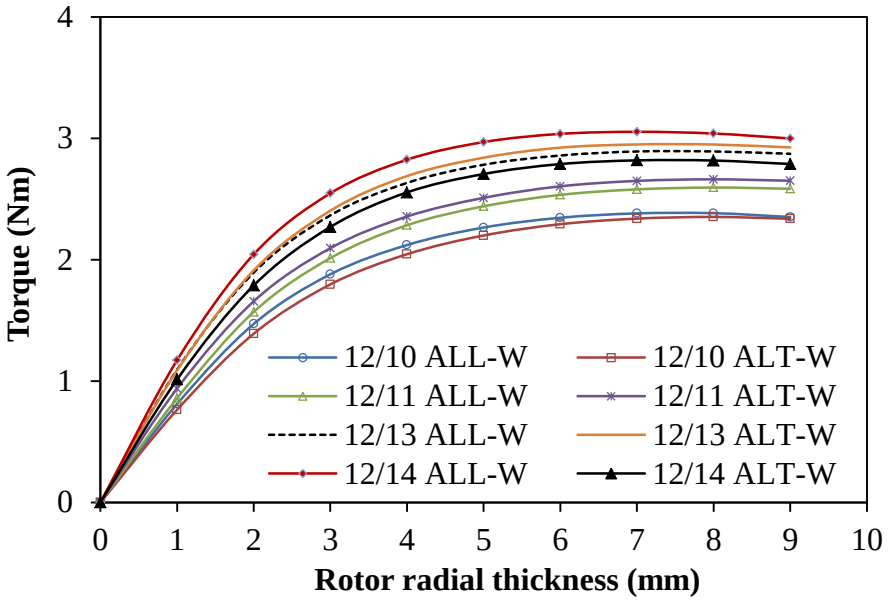

Fig.2.4 Variation of average torque with rotor radial thickness, i_d=0.

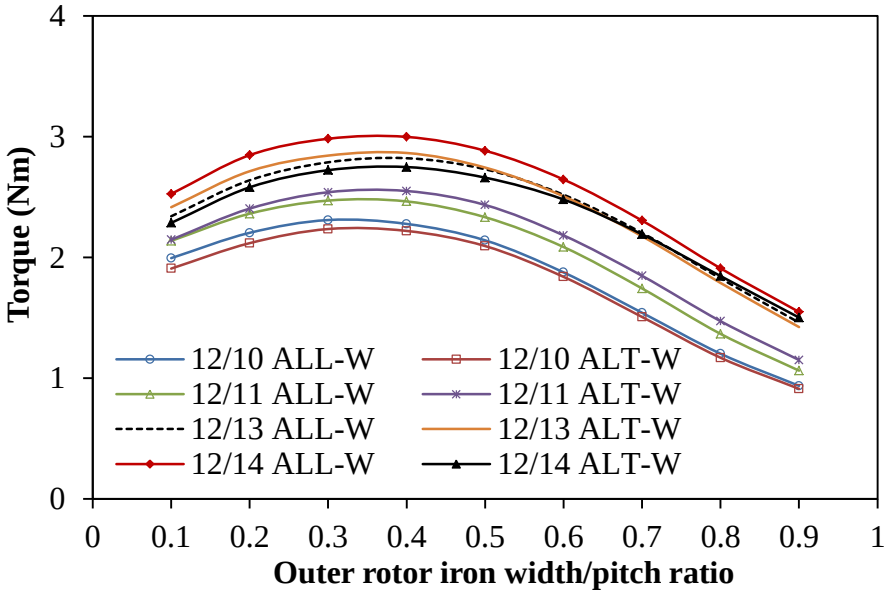

(a) Torque versus outer rotor iron width/pitch ratio

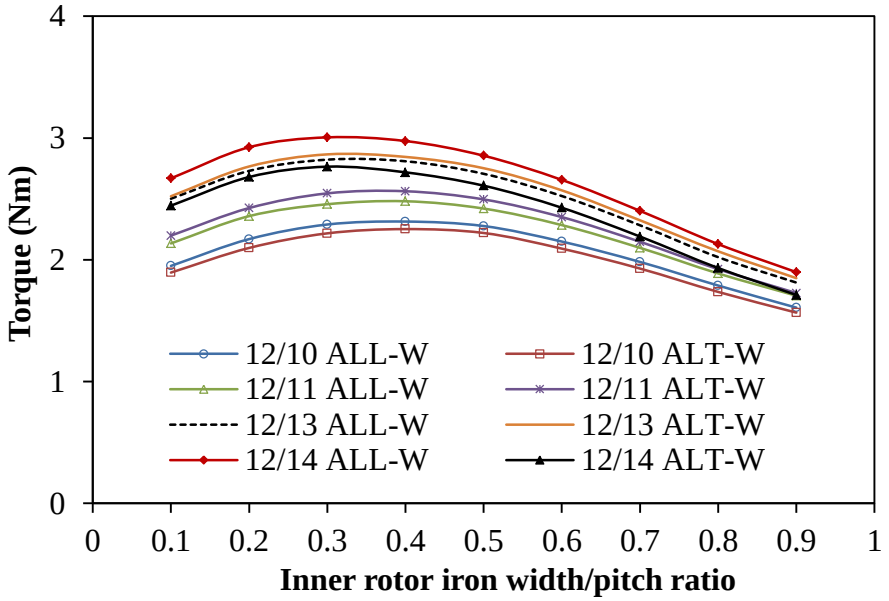

(b) Torque versus inner rotor iron width/pitch ratio

Fig.2.5 Variation of average torque with rotor inner and outer pole arcs, i_d=0.

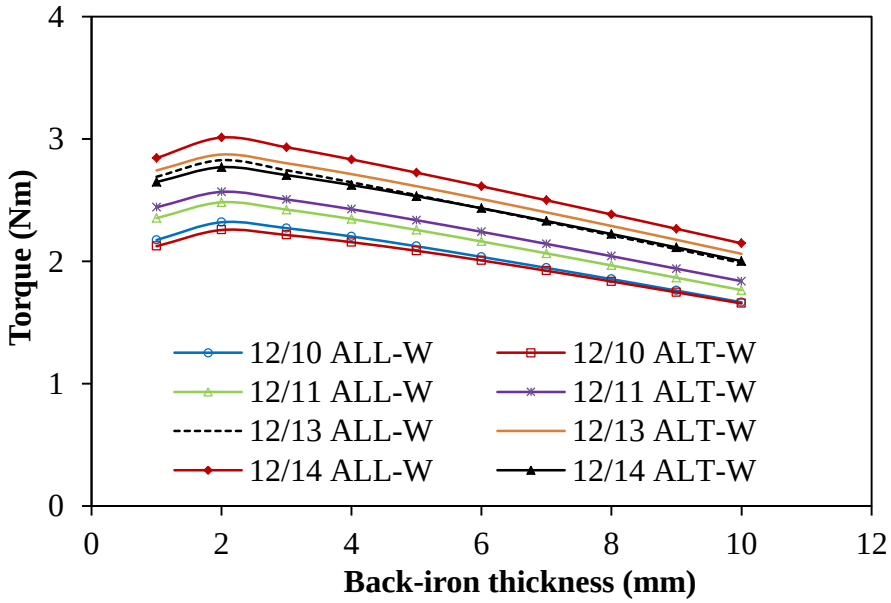

Fig.2.6 Variation of average torque with outer stator back-iron thickness, i_d=0.

2.3 Feasible stator and rotor pole combinations

The electrical and mechanical degrees of the developed machines are related by:

$$Elec.(°) = N_r * mech.(°) \tag{2.1}$$

where N_r is the rotor pole number.

Similarly, the stator and rotor pole combinations (N_s and N_r) of the analysed machines are given by:

$$N_r = N_s \pm j \tag{2.2}$$

where j is an integer 1 or 2. The feasible stator and rotor pole combinations of the analysed machines are similar to those stated in [CHE10b].

2.4 Electromagnetic performance

The open-circuit phase flux-linkage and back-EMF waveforms of the analysed machines with their respective harmonic spectra are shown in Figs.2.7 and 2.8. It is obvious that the waveforms are symmetrical and sinusoidal with the rotor position, although the 10- and 14-pole machines exhibit significant amount of harmonics as seen in the spectra of Fig.2.8. Meanwhile, in order to predict the voltage harmonics of the machines, we have evaluated the total harmonic distortions (THD) in the back-EMFs by the equation given below:

$$THD = \frac{\sqrt{\sum_{i=2}^{\infty} V_i}}{V_1} \tag{2.3}$$

where V_i is the *rms* value of the *ith* harmonic, and V_1 is the fundamental magnitude of the back-EMF. The variations of the THD under different load conditions are shown in Fig.2.9.

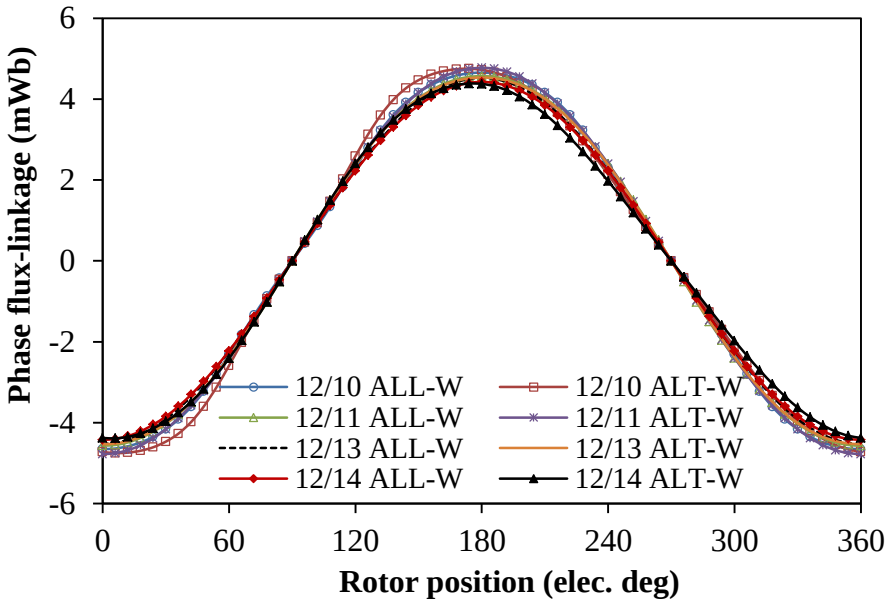

(a) Waveforms

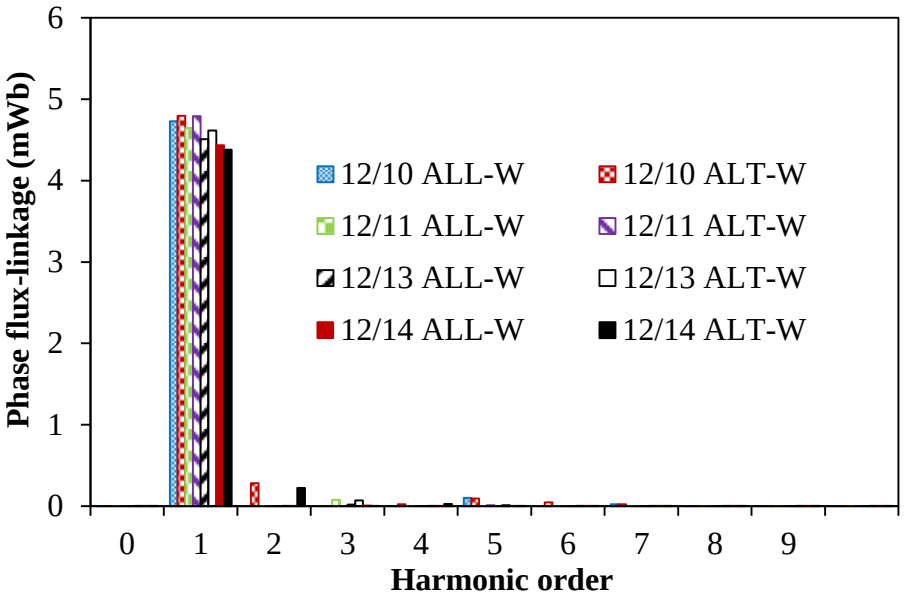

(b) Spectra

Fig.2.7 Comparison of open-circuit flux linkage variation with rotor position.

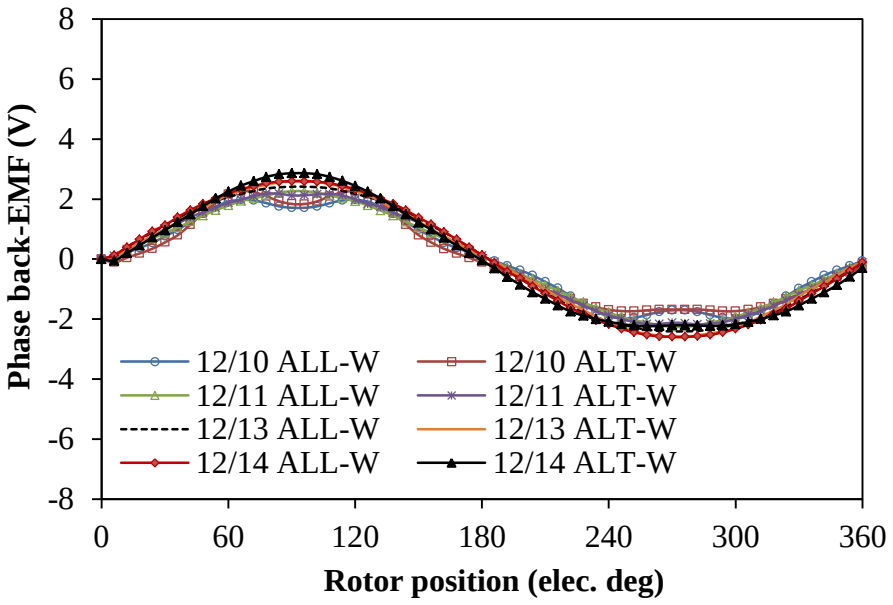

(a) Waveforms

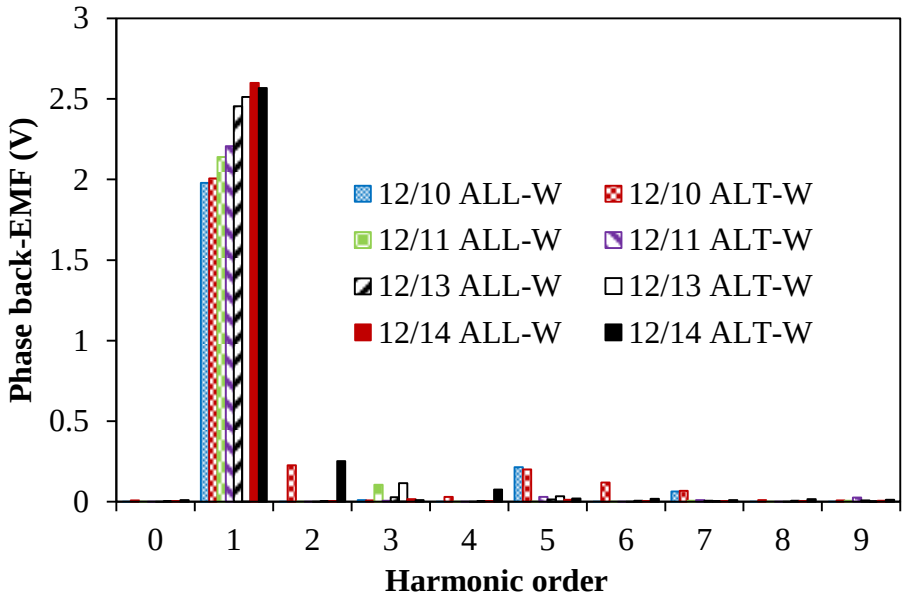

(b) Spectra

Fig.2.8 Comparison of phase back-EMF variation with rotor position, 400rpm.

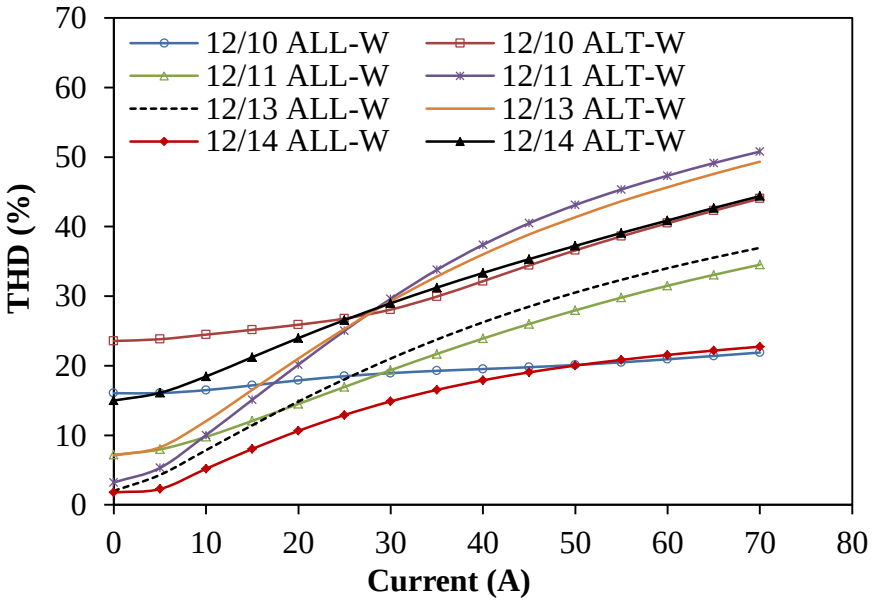

Fig.2.9 Variation of total harmonic distortions (THD) with *q*-axis current.

Fig.2.10 shows the cogging torque waveforms and spectra of the analysed machines. The cogging torque of the analysed machines having even-rotor poles is quite large especially that of the 10-pole machine when compared with the analysed odd-rotor pole machines. This is likely due to the existence of the 5^{th} and 7^{th} harmonic order of the back-EMF. It is worth noting that the cogging torque orders of the analysed machines having even- and odd-rotor pole numbers are multiples of six and twelve, respectively. The cogging torque could be reduced by taking it into account during the design/optimization process, but usually at the expense of some percentage of the electromagnetic torque.

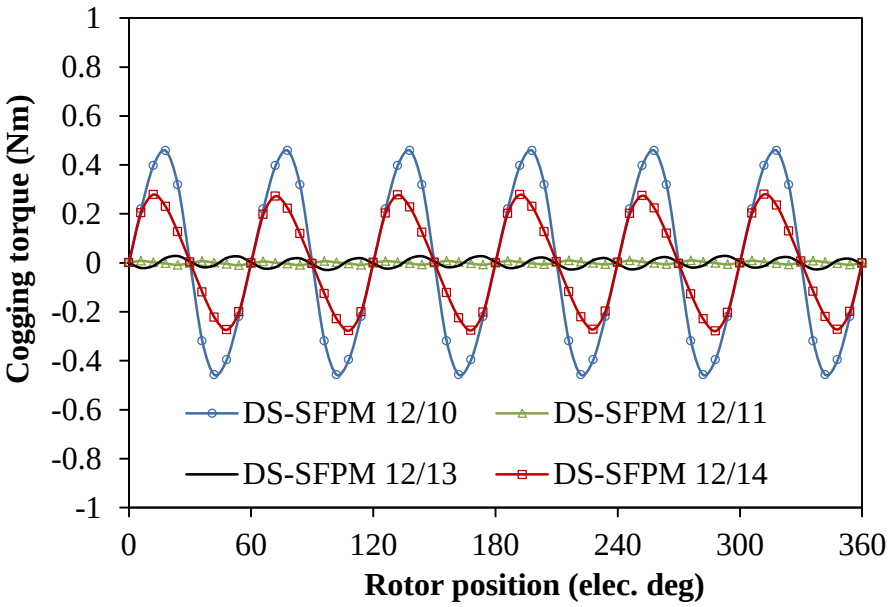

(a) Waveforms

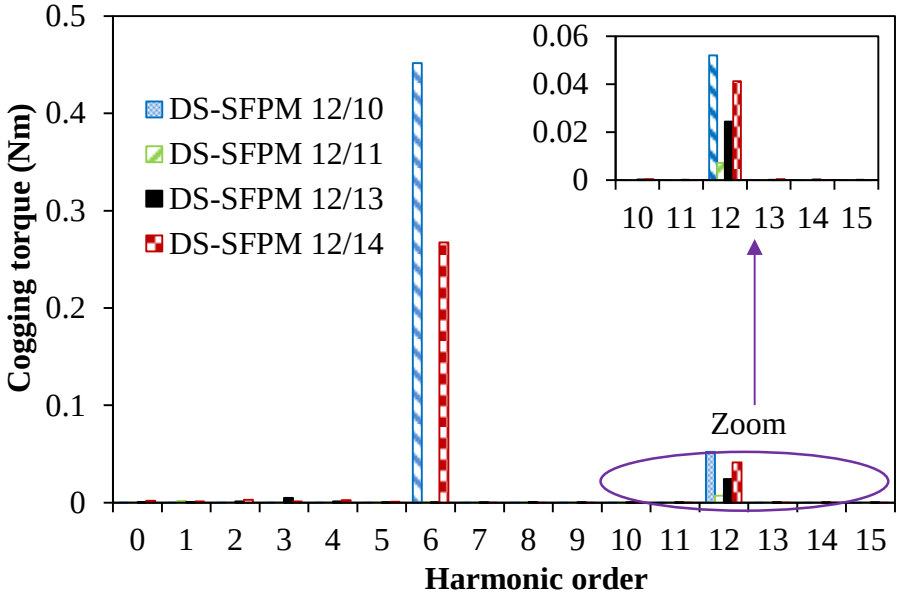

(b) Spectra

Fig.2.10 Comparison of cogging torque variation with rotor position.

The torque profile of the analysed machines is given in Fig.2.11. It can be seen that the developed all-pole wound DS-SFPM machine with N_r=14 seems to be the best candidate in terms of torque production. Moreover, it has good overload capability as seen from Figs.2.13 and 2.14.

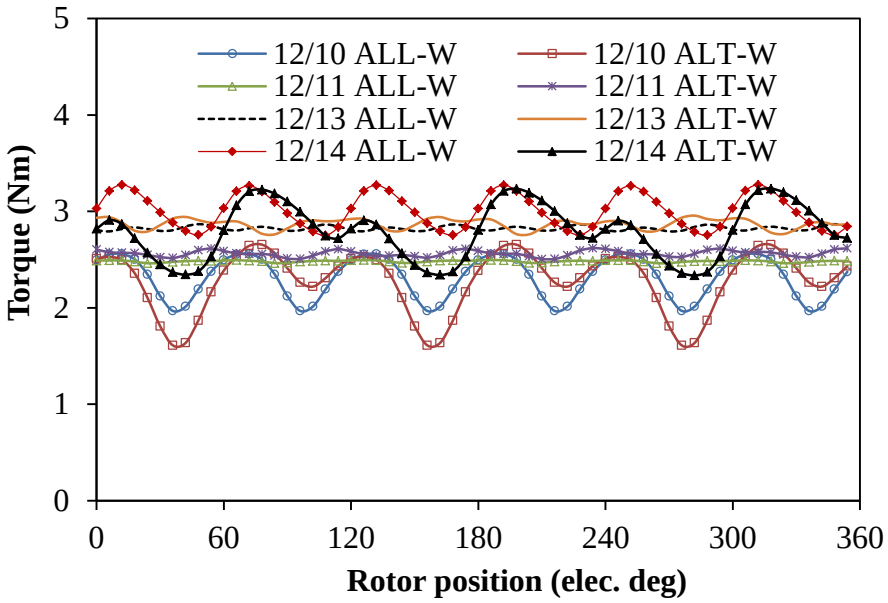

(a) Waveforms

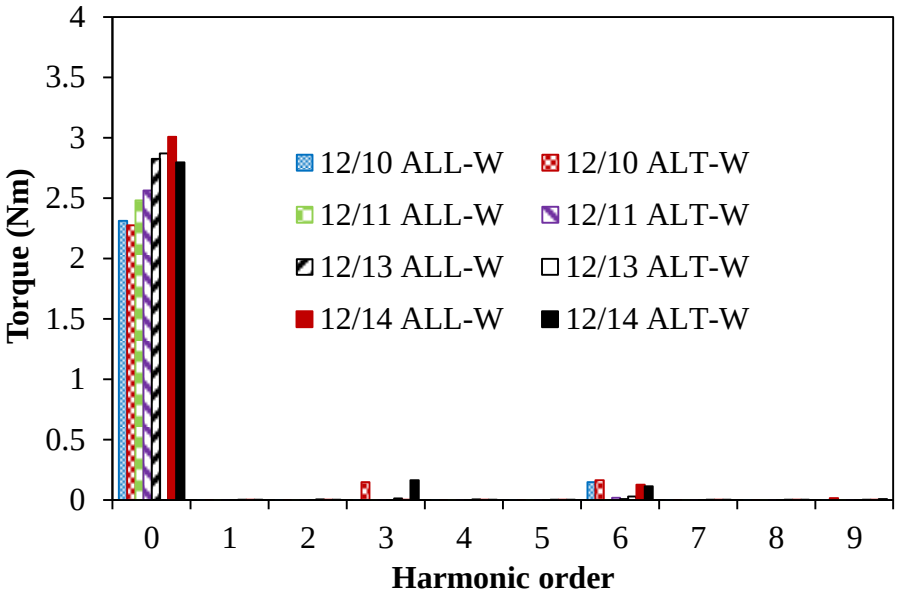

(b) Spectra

Fig.2.11 Comparison of torque characteristics (copper loss = 30W, i_d=0).

The torque ripple which is the ratio of the difference between the maximum and minimum torque to the average torque over one electric cycle is given by:

$$T_{ripple} = \frac{T_{max} - T_{min}}{T_{avg}} * 100\% \quad (2.4)$$

where T_{max}, T_{min}, and T_{avg} are the maximum, minimum and average torque respectively.

The comparison of the torque ripple at different peak currents is depicted in Fig.2.12. It can be seen that the developed machines having N_r=even exhibits higher torque ripple than their odd-rotor pole counterparts. This is because the machines with even-rotor pole numbers are characterised by a large amount of harmonics.

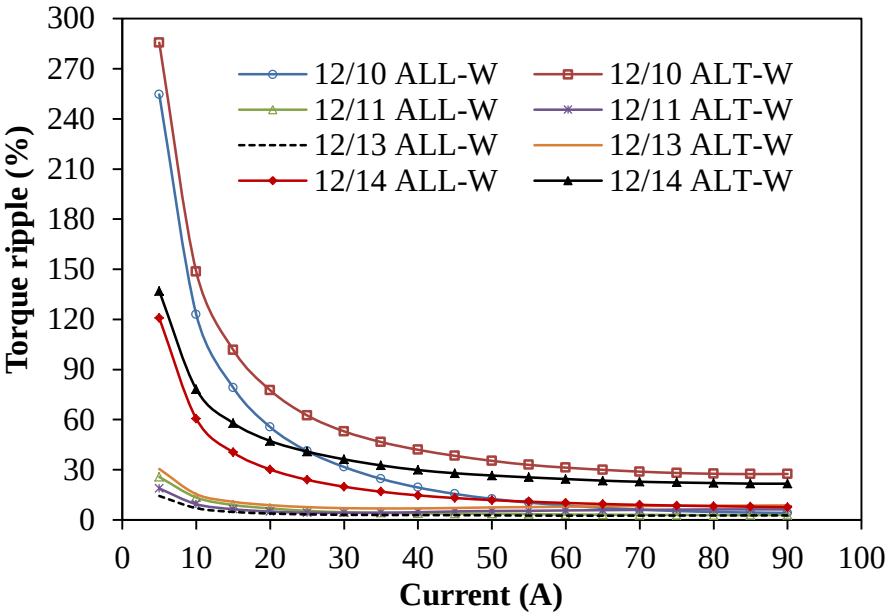

Fig.2.12 Variation of torque ripple with q-axis current, i_d=0.

The saturation curves of the analysed machines are depicted in Figs.2.13 and 2.14. It should be noted that the all-pole-wound 12-slot/14-pole machine has the largest torque profile at all the conditions.

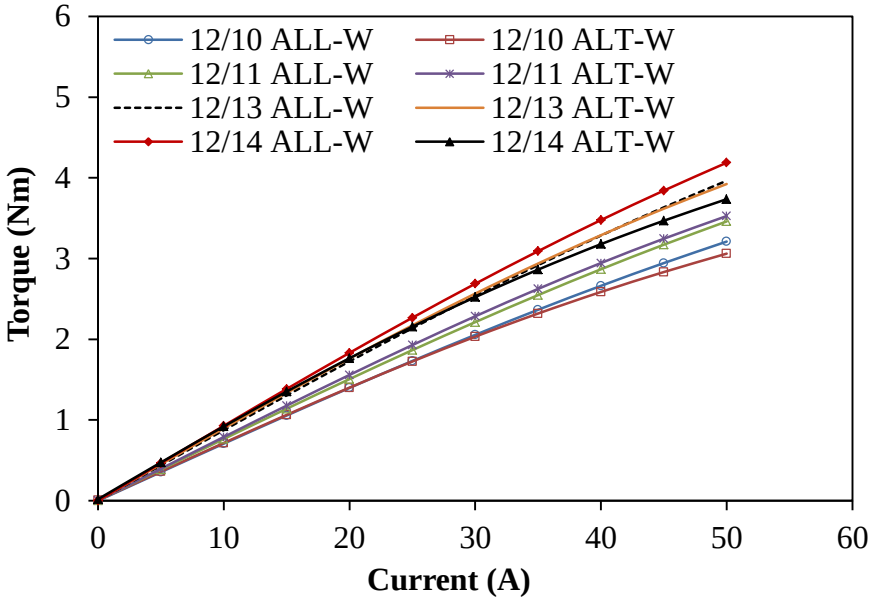

Fig.2.13 Comparison of average torque versus current, i_d=0.

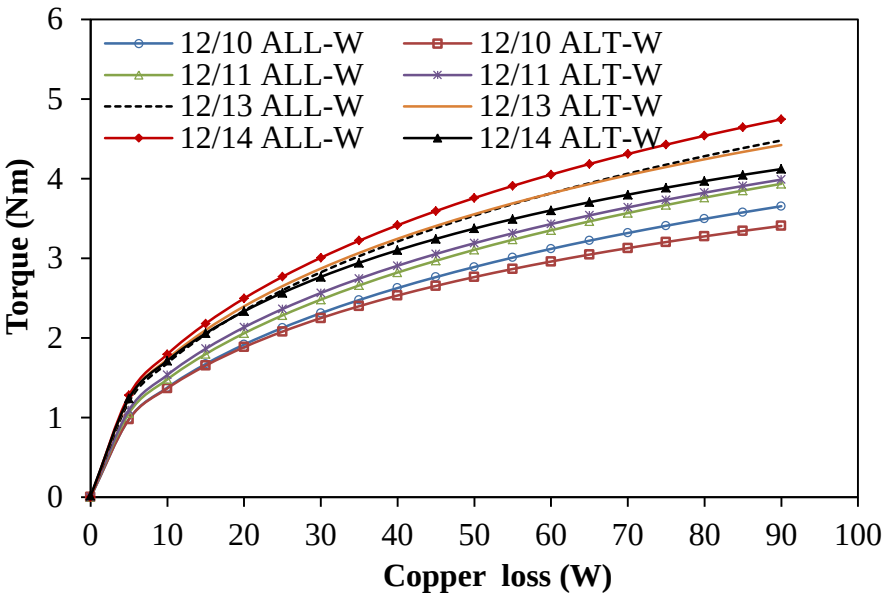

Fig.2.14 Variation of average torque with copper loss, i_d=0.

2.5 Inductance characteristics

The self- and mutual-inductances of the developed machines are shown in Figs.2.15 and 2.16 respectively. We could see that the 12-slot/10-pole machine having alternate-pole-wound configuration has the largest self-inductance amongst the analysed machines. The developed machines having alternate-pole-wound with 11- , 13- , and 14-rotor poles have similar self-inductance values. Moreover, the lowest values of mutual-inductances are seen in the even-rotor pole machines whose mutual-inductance values are quite similar. From the winding inductance characteristics of the developed machines, we could infer that the 10-pole machine having alternate-pole-wound topology may likely be a good candidate for fault tolerant capability, since it exhibits the highest and lowest amount of self- and mutual-inductances, respectively.

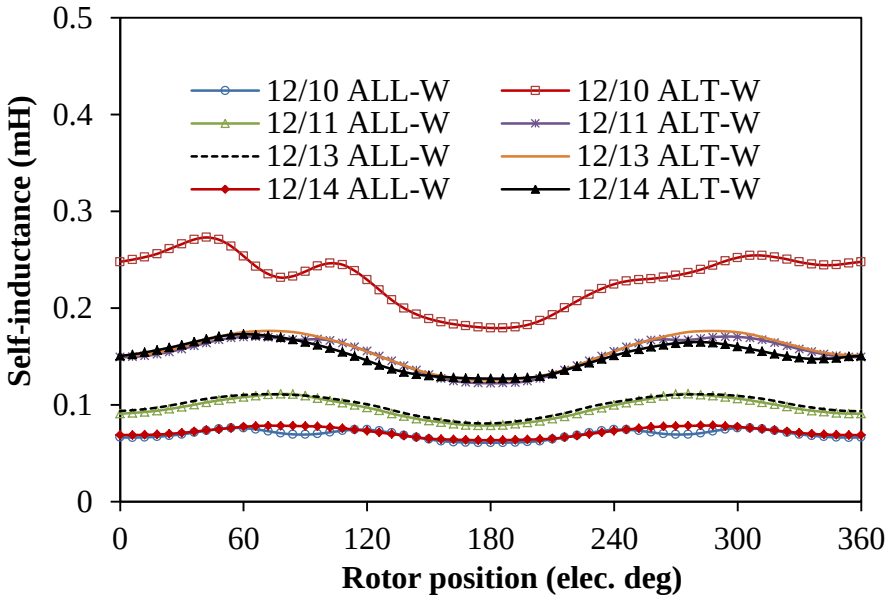

Fig.2.15 Variation of self-inductance with rotor position, *I*=15A.

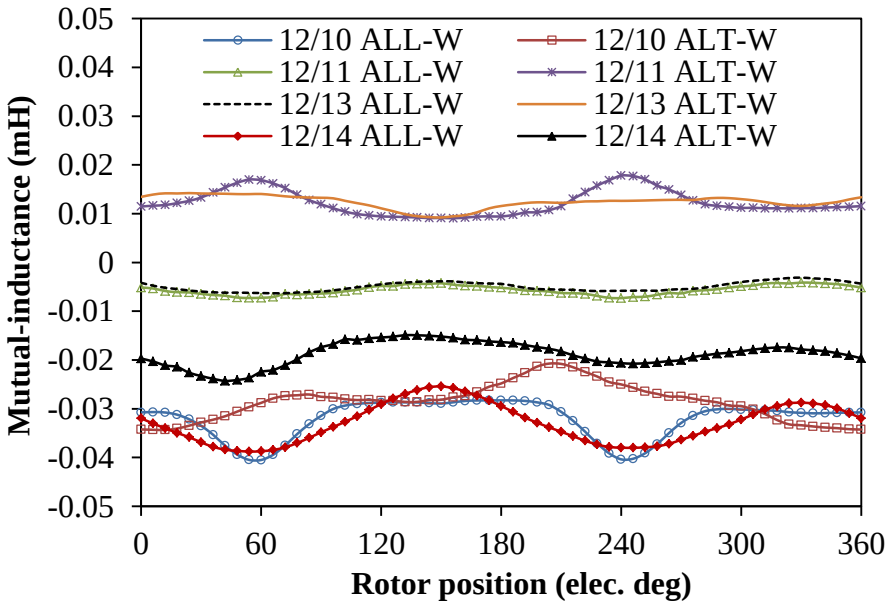

Fig.2.16 Variation of mutual-inductance with rotor position, *I*=15A.

2.6 Losses and efficiency profiles

Precise prediction of losses in the design of electrical machines is of utmost importance since this property influences the overall efficiency of the machine, to a great extent. Thus, we have given an adequate loss analysis in this section. The core losses of the analysed machines can be expressed by the classical iron loss equation given by:

$$P_{loss} = K_h B_m^2 f + K_e (B_m f)^{1.5} + K_c (B_m f)^2 \quad (2.5)$$

where B_m is the maximum value of the magnetic flux density, f is the frequency; K_h, K_e, and K_c are the loss coefficients for hysteresis, excess and eddy current losses respectively. Consequently, the efficiency of the machine is expressed as follows:

$$\eta = \frac{P_{out}}{P_{out} + losses} = \frac{2\pi NT}{(2\pi NT) + P_{cu} + P_{iron} + P_{mag}} * 100\% \quad (2.6)$$

where P_{out} is the mechanical output (W), T is the average torque (N.m), N is the rotational speed (rad/s), P_{iron}, P_{mag} and P_{cu} are iron, PM eddy current and copper losses, respectively. The PM eddy current loss in the analysed DS-SFPM machines could be reduced by means of magnet segmentation as proposed in [ZHU08]. Meanwhile, the PM eddy loss is insignificant compared to the core and copper losses obtainable in the analysed machines. The on-load variations of magnet eddy current, rotor, stator and total iron loss with speed are shown in Fig.2.17. The losses vary differently due to the varying structures of the machines as well as the electrical frequencies.

It is worth noting that the 10-pole machines have the least amount of magnet eddy current loss and total core loss amongst the compared machines as seen in Figs.2.17(d) and (e). Similarly, the largest amount of the magnet eddy current loss and the total core loss is obtained in the 14-pole machines. This indicates that the loss profile of the developed machines is heavily dependent on its electrical frequency. More importantly, the developed 12-slot/14-pole DS-SFPM machine with all-pole-wound configuration exhibits the highest efficiency amongst the compared topologies as seen from Fig.2.18 and in Table 2.1.

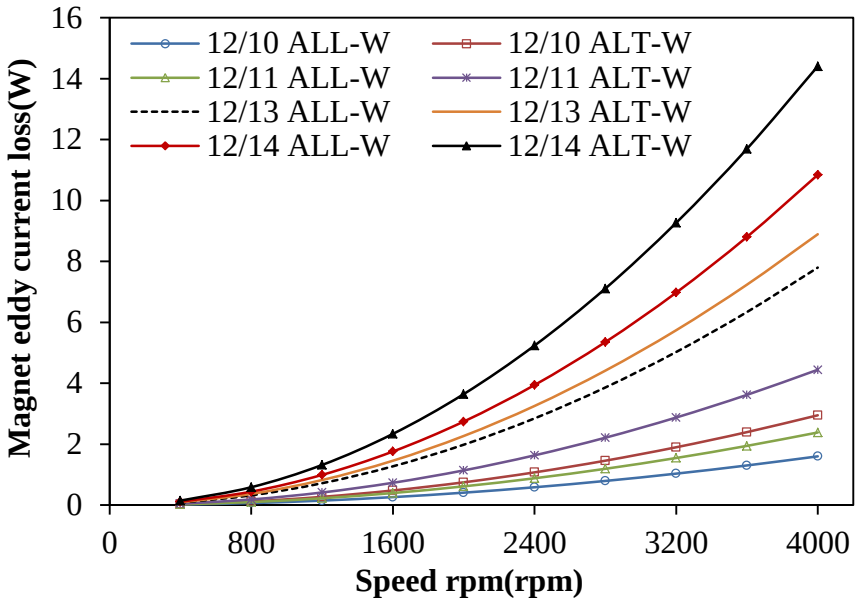

(a) PM eddy current loss versus speed

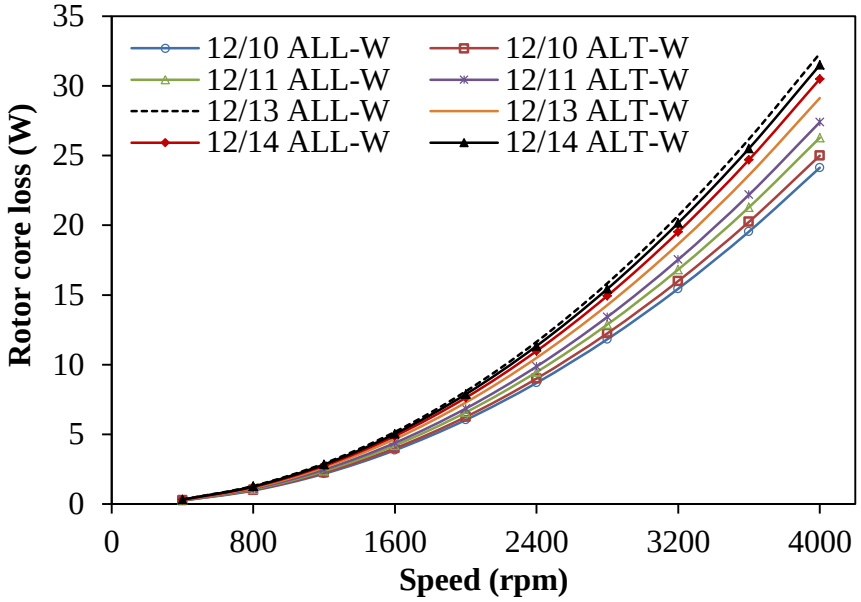

(b) Rotor core loss versus speed

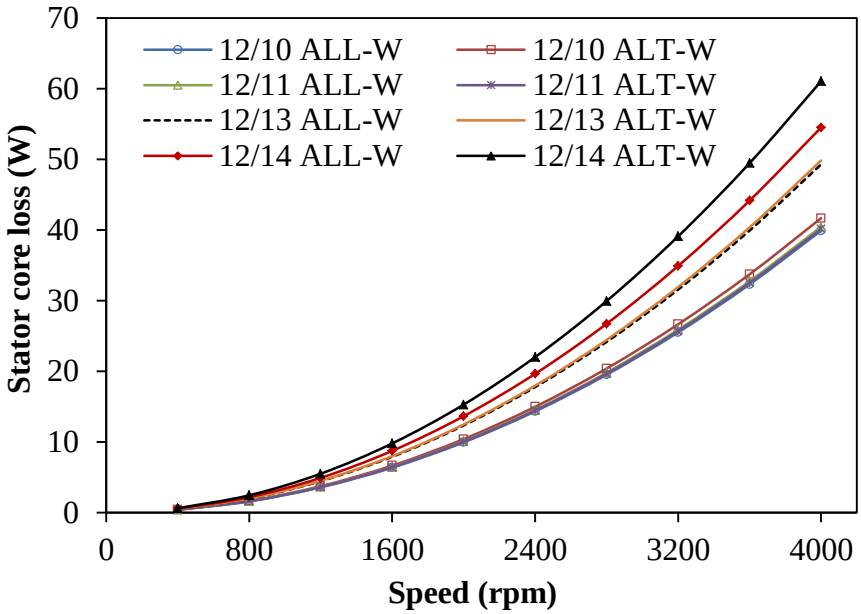

(c) Stator core loss versus speed

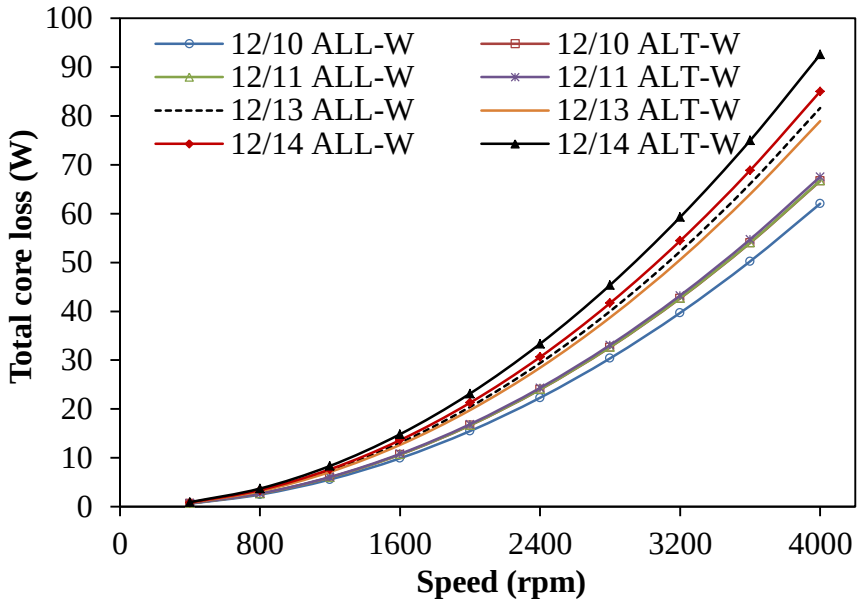

(d) Total core loss versus speed

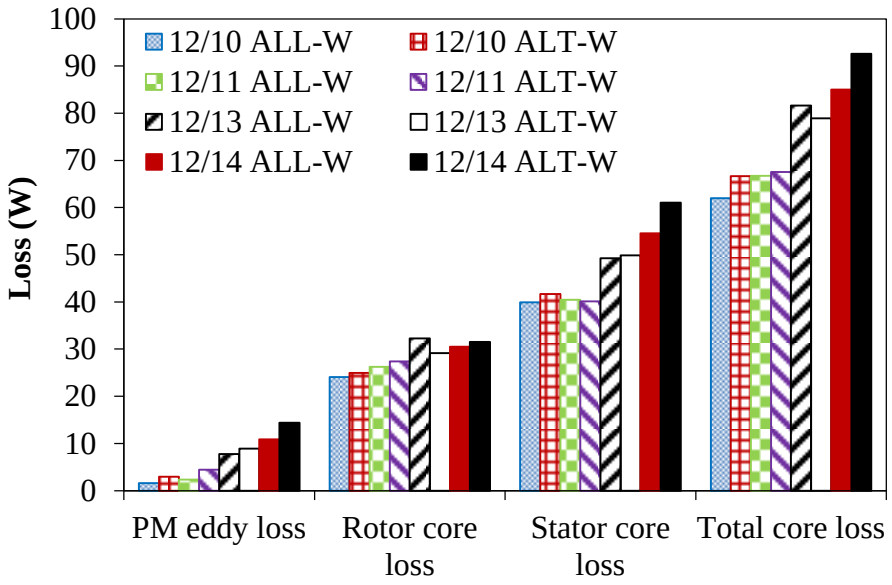

(e) Comparison of losses, 4000rpm

Fig.2.17 Comparison of losses in the DS-SFPM machines, *I*=15A.

It is worth noting that the lowest efficiency is seen in the alternate-pole-wound 12-slot/14-pole machine, owing to its high frequency and also large amount of harmonics. This is because of its inherent high amount of core loss and PM eddy current loss.

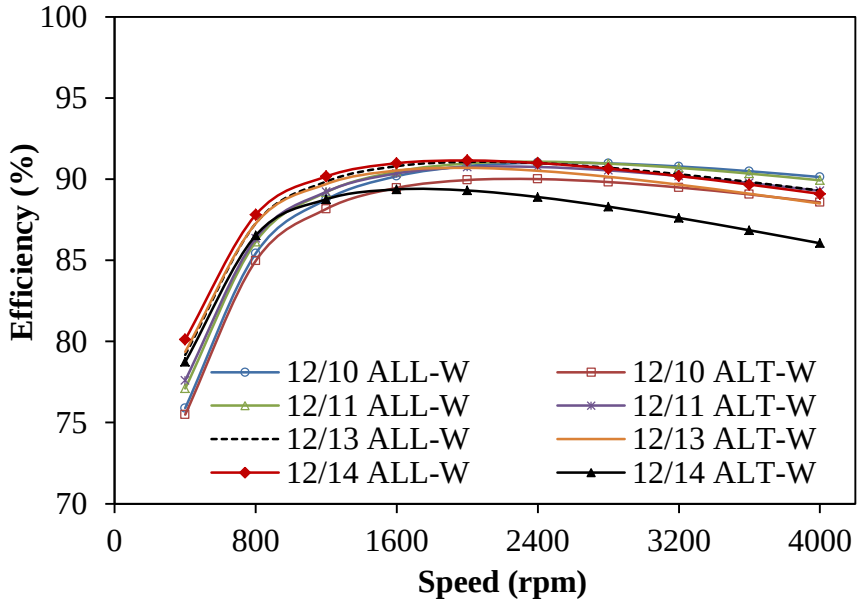

Fig.2.18 Comparison of efficiency, copper loss=30W.

2.7 Torque/power-speed characteristics

The torque- and power-speed characteristics of the analysed machines are shown in Figs. 2.19 and 2.20, respectively. The computations are carried out at I_{max} and V_{dc} of 15A and 22.9V respectively. The predicted results show that the all-pole-wound 12/14-pole machine has the largest torque potential.

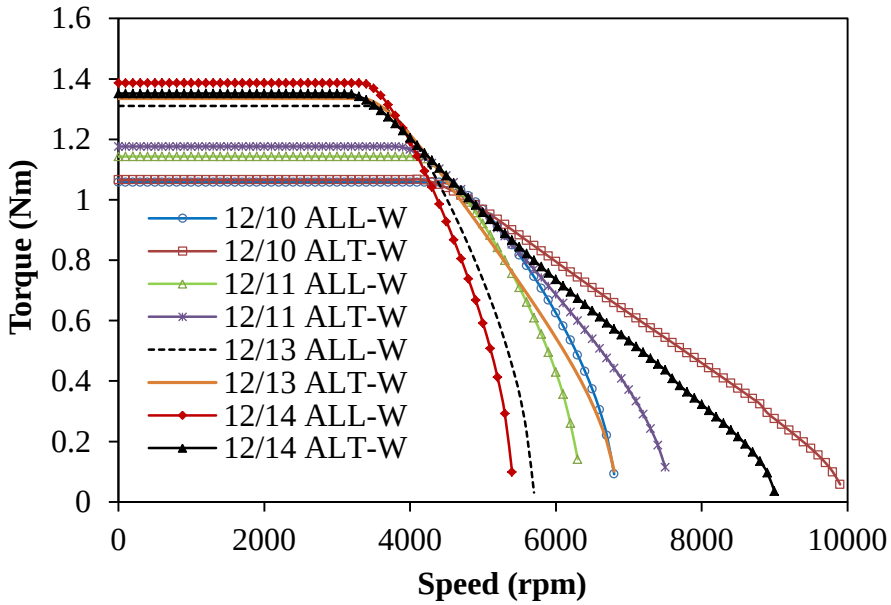

Fig.2.19 Comparison of torque-speed characteristics, (V_{dc} = 22.9V, I_{max} = 15A).

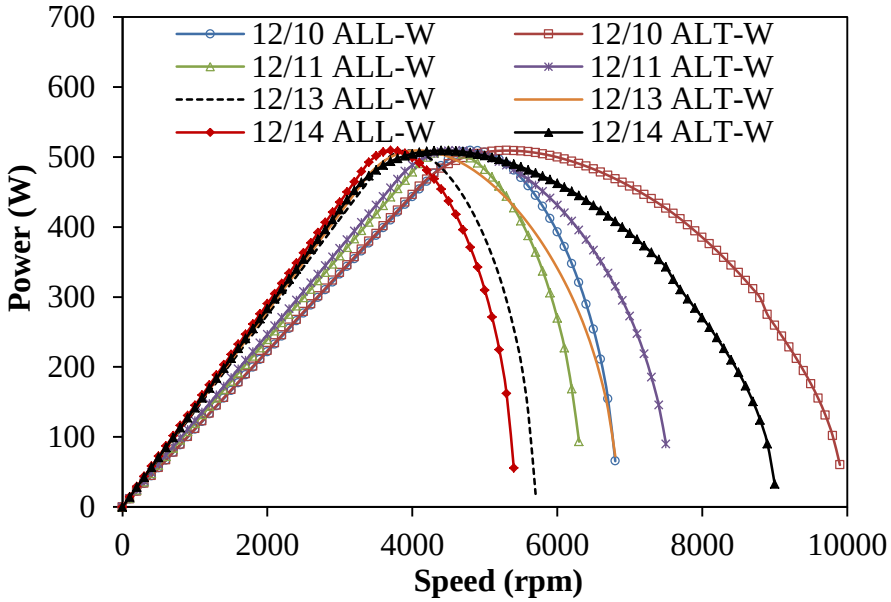

Fig.2.20 Comparison of torque-speed characteristics, (V_{dc} = 22.9V, I_{max} = 15A).

The PM flux-linkages of the developed machines at different load conditions are compared in Fig.2.21. It is observed that the values of the flux-linkages are inversely related to the machine's electrical frequencies, i.e. the higher the frequency, the lower the magnitude of the PM flux-linkage. The variations of the PM flux-linkage with different *q*-axis current are essentially constant, although with a little decrease as the load increases due to the armature reaction which tends to saturate the electromagnetic circuit.

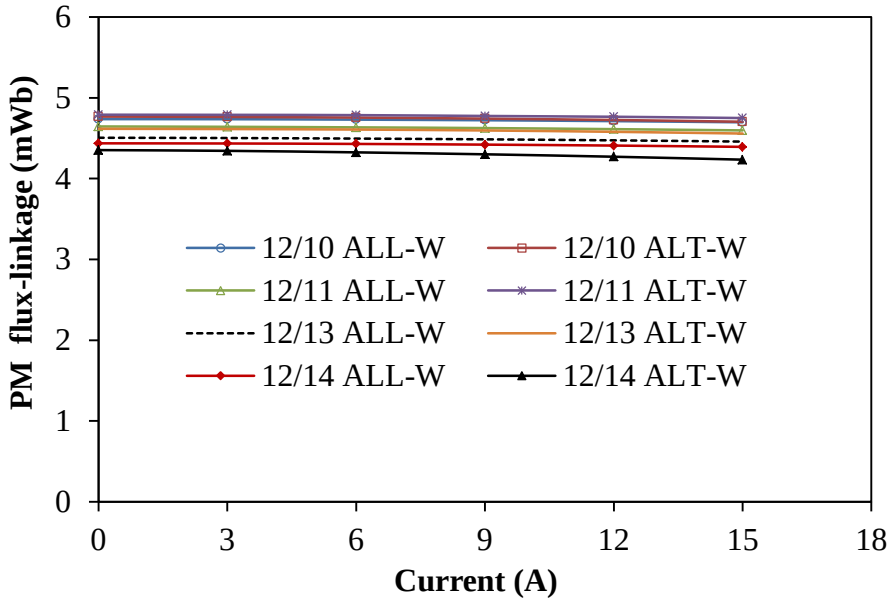

Fig.2.21 Variation of PM flux-linkage with *q*-axis current.

2.8 Summary

In this chapter, double-stator switched flux permanent magnet (DS-SFPM) machines having 12-separate stator slots are developed and analysed. Moreover, the influence of design parameters on the average torque of the developed machines is given. It is worth noting that the design parameters of these machines are optimized globally at a set condition of fixed copper loss (30W). Further, quantitative comparison of the electromagnetic performances of the machines having all- and alternate-pole-wound topologies is presented by 2-dimensional finite element analysis (2D-FEA). The analyses show that the all-pole wound 12-slot/14-pole machine delivers the largest torque amongst all the compared machines, under all operating conditions.

Furthermore, a comprehensive study of the core and PM eddy current losses in these machines are also presented, together with their efficiency characteristics. The torque- and power-speed characteristics as well as the winding inductances of the machines are also illustrated in this chapter. Moreover, the effects of load on the total harmonic distortion of the voltage and torque ripple of the analysed machines are also given in this chapter.

The developed machines could have wide range of applications including automotive, aerospace, and wind power generation. It is worth mentioning that the analysed 12-slot/14-pole DS-SFPM machine with all-pole wound topology could deliver not only higher torque density, but also better efficiency than its compared counterparts.

CHAPTER 3

DOUBLE-STATOR SWITCHED FLUX PM MACHINES HAVING 6-STATOR TEETH/POLES

3.1 Introduction

Switched flux permanent magnet (SFPM) machines exhibit numerous advantages including but not limited to high torque/power capability, good thermal dissipation potential, better efficiency, rugged rotor structure and good flux-weakening capability. Hence, a handful of literature is available in this area for over last decade [HOA97], [ZHU05], [HOA07], [HUA08] and [CHE10a]. Unfortunately, PM machines are prone to the risk of demagnetization, particularly with ferrite magnets as identified in [FAS14] and [LI15]. Moreover, the cost of NdFeB magnets is a major concern. Thus, low-cost alternatives for PM machines are under consideration, including switched reluctance machines especially the double stator type [ABB10]. The influence of rotor pole numbers of SFPM machines is demonstrated in [CHE10]. Similarly, many research efforts on the optimal designs of PM machines to enhance the performance are readily available in literature [SIZ13], [CHE11c] and [ASH11]. The saliency ratio of interior permanent magnet (IPM) and flux-weakening capability of SFPM machines are given in [KIM07], [ZHA13] and [ZHU15] respectively. The flux weakening factor given in [ZHU15b] is used as flux weakening performance index of the analysed machines, and the larger this factor, the better the flux weakening performance.

Due to the capability of the double air-gap machines to produce larger torque density than the equivalent single airgap-type of the same size and under the same condition, a lot of researchers have paid their attention towards double-stator machines with dual air-gaps, particularly the magnetically-geared machines [CHA07], [WAN11a], [WAN09], [LIU12], and [KIM16]. It is worth noting that the numbers of stator pole and rotor iron pole pieces in [KIM16] are similar. Thus, the PM usage of the machine in [KIM16] is much higher than that of the developed machines for a given machine size, and thus the cost of production would also be higher.

In this chapter, the feasible stator and rotor pole number combinations (N_s and N_r) and the influence of rotor pole numbers on the overall performance of double-stator switched flux PM (DS-SFPM) machines are quantitatively compared. The 13-rotor pole machine is found

to be the most promising candidate in terms of high output torque and better flux-weakening capability.

The schematic diagrams of the developed machines as well as the conventional SFPM machines are shown in Fig.3.1. The machines comprise of a flux-modulator and identical salient-pole double stators equipped with non-overlapping concentrated armature windings. Since the stators are furnished with concentrated armature coils, it implies that shorter end-windings, and hence, lower copper losses are achieved. It is worth mentioning that the armature windings are allocated to the separate stators according to the ratio of the slot areas, so as to maintain similar level of saturation at both inner and outer stators. All the machines are optimized using the genetic algorithm approach with a fixed value of copper loss (30W); the design objective is to realize the maximum average torque. Note that circumferential PMs having opposite polarity are sandwiched in-between the stator poles in each stator. Similarly, for torque production, the PMs that are directly opposite to each other in both stators must be of reverse polarity. The magnetic flux reverses its direction of flow over half an electric cycle, in consonant with the principles of SFPM machines. Note that the electromagnetic circuit of these machines is in series. Therefore, this would reduce control complexities. Further, the aforementioned circuit is primarily dominated by the flux path due to the magnets. Consequently, the DS-SFPM machines produce significant amount of PM torque with negligible reluctance torque.

The machines have dual-operating principle; similar to that of flux-modulated magnetically-geared machines and switched flux PM machines.

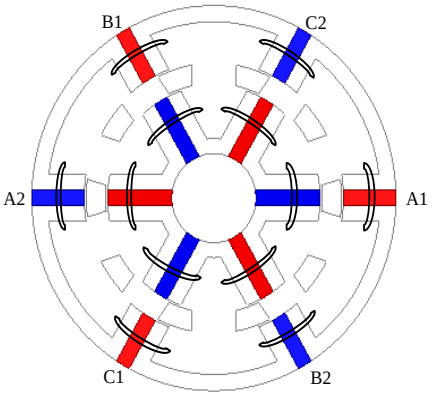

(a) Developed DS-SFPM 6/10

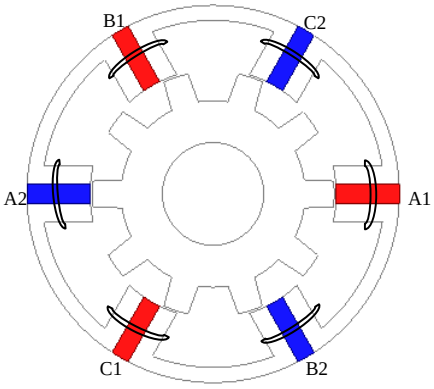

(b) Conventional SFPM 6/10

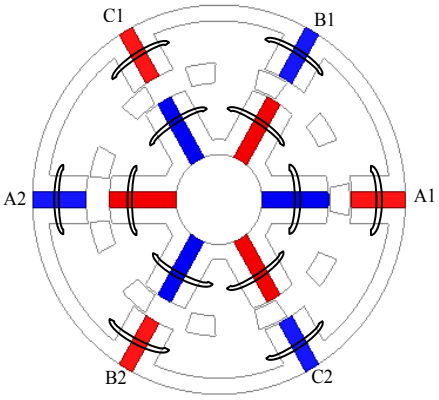

(c) Developed DS-SFPM 6/11

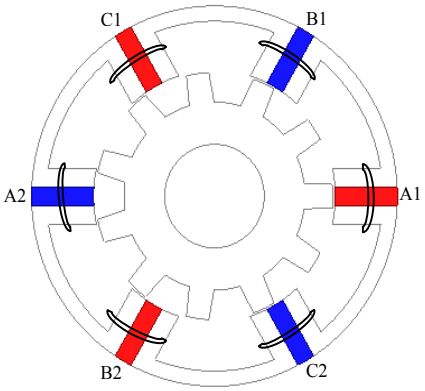

(d) Conventional SFPM 6/11

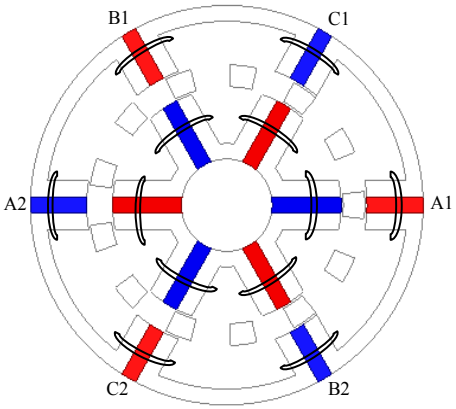

(e) Developed DS-SFPM 6/13

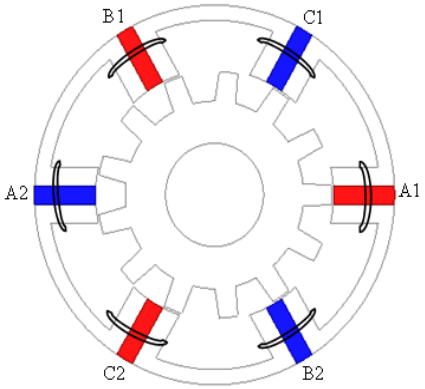

(f) Conventional SFPM 6/13

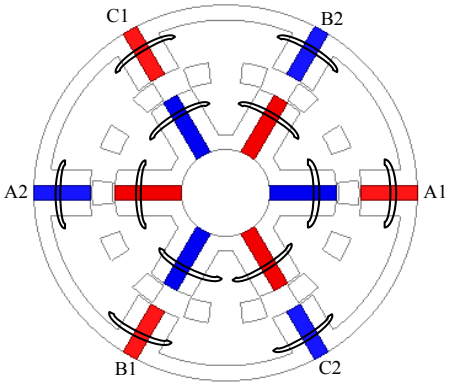

(g) Developed DS-SFPM 6/14

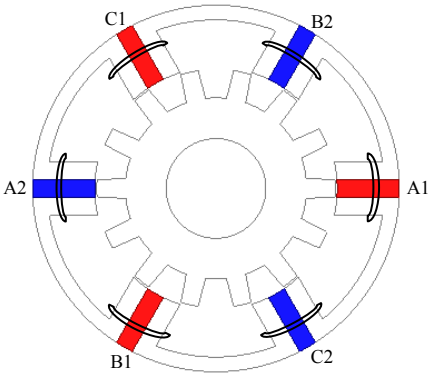

(h) Conventional SFPM 6/14

Fig.3.1 Cross-sections of the proposed DS-SFPM machines.

As shown in Fig.3.26, the DS-SFPM machines seem to produce higher electromagnetic torque than its equivalent single-stator counterparts, due to its peculiar advantage of combined working-effect of flux-modulation and flux-switching. Fig.3.2 shows the schematic diagram of the developed DS-SFPM machine having 4-rotor iron pieces, held together by iron brigdes of about 0.5mm thickness.

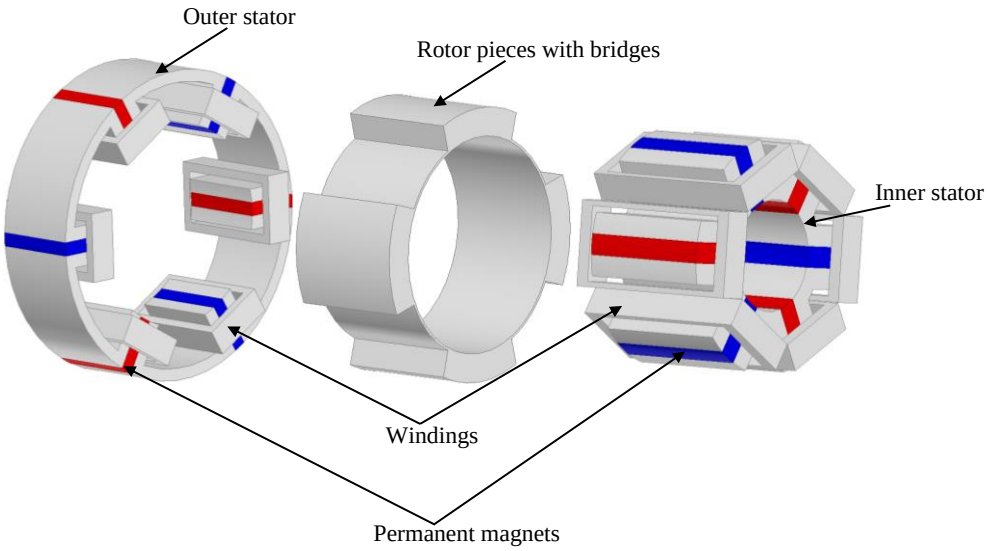

Fig.3.2 Schematic diagram of the developed DS-SFPM machine.

The coil-EMF phasors and winding configurations of the DS-SFPM machines are depicted in Fig.3.3. It is worth noting that the following pairs of machines have similar winding topology: 4- and 10-rotor pole machines, 5- and 11-rotor pole machines, 7- and 13-rotor pole machines, and 8- and 14-rotor pole machines, respectively. Further, the values of the main machine parameters with its corresponding optimum values are listed in Table 3.1.

In general, the stator and rotor pole combinations of the developed machines with odd- and even-rotor pole numbers is represented by (3.1):

$$N_r = kN_s \pm j \tag{3.1}$$

where k and j= integers 1, 2…, N_r and N_s are the numbers of rotor- and stator-poles respectively.

For clarity, the considered machines in this chapter could be broadly group into two: $N_r=N_s\pm j$ and $N_r=2N_s\pm j$ with j=1 and or 2.

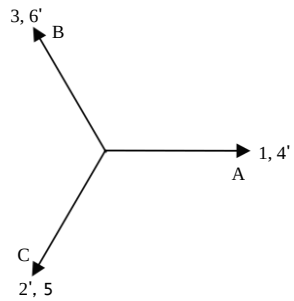

(a) 4-rotor-pole

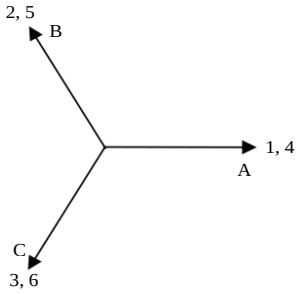

(b) 5-rotor-pole

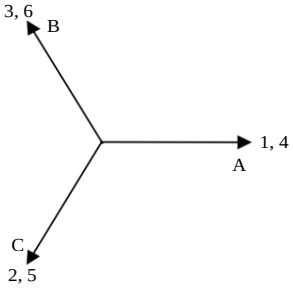

(c) 7-rotor-pole

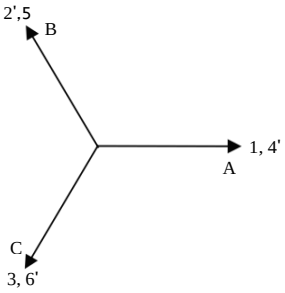

(d) 8-rotor-pole

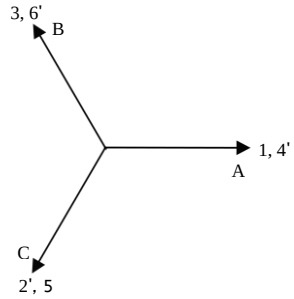

(e) 10-rotor-pole

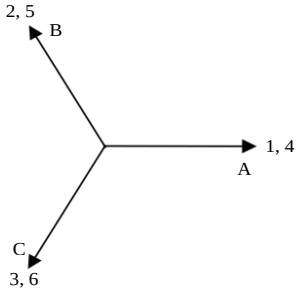

(f) 11-rotor-pole

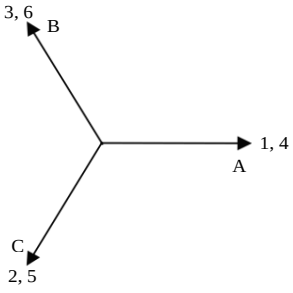

(g) 13-rotor-pole

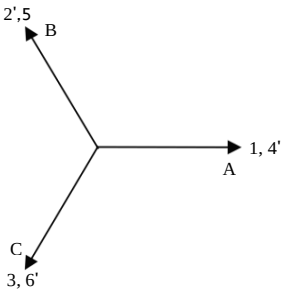

(h) 14-rotor-pole

Fig.3.3 Coil EMF phasors and winding configurations of DS-SFPM machines.

TABLE 3.1 MAIN PARAMETERS OF OPTIMIZED DS-SFPM MACHINES

Parameter	Value			
Outer stator slot number	6			
Inner stator slot number	6			
Air-gap length (mm)	0.5			
Active axial length (mm)	25			
Machine outer diameter (mm)	90			
Outer stator turns/coil	24			
Inner stator turns/coil	12			
Total number of turns/phase	72			
PM remanence (T)	1.2			
Rotor pole number, N_r	**10**	**11**	**13**	**14**
Split ratio	0.71	0.71	0.71	0.70
Rotor radial thickness (mm)	4.76	4.62	4.93	4.86
PM thickness (mm)	3.58	3.59	3.58	3.66
Outer rotor arc/pitch ratio	0.45	0.41	0.40	0.43
Inner rotor/pitch ratio	0.36	0.36	0.40	0.41
Back-iron thickness (mm)	3.81	3.68	3.57	3.60
PM volume (k.mm^3)	15.51	15.6	15.39	15.8
PM volume of DS-SFPM 12/14 (k.mm^3)	22.61			
Torque/PM vol. (k.Nm/mm^3)	0.19	0.31	0.35	0.24
Torque ripple (%)	166.8	7.56	10.5	9.69
Total harmonic distortion, THD (%)	22.38	3.06	4.61	8.06
Rotor pole number, N_r	**4**	**5**	**7**	**8**
Split ratio	0.67	0.59	0.55	0.57
Rotor radial thickness (mm)	7	7	6	6
Outer rotor arc/pitch ratio	0.4	0.4	0.4	0.4
Inner rotor/pitch ratio	0.5	0.5	0.4	0.4

3.2 Machine optimization and influence of leading design parameters on the average torque

In order to obtain the optimum electromagnetic performance of the machine we have optimized all the developed machines using the evolutionary computational method. The design/optimization target is to realize the maximum average torque. The leading design

parameters that were considered include: the split-ratio, the PM thickness, the rotor radial thickness, the rotor iron pole arc/pole pitch, and the stator back-iron thickness. The optimum values of the design parameters for the DS-SFPM machines having $N_r=2N_s\pm j$ are listed in Table 3.1. For fair comparison, it is worth noting that we have kept the same outer diameter of these machines at fixed copper loss condition of 30W.

3.2.1 Split ratio

The average torque of the developed machine is influenced by its split ratio which is defined as the ratio of the outer airgap diameter to the outer machine diameter. Note that the outer airgap is the assumed working airgap in this machine. The average torque would increase initially as the split ratio increases as seen in Fig.3.4, until a point when magnetic saturation becomes severer due to reduced slot area, and consequently, a decreased torque would emerge due to less flux per pole.

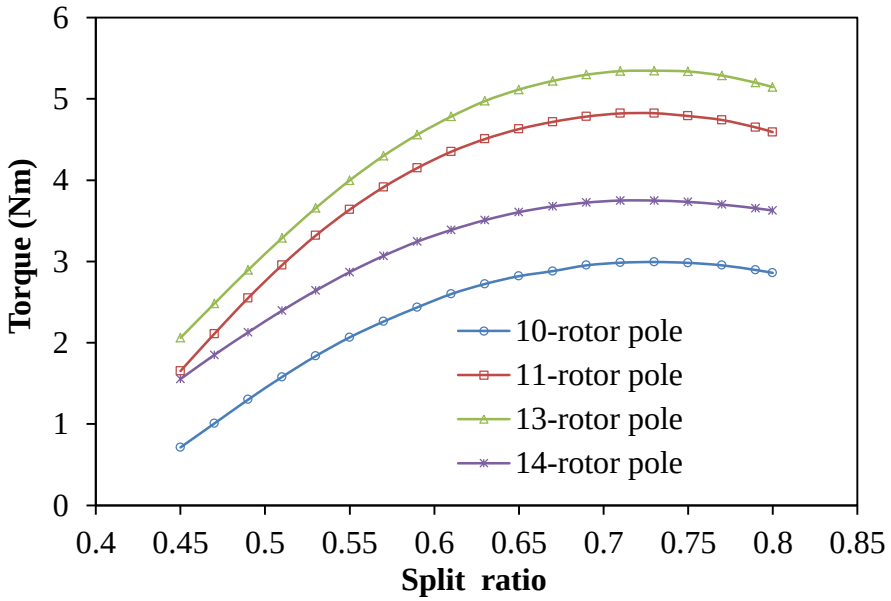

Fig.3.4 Variation of average torque with split ratio, i_d=0.

3.2.2 PM thickness

Similarly, as the PM size increases, there would be a corresponding increase in the rate of change of flux with time and thus the back-EMF. This would lead to enhanced output torque. Hence, the average torque would continue to increase until a certain value when an increased PM thickness leads to significant reduction of the spaces for the armature conductors, and then the average torque would subsequently decrease. The variation of average torque with

PM thickness is shown in Fig.3.5.

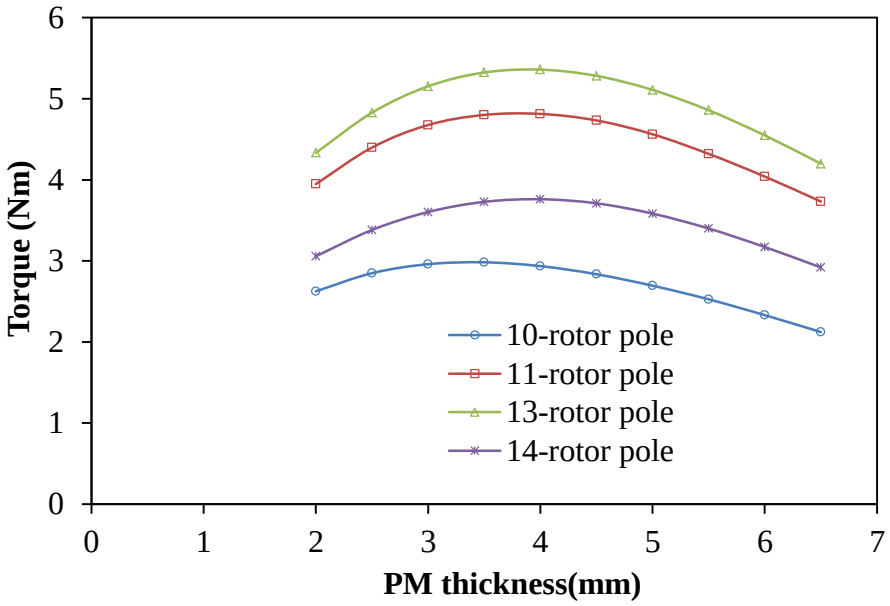

Fig.3.5 Variation of average torque with PM thickness, i_d=0.

3.2.3 Rotor radial thickness

The variation of the average torque with rotor radial thickness is depicted in Fig.3.6. A smaller size of the modulating iron pieces implies that the rotor iron could be easily saturated, and thus for the same electric loading, there would be lower output torque. Also, when the rotor size is increased significantly, it could lead to smaller slot area, and hence, smaller phase current at fixed copper loss, and consequently, a reduced output torque.

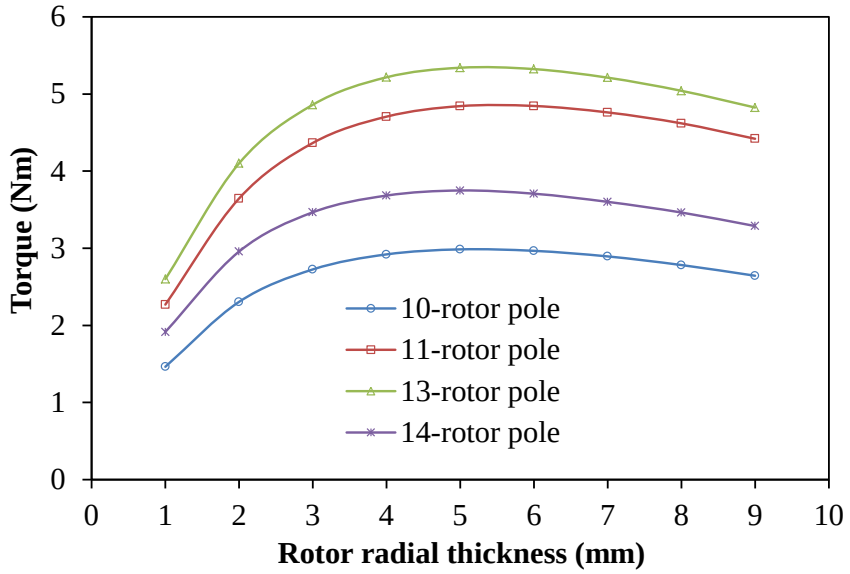

Fig.3.6 Variation of average torque with rotor radial thickness, i_d=0.

3.2.4 Rotor iron pole arc/pole pitch

Also, Figs.3.7 (a) and (b) show the variation of average torque with the rotor pole arcs. The ratio of the rotor pole arc to its pitch ratio is dependent on the rate of change of the modulated magnetic flux around the airgaps. Thus, the resultant amount of flux-linkages on the pole arcs would be proportional to the produced output torque. The maximum value of the average torque would occur on these separated arcs when the largest amount of magnetic flux surrounds the arcs consecutively.

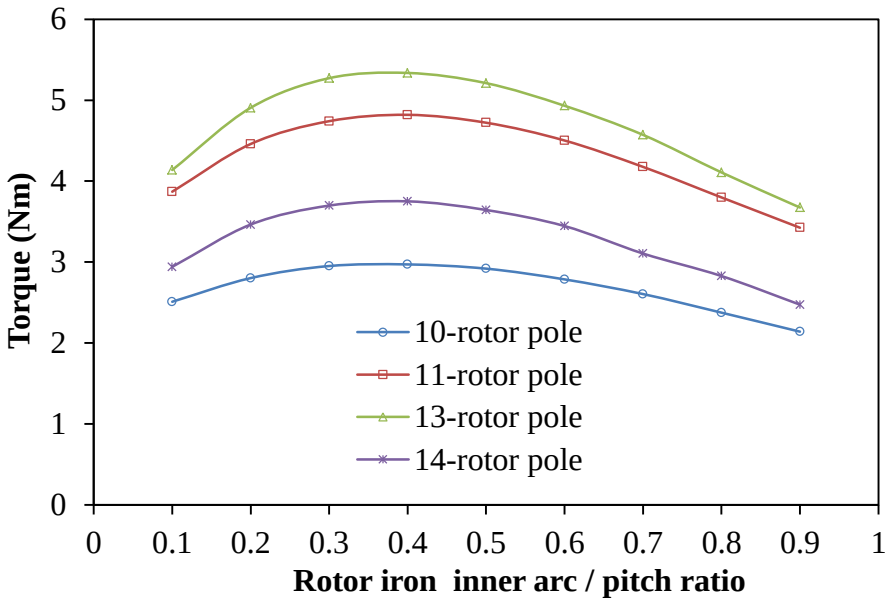

(a) Torque versus rotor inner arc/pitch ratio

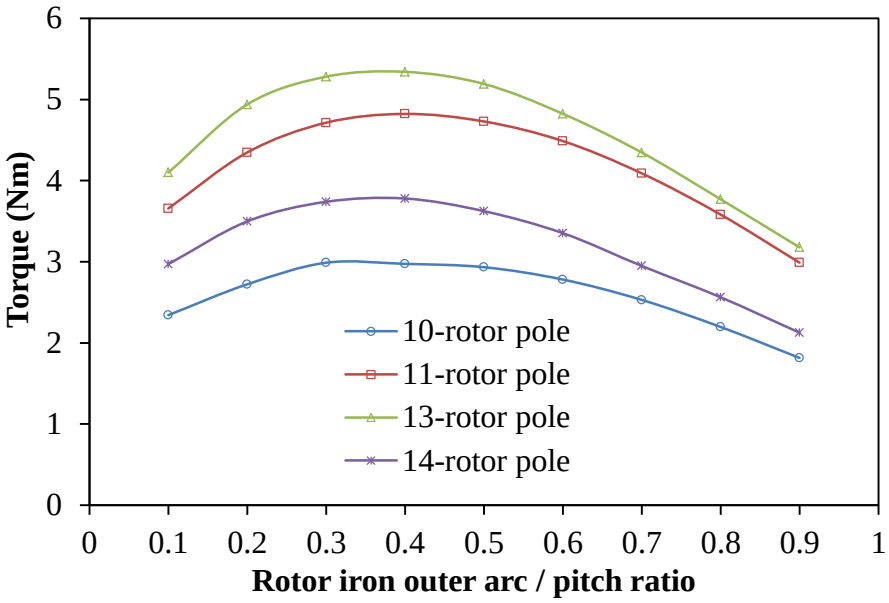

(b) Torque versus rotor outer arc/pitch ratio

Fig.3.7 Variation of average torque with rotor inner and outer pole arcs, i_d=0.

3.2.5 Back-iron thickness

Further, the output torque is very sensitive to the variation of the back-iron thickness. Clearly, it can be seen from Fig.3.8 that there is an optimal stator yoke. A sharp reduction on the average torque when the stator yoke thickness is decreased as although the slot area is increased the stator yoke will be significantly saturated. Similarly, the performance would be deteriorated when the stator yoke is enlarged beyond a certain value due to higher flux leakage, reduced slot area and increased copper loss.

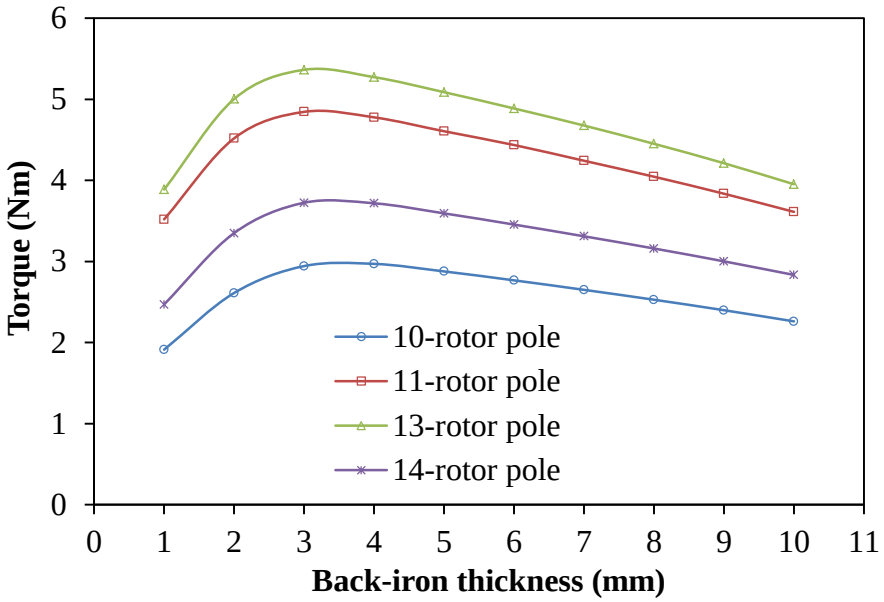

Fig.3.8 Variation of average torque with outer stator back-iron thickness, i_d=0.

Furthermore, the effects of leading design parameters on the magnitude of the back-EMF of DS-SFPM machines having N_r=N_s±j are displayed in Figs.3.9 (a)-e. The optimum values of the design parameters which include the split-ratio, the stator back-iron thickness, the rotor iron outer arc/pitch ratio, the rotor iron inner arc/pitch ratio and the rotor radial thickness as a function of fundamental amplitude of the back-EMF are listed in Table 3.1.

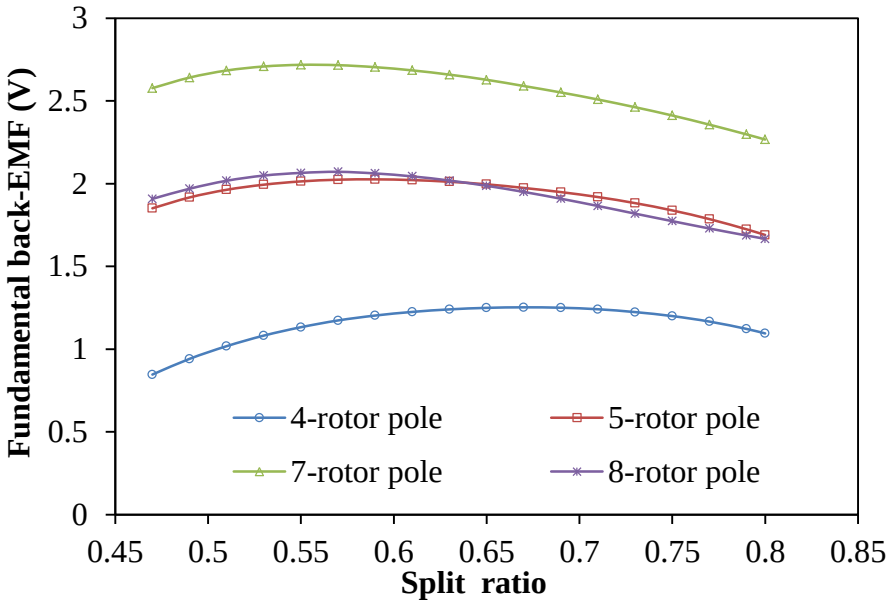
Fundamental back-EMF (V)
3
2.5
2
1.5
1
0.5
0
0.45
0.5
0.55
0.6
0.65
0.7
0.75
0.8
0.85
Split ratio
4-rotor pole
5-rotor pole
7-rotor pole
8-rotor pole

(a)

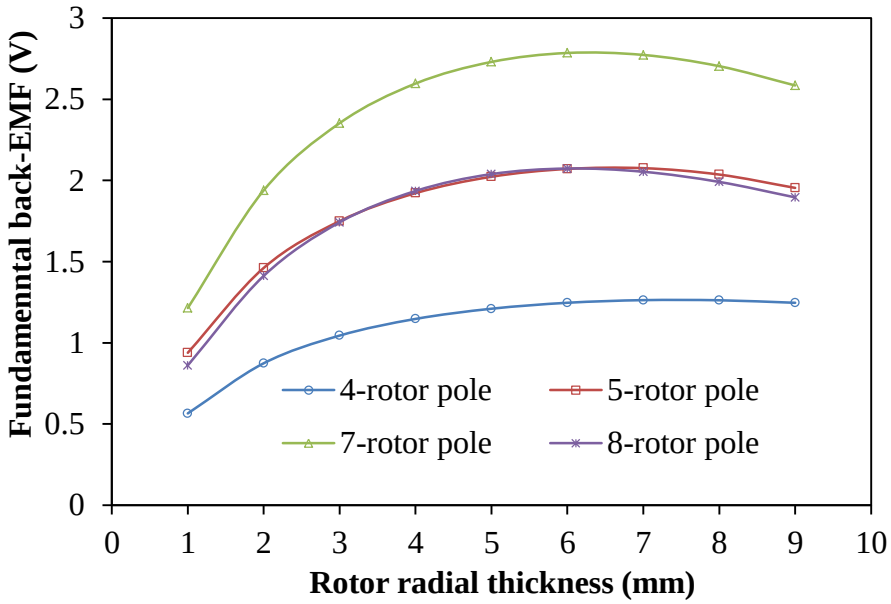
Fundamenntal back-EMF (V)
3
2.5
2
1.5
1
0.5
0
0
1
2
3
4
5
6
7
8
9
10
Rotor radial thickness (mm)
4-rotor pole
5-rotor pole
7-rotor pole
8-rotor pole

(b)

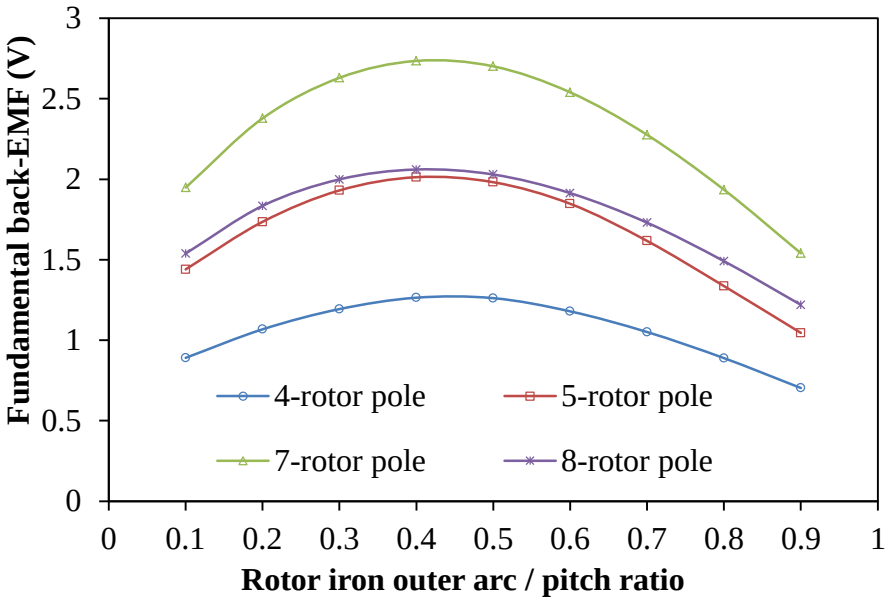
Fundamental back-EMF (V)
3
2.5
2
1.5
1
0.5
0
0
0.1
0.2
0.3
0.4
0.5
0.6
0.7
0.8
0.9
1
Rotor iron outer arc / pitch ratio
4-rotor pole
5-rotor pole
7-rotor pole
8-rotor pole

(c)

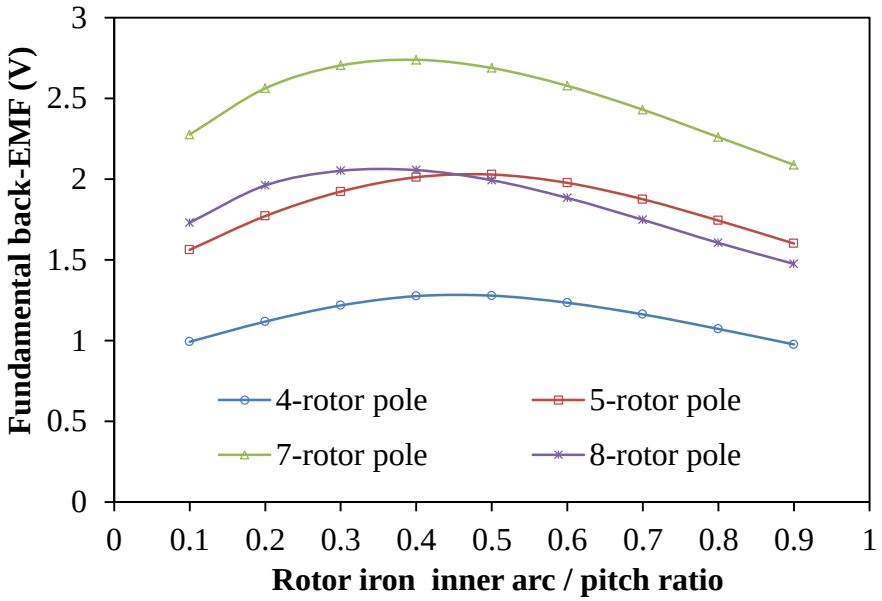
Fundamental back-EMF (V)
3
2.5
2
1.5
1
0.5
0
0
0.1
0.2
0.3
0.4
0.5
0.6
0.7
0.8
0.9
1
Rotor iron inner arc / pitch ratio
4-rotor pole
5-rotor pole
7-rotor pole
8-rotor pole

(d)

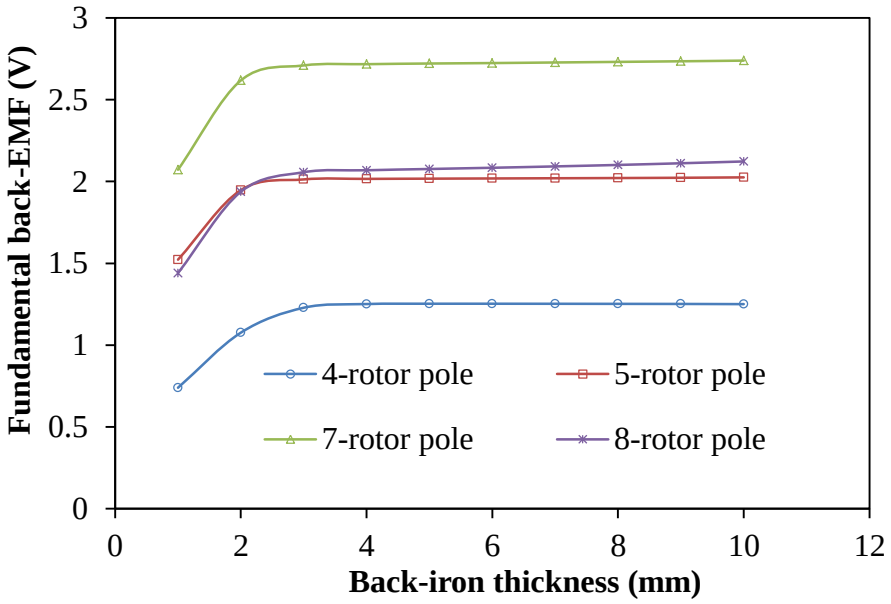

(e)

Fig.3.9 Variation of fundamental magnitude of the open-circuit back-EMF with design parameters, 400rpm: (a) split-ratio, (b) rotor radial thickness, (c) rotor iron outer arc/pitch ratio, (d) rotor iron inner arc/pitch ratio and (e) stator back-iron thickness.

3.3 Influence of rotor pole numbers on the electromagnetic performance

The optimum combination of rotor-poles /stator-slots of the developed DS-SFPM machines have a great impact on the overall performance of the machines. Thus, in this section, we have investigated and quantitatively compared the influence of stator and rotor pole combinations stated in (3.1) on the machine's performances.

3.3.1 Open-circuit waveforms and spectra

The open-circuit flux-linkages of the individual coils with their corresponding spectra are displayed in Figs.3.10-3.13. Note that the respective pairs of the phase coils have identical waveforms and same fundamental values. The phase flux-linkage and back-EMF waveforms with their corresponding harmonic spectra of the analysed machines are given in Figs.3.14-3.17. It is worth noting that the largest amplitude of the flux-linkages is obtained in the 11-rotor pole machine. Although the 11-rotor pole machine possesses higher peak-to-peak value of flux-linkage than the 13-rotor pole machine, its back-EMF is lower due to its lower electrical frequency.

It is obvious from Figs.3.14 and 3.15 that the flux-linkage waveforms of the machines having odd-rotor pole number are both symmetrical and almost sinusoidal about the rotor position

unlike the machines with even-rotor pole number whose waveforms are asymmetric and non-sinusoidal. Moreover, the amount of flux that links the stators and the rotor via the airgap in the analysed machines over one electrical period are more in the machines with odd-rotor pole numbers, although PM machines with $N_r=kN_s\pm1$ are generally characterized by an unbalanced magnetic force. The magnitude of flux-linkages in the developed machines are inversely proportional their varying rotor pole numbers and consequently this is manifested in the resultant flux per pole in the various machines. In other words, the higher the rotor pole number, lesser the resultant flux-linkage.

Similarly, it could be observed that the back-EMF waveforms of all the machines having $N_r=kN_s\pm1$ are symmetrical about the rotor position. The back-EMF waveforms of the 4 and 10-rotor pole machines are both asymmetrical and non-sinusoidal, which accounts for the reason why they have a bit of the even order harmonic components in their harmonic spectra.

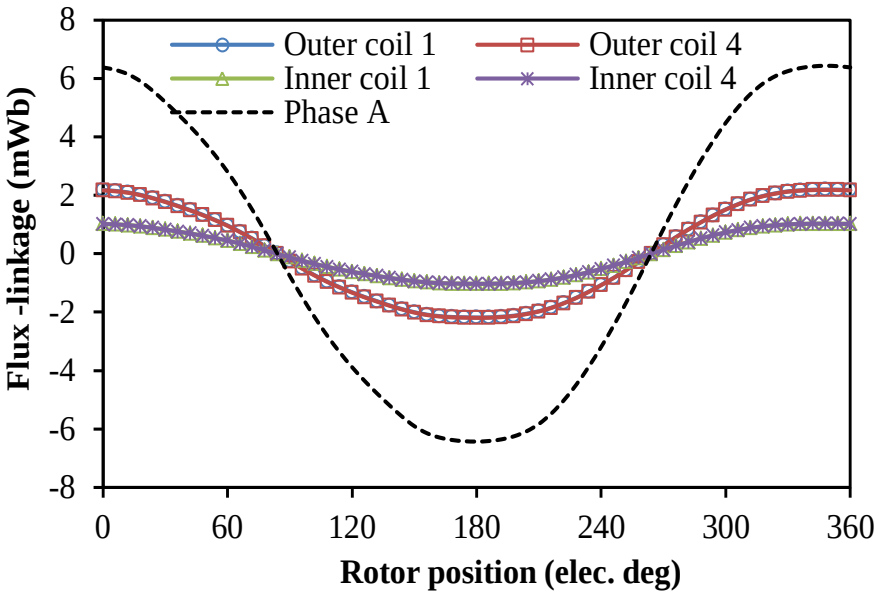

(a) Waveforms

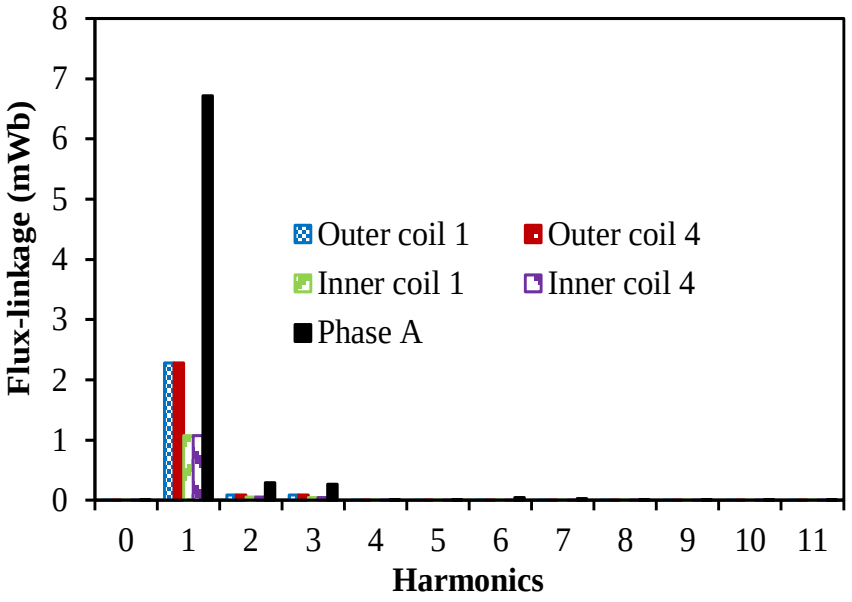

(b) Spectra

Fig.3.10 Coil and phase flux-linkages in 10-rotor pole DS-SFPM machine.

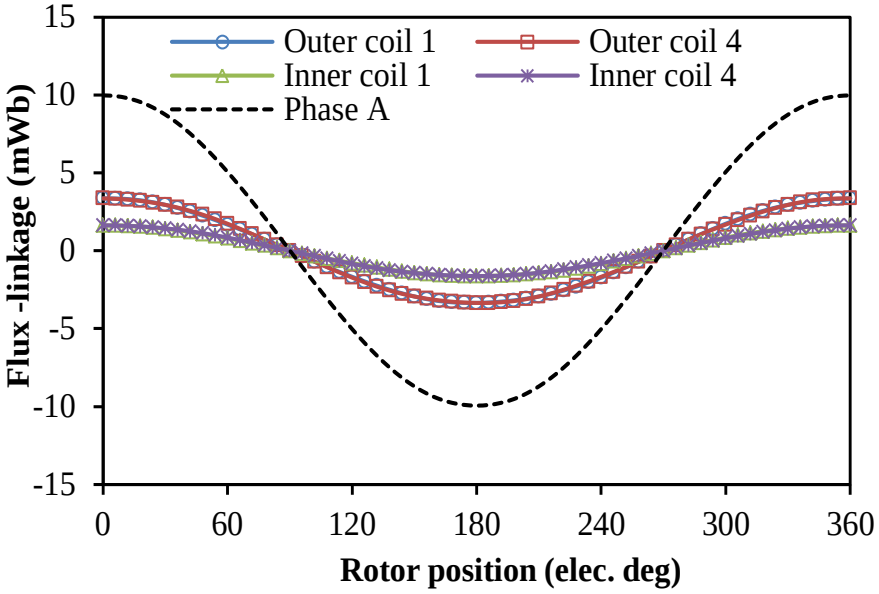

(a) Waveforms

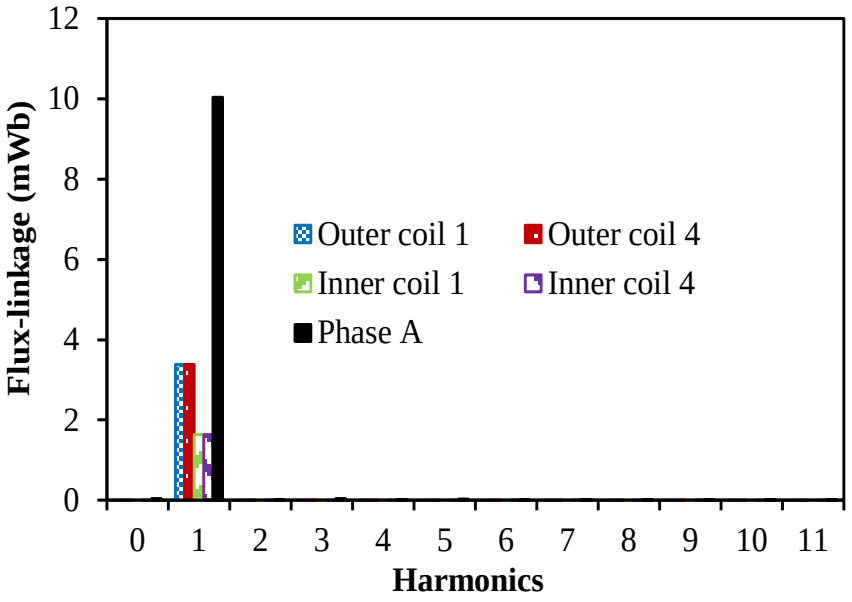

(b) Spectra

Fig.3.11 Coil and phase flux-linkages in 11-rotor pole DS-SFPM machine.

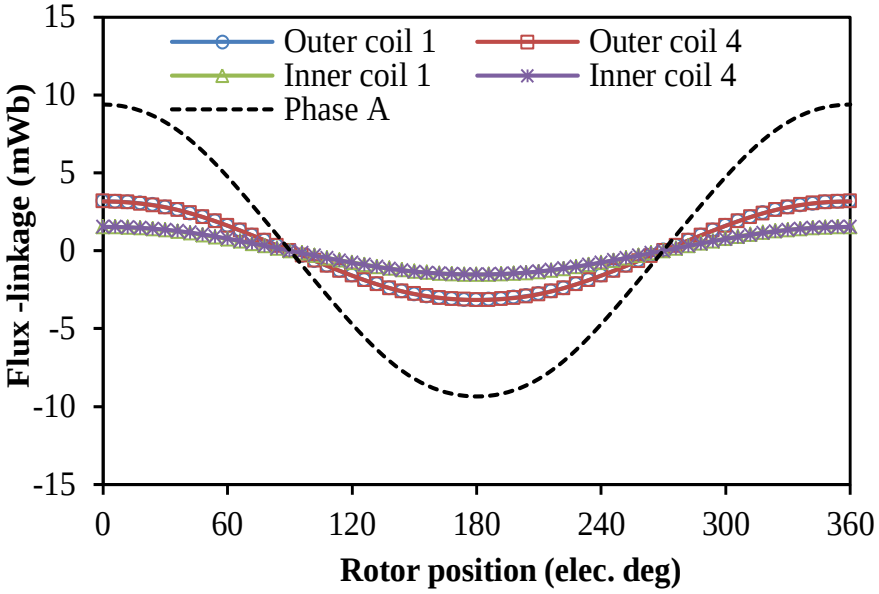

(a) Waveforms

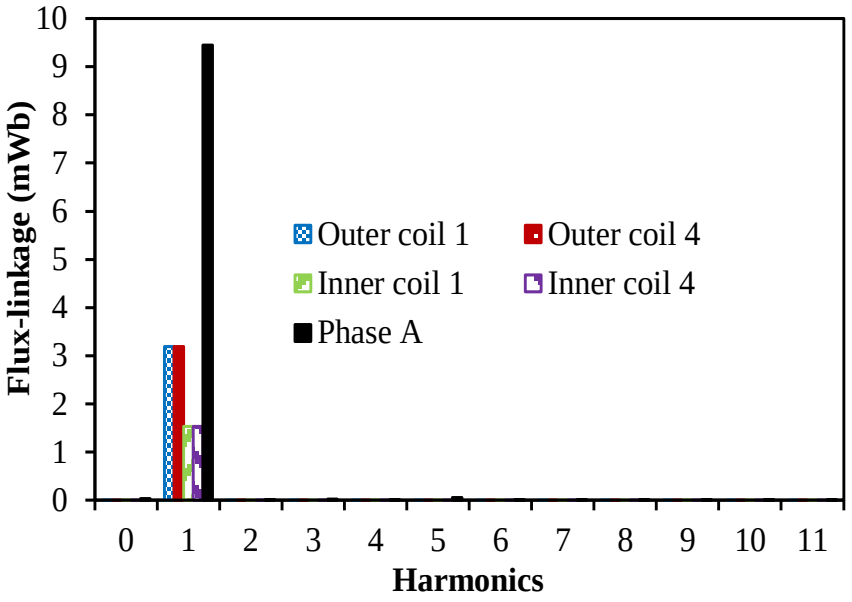

(b) Spectra

Fig.3.12 Coil and phase flux-linkages in 13-rotor pole DS-SFPM machine.

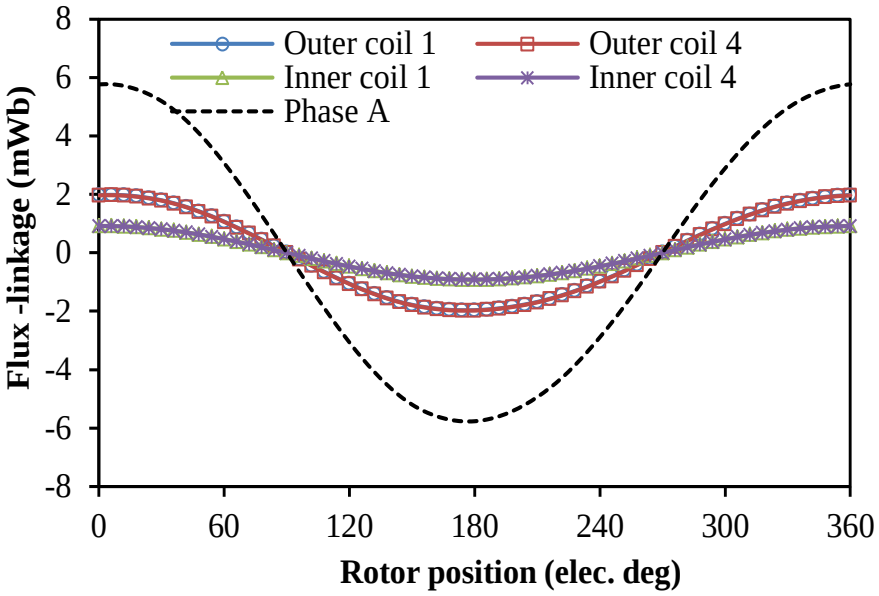

(a) Waveforms

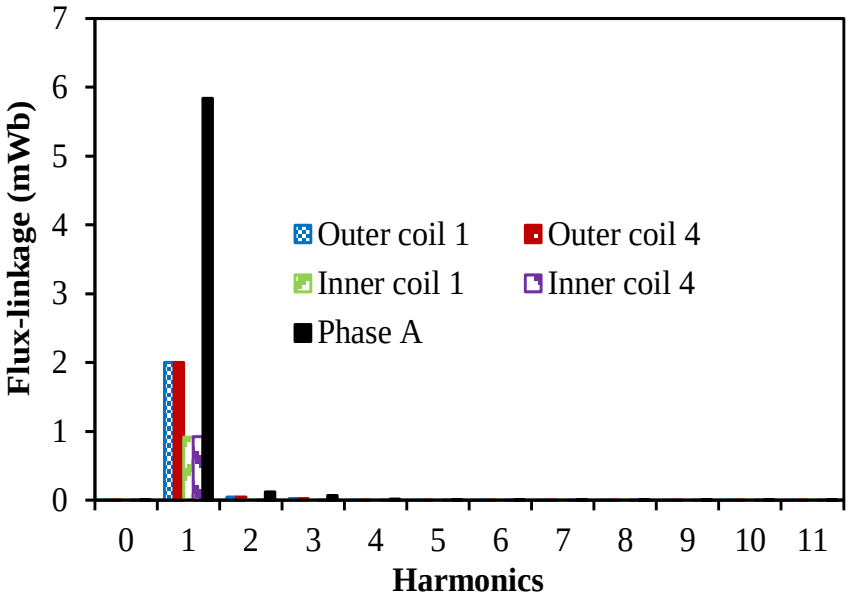

(b) Spectra

Fig.3.13 Coil and phase flux-linkages in 14-rotor pole DS-SFPM machine.

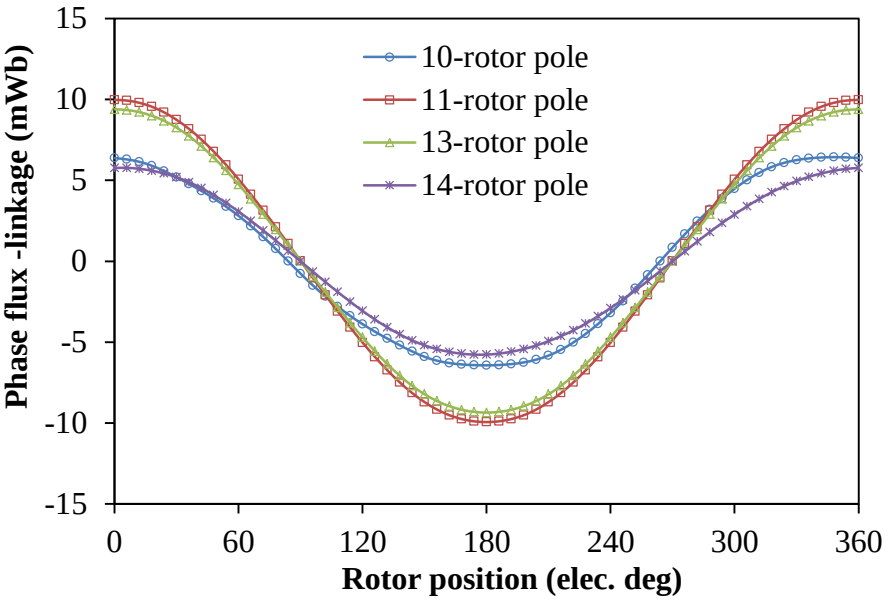

(a) Waveforms

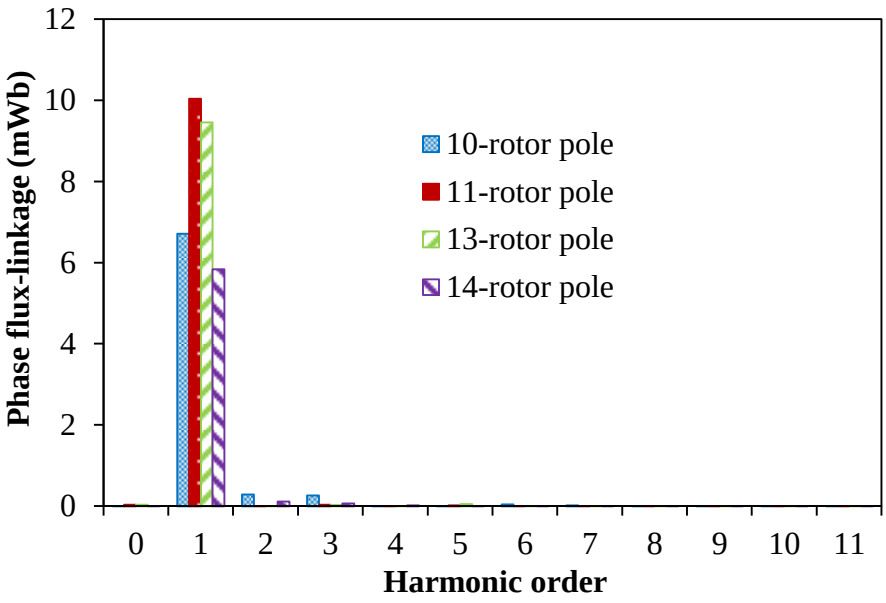

(b) Spectra

Fig.3.14 Comparison open-circuit phase flux-linkage, i_d=0.

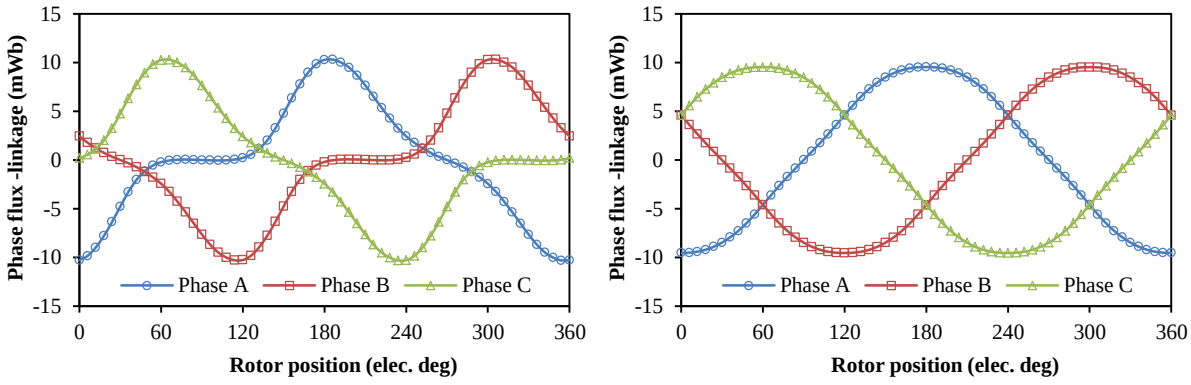

(a) 4-rotor-pole (b) 5-rotor-pole

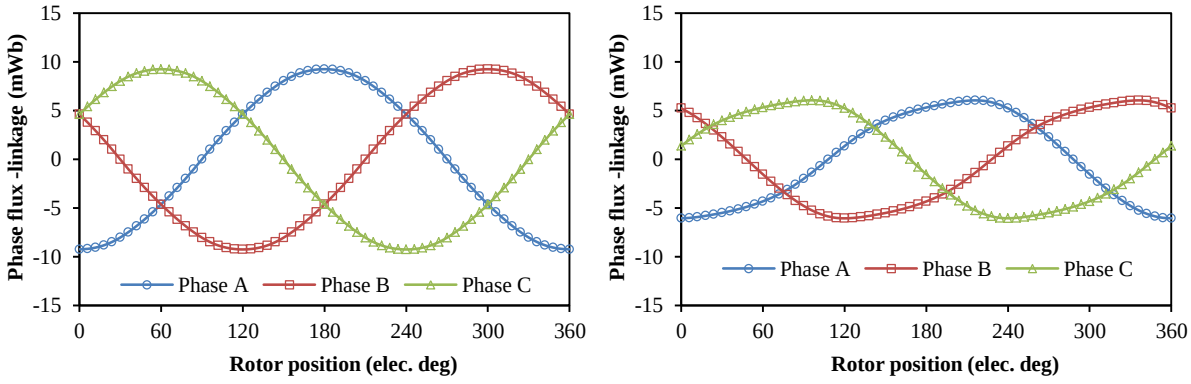

(c) 7-rotor-pole (d) 8-rotor-pole

Fig.3.15 Three phase open-circuit flux-linkage variation with rotor position.

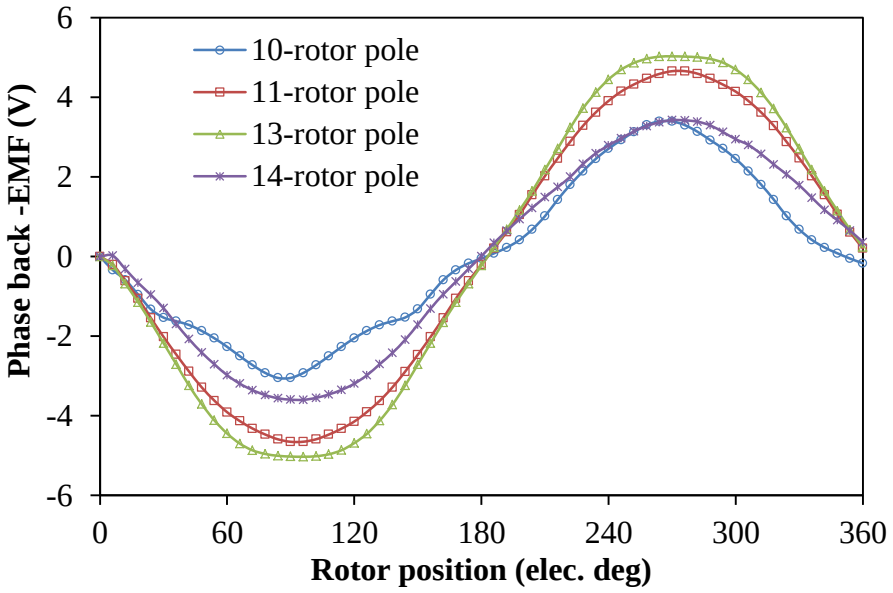

(a) Waveforms

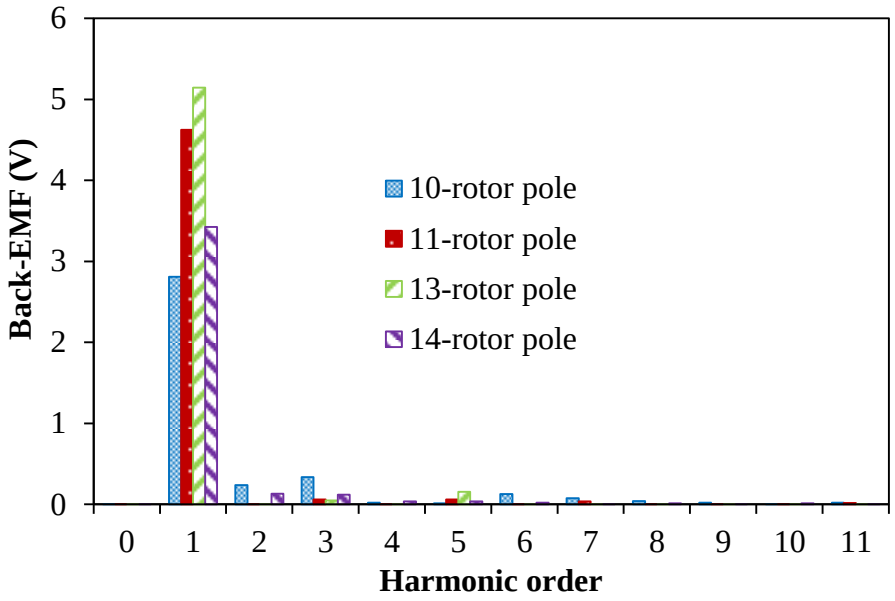

(b) Spectra

Fig.3.16 Comparison of phase back-EMF at 400rpm when i_d=0.

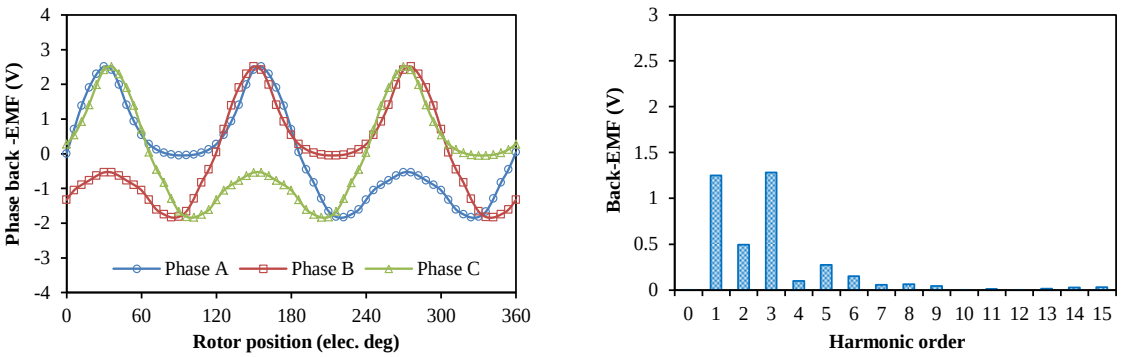

(a) 4-rotor-pole

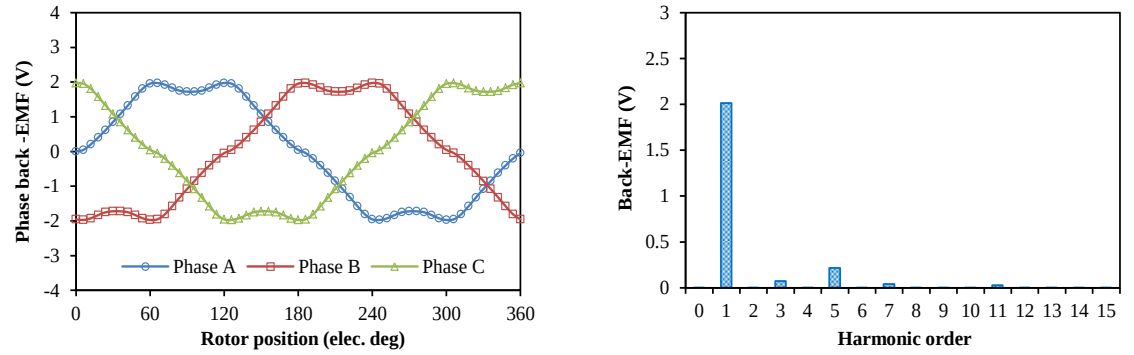

(b) 5-rotor-pole

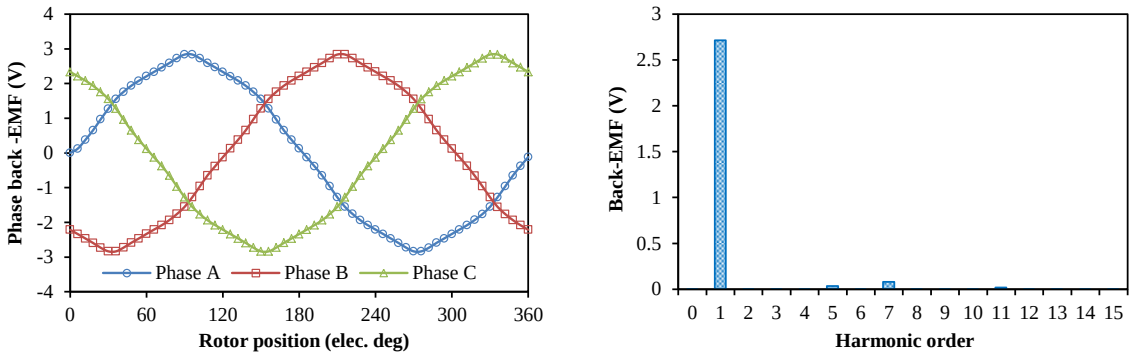

(c) 7-rotor-pole

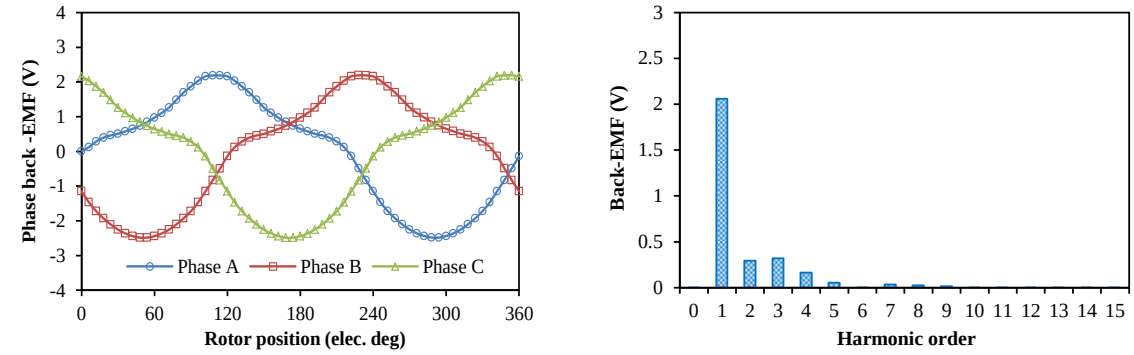

(d) 8-rotor-pole

Fig.3.17 Three-phase open-circuit back-EMF waveforms and spectra, 400rpm.

More importantly, the 13-rotor pole machine exhibits the largest fundamental value of back-EMF and thus the largest torque profile under all conditions. Since the waveforms are not quite sinusoidal, it implies that the analysed machines are not free of ripples, harmonics and voltage distortions. Although the machines with N_r= even number suffer from high torque ripple, the 4-rotor pole machines has the lowest output torque. Moreover, it has a noticeable 6^{th} order harmonic in its torque spectrum which may be attributed to the asymmetric nature of its back-EMF waveform.

The back-EMFs of the developed machines are calculated mathematically as a function of change of its flux linkage according to (3.2), from the Faraday's law of electromagnetic induction.

$$E = -\Delta\psi \Big/ \Delta t = -N\omega \, {}^{d\phi}\!/_{d\theta} \tag{3.2}$$

ψ= flux linkage, ϕ=phase flux, N = Number of turns per phase, θ = rotor position, and ω the angular speed of the machine.

The radial component of the air-gap flux densities of the DS-SFPM machines are shown in Fig.3.18. The torque production of these machines is a function of its modulated flux densities around the air-gap. Hence, it could be seen that the maximum peak-to-peak value of the flux densities occurs in the 13-rotor pole machine which, in turn, is reflected in the magnitude of its output electromagnetic torque.

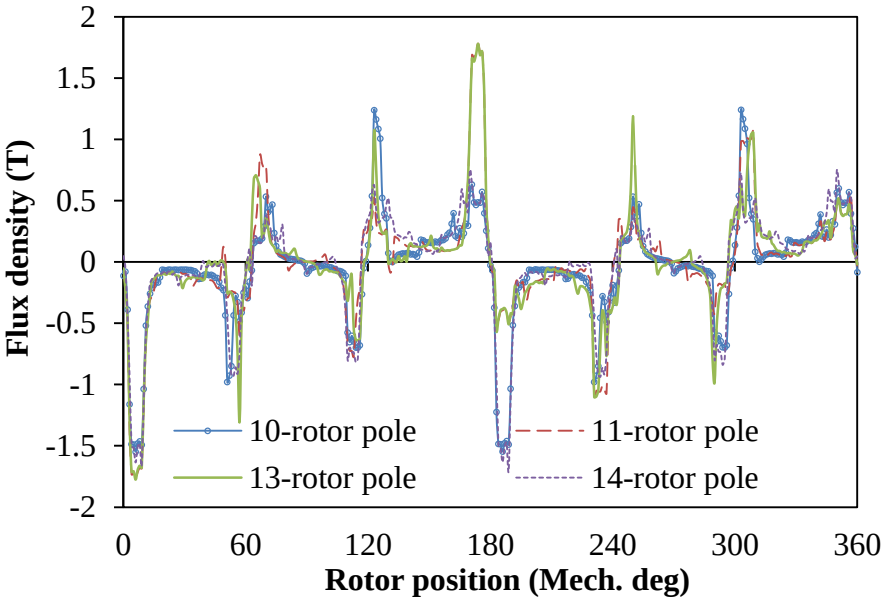

Fig.3.18 Variation of open-circuit air-gap flux density.

3.3.2 Torque ripple and total harmonic distortion

The variations of the torque ripple and total harmonic distortion (THD) of the voltage with the machine design parameters are shown in Figs.3.19 (a)-(e). It is obvious that significant amount of both the torque ripple and the total harmonic distortion is obtained in the even rotor pole machines. This implies that larger noise and vibration would be inherent in these machines. Further, the torque ripples associated with the analysed 4- and 8-rotor pole

machines are considerably high, thus making it inappropriate for critical applications such as aerospace.

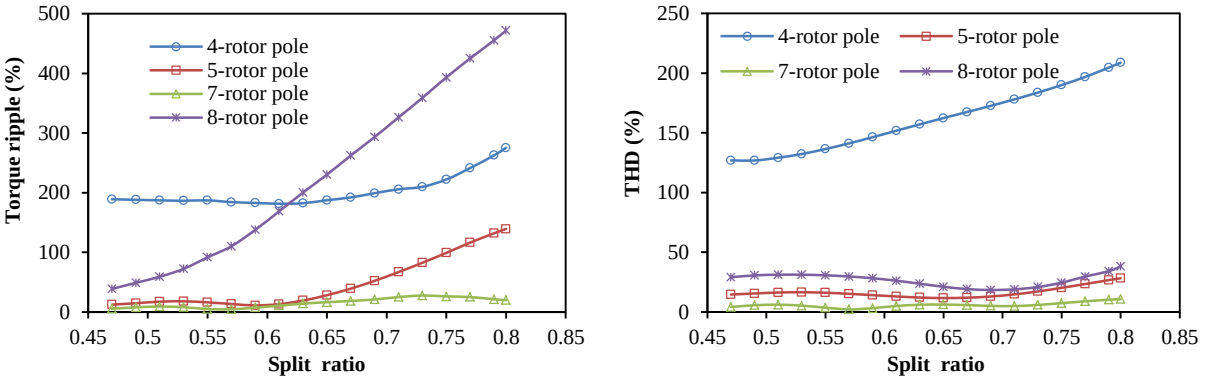

(a) Torque ripple/THD versus split ratio

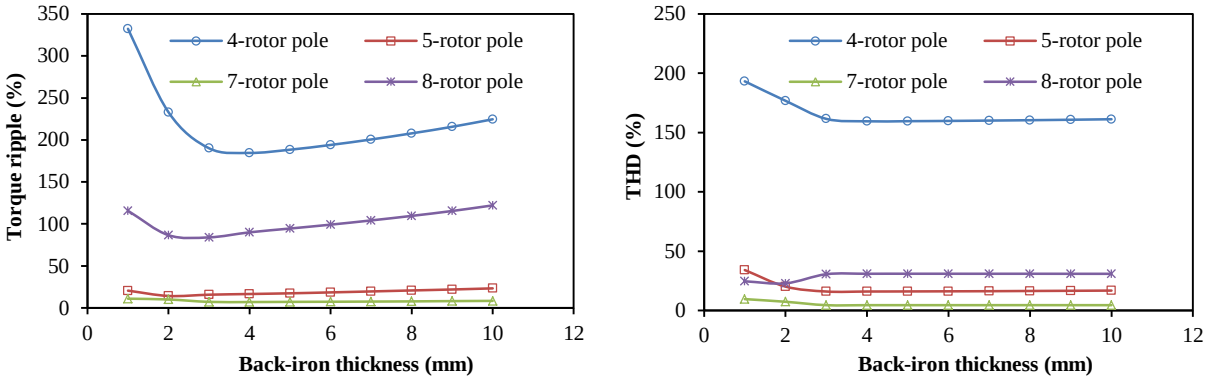

(b) Torque ripple/THD versus back-iron

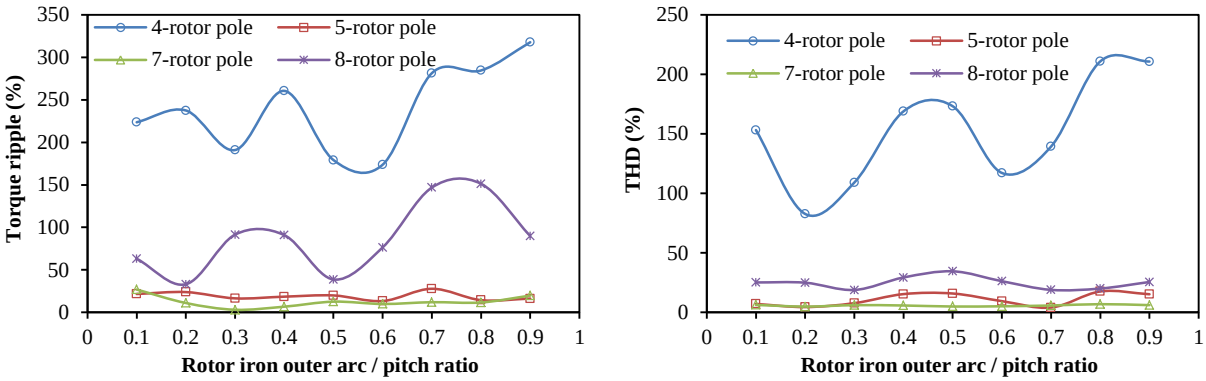

(c) Torque ripple/THD versus rotor iron outer arc

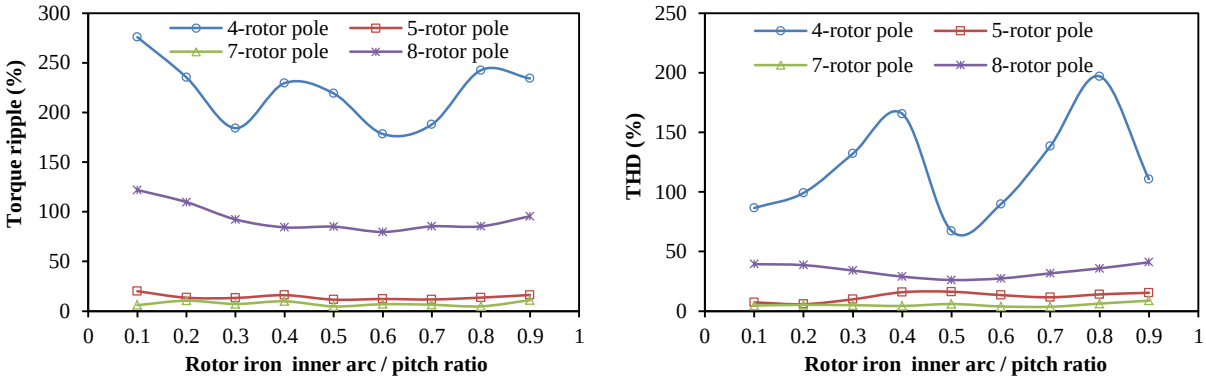

(d) Torque ripple/THD versus rotor iron inner arc

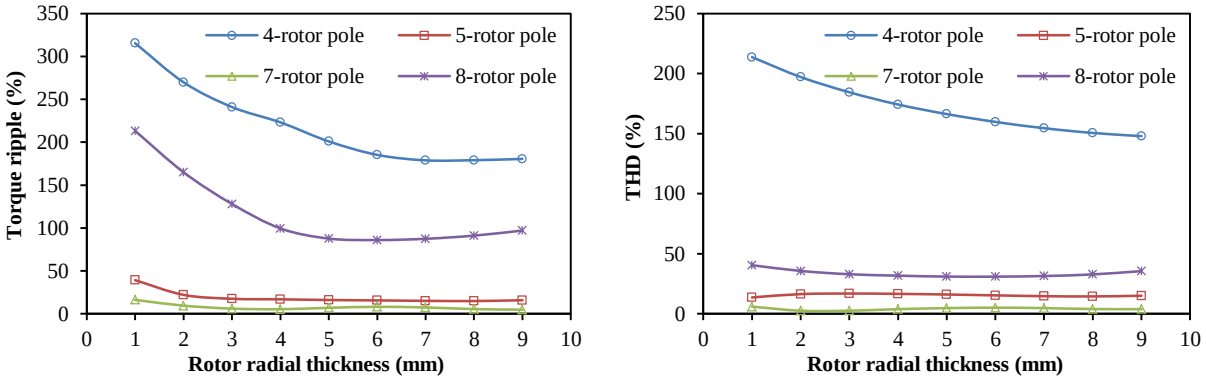

(e) Torque ripple/THD versus rotor radial thickness

Fig.3.19 Comparison of torque ripple and THD with leading design parameters.

3.3.3 Load characteristics

The electromagnetic torque waveforms and spectra of the analysed machines are shown in Figs.3.20 and 3.21. Note that the 13-rotor pole machine has the largest peak to peak and average value of torque. As aforementioned, it is obvious from Fig.3.26 that the developed machines could produce larger torque density than its conventional single-stator counterpart. Similarly, the saturation curves of the DS-SFPM machines are shown in Figs.3.22-3.24. Clearly, the machines with $N_r=2N_s\pm1$ seem to possess higher torque than the rest of other compared machines. The even-rotor pole machines suffer most of this low-torque syndrome. Additionally, the 10-rotor machine has significantly high amount of torque pulsations amongst the analysed machines due to presence of harmonics. It is worth noting that the 4-, 8- and 10-rotor pole machines have dominant 3rd order harmonics as seen in the torque harmonic spectra of Fig.3.21.

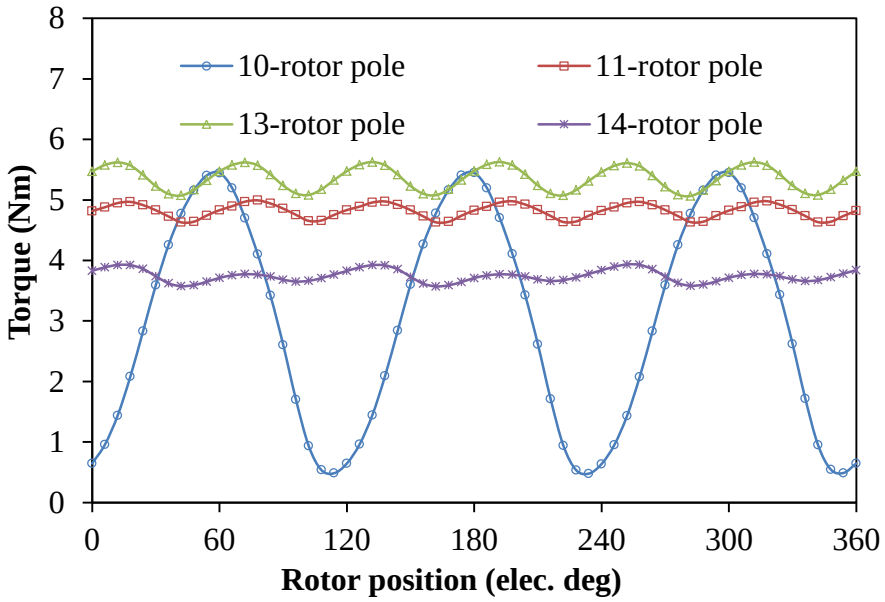

(a) Waveforms

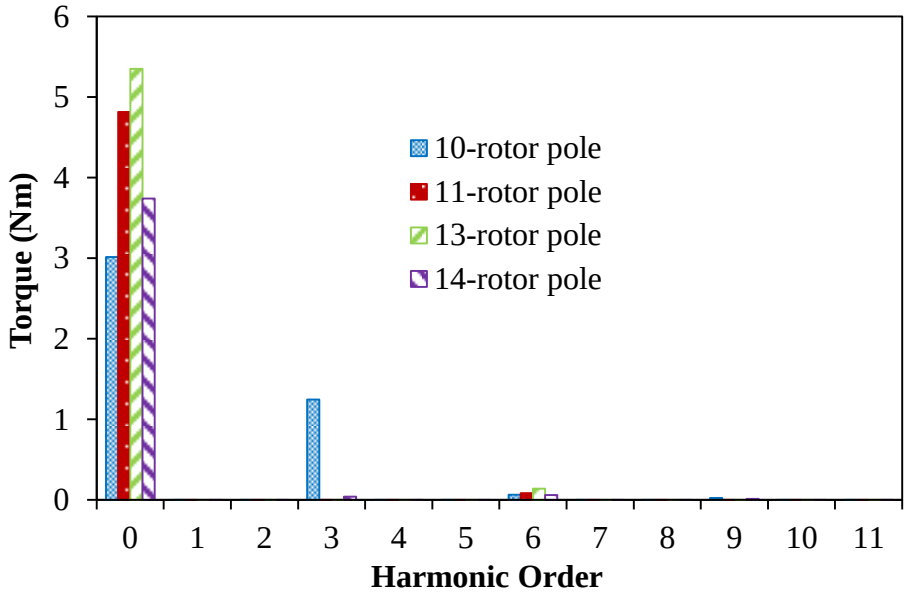

(b) Spectra

Fig.3.20 Variation of torque with rotor position when copper loss = 30W and i_d=0.

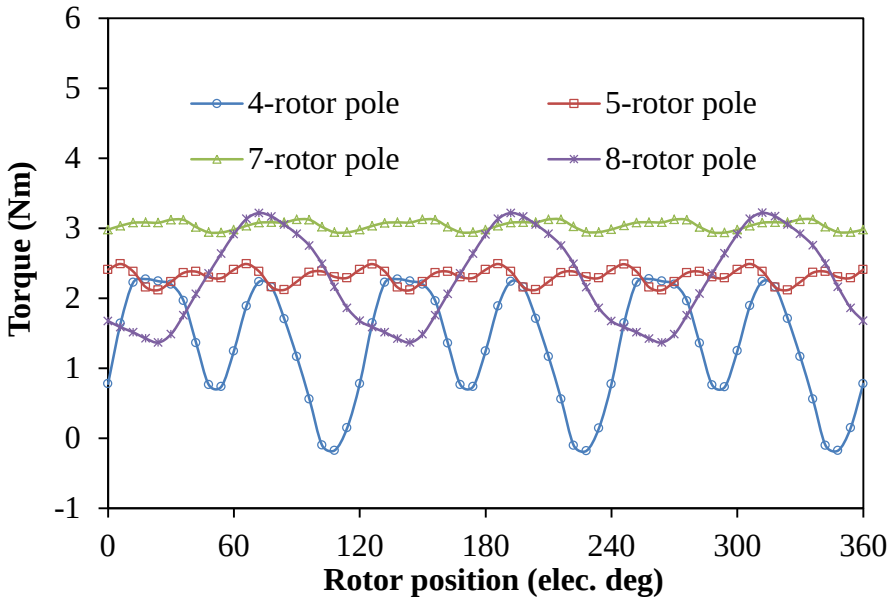

(a) Waveforms

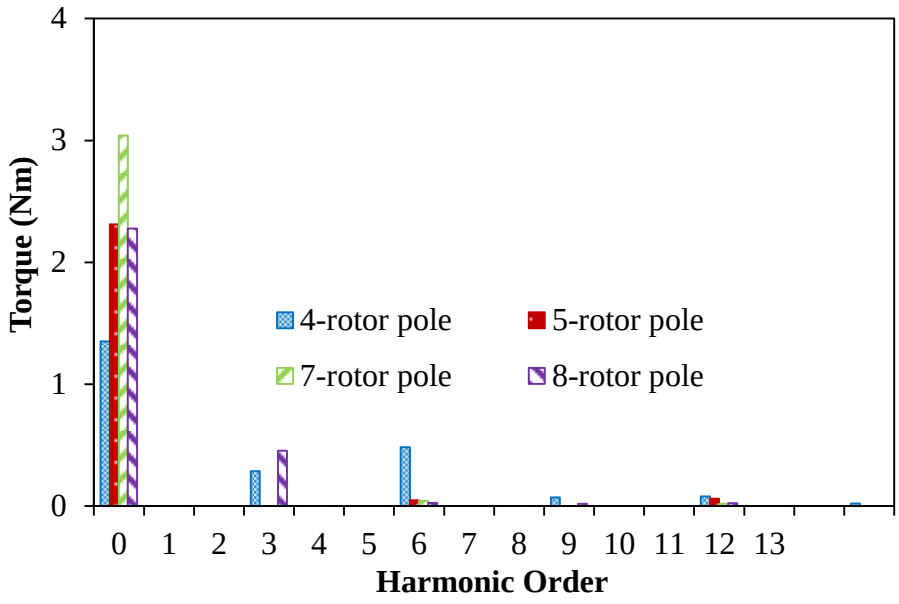

(b) Spectra

Fig.3.21 Variation of torque with rotor position when copper loss = 30W and i_d=0.

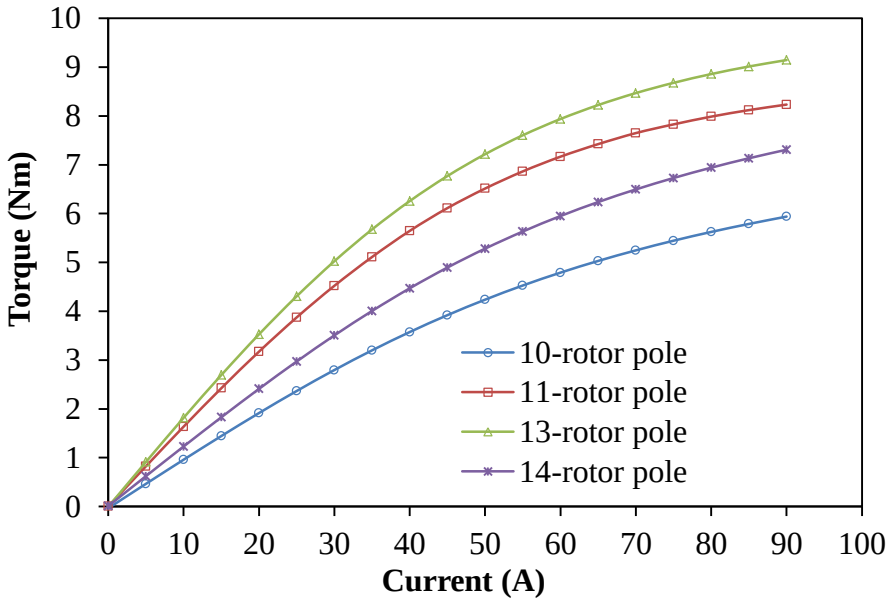

(a)

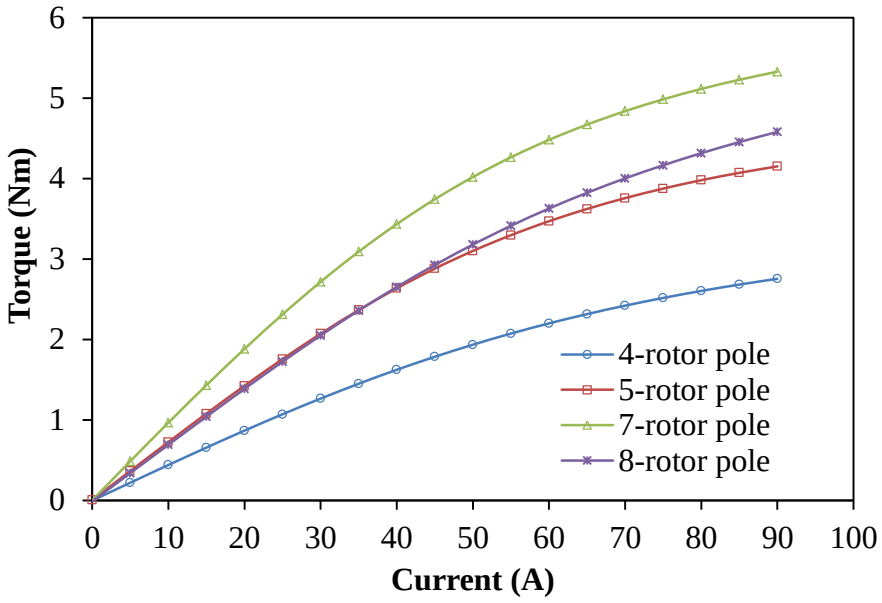

(b)

Fig.3.22 Variation of torque versus current when i_d=0.

The average torque versus current plots of the developed machines is shown in Fig.3.22. It can be seen that the overload/saturation withstand capability of the 13- and 7-rotor pole machines are quite higher compared to the other analysed machines.

The torque variation with current angle under zero *d*-axis control is shown in Fig.3.23. The maximum torque of these machines is produced when the rotor is aligned to the *d*-axis position, as seen from the dotted line of Fig.3.23. Similarly, the torque versus copper loss

curves is displayed in Fig.3.24. It reveals that the machines with $N_r=2N_s\pm1$ has higher overload potential than those of $N_r=2N_s\pm2$. Similarly, machines with $N_r=N_s\pm1$ exhibits larger overload capability than the ones having $N_r=N_s\pm2$. Nevertheless, it could be observed that the rate of change in torque with copper loss would be slower beyond the rated copper loss, due to saturation effect of the electromagnetic circuit.

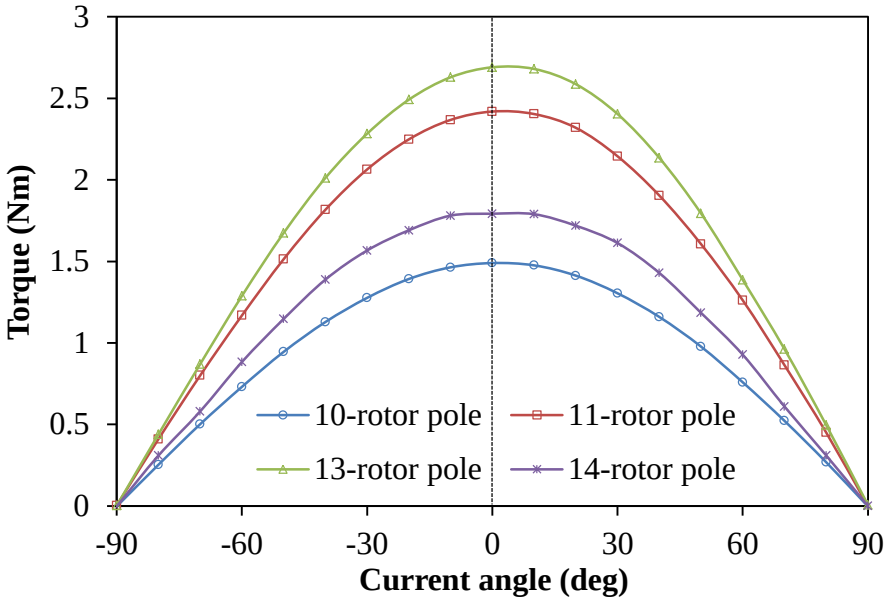

(a) Torque versus current angle

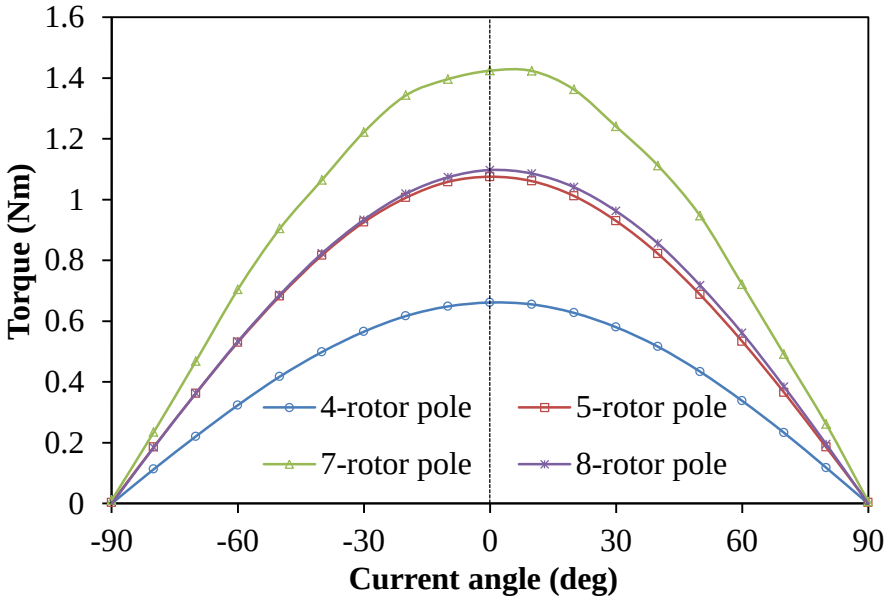

(b) Torque versus current angle

Fig.3.23 Variation of torque versus current angle when i_d=0 and I_{max}=15A.

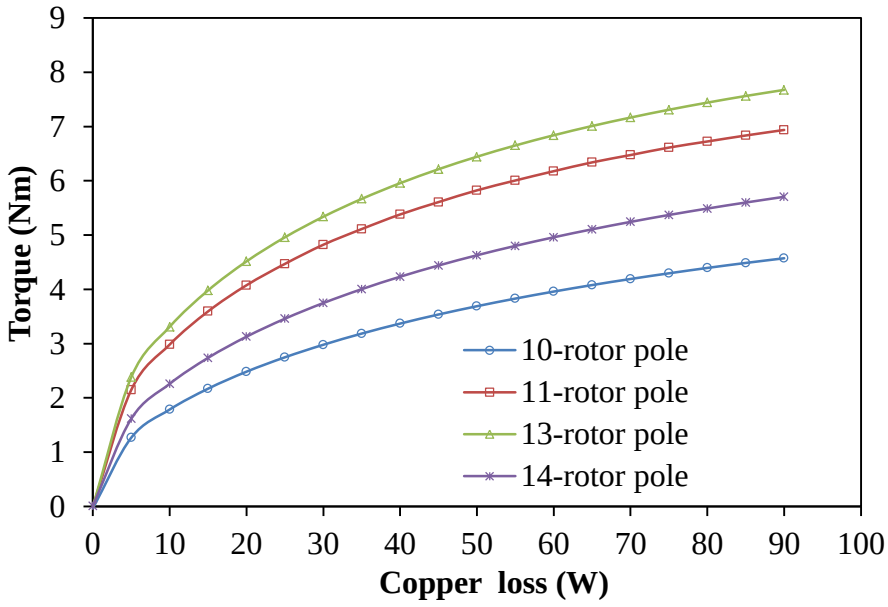

(a)

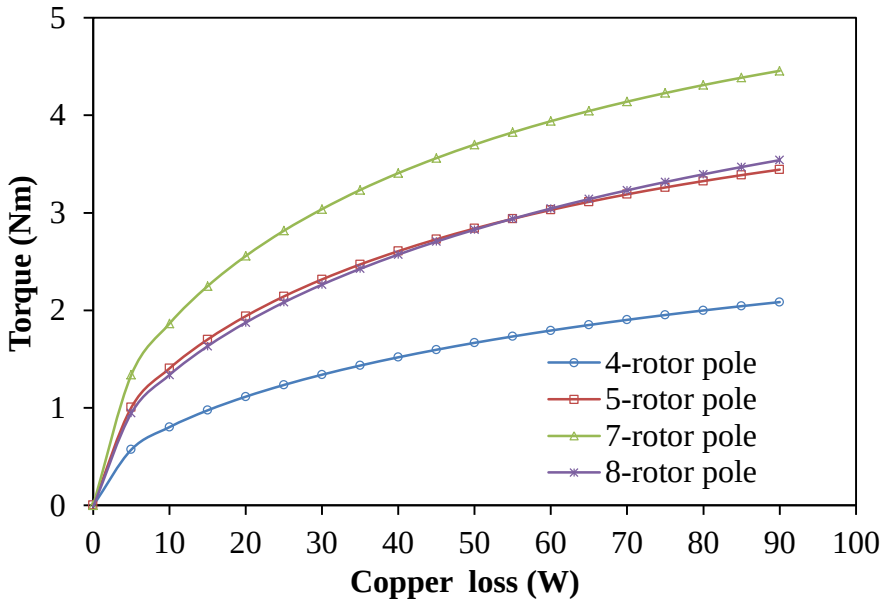

(b)

Fig.3.24 Variation of torque versus copper loss in DS-SFPM machines, i_d=0.

It could be inferred from Figs.3.25 (a) and (b) that the odd-rotor number pole machines seem to be the most promising options in cost-sensitive applications since it utilizes less magnet volume for the same machine size.

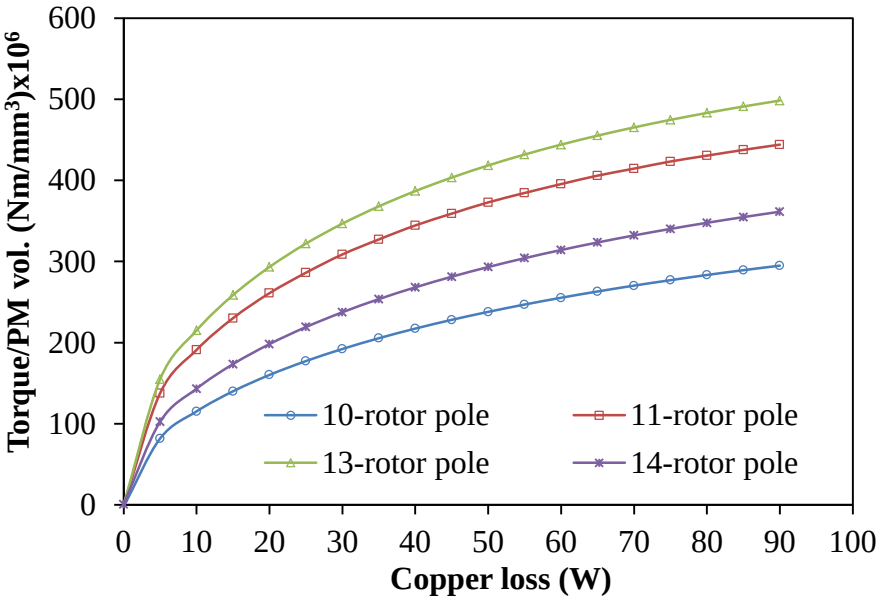

(a)

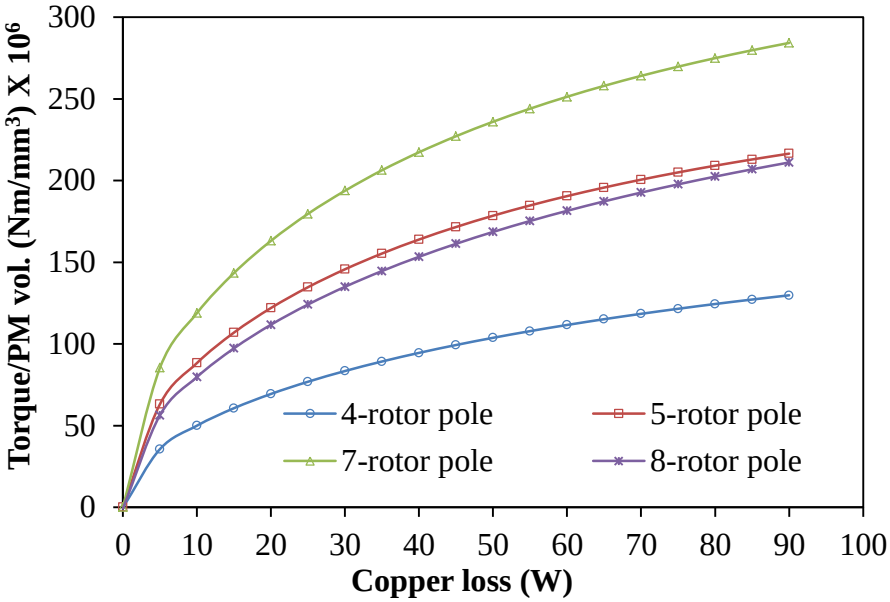

(b)

Fig.3.25 Comparison of torque/PM usage with copper loss.

The electromagnetic performances of the developed DS-SFPM machines with their equivalent single-stator type are compared quantitatively in Fig.3.26. Although the flux-linkage waveform of the DS-SFPM machines is relatively lower than that of the compared SFPM machines, it produces the largest torque density. This is because the electric loading, which has significant impact on the output torque of the machines, varies directly with its slot area under a fixed condition of copper loss and packing factor.

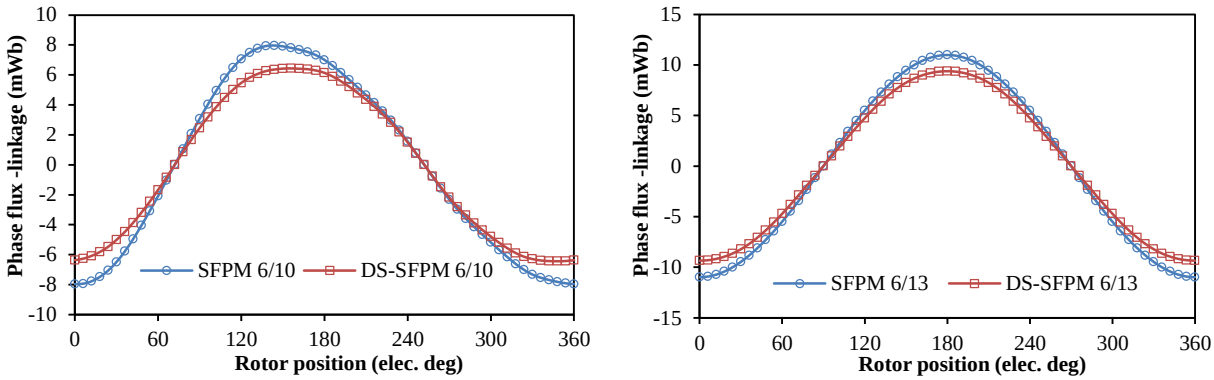

(a) Flux-linkage versus rotor position

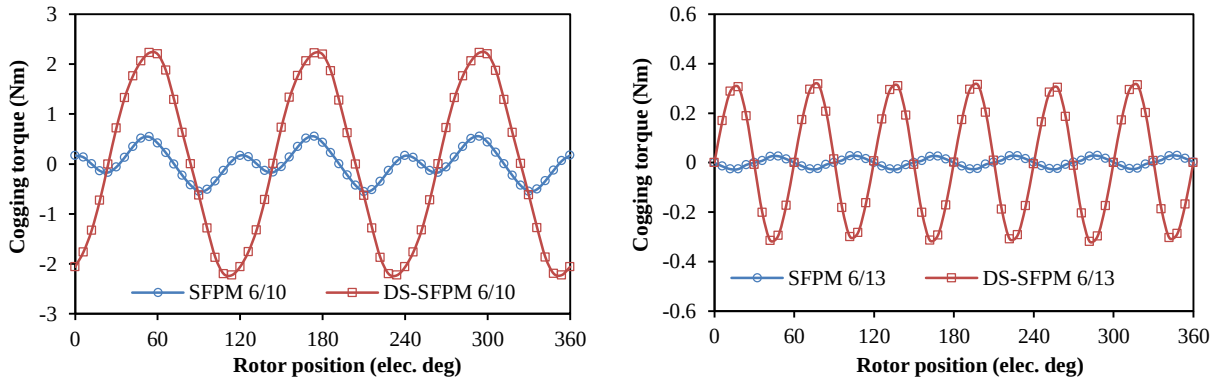

(b) Cogging torque versus rotor position

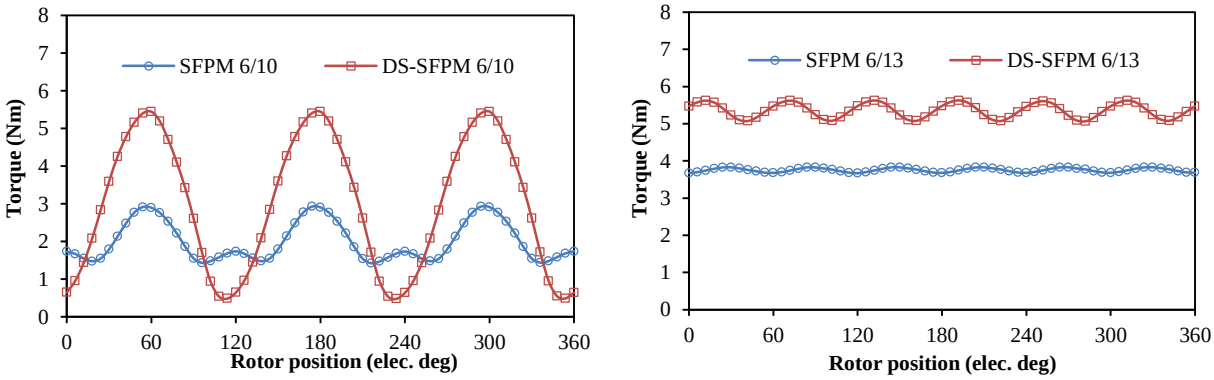

(c) Torque versus rotor position

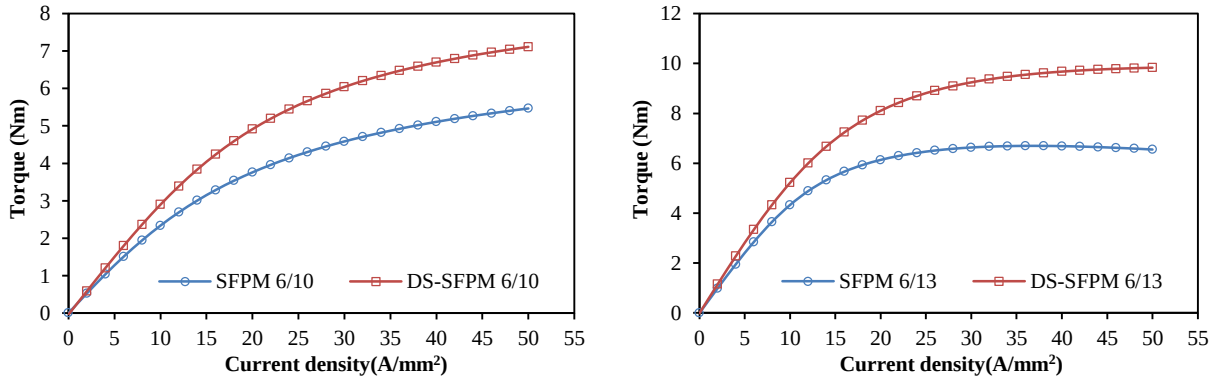

(d) Torque versus current density

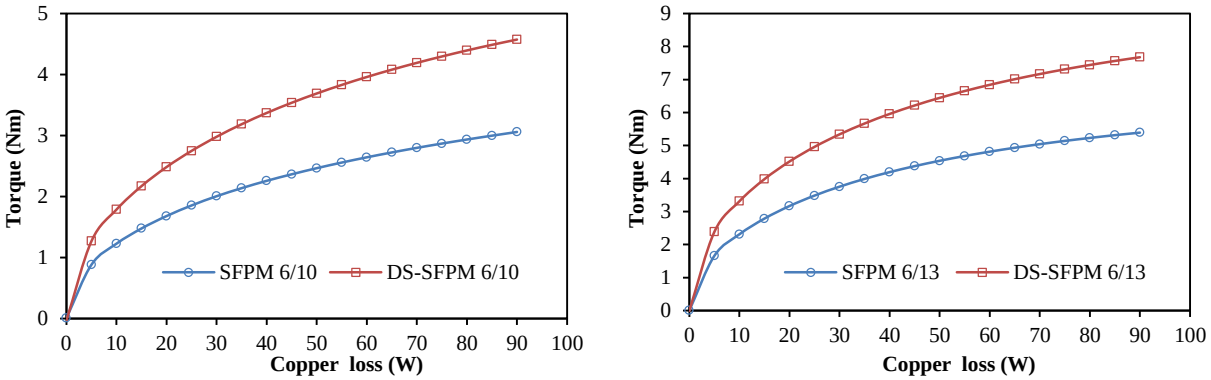

(e) Torque versus copper loss

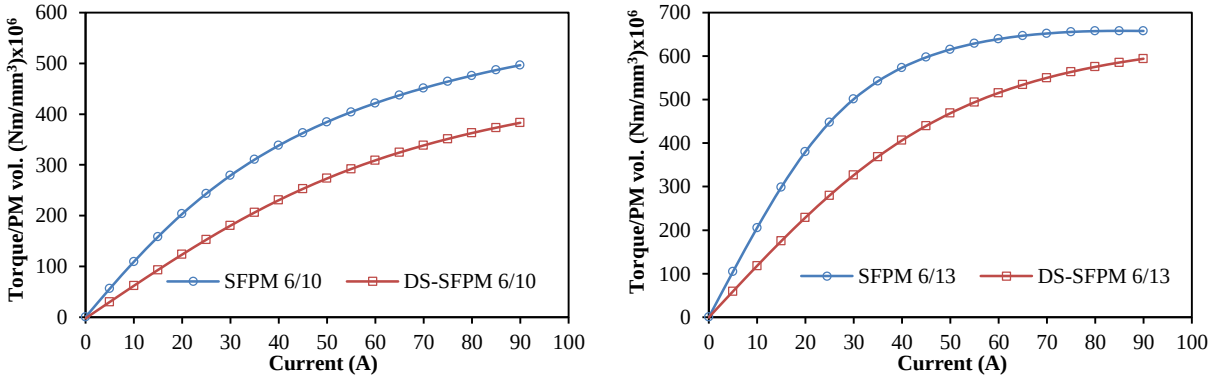

(f) Torque per magnet volume versus current

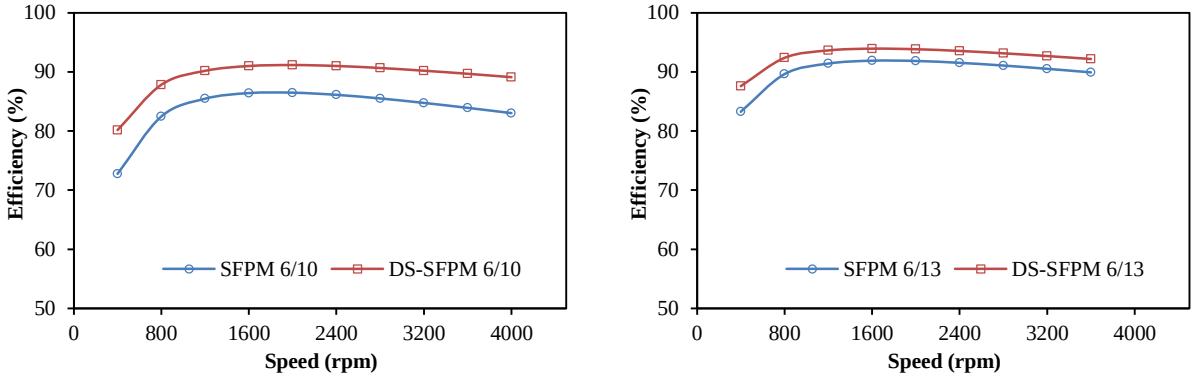

(g) Efficiency

Fig.3.26 Comparison SFPM and DS-SFPM machines, i_d=0.

3.3.4 Field distributions

The magnetic flux lines and the flux densities of the developed DS-SFPM machines at open circuit condition (i_d=0) are displayed in Figs.3.27 and 3.28 below. From flux density contour plots, it could be seen that the teeth of both inner and outer stators as well as the top parts of the modulating pieces are prone to heavier saturation than the other part of the machines; the situation would deteriorate more during load operation. Basically, the identified parts are the magnetic pathways between both stators and the rotor with high amount flux lines.

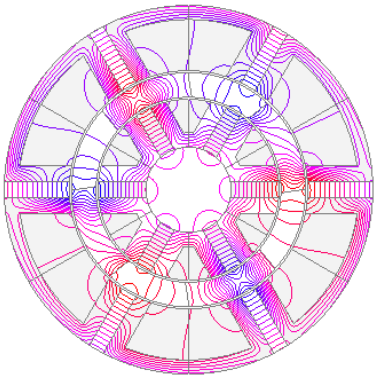

(a) DS-SFPM 6/4

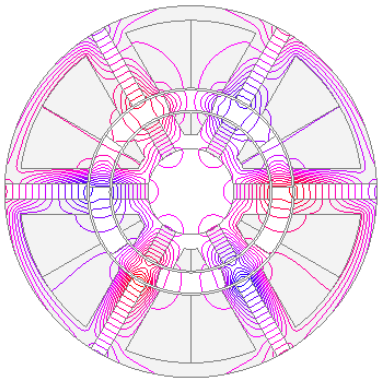

(b) DS-SFPM 6/5

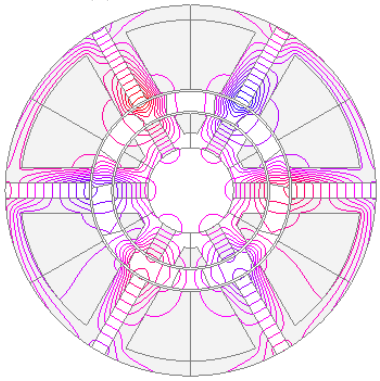

(c) DS-SFPM 6/7

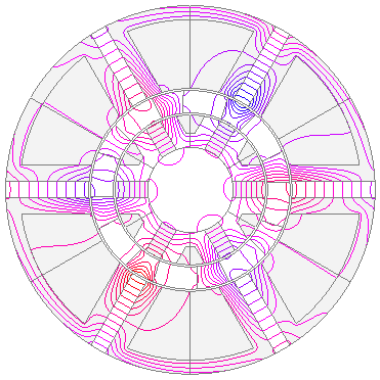

(d) DS-SFPM 6/8

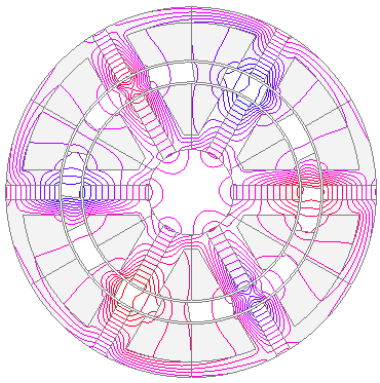

(e) DS-SFPM 6/10

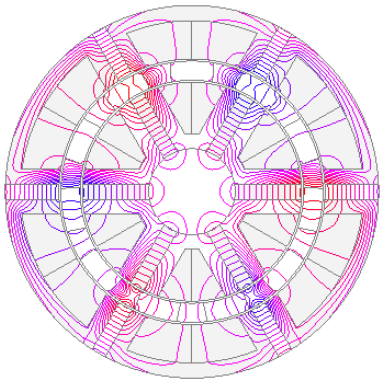

(f) DS-SFPM 6/11

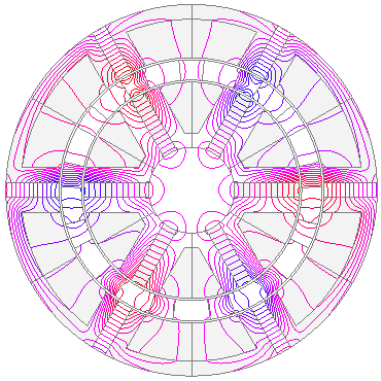

(g) DS-SFPM 6/13

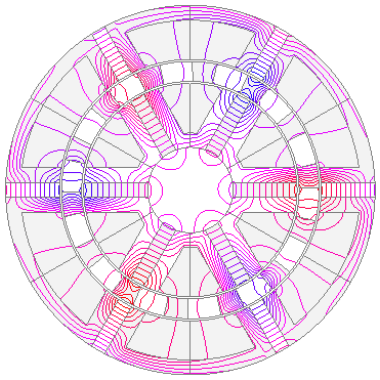

(h) DS-SFPM 6/14

Fig.3.27 Open circuit field distributions of DS-SFPM machines at *d*-axis rotor position.

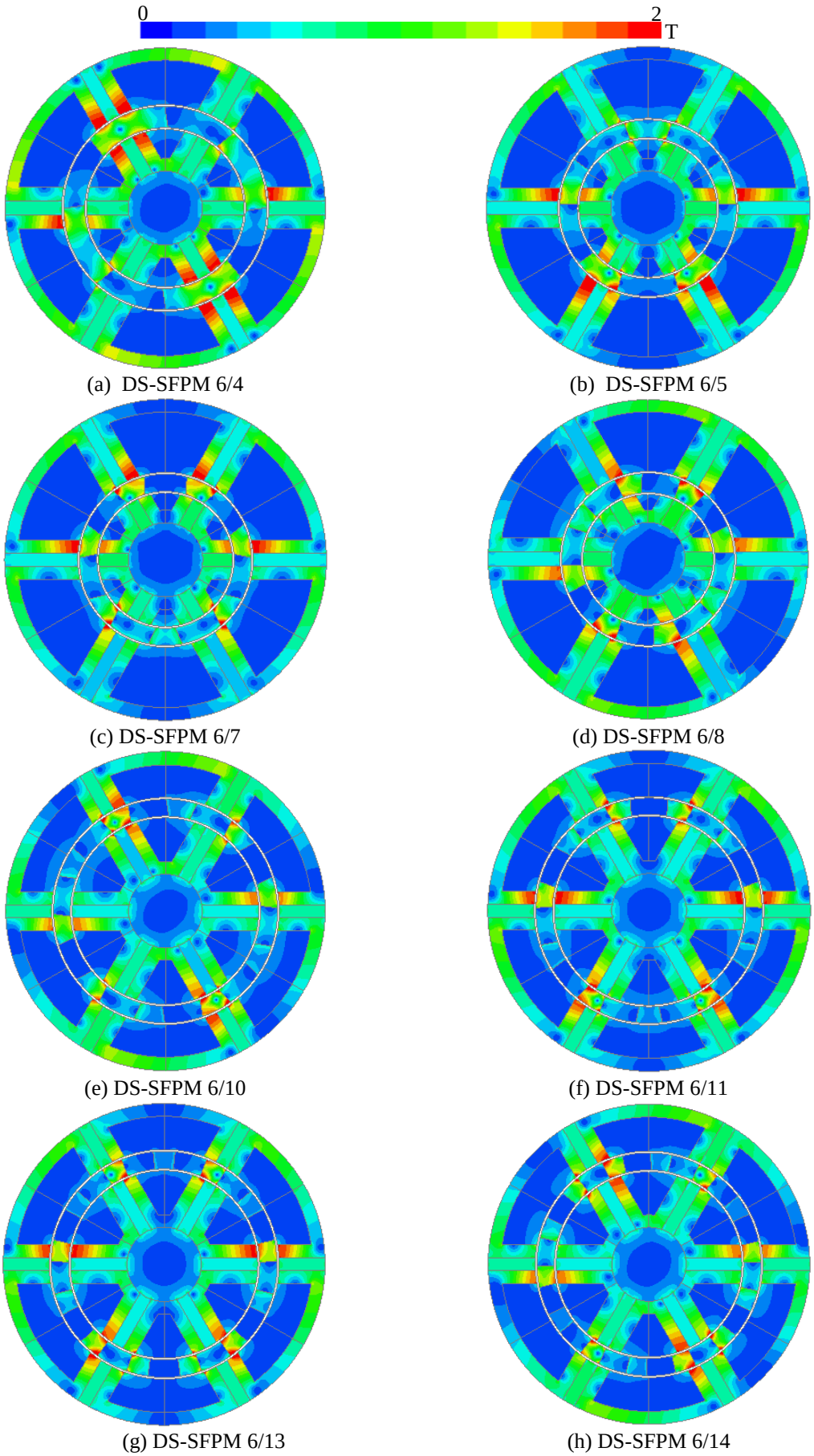

(a) DS-SFPM 6/4 (b) DS-SFPM 6/5

(c) DS-SFPM 6/7 (d) DS-SFPM 6/8

(e) DS-SFPM 6/10 (f) DS-SFPM 6/11

(g) DS-SFPM 6/13 (h) DS-SFPM 6/14

Fig.3.28 Open circuit flux densities of DS-SFPM machines at *d*-axis rotor position.

3.4 Inductance characteristics

The variation of self- and mutual-inductance waveforms with rotor position at i_d=0 control is depicted in Figs.3.29 and 3.30. The self-inductances of these machines are quite similar. It could be observed that the machines with odd-rotor pole numbers have better fault-tolerant capability, since they possess lower mutual inductance values than the even-number rotor pole machines. This simply implies that there would be very low magnetic coupling between the phases of the machines. The inductances are mathematically expressed by equations (3.3) and (3.4).

$$L_{aa} = (\psi_{aa} - \psi_{PM})/I \tag{3.3}$$

$$M_{ab} = (\psi_{ab} - \psi_{PM})/I \tag{3.4}$$

where ψ_{aa} = the total excited flux-linkage in windings of phase A due the PMs and phase A current, ψ_{ab} = the total excited flux-linkage in windings of phase A due to the PMs and phase B current, ψ_{PM} = the open-circuit flux-linkage of phase A due to the magnets only, I = the applied current, L_{aa} and M_{ab} are the self- and mutual-inductances respectively.

3.4.1 Self-inductance

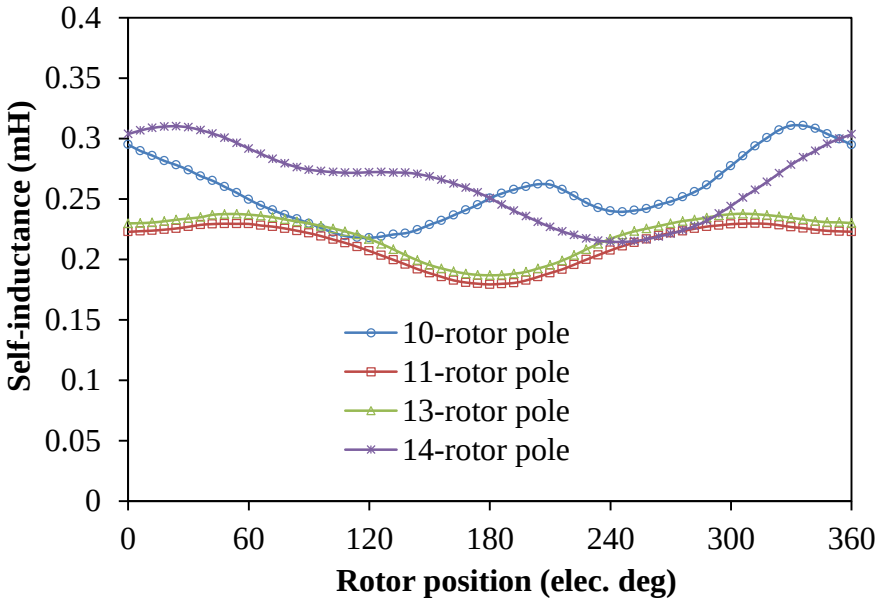

(a)

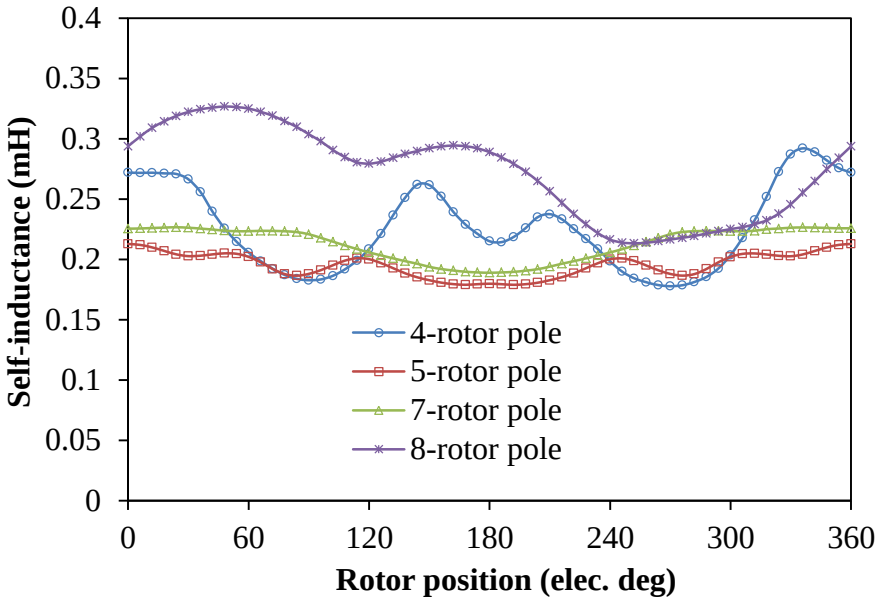

(b)

Fig.3.29 Variation of self-inductance with rotor position, *I*=15A.

3.4.2 Mutual-inductance

The mutual-inductance plots of the developed machines are shown in Fig.3.30. Obviously, the machines with odd rotor pole numbers exhibit the least amount of mutual inductance which implies that there would be less magnetic coupling in the phases of these machines which is a desirable quality for fault-tolerant operation.

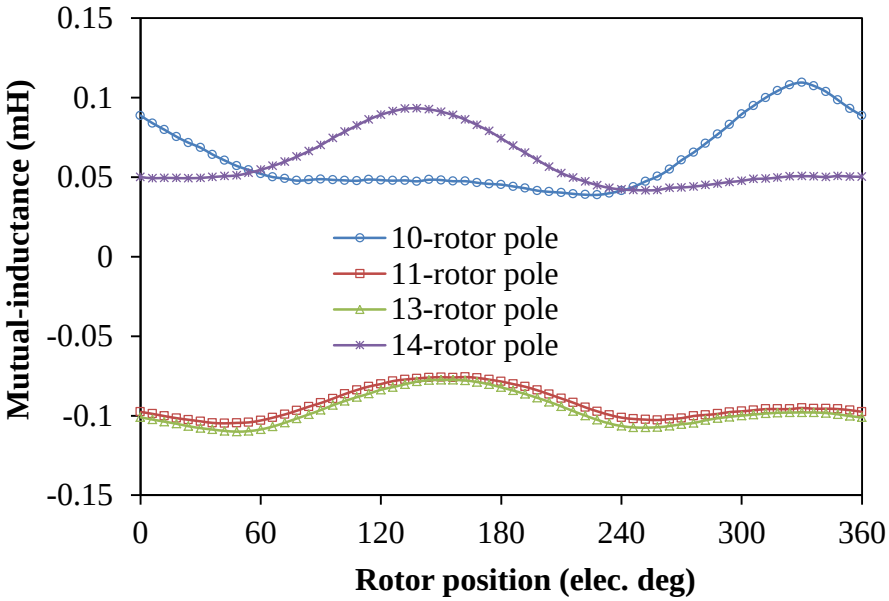

(a)

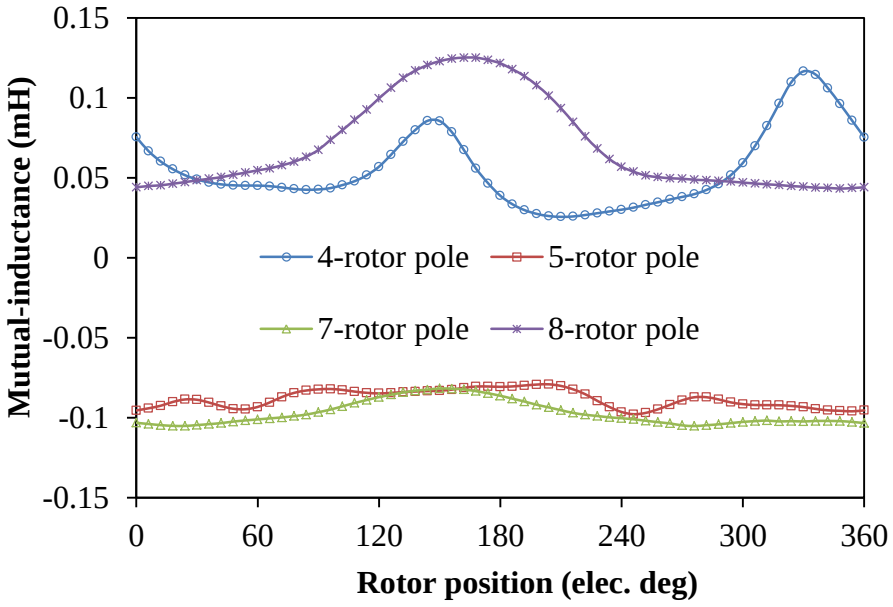

(b)

Fig.3.30 Variation of mutual-inductance with rotor position, *I*=15A.

3.5 Torque/power-speed characteristics

The torque- and power-speed characteristics of the DS-SFPM machines are illustrated in Figs.3.31 and 3.32 respectively. The flux-linkage and cross coupling method in [QI09] is adopted in calculation of torque-speed curves. The calculation was conducted at a maximum current of 15A and *dc* supply voltage of 22.9V. Although the 13-rotor pole machine has low base and maximum speeds, its output power and torque are better compared to the other DS-SFPM machines.

3.5.1 Flux-weakening capabilities

In general, the flux-weakening factor, K_{fw} given by (3.5), is used to estimate the flux-weakening capability of PM machines.

$$K_{fw} = L_d I_m / \psi_{PM} \tag{3.5}$$

where L_d = *d*-axis inductance, I_m = maximum current and ψ_{PM} = PM flux-linkage.

The values of the output torque and power of the machines are given in Table 3.2. Also, it can be seen from Table 3.2 that the machines with N_r=*13* has the highest value of K_{fw}. This implies that the best flux-weakening potential would be obtainable in the 13-rotor poles machine [ZHU15]. This is followed by the 14-rotor pole machine. It is worth mentioning that

the optimum flux weakening capabilities of these machines are also reflected in the ratio of the maximum speed to the base speed of the individual machines. However, it should also be noted that all the machines are optimized for the maximum torque for the fixed copper loss, and consequently, the optimized machine would have the maximum torque in the constant torque region, rather than the optimal constant power (flux weakening) operation region, such as the optimal base speed and maximum speed etc.

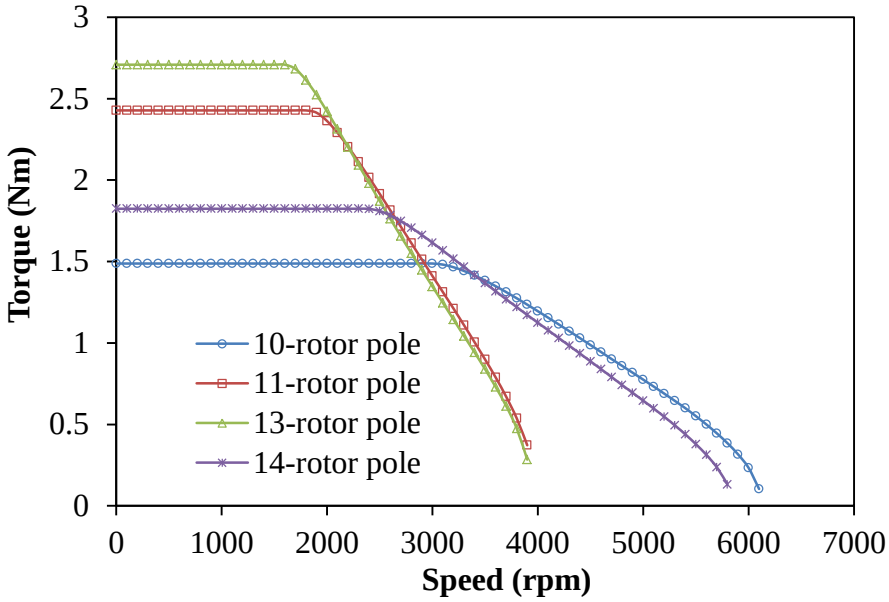

(a)

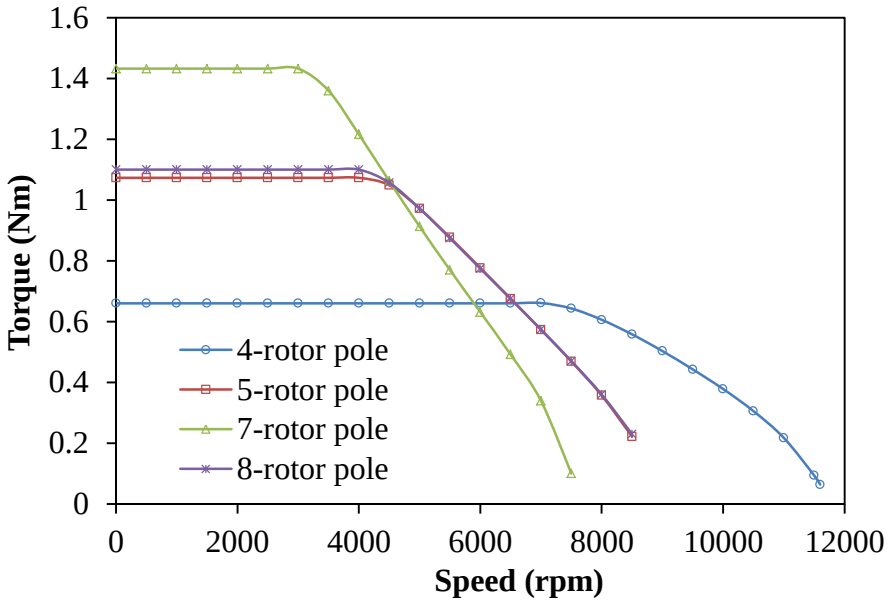

(b)

Fig.3.31 Comparison of torque-speed characteristics, (V_{dc} = 22.9V, I_{max} = 15A).

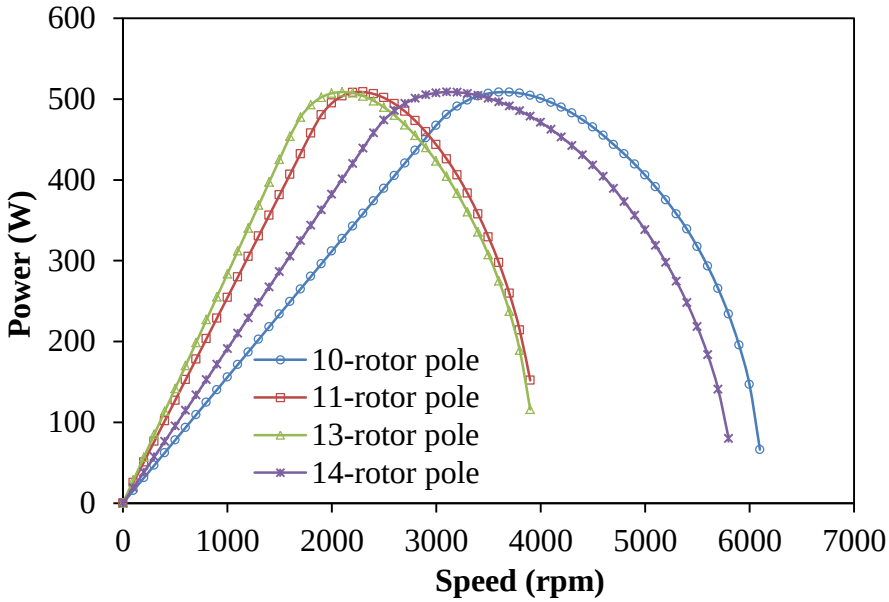

(a)

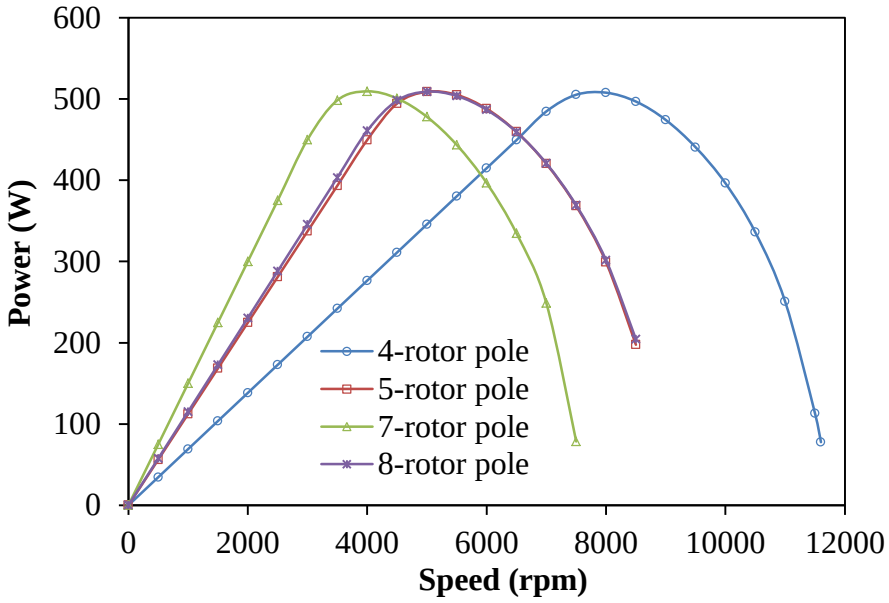

(b)

Fig.3.32 Comparison of power-speed characteristics, (V_{dc} = 22.9V, I_{max} = 15A).

Note that the largest values of *d*- and *q*-axis inductances are obtained in the 13-rotor pole machines. The saliency ratio of IPM machines is given as the ratio of the *q*-axis to *d*-axis inductance in [ZHA13]. However, as can be seen from Table 3.2 that all machines have saliency ratios very close to unity so that the reluctance torque is negligible.

TABLE 3.2 FLUX WEAKENING CAPABILITY, INDUCTANCES AND SALIENCY RATIOS

Item	Value							
Rotor pole number, N_r	**4**	**5**	**7**	**8**	**10**	**11**	**13**	**14**
D-axis inductance, L_d (mH)	0.181	0.317	0.341	0.204	0.2107	0.338	0.3482	0.2113
Q-axis inductance, L_q (mH)	0.241	0.303	0.340	0.210	0.2265	0.335	0.3552	0.2063
Saliency ratio, L_q/L_d	1.33	0.96	0.997	1.03	1.07	0.99	1.02	0.98
PM flux (mWb)	7.41	9.63	9.27	6.15	6.73	10.04	9.4	5.8
K_{fw}	0.37	0.49	0.55	0.49	0.47	0.50	0.55	0.54
Base speed (rpm)	6800	4100	3000	3900	2900	1700	1500	2300
Maximum speed (rpm)	11600	8800	7500	8900	6100	3900	3900	5800
Max. speed/base speed	1.71	2.15	2.50	2.28	2.10	2.29	2.6	2.52
Maximum torque (Nm)	0.66	1.07	1.43	1.10	1.49	2.43	2.72	1.82
Maximum power (W)	507.80	508.97	509.42	509.03	508.54	508.68	508.73	508.69
Self-inductance, L_{aa} (mH)	0.226	0.195	0.213	0.273	0.257	0.213	0.220	0.263
Mutual-inductance, M_{ab} (mH)	0.06	-0.09	-0.097	0.07	0.0618	-0.093	-0.097	0.0595
M_{ab}/L_{aa}	0.2655	-0.462	-0.455	0.256	0.241	-0.437	-0.441	0.226
Torque density (k.Nm/m^3)	8.49	14.54	19.12	14.31	18.96	30.28	33.67	23.53
Power factor	0.75	0.5	0.9	0.9	0.9	0.9	0.9	0.9
Efficiency (%)	88.49	93.58	93.48	90.25	91.17	94.09	93.94	90.99

3.6 Losses and efficiency

Since the output of the electrical machines is dependent on its losses. Moreover, accurate prediction of losses in electrical machines could help to give insight about its thermal/heat dissipation design limits. Hence, we have devoted this section to the investigation of permanent magnet edddy current losses and core loss analysis under load and no-load conditions at various speed and rotor positions. It is worth noting that the machines' losses

are dependent on load and their respective electrical frequencies. The variation of both PM eddy current losses and total core losses of the DS-SFPM machines are displayed in Figs.3.33-3.37. The predicted results reveal that the 8-rotor pole machine has the highest value of PM eddy current loss due to its large amount of harmonics as well as relatively high electrical frequency. Moreover, the 4-rotor machine exhibits the largest amount of total core losses amongst its counterparts. This is possibly due to its enormous harmonics.

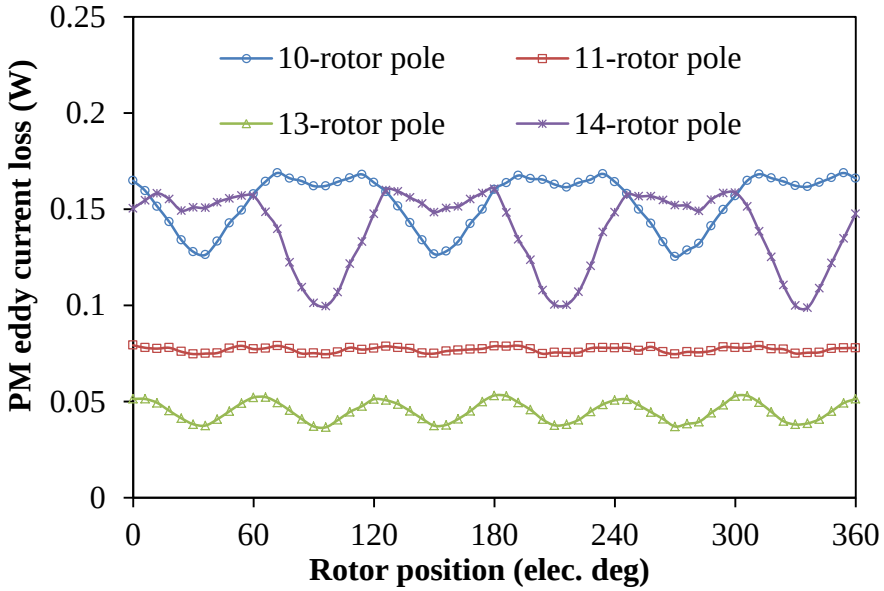

(a) Loss versus rotor position

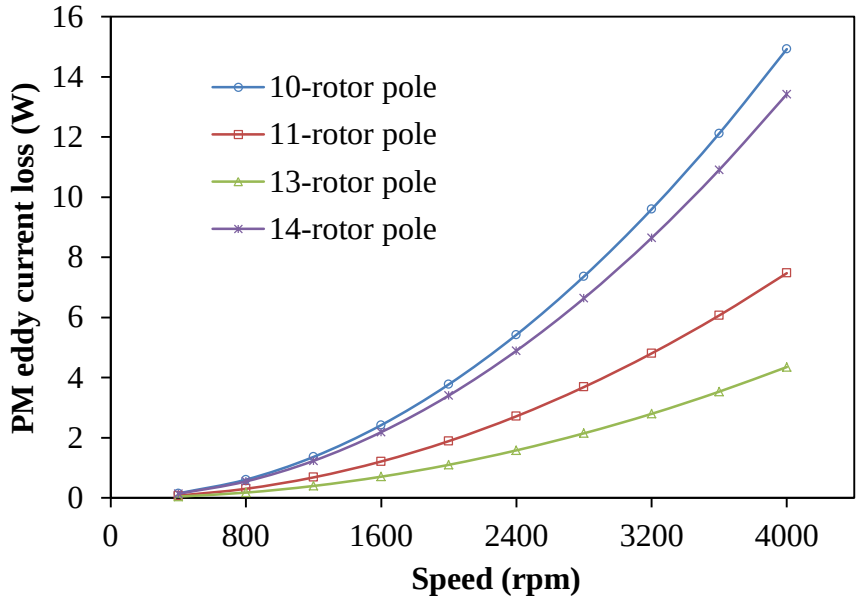

(b) Loss versus speed

Fig.3.33 Variation of PM eddy current losses, 400rpm, no load.

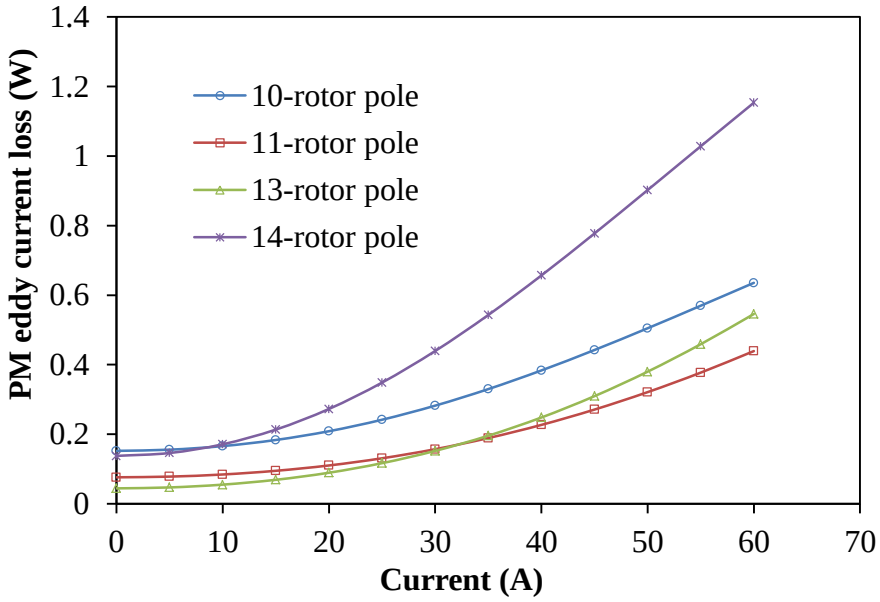

Fig.3.34 Variation of PM eddy current losses with current, 400rpm.

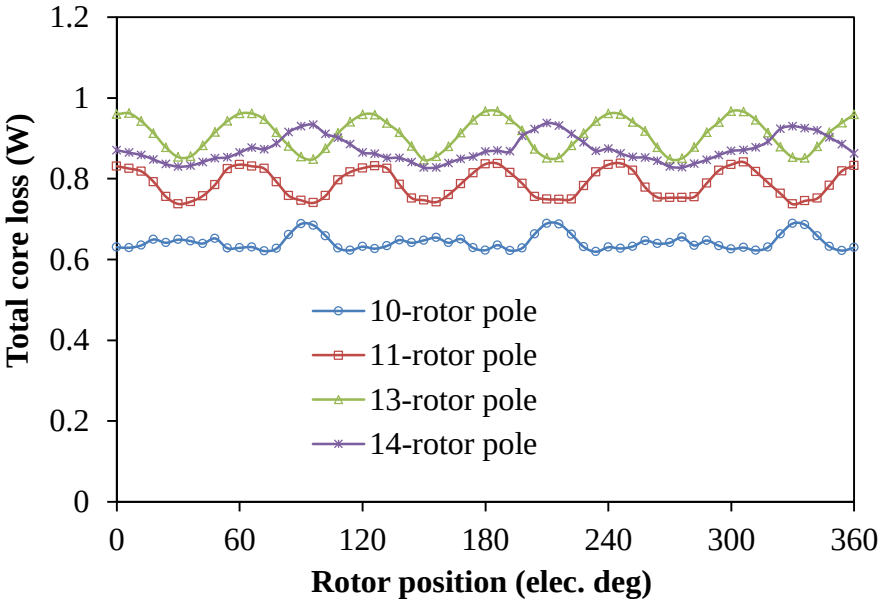

(a) Loss versus rotor position

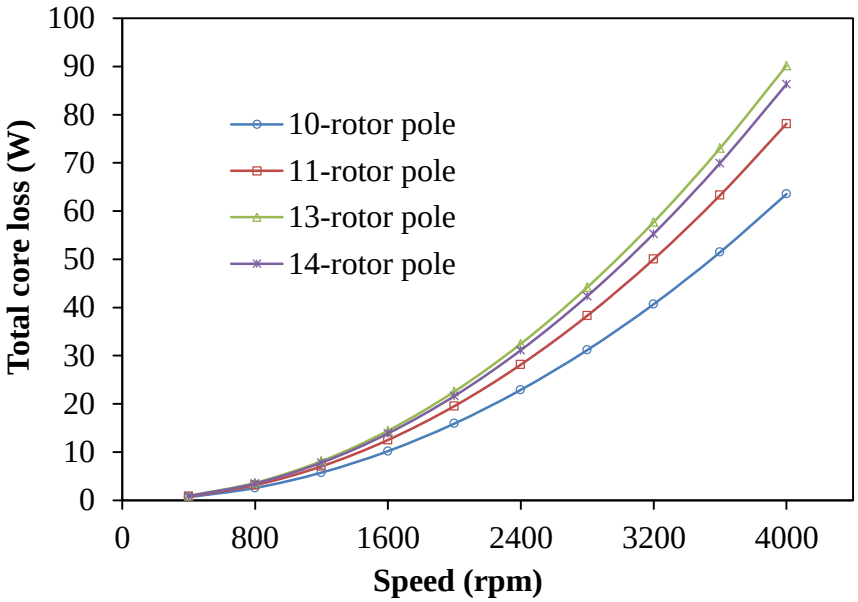

(b) Loss versus speed

Fig.3.35 Variation of total core losses, 400rpm, no load.

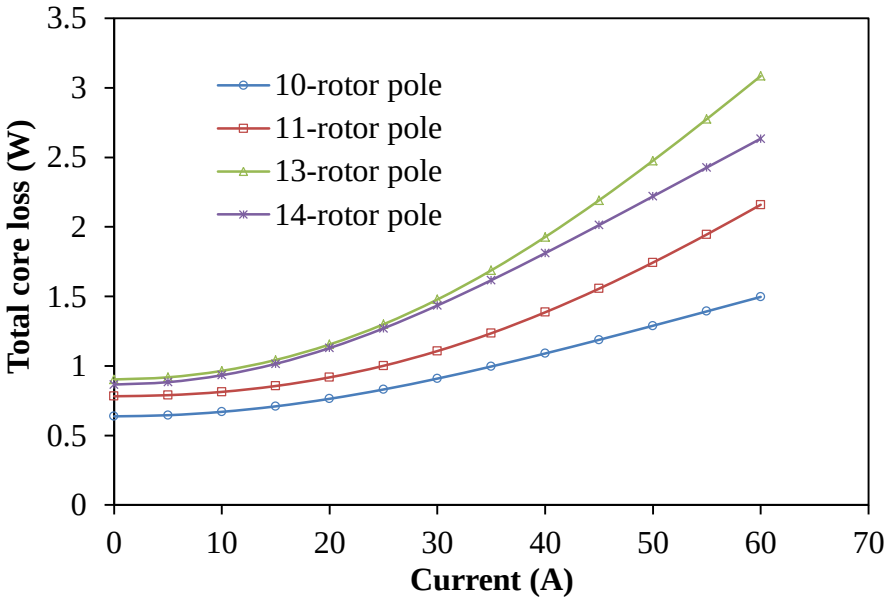

Fig.3.36 Variation of total core losses with currrent , 400rpm

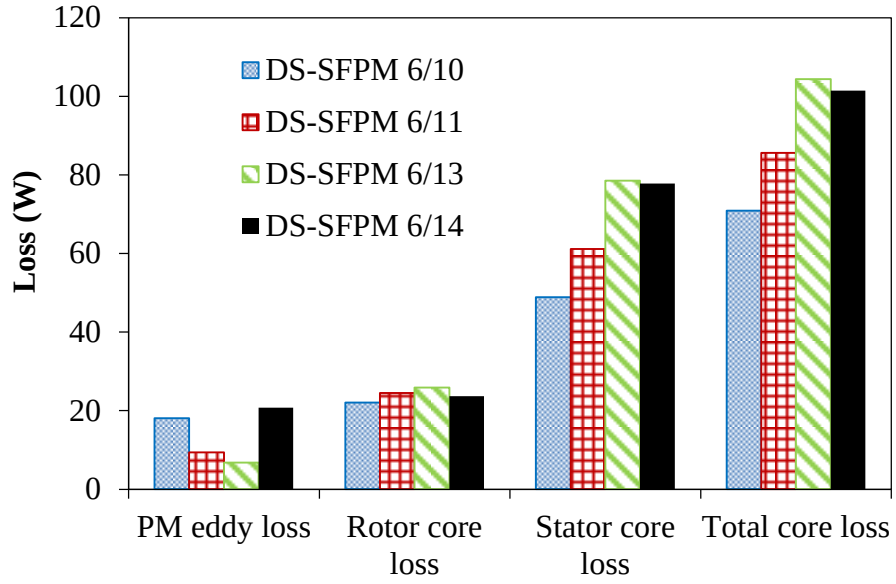

(a)

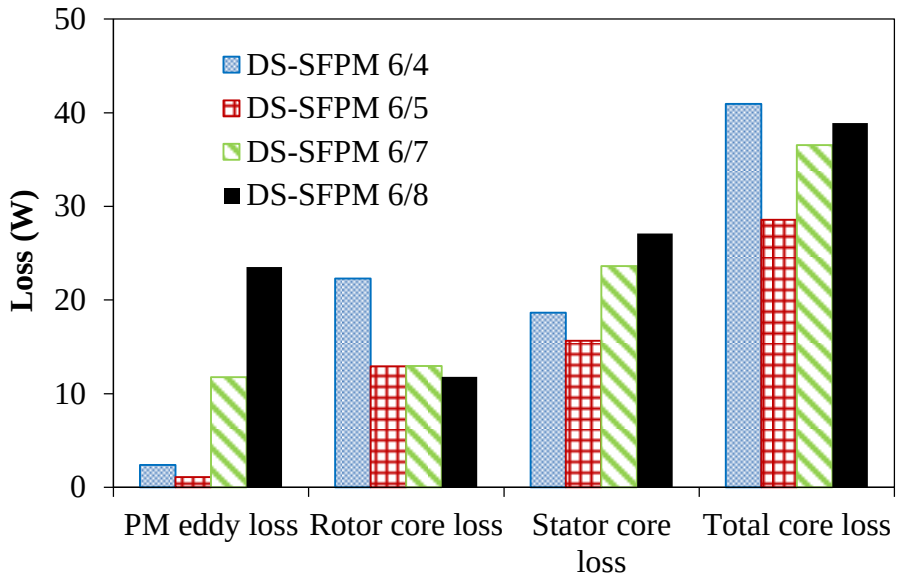

(b)

Fig.3.37 Comparison of losses in DS-SFPM machines, I=15A, 4000rpm.

The influences of the design parameters on the loss characteristics of the developed machines at no-load are displayed in Figs.3.38 (a)-(e). Depending on the objective(s), the machines could be designed to have minimum loss by employing the optimum values of the main design parameters. It is worth noting from Fig.3.38 that the 4-rotor pole machines exhibits the largest loss whilst the least loss occurs in the 5-rotor pole machines. The loss characteristics of the 7-and 8-rotor pole machines are almost identical in each variation with leading design parameters.

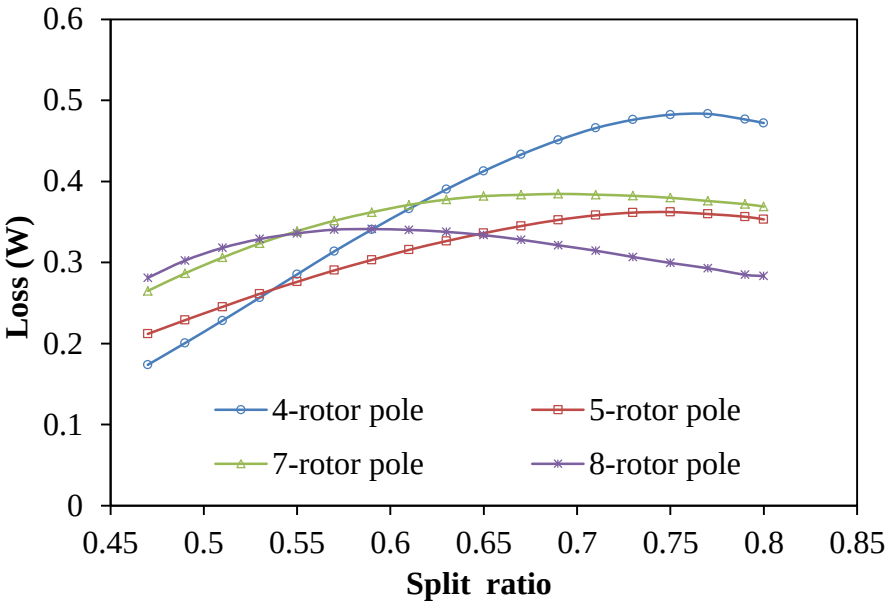

(a) Loss versus split ratio

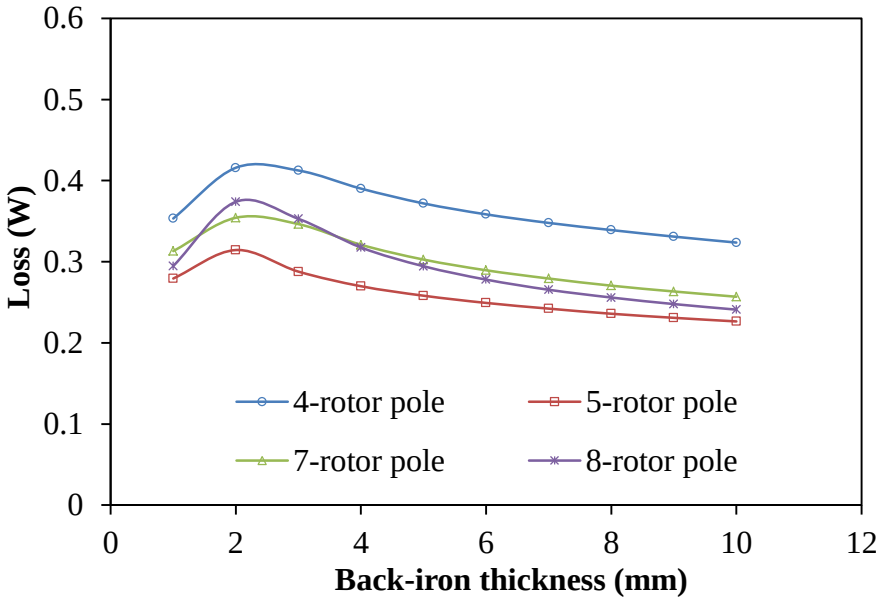

(b) Loss versus back-iron thickness

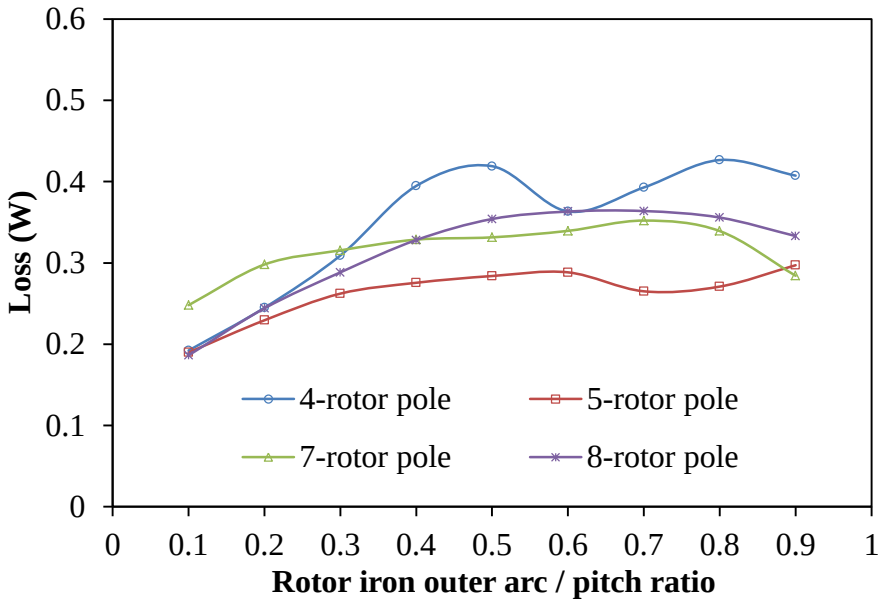

(c) Loss versus rotor iron outer arc / pitch ratio

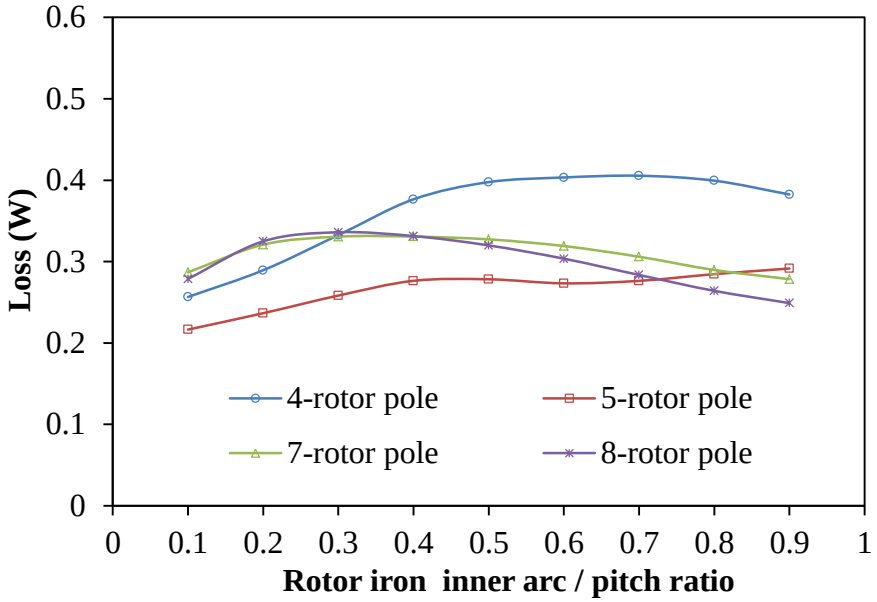

(d) Loss versus rotor iron inner arc / pitch ratio

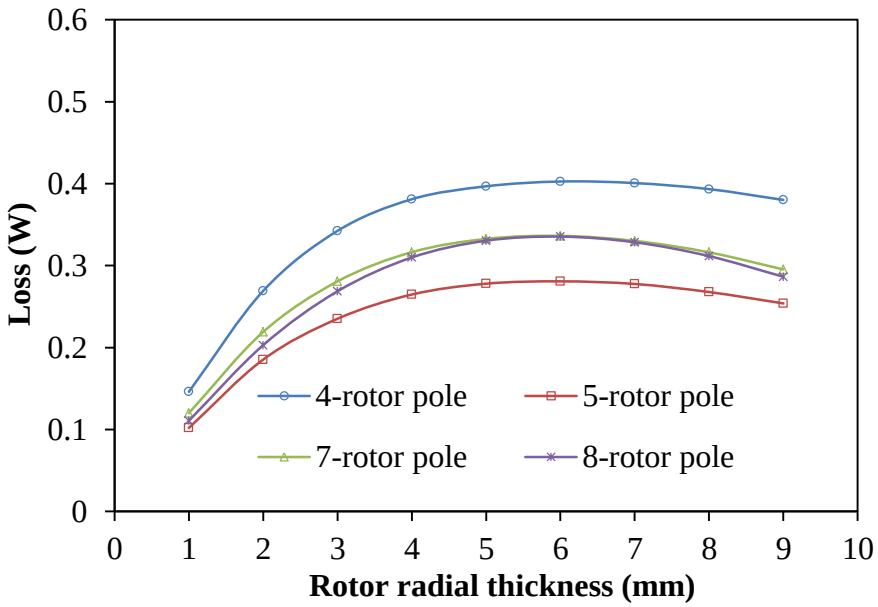

(e) Loss versus rotor radial thickness (mm)

Fig.3.38 Variation of total core losses in DS-SFPM machines with design parameters, no-load, 400rpm.

The variation of overall efficiency of the DS-SFPM machines with rotor speed is shown in Figs.3.39 (a) and (b). From the plots, it is obvious that the developed 13-rotor pole machine exhibits the highest efficiency amongst the compared machines. This is followed by the 5-rotor pole machine, the worst being the 4-rotor pole machine. Moreover, the efficiencies of these machines are listed in Table 3.2.

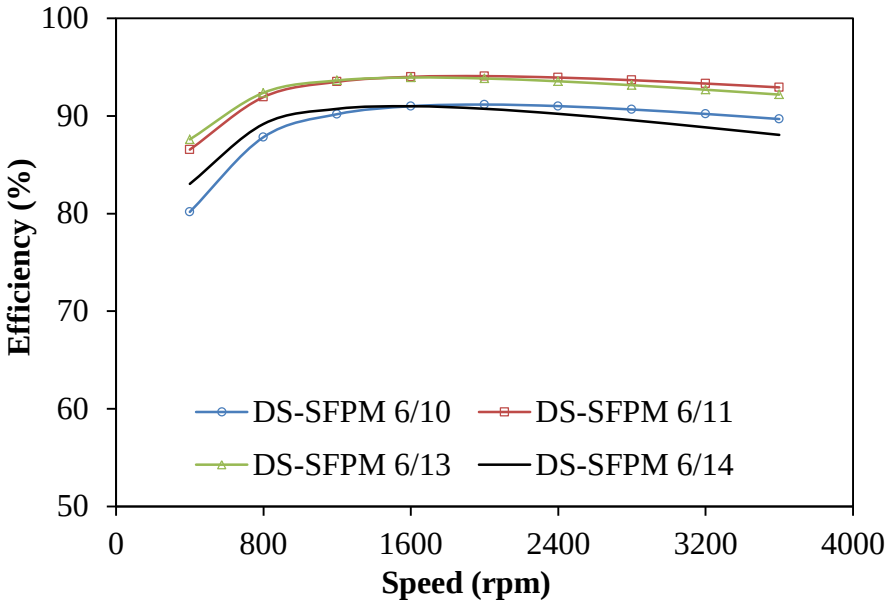

(a)

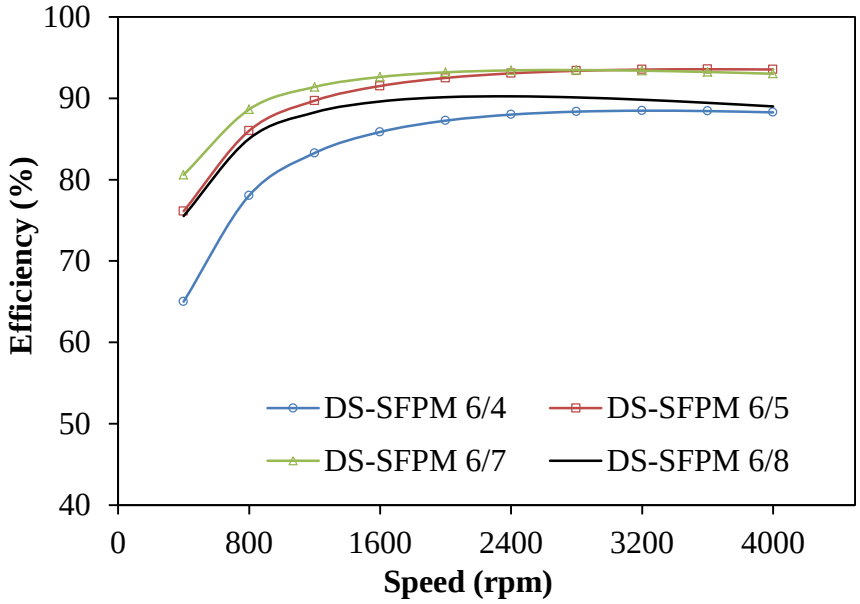

(b)

Fig.3.39 Comparison of efficiency in DS-SFPM machines, copper loss=30W.

3.6.1 Unbalanced magnetic force

It is clear from Figs.3.40-3.41 that the 5-pole machine suffers from significant amount of UMF relatively to the other compared machines. In general, it is clear that the magnitudes of the UMF in the rotor of these machines are inversely related to the rotor pole number; although the 11- and 13-rotor pole machines seem to be quite similar in the magnitude of their UMFs. Obviously, the analysed 5- and 7-rotor machines would be very unsuitable for applications where minimum unbalanced magnetic force is required. The variations of magnitude of UMF with rotor position on no load and on load are given in Figs 3.40 and 3.41.

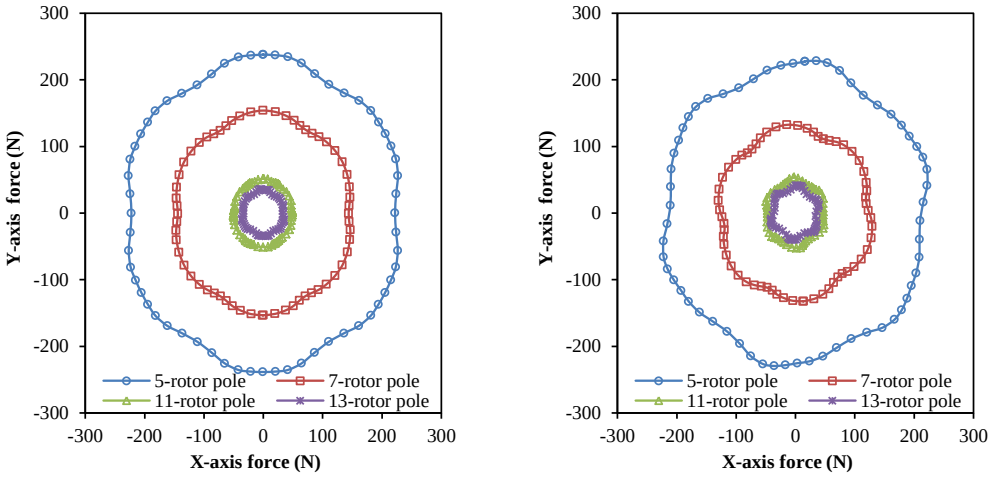

(a) I=0A (b) I=15A

Fig.3.40 Comparison of UMF on load and no load conditions, i_d=0

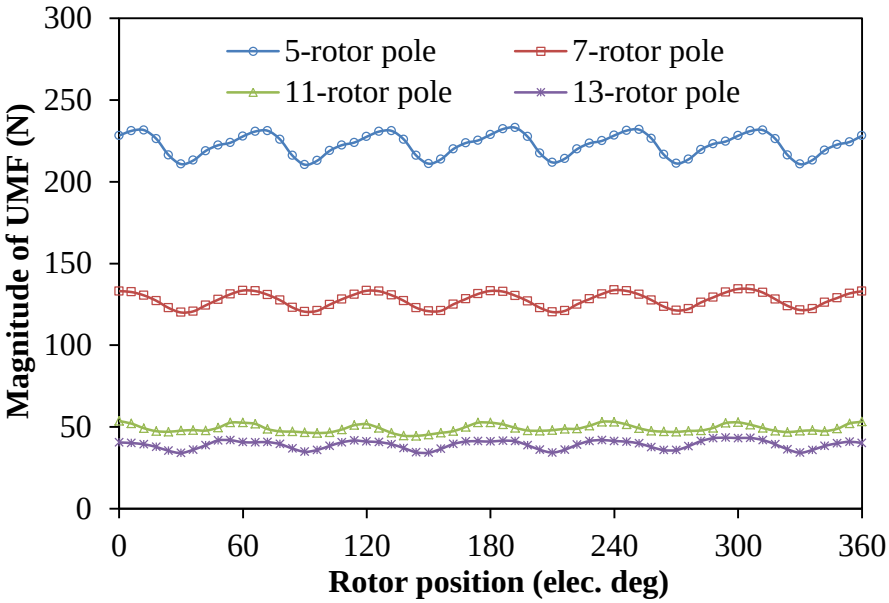

(a) Magnitude of UMF versus rotor position, I=15A

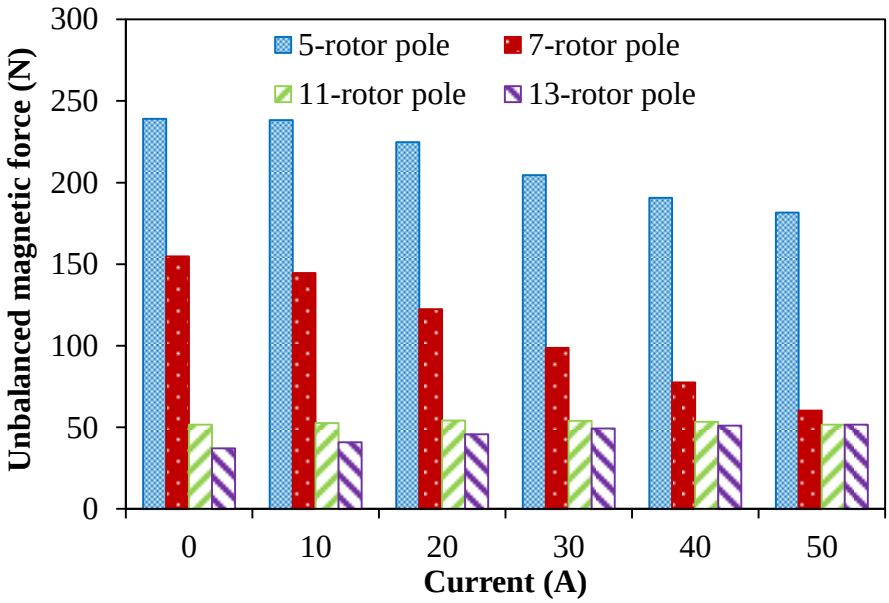

(b) Magnitude of UMF versus current

Fig.3.41 Comparison of UMF, i_d=0.

3.7 Experimental validation

The manufactured prototype is shown in Fig.3.42. The FEA predicted results are compared with the experiments as seen in Figs.3.44-3.49.

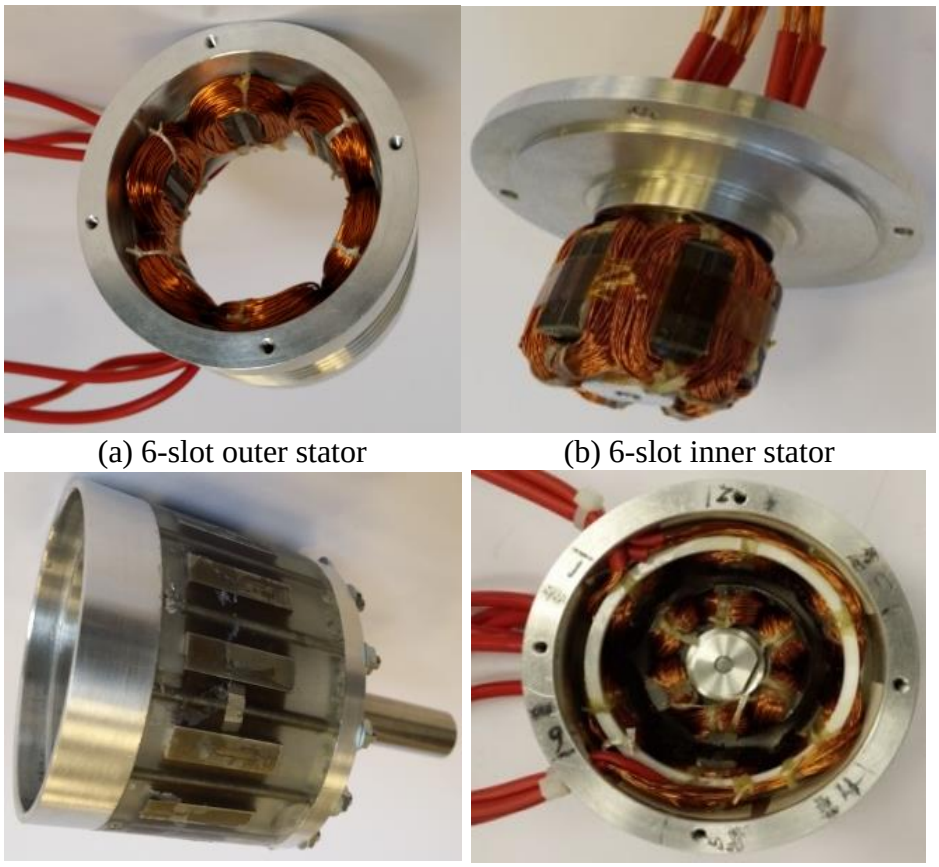

(a) 6-slot outer stator (b) 6-slot inner stator

(c) 13-pole cup-rotor (d) Assembled stators

Fig.3.42 Manufactured prototype of 13-pole DS-SFPM machine.

The developed machine is fabricated and shown in Fig.3.42, which comprises of an inner stator, an outer stator and a cup-rotor shaped modulating iron segments. The predicted 3D-FEA open circuit flux density distribution of the prototype machine is shown in Fig.3.43. Figs.3.44-3.47 show the comparison of open-circuit back-EMF waveforms and spectra of the manufactured prototype at different operating modes i.e. with the inner stator alone, the outer stator alone, and a series connection of the same phases.

Although the fundamental magnitude of the 2D-FEA is quite higher than the experimental results, this discrepancy is mainly due to the end-effects which have been accounted for in the 3D-FEA results. Note that the error difference between the predicted 3D-FEA and measured results is about 15% which is reasonably acceptable considering the fact that the accuracy of the results could be adversely affected by the manufacturing error.

Figs.3.48 and 3.49 show the comparison of the torque characteristics of the developed machine with the combined stators in operation. Again, an error difference of ~12% is obtained in the torque characteristic between the measured and predicted results. This could be attributed to the manufacturing tolerances.

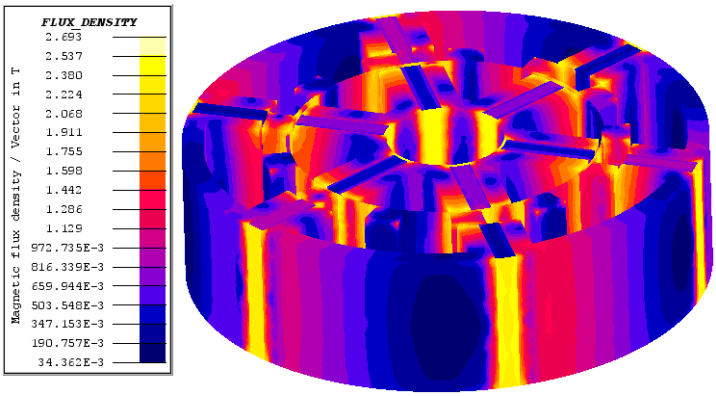

Fig.3.43 3D-Flux density distribution of the DS-SFPM machine, open circuit.

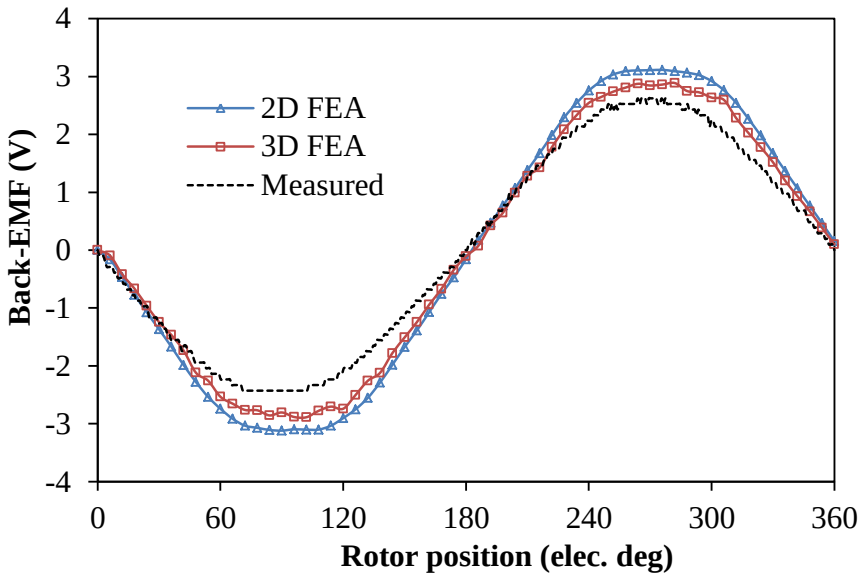

(a) Waveforms

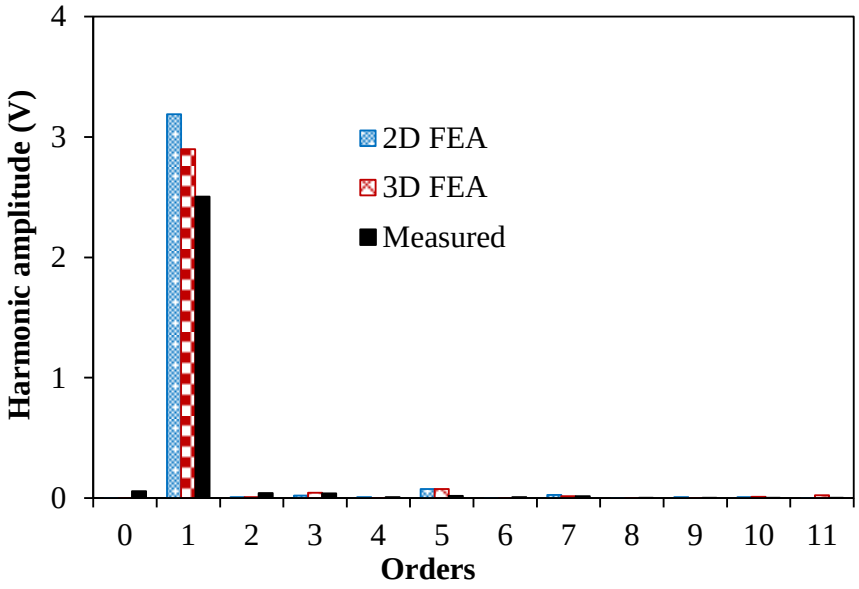

(b) Spectra

Fig.3.44 Comparison of the outer stator phase back-EMF variation with rotor position, 400rpm.

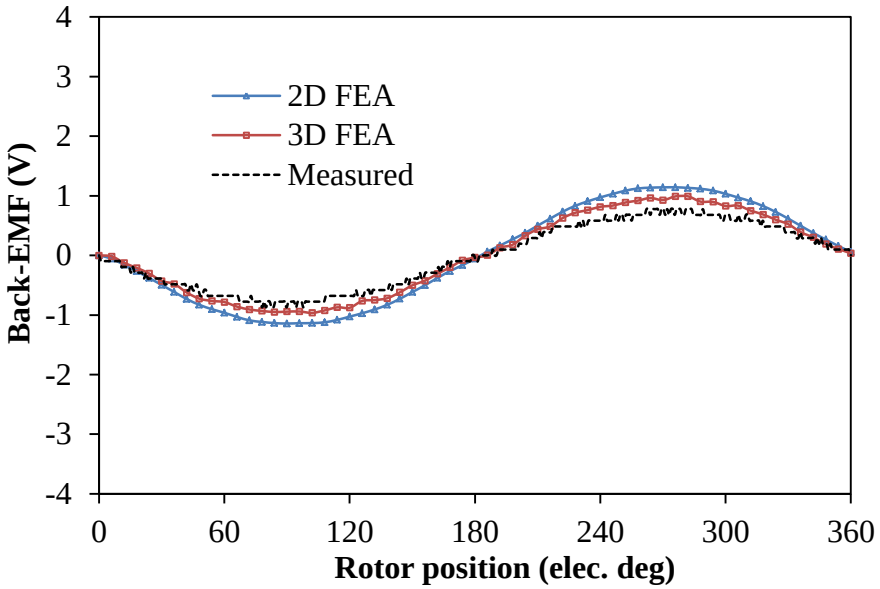

(a) Waveforms

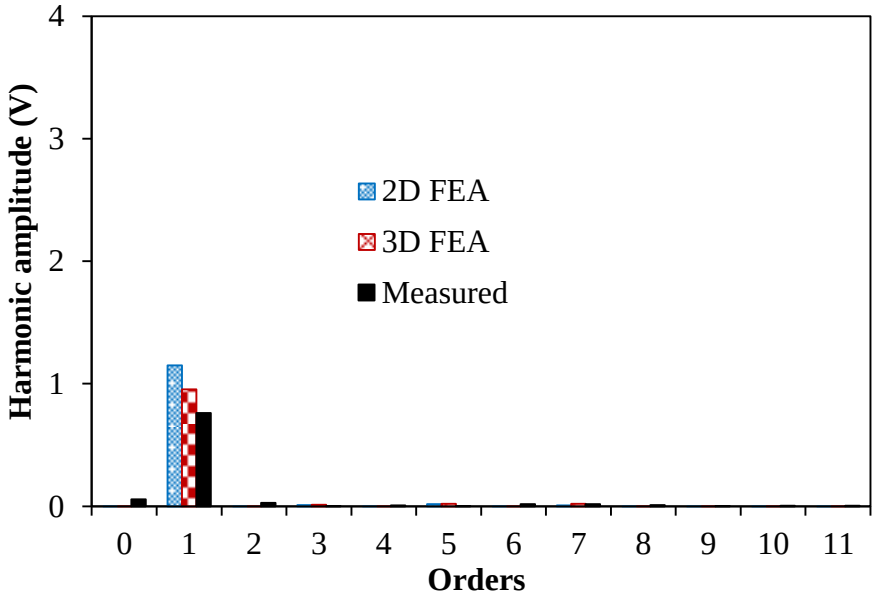

(b) Spectra

Fig.3.45 Comparison of the inner stator phase back-EMF variation with rotor position, 400rpm.

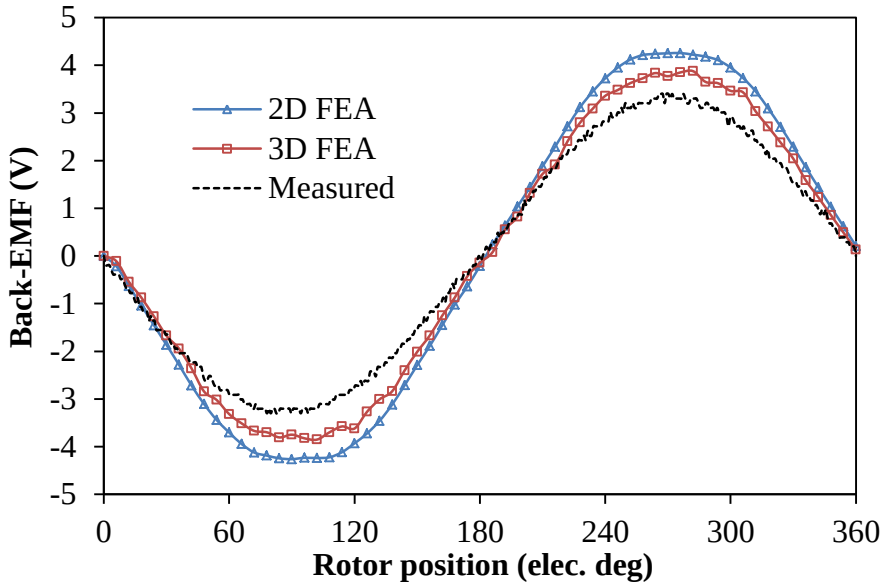

(a) Waveforms

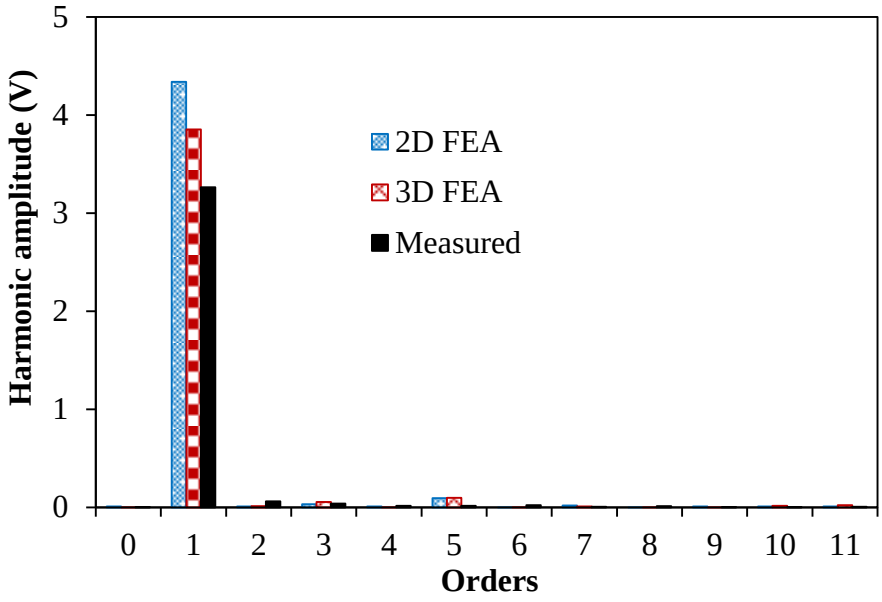

(b) Spectra

Fig.3.46 Comparison of phase back-EMF of prototype DS-SFPM, 400rpm.

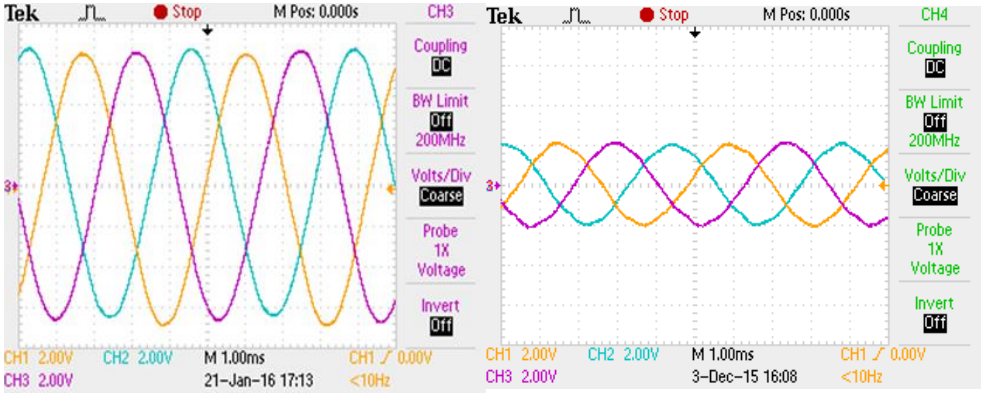

(a) Outer stator back-EMF (b) Inner stator back-EMF

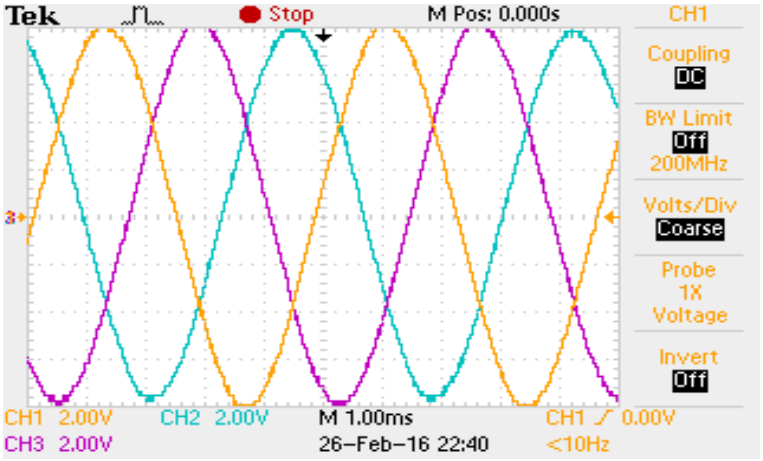

(c) Total back-EMF of series connected inner and outer stators, 2V/div

Fig.3.47 Measured phase back-EMF of the DS-SFPM machines at 400rpm.

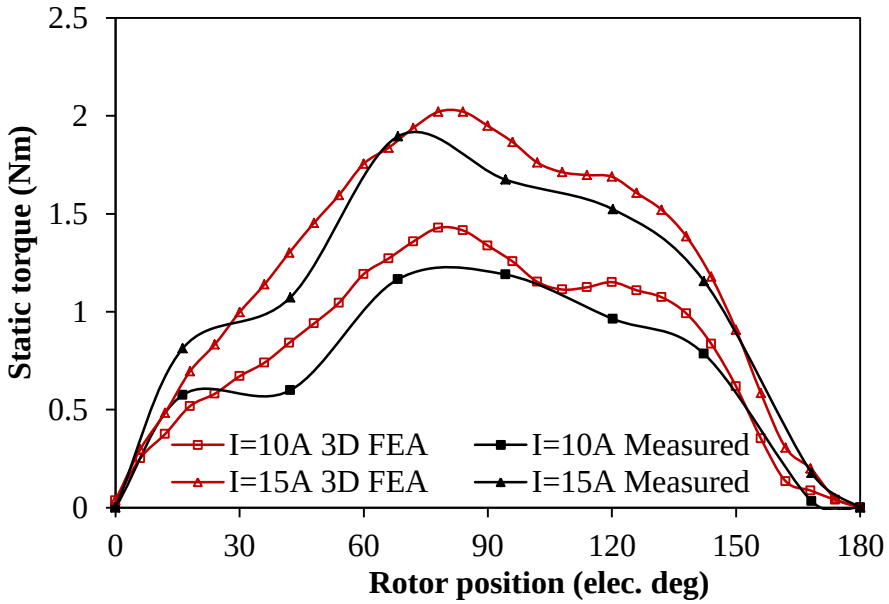

Fig.3.48 Comparison of static torque with different load current of the prototype (I_a=-2I_b =-2I_c).

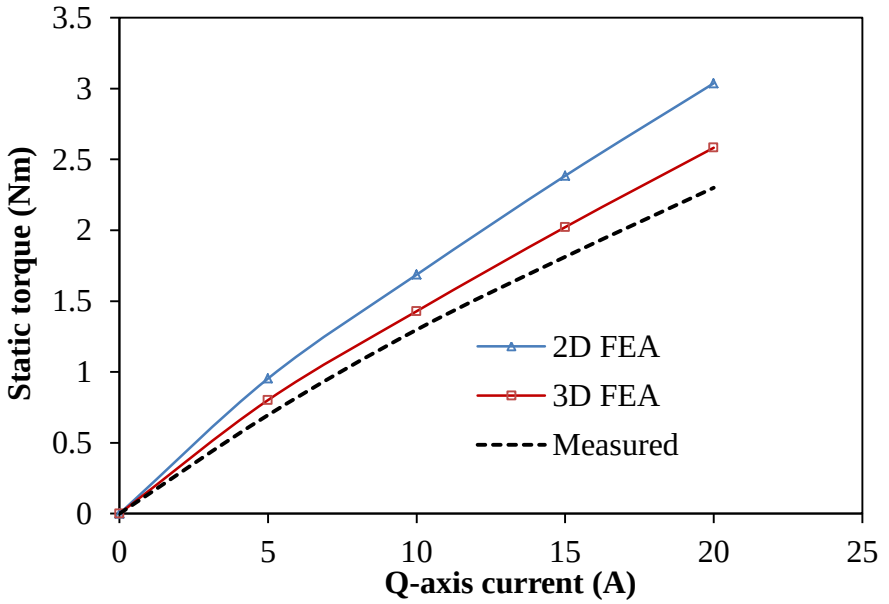

Fig.3.49 Comparison of peak torque versus current.

In order to reduce the cost, we have manufactured only one prototype having 13-rotor pole number since it seems to be the most promising candidate amongst the other compared machines. Note that the rotor iron pieces are mechanically supported with iron bridges of about 0.5mm thickness. Also, both stators are made of laminated steel sheets in order to reduce the iron losses. Error differences are about 15% and 12% between the 3D FE predicted and measured results of the back-EMF and static torque respectively. The discrepancies are primarily due the manufacturing tolerance.

3.8 Summary

The influence of rotor pole number on the electromagnetic performance of double-stator switched flux PM machines is investigated. The analyses show that the machine with 13-rotor pole exhibits the largest fundamental back-EMF and hence the largest power and torque densities amongst the compared machines. Also, the developed DS-SFPM machines could deliver higher electromagnetic torque than their equivalent single-stator counterparts. The flux weakening capability of these machines is defined as the ratio of the maximum speed to the base speed. Although the maximum speed of the 13-rotor pole machine is low, it has the best flux-weakening capability amongst the other compared DS-SFPM machines since the ratio of its maximum speed to the base speed is high. Furthermore, the DS-SFPM machine having 13-rotor has the least amount of UMF on the rotor which is desirable in most applications. Further, it exhibits the least amount of magnet eddy current loss owing to its minimum PM usage despite its high electrical frequency, which again is an admirable quality although it has high core loss. It is worth mentioning that the developed machines are characterized by high cogging torque when compared to other PM machines. Nevertheless, the effect is negligible when compared to its output electromagnetic torque. Finally, the FEA results are validated by experiments with good agreement.

CHAPTER 4
SWITCHED FLUX PM MACHINES HAVING TWO SEPARATE STATORS WITH E-CORE OUTER STATOR STRUCTURE

4.1 Introduction

Although the switched flux machine was firstly introduced as a single-phase generator in 1955 [RAU55], it did not attract much attention until recently multi-phase switched flux permanent magnet (SFPM) machines have been investigated extensively [HOA97], [ZHU05], [HOA07], [HUA08], [CHE10a], [OWE10], [WU15a], [RAM11], [CHE11a], [SUL11], and [GAU14]. SFPM machines have many special features [ZHU07a], [ZHU10], [ZHU11], and [CHE11b], including PMs on the stator, salient pole stator with non-overlapping concentrated windings, salient pole rotor without windings or PMs, torque production due to reluctance action but negligible reluctance torque, sinusoidal back-EMFs and high torque density, etc. However, as stator-PM machines, SFPM machines also have obvious demerits. Since both PMs and armature windings are housed on the stator and the rotor is very simple, the stator becomes very crowded but the rotor space is not fully utilized compared with the conventional rotor-PM machines. Consequently, the slot area for windings is reduced, resulting in potential increased copper loss. In addition, since the PMs are placed adjacent to the windings, the PMs may experience overheating and also potential demagnetization. To overcome these demerits, novel partitioned stator (PS) SFPM (PS-SFPM) machines have been developed recently [ZHU14] and [EVA15]. In PS-SFPM machines, there are two stators and two air-gaps, the windings being located in one stator and the PMs placed on the other stator, while the rotor is made only of iron pieces and sandwiched between two stators. It is shown in [ZHU14] and [EVA15] that PS-SFPM machines can exhibit significantly higher torque density than the conventional SFPM machines.

It is worthy emphasizing that although the novel PS-SFPM machines have two stators, they are different from the conventional double stator machines [TOB99], [CHA09], [NIU08], and [WAN11b] which have two identical stators but the PS-SFPM machines have two completely different stators which respectively accommodate the armature windings only or the PMs only. On the other hand, from the torque generation point of view, the PS-SFPM machines can also be ascribed as a novel type of magnetically geared machine [ZHU14], [GER15a], [GER15b], [ZHU15c] and [AWA16a].

Since the introduction of concept of PS-SFPM machines, many PS-SFPM machine topologies have been developed based on the topologies of conventional SFPM machines. [ZHU15c] proposed a new PS machine based on the flux reversal machine, while [WU15b] introduced the PS doubly salient machine. [ZHU15d] proved that all stator-PM machines having PMs on the stator can be unified by the PS machine concept. Therefore, machine topologies and design techniques for the conventional stator-PM machines can be adopted for the PS machines.

On the other hand, all- and alternate-pole-wound non-overlapping winding techniques are widely used to increase the torque density and particularly alternate-pole-wound are often employed to improve the fault tolerance capability in the conventional rotor-PM machines, [JAH86], [ELR10], [PAR05], and [BIA06]. Consequently, it has also been introduced to SFPM machines [CHE10a] and [OWE10]. Thus, following the aforementioned discussions, all- and alternate-pole-wound non-overlapping winding techniques may also be introduced into the PS-SFPM machines in order to further increase the torque density and enhance the fault tolerance capability.

It should be mentioned that the original topologies of PS-SFPM machines described in [ZHU14] and [EVA15] have a strict restriction that the outer stator pole number must be equal to the inner stator pole number. In this chapter, it will be extended to the case that the PM stator pole number may be half of that of the armature stator pole number. All investigations will be carried out by 2-dimentional (2D) finite element analysis (FEA). A prototype machine is manufactured and tested to validate the analyses.

In [EVA15], 12-stator-pole PS-SFPM machines having 10-, 11-, 13- and 14-rotor-pole rotors with all- and alternate-pole-wound are comparatively analysed. The results show that among the four analysed machines with all-pole-wound, the 12/11 stator/rotor-pole one can deliver the highest torque. This is also true for the machine with alternate-pole-wound. As described in [EVA15], the original design of PS-SFPM has a strict limit that N_{so} must be always equal to N_{si}, i.e.

$$N_{so} = N_{si} \tag{4.1}$$

Nevertheless, the conventional SFPM machine may have the number of PMs as half of the

stator slot numbers. Thus, this concept could be adopted in PS-SFPM machines as well, which leads to the constrains as:

$$N_{so} = 2N_{si} \tag{4.2}$$

By way of example, Fig.4.1 shows the schematic diagram of the proposed machines which has 12 outer stator slots or poles (N_{so}) and 6 inner stator poles (N_{si}).

Thus, a novel PS-SFPM machine with all-pole-wound topology can be proposed as shown in Fig.4.1 (a) which still has 12 slots but the number of PMs is halved. Further, the corresponding alternate-pole-wound topology, Fig.4.1 (b), can also be proposed for comparative study. The proposed machines having all- and alternate-pole-wound topologies as well as different rotor poles are globally optimized by genetic algorithms using 2D FEA for maximum average torque under the fixed copper loss of 30W. It is worth mentioning that the series turns per phase of these machines are kept the same in the analysis. Their main parameters are listed in Tables 4.1 and 4.2. For convenience, we have designated the machines having all- and alternate-pole-wound configurations as ALL-W and ALT-W, respectively.

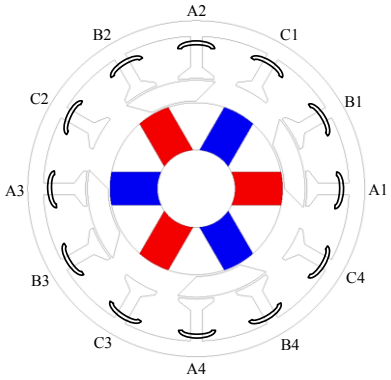

(a) ALL-W 6/4

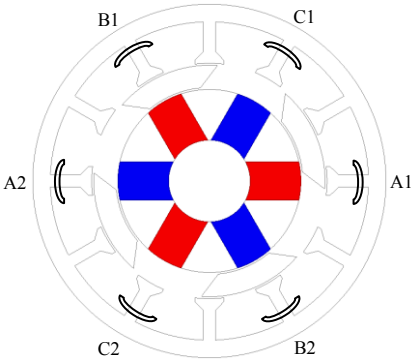

(b) ALT-W 6/4

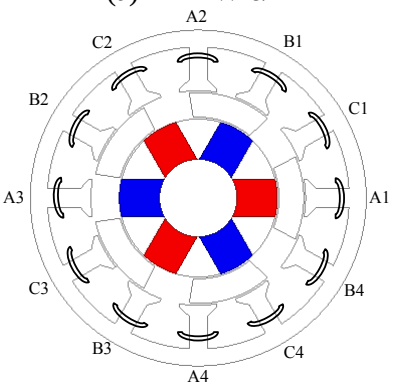

(c) ALL-W 6/5

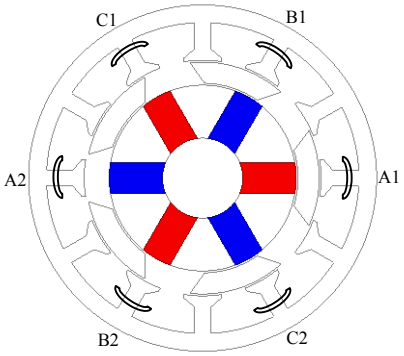

(d) ALT-W 6/5

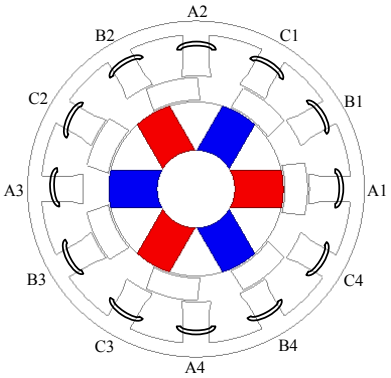

(e) ALL-W 6/7

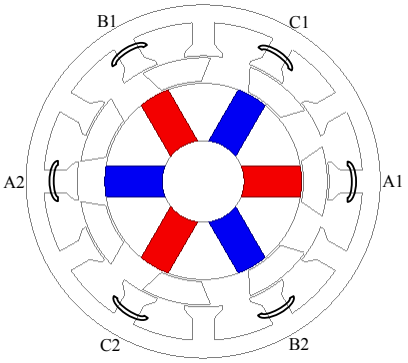

(f) ALT-W 6/7

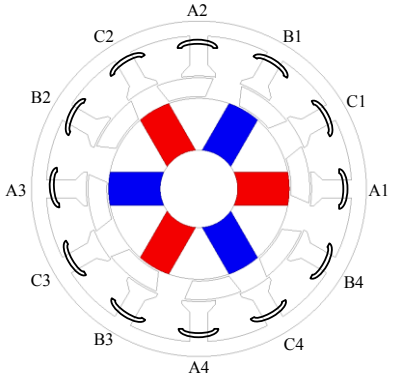

(g) ALL-W 6/8

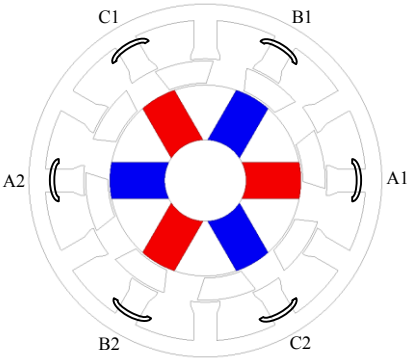

(h) ALT-W 6/8

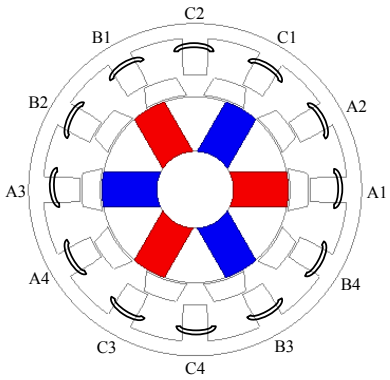

(i) ALL-W 6/10

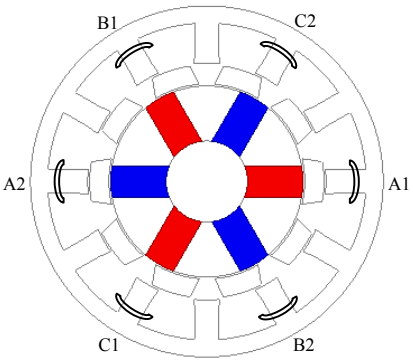

(j) ALT-W 6/10

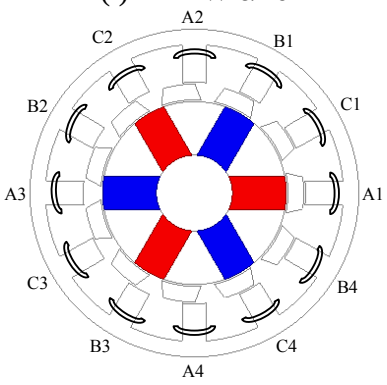

(k) ALL-W 6/11

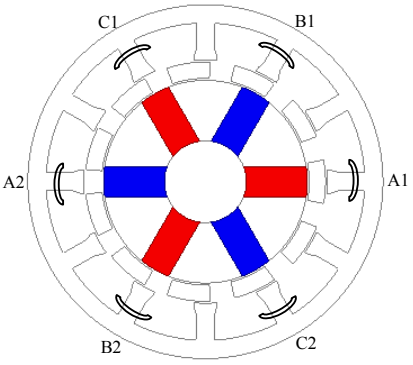

(l) ALT-W 6/11

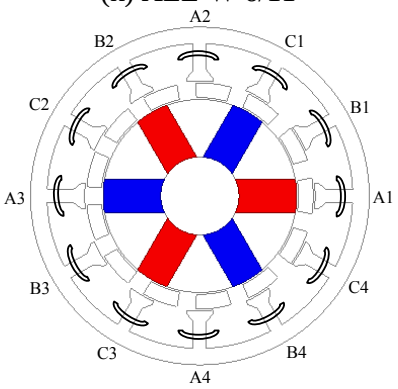

(m) ALL-W 6/13

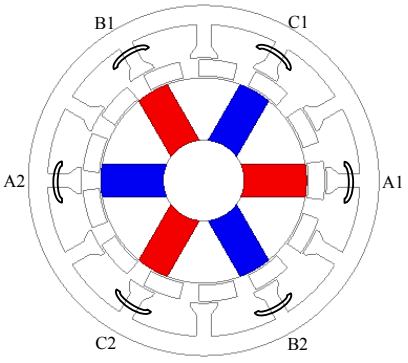

(n) ALT-W 6/13

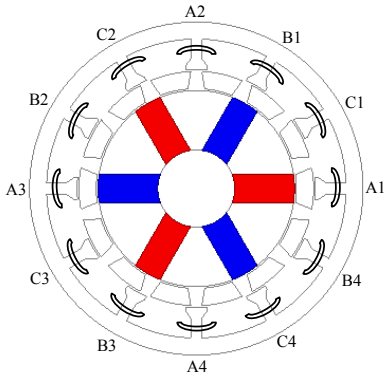

(o) ALL-W 6/14

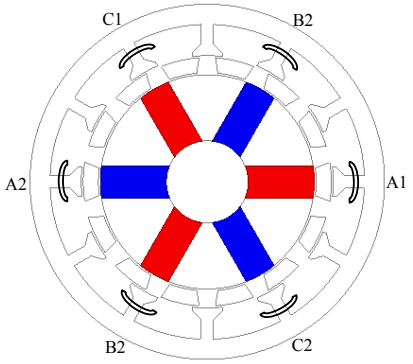

(p) ALT-W 6/14

Fig.4.1 Cross-sections of the proposed machines

TABLE 4.1 PARAMETERS OF ANALYSED ALL-POLE-WOUND MACHINES

Item	**Value**							
Machine topology	**All-pole-wound**							
Rotor pole number, N_r	**4**	**5**	**7**	**8**	**10**	**11**	**13**	**14**
No. of outer stator slots, N_s	12							
No. of inner stator slots, P_s	6							
Number of phases, m	3							
No. of turns/coil	18							
Coils/phase	4							
Outer stator diameter (mm)	90							
Airgap length (mm)	0.5							
Active stack length (mm)	25							
Split ratio	0.65	0.63	0.67	0.67	0.69	0.67	0.67	0.71
Slot opening/slot pitch ratio	0.39	0.34	0.51	0.43	0.62	0.60	0.57	0.65
Rotor radial thickness (mm)	5.50	6.61	5.99	5.01	5.01	4.31	3.92	4.66
PM thickness (mm)	8.78	9.86	9.92	8.83	9.38	9.20	8.95	7.66
Outer rotor iron width/pitch ratio	0.56	0.64	0.53	0.66	0.47	0.52	0.66	0.79
Inner rotor iron width/pitch ratio	0.33	0.60	0.60	0.51	0.72	0.75	0.64	0.62
Stator back-iron thickness (mm)	4.19	4.55	3.66	3.96	3.93	4.24	4.39	4.60
Stator tooth width (mm)	3.20	4.89	6.83	4.78	6.77	6.64	3.49	3.00

TABLE 4.2 PARAMETERS OF ANALYSED ALTERNATE-POLE-WOUND MACHINES

Item	**Value**							
Machine topology	**Alternate-pole-wound**							
Rotor pole number, N_r	**4**	**5**	**7**	**8**	**10**	**11**	**13**	**14**
No. of outer stator slots, N_s	12							
No. of inner stator slots, P_s	6							
Number of phases, m	3							
No. of turns/coil	36							
Coils/phase	2							
Outer stator diameter (mm)	90							
Airgap length (mm)	0.5							
Active stack length (mm)	25							
Split ratio	0.66	0.68	0.71	0.68	0.67	0.68	0.70	0.71
Slot opening/slot pitch ratio	0.53	0.40	0.42	0.53	0.60	0.64	0.58	0.55
Rotor radial thickness (mm)	5.66	5.48	6.03	5.68	4.91	4.15	4.18	3.84
PM thickness (mm)	9.68	7.95	7.92	9.32	8.15	7.82	8.40	8.13
Outer rotor iron width/pitch ratio	0.59	0.67	0.64	0.64	0.54	0.64	0.66	0.71
Inner rotor iron width/pitch ratio	0.53	0.47	0.46	0.49	0.75	0.63	0.69	0.57
Stator back-iron thickness (mm)	4.46	4.61	4.49	4.11	4.37	4.64	4.93	5.10
Stator tooth width (mm)	3.12	4.11	5.64	5.86	5.91	4.55	3.69	3.01

The flux density distributions of the analysed machines at both open circuit and different copper loss conditions are displayed in Figs.4.2 and 4.3. Fig.4.4 shows the open circuit equipotential distributions of the analysed machines. It is worth noting that the flux densities and equipotential distributions of the ALL-W and ALT-W machines of the same rotor pole number are similar but not exactly the same since they have different physical geometries. As

shown in Figs.4.2 and 4.3, the outer and inner stator steel edges, the outer stator tooth, and the rotor edges are more easily to undergo saturation than the other parts of the analysed machines when subjected to high copper loss.

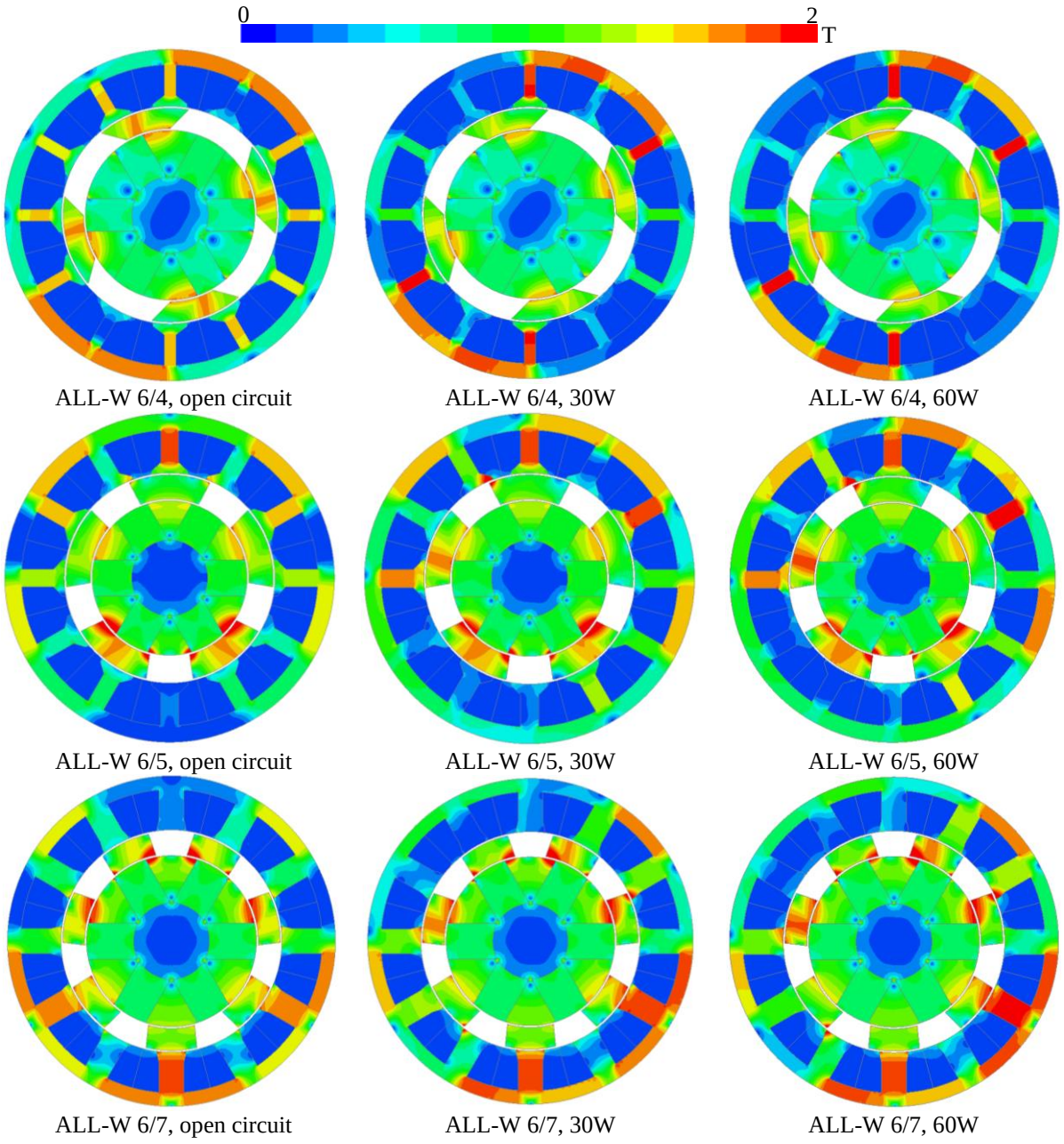

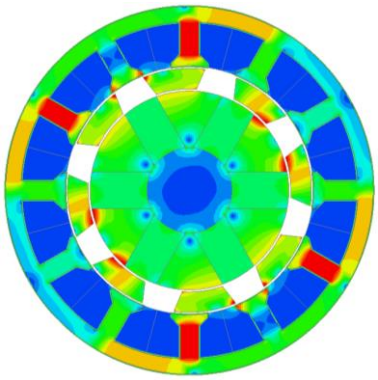

ALL-W 6/8, open circuit

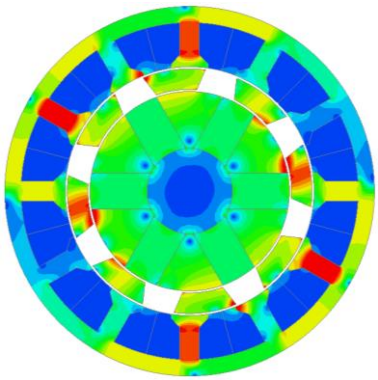

ALL-W 6/8, 30W

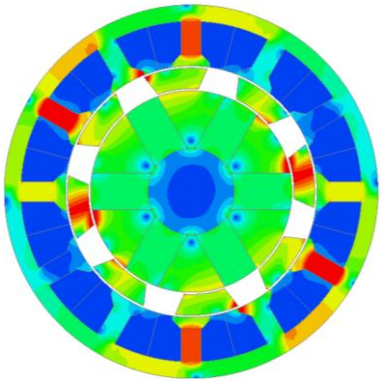

ALL-W 6/8, 60W

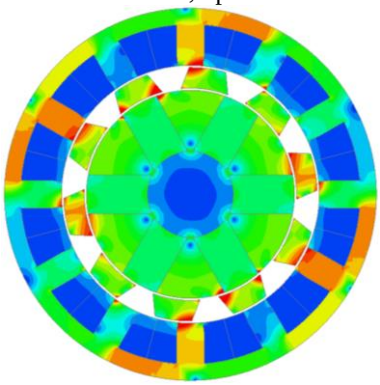

ALL-W 6/10, open circuit

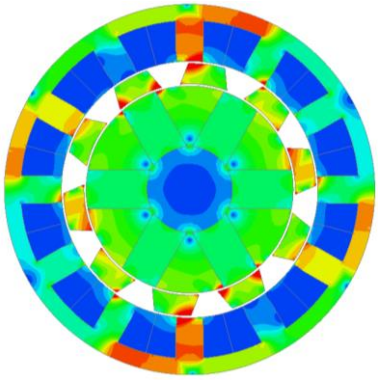

ALL-W 6/10, 30W

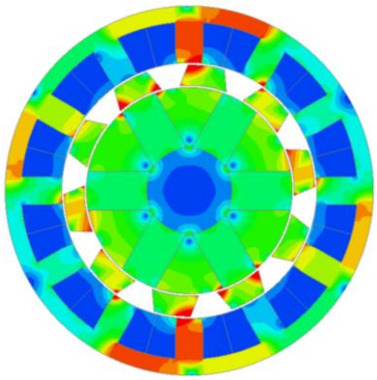

ALL-W 6/10, 60W

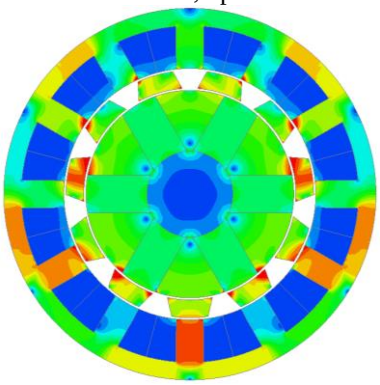

ALL-W 6/11, open circuit

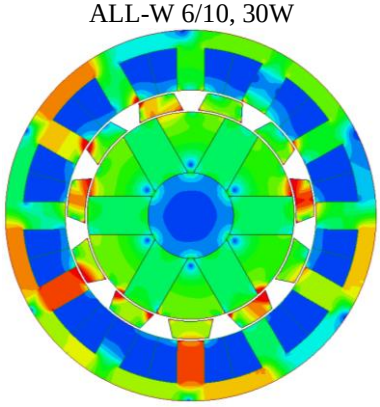

ALL-W 6/11, 30W

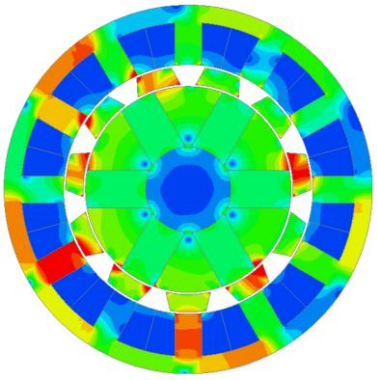

ALL-W 6/11, 60W

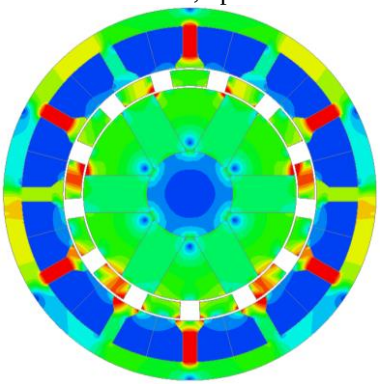

ALL-W 6/13, open circuit

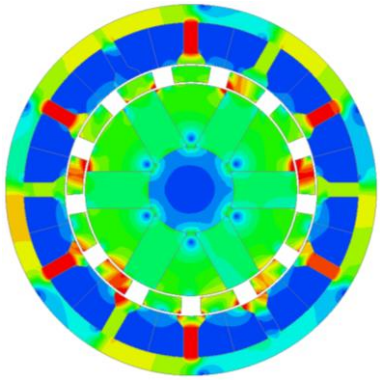

ALL-W 6/13, 30W

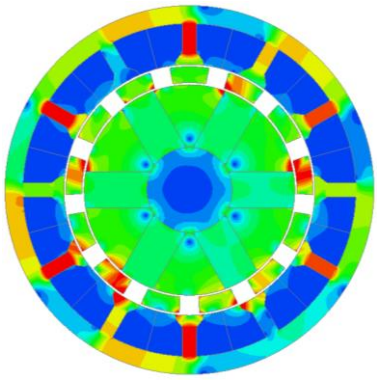

ALL-W 6/13, 60W

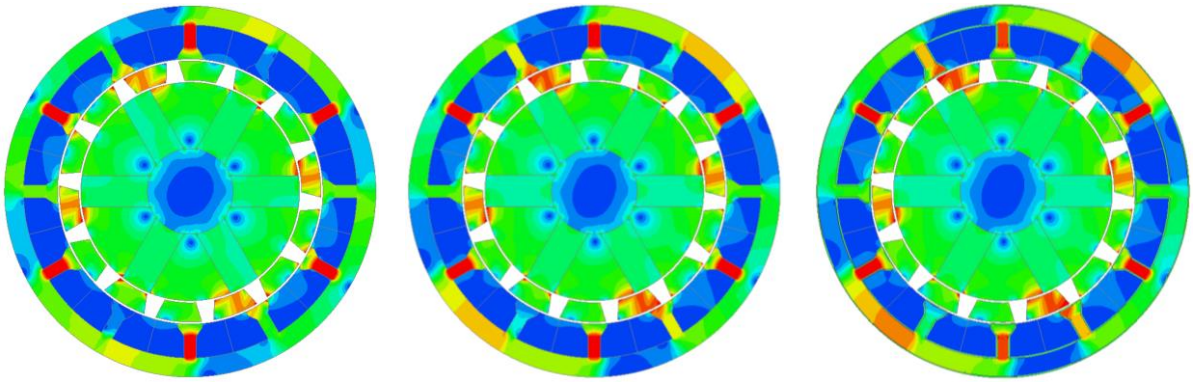

ALL-W 6/14, open circuit　　ALL-W 6/14, 30W　　ALL-W 6/14, 60W

Fig.4.2 Flux density distributions of all-pole-wound machines, rotor at *d*-axis position.

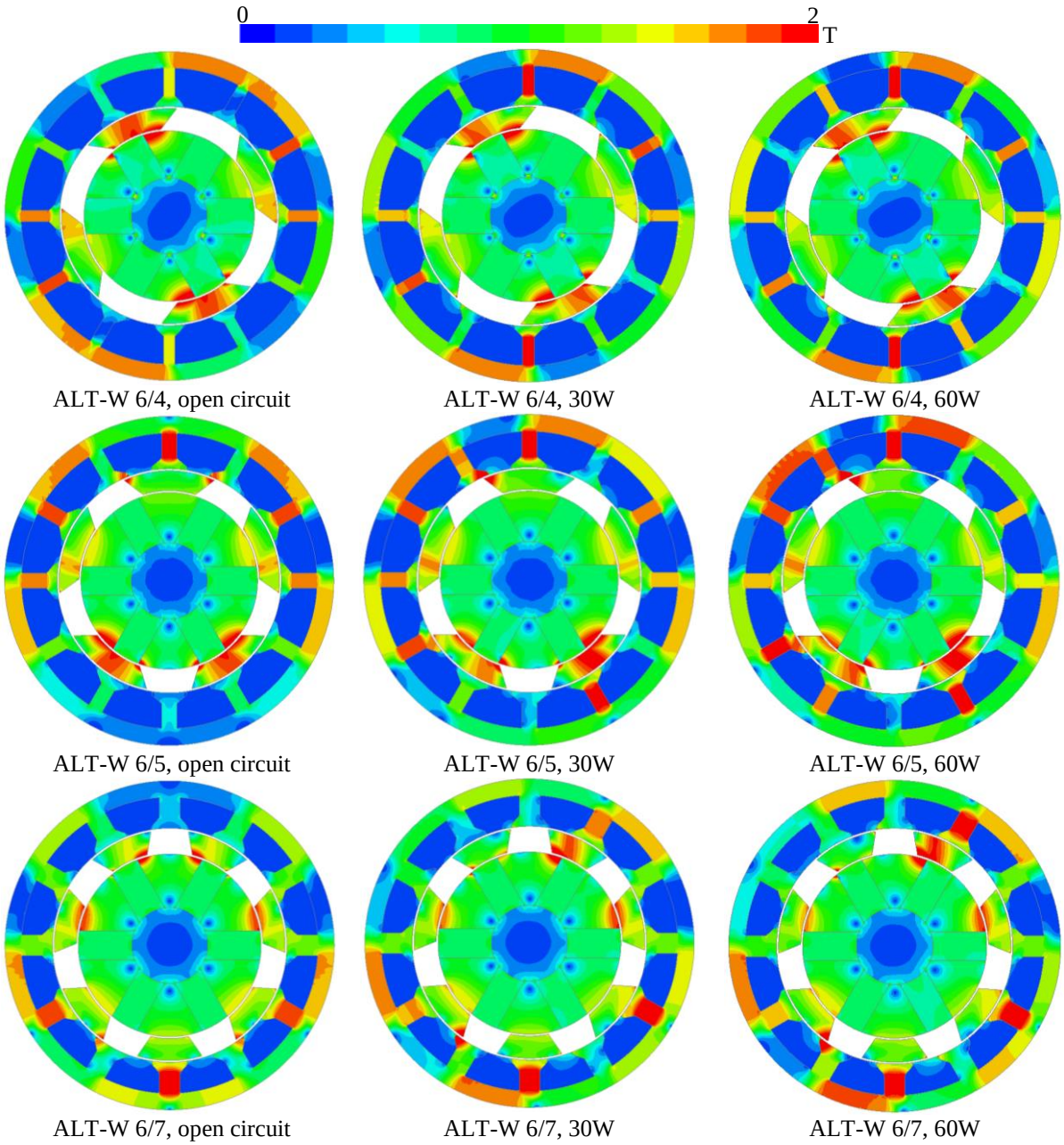

ALT-W 6/4, open circuit　　ALT-W 6/4, 30W　　ALT-W 6/4, 60W

ALT-W 6/5, open circuit　　ALT-W 6/5, 30W　　ALT-W 6/5, 60W

ALT-W 6/7, open circuit　　ALT-W 6/7, 30W　　ALT-W 6/7, 60W

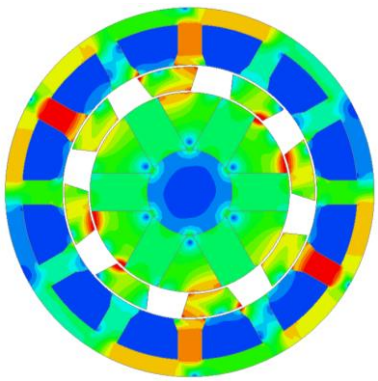

ALT-W 6/8, open circuit

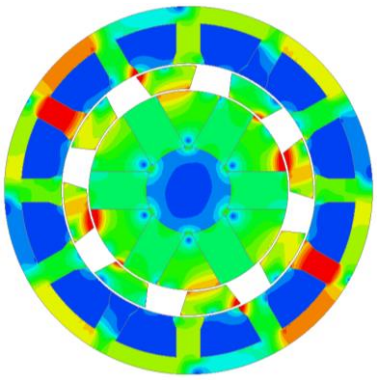

ALT-W 6/8, 30W

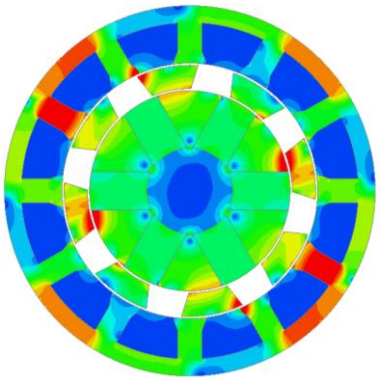

ALT-W 6/8, 60W

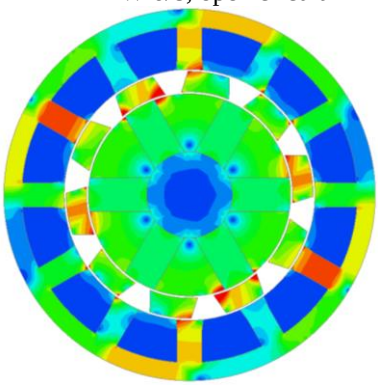

ALT-W 6/10, open circuit

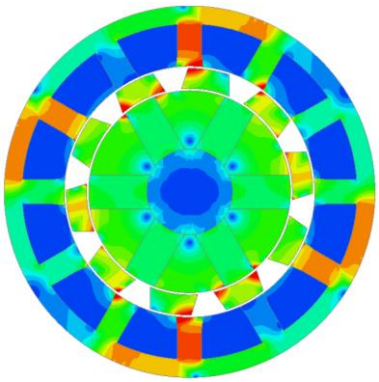

ALT-W 6/10, 30W

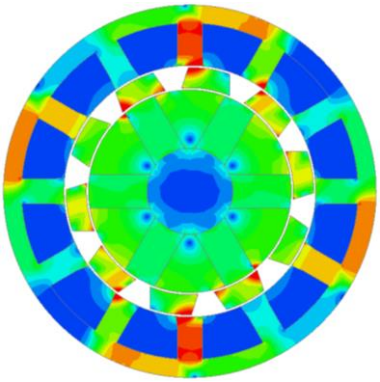

ALT-W 6/10, 60W

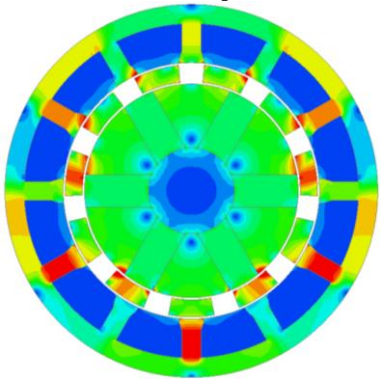

ALT-W 6/11, open circuit

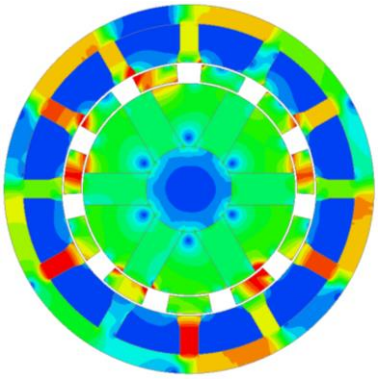

ALT-W 6/11, 30W

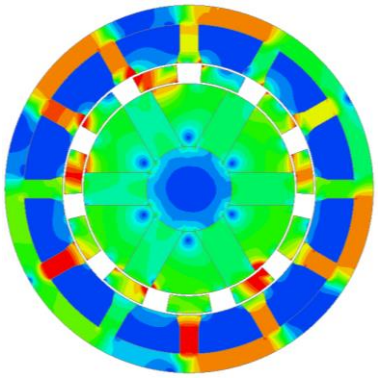

ALT-W 6/11, 60W

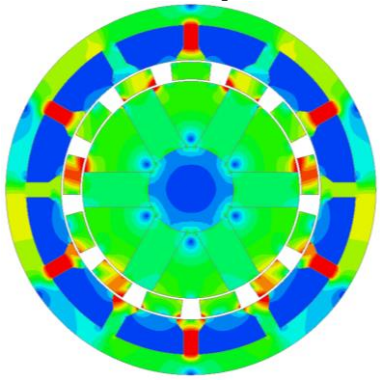

ALT-W 6/13, open circuit

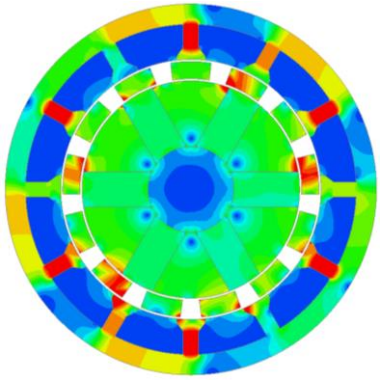

ALT-W 6/13, 30W

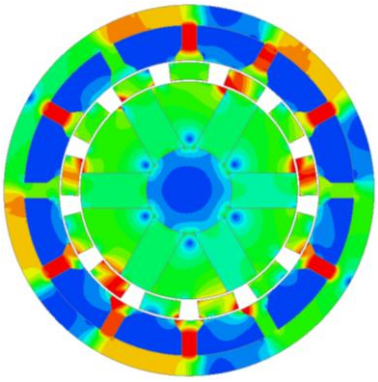

ALT-W 6/13, 60W

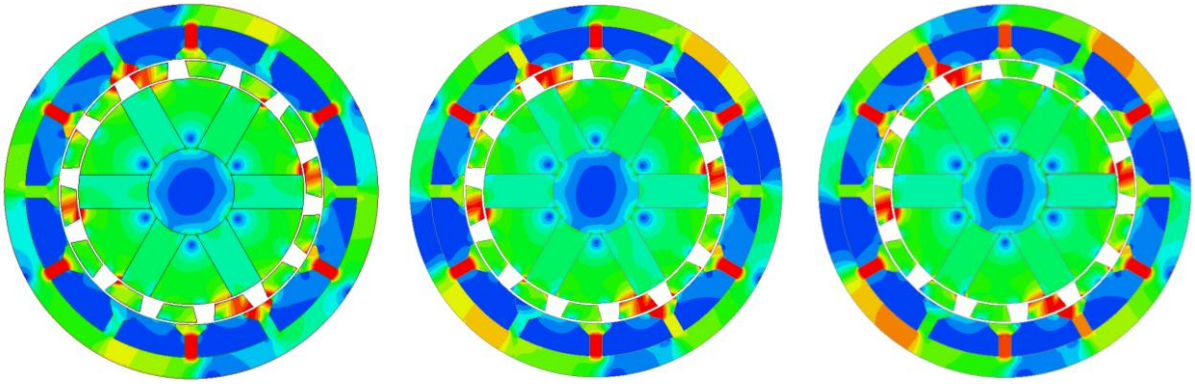

ALT-W 6/14, open circuit　　ALT-W 6/14, 30W　　ALT-W 6/14, 60W

Fig.4.3 Flux density distributions of alternate-pole-wound machines, rotor at *d*-axis position.

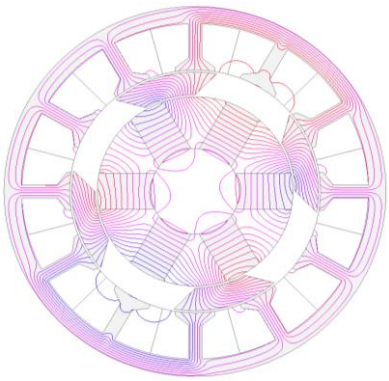

(a) ALL-W 6/4

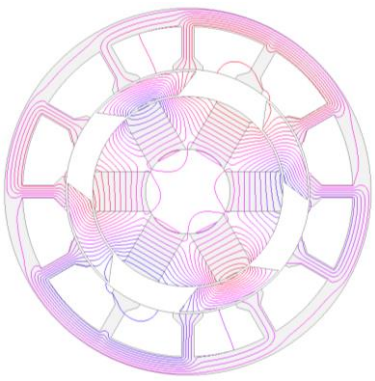

(b) ALT-W 6/4

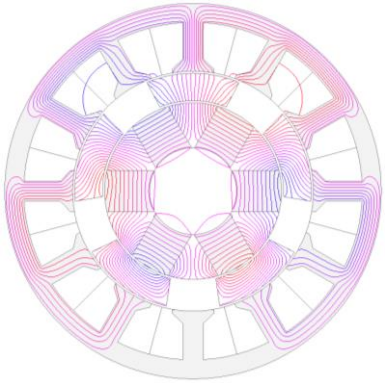

(c) ALL-W 6/5

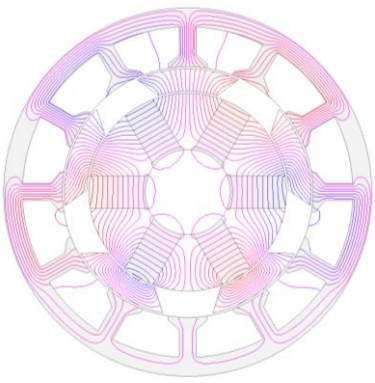

(d) ALT-W 6/5

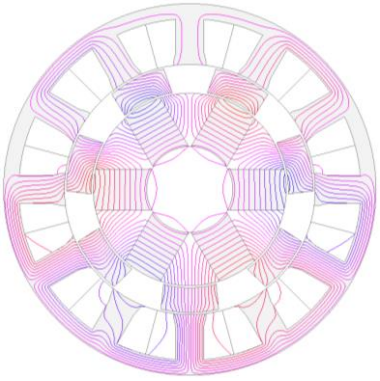

(e) ALL-W 6/7

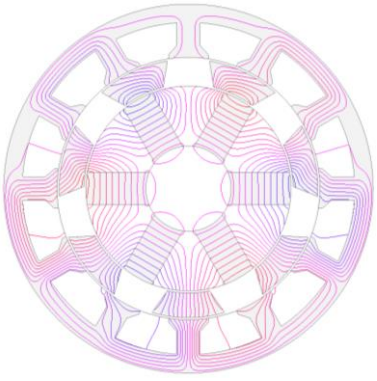

(f) ALT-W 6/7

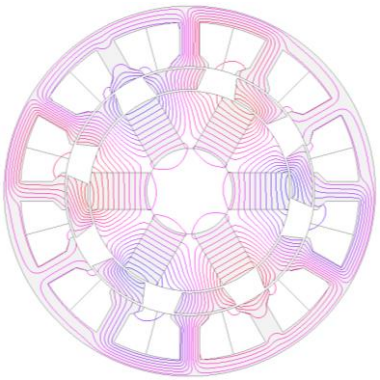

(g) ALL-W 6/8

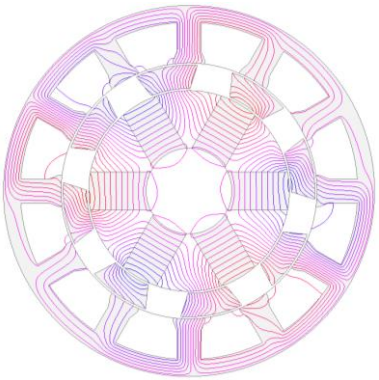

(h) ALT-W 6/8

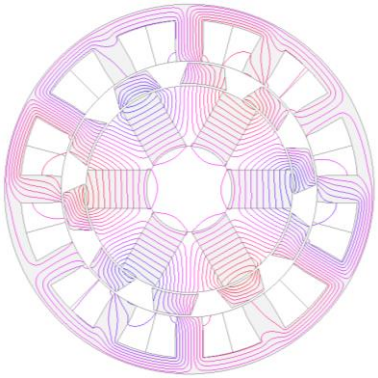

(i) ALL-W 6/10

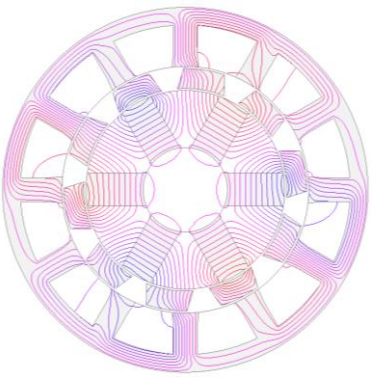

(j) ALT-W 6/10

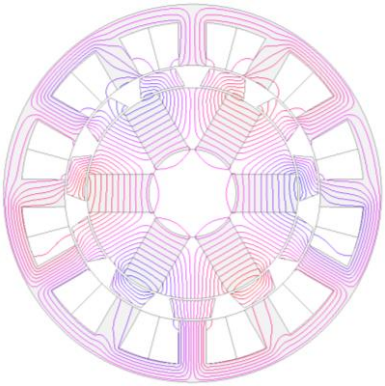

(k) ALL-W 6/11

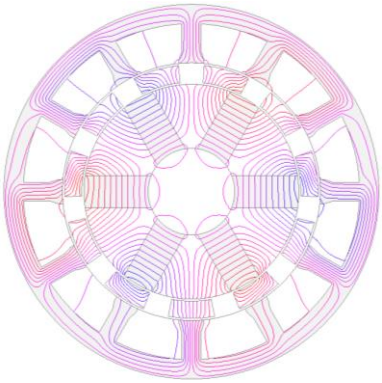

(l) ALT-W 6/11

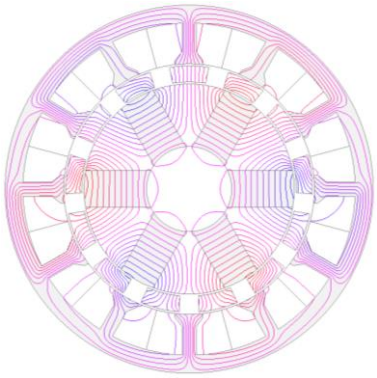

(m) ALL-W 6/13

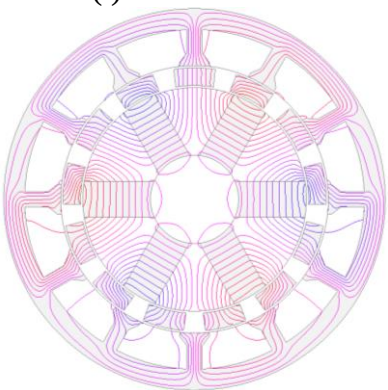

(n) ALT-W 6/13

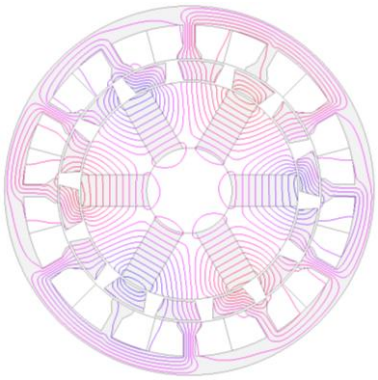

(o) ALL-W 6/14

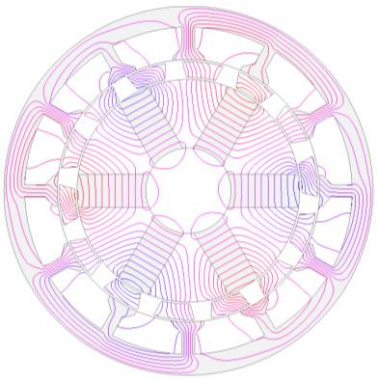

(p) ALT-W 6/14

Fig.4.4 Open-circuit field distributions of analysed all- and alternate-pole-wound machines, rotor at *d*-axis rotor position.

4.2 Machine optimization and influence of leading design parameters on the average torque

The overall performance of the developed machines is influenced by the design parameters to a large extent. Thus, it is imperative to investigate the effect of the design parameters on the electromagnetic performance. The optimized machine parameters include: split ratio, PM thickness, rotor radial thickness and arcs, and stator back-iron thickness. The optimal values of the leading design parameters are listed in Tables 4.1 and 4.2. It is worth mentioning that the 4-pole machine suffers from poor torque density in all the analysed cases.

The mechanical angle between the *d*- and *q*-axes of the analysed machines is given by (4.3).

$$\theta_{d-q\ axis} = \left|{}^{90}/_{N_r}\right| \tag{4.3}$$

Fig.4.5 shows the variation of average torque with split ratio (which is defined as the ratio of the inner airgap radius to the outer diameter of the machine). Larger torque is obtained in the 10-pole and 11-pole machines for the analysed all- and alternate-pole-wound topologies with optimum split-ratios, respectively.

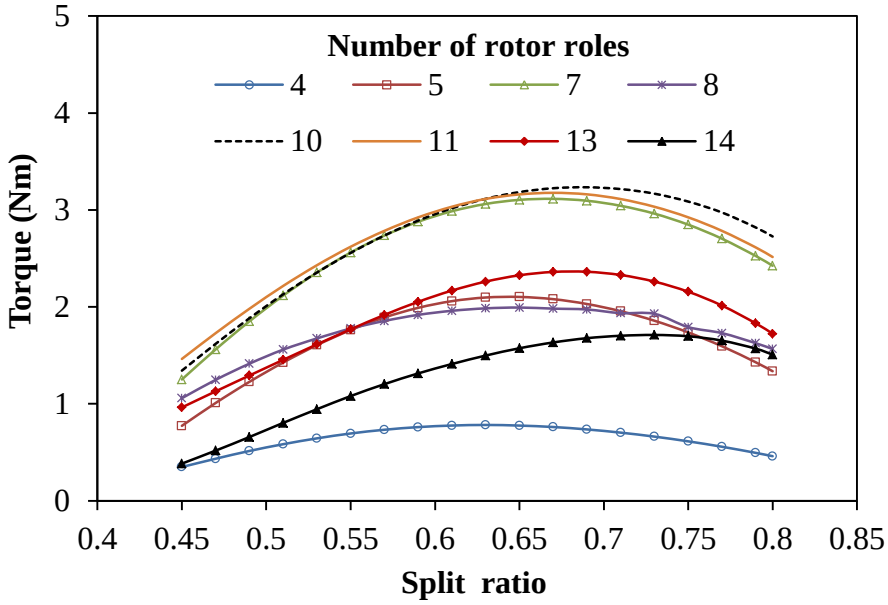

(a) All-pole-wound

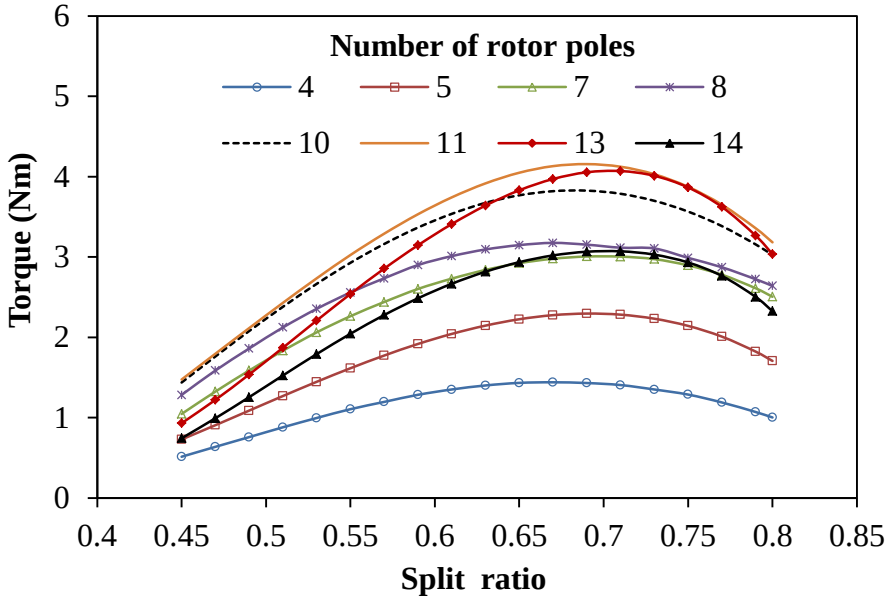

(b) Alternate-pole-wound

Fig.4.5 Variation of average torque with split ratio, i_d=0.

The variation of average torque with slot opening/slot pitch ratio is shown in Fig.4.6. For each of the analysed machines, we could see that there is an optimum value of the above mentioned design parameter. The average torque increases initially with the slot opening/slot pitch ratio. As the tooth-tip width is small, there will be significant magnetic saturation of the tooth. Thus, as the tooth-tip width increases, the output torque will be increased. However, as the tooth-tip width continues to increase beyond a certain value, there may be decreased slot area for the winding and thus reduced phase current for the fixed copper loss which will

eventually lead to decreased output torque. Therefore, an optimum slot opening/slot pitch ratio exists.

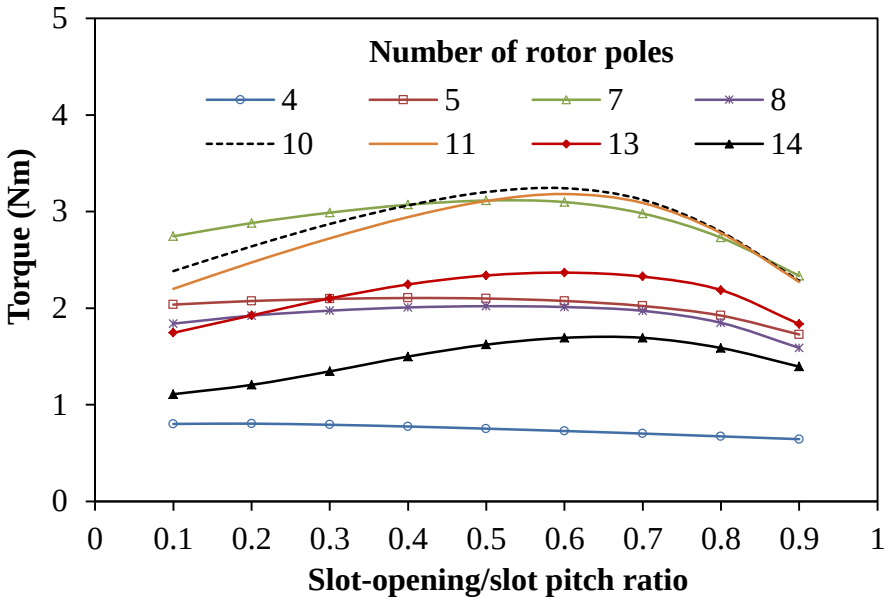

(a) All-pole-wound

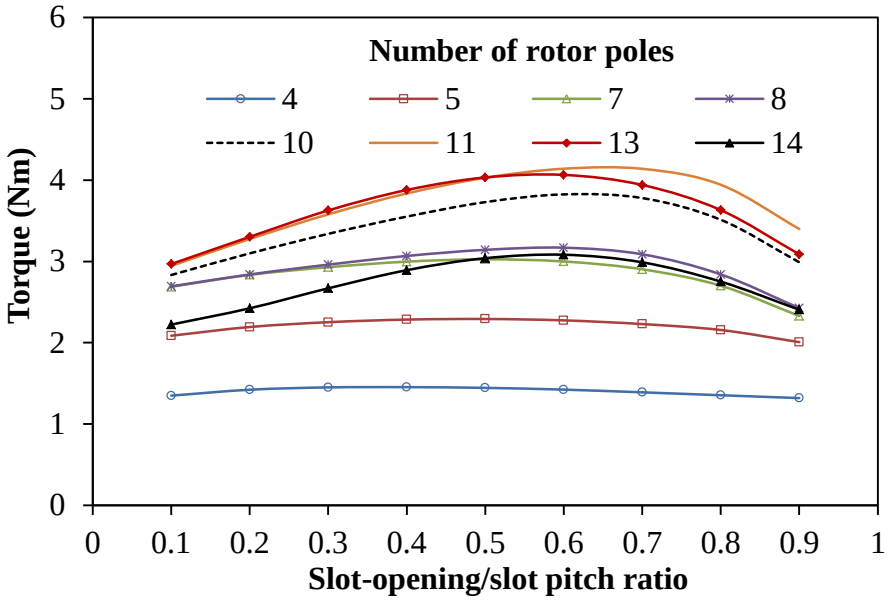

(b) Alternate-pole wound

Fig.4.6 Variation of average torque with slot opening/slot pitch ratio, i_d=0.

Similarly, the variation of average torque with the rotor radial thickness is depicted in Fig.4.7. An optimum rotor radial thickness will be obtained when there is a balance between the saturation effect due to thinner rotor radial width and the impact of small slot area due to the effect of over enlarged rotor radial thickness. A compromise between these two situations

will yield an optimum result. The optimum values of the radial thickness are given in Tables 4.1 and 4.2.

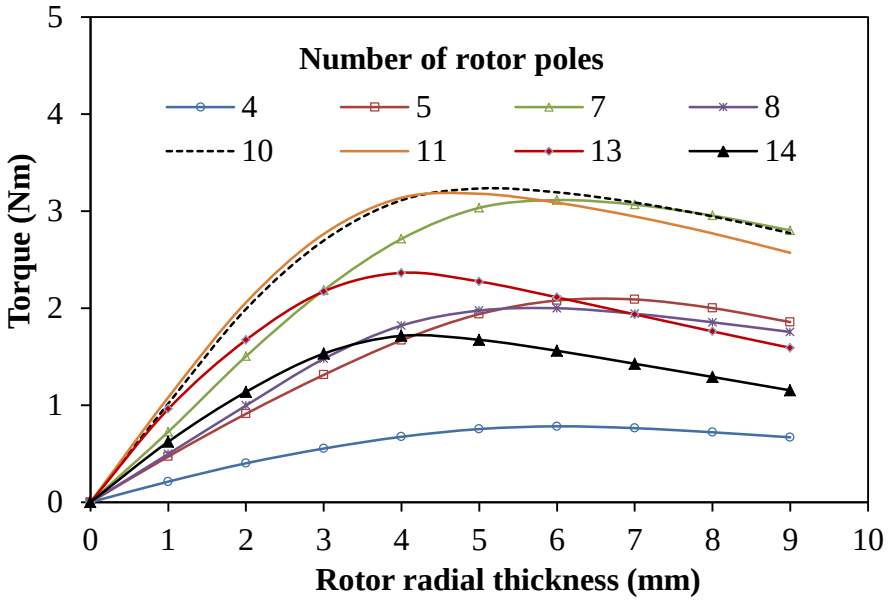

(a) All-pole-wound

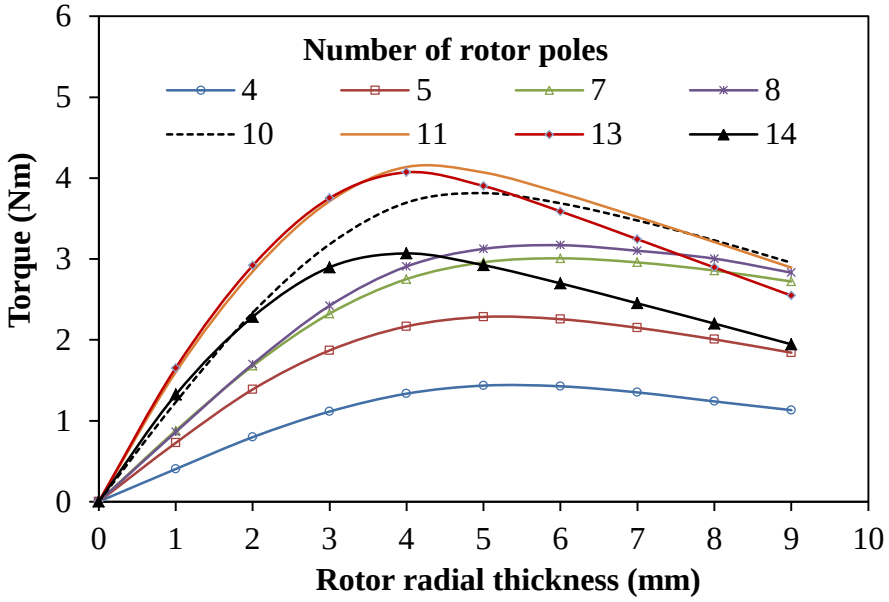

(b) Alternate-pole-wound

Fig.4.7 Variation of average torque with rotor radial thickness, i_d=0.

Further, the variation of average torque with both outer and inner arcs/pitch ratio is shown in Figs.4.8. The optimum values of these parameters are given in Tables 4.1 and 4.2.

(I) All-pole wound (II) Alternate-pole wound

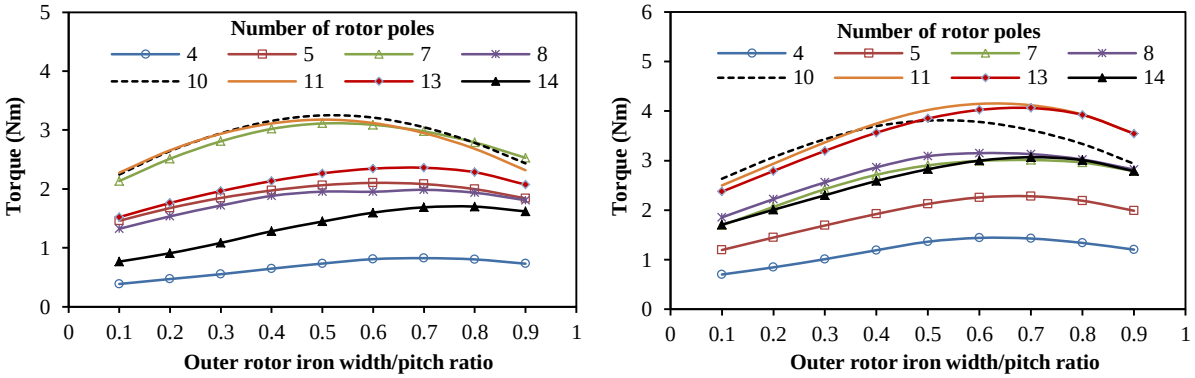

(a) Torque versus outer rotor iron width/pitch ratio pole

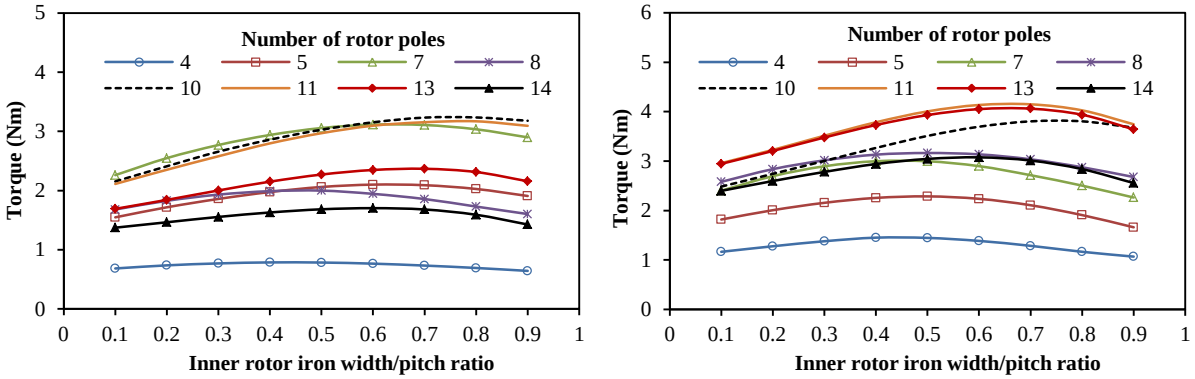

(b) Torque versus inner rotor iron width/pitch ratio pole

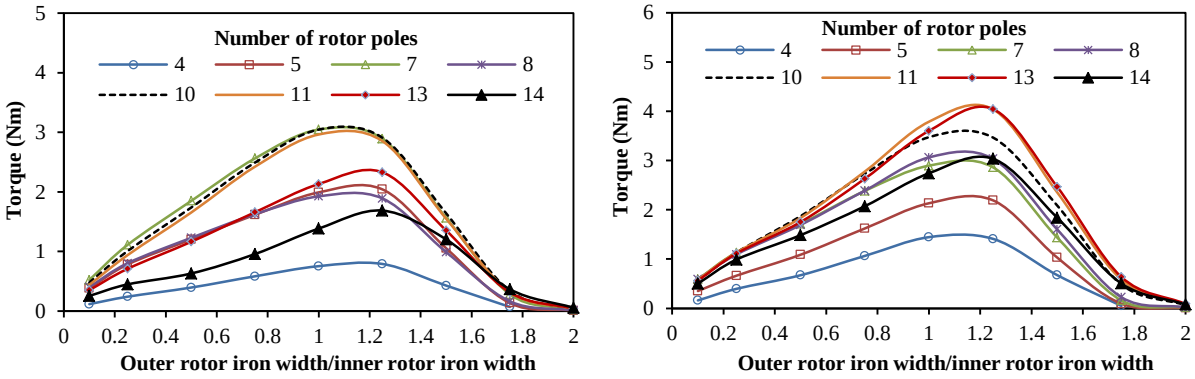

(c) Outer rotor iron width/inner rotor iron width

Fig.4.8 Variation of average torque with outer and inner rotor pole arc.

Moreover, it can be seen from Figs.4.9 and 4.10 that the average torques of the machines are sensitive to both the back-iron thickness and the stator tooth-width as they affect the magnetic saturation as well as the available slot areas. Therefore, there is an optimum for either the back-iron thickness or the stator tooth-width.

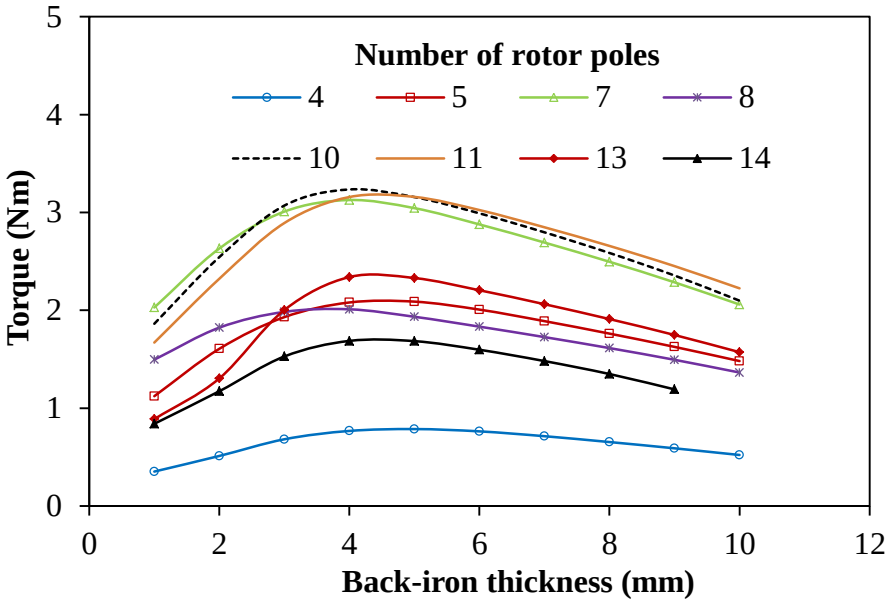

(a) All-pole-wound

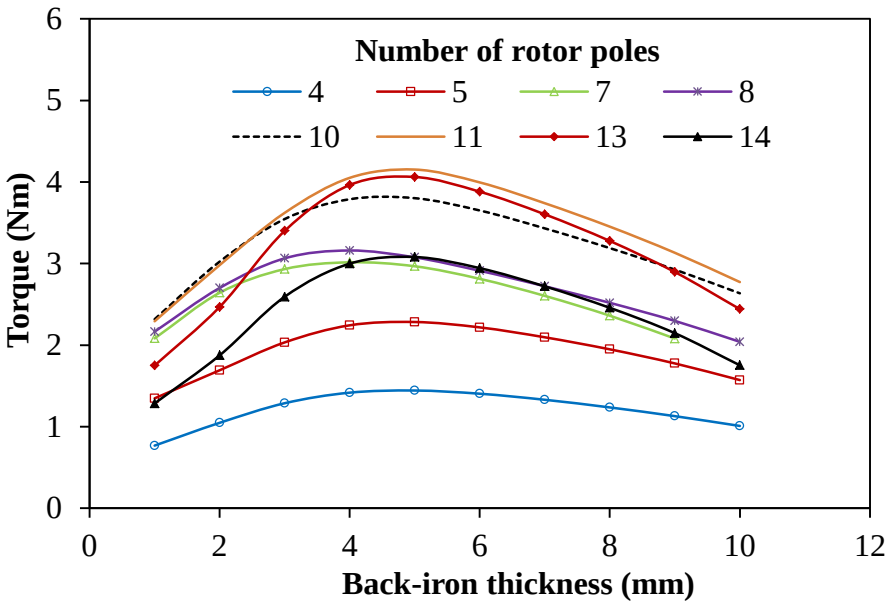

(b) Alternate-pole-wound

Fig.4.9 Variation of average torque with outer stator back-iron thickness, i_d=0.

(I) All-pole wound (II) Alternate-pole wound

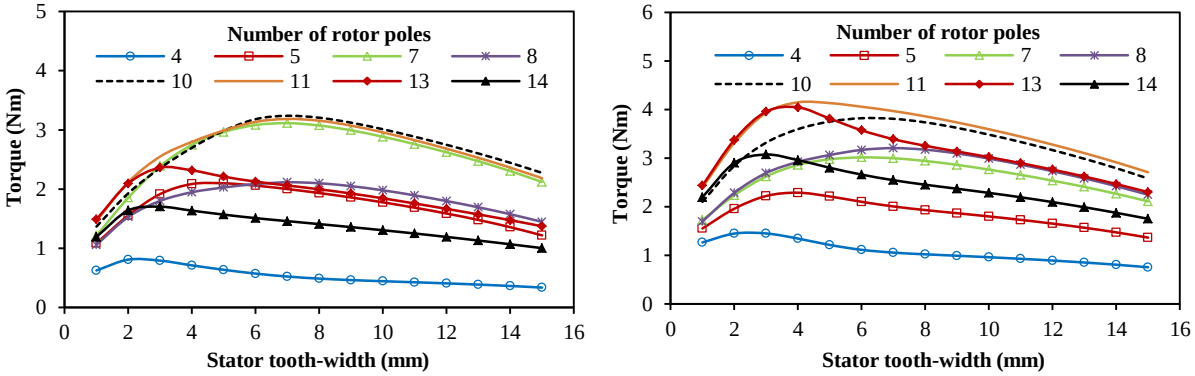

(a) Torque versus stator tooth width

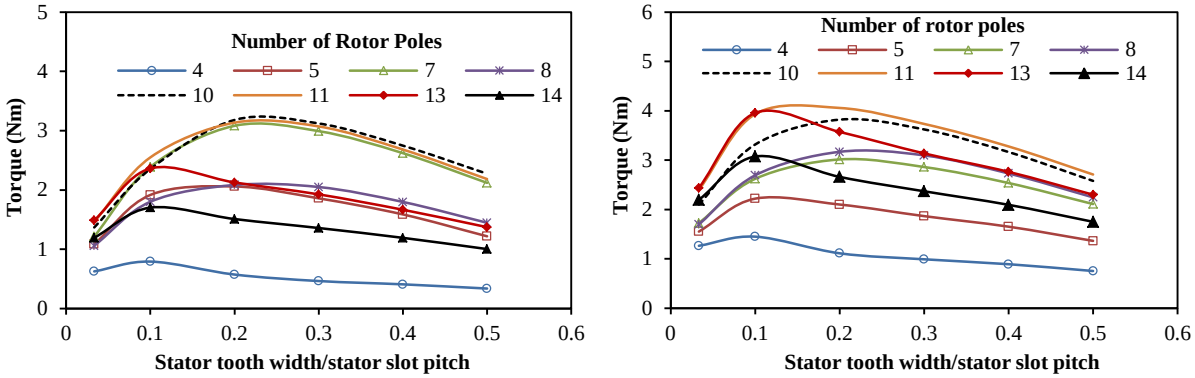

(b) Torque versus stator tooth width/stator slot pitch

Fig.4.10 Variation of average torque with stator tooth-width, i_d=0.

4.3 All- and alternate-pole wound machine configurations

In this section, we will present the electromagnetic performance of the all- and alternate-pole wound machines at both open-circuit and on-load conditions, which include the coil/phase flux-linkages, back-EMFs, and torque characteristics. The winding inductance characteristics will also be given.

4.3.1 Open-circuit coil and phase flux linkage and emf waveforms/spectra

The waveforms and spectra of the coil and phase flux linkages and emfs of the analysed machines having different rotor-pole combinations with various rotor positions is shown in Fig.4.11. For the all-pole-wound machines, it is worth noting that the orthogonal coils always have different coil flux linkage and emf waveforms, while the diametrically opposite coils will have the same coil flux linkage and emf waveforms if the number of rotor poles is even, otherwise, i.e. when the number of rotor poles is odd, their waveforms also differ. For the alternate-pole-wound machines, there are only the diametrically opposite coils but no

orthogonal coils in the same phase. The same conclusions can be obtained. In general, for the same rotor pole number, the all-pole-wound machines will have less harmonics but also relatively lower amplitudes, compared to the alternate-pole-wound machines.

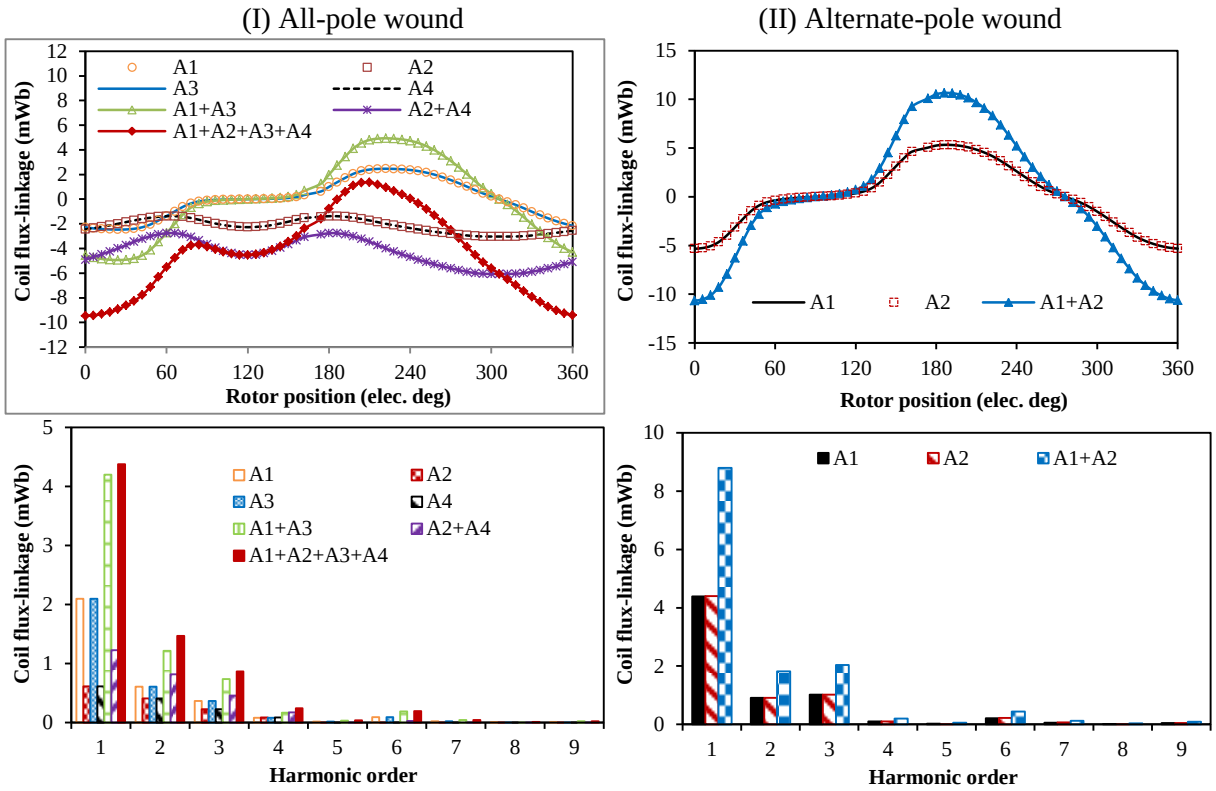

(a) 4-rotor-pole

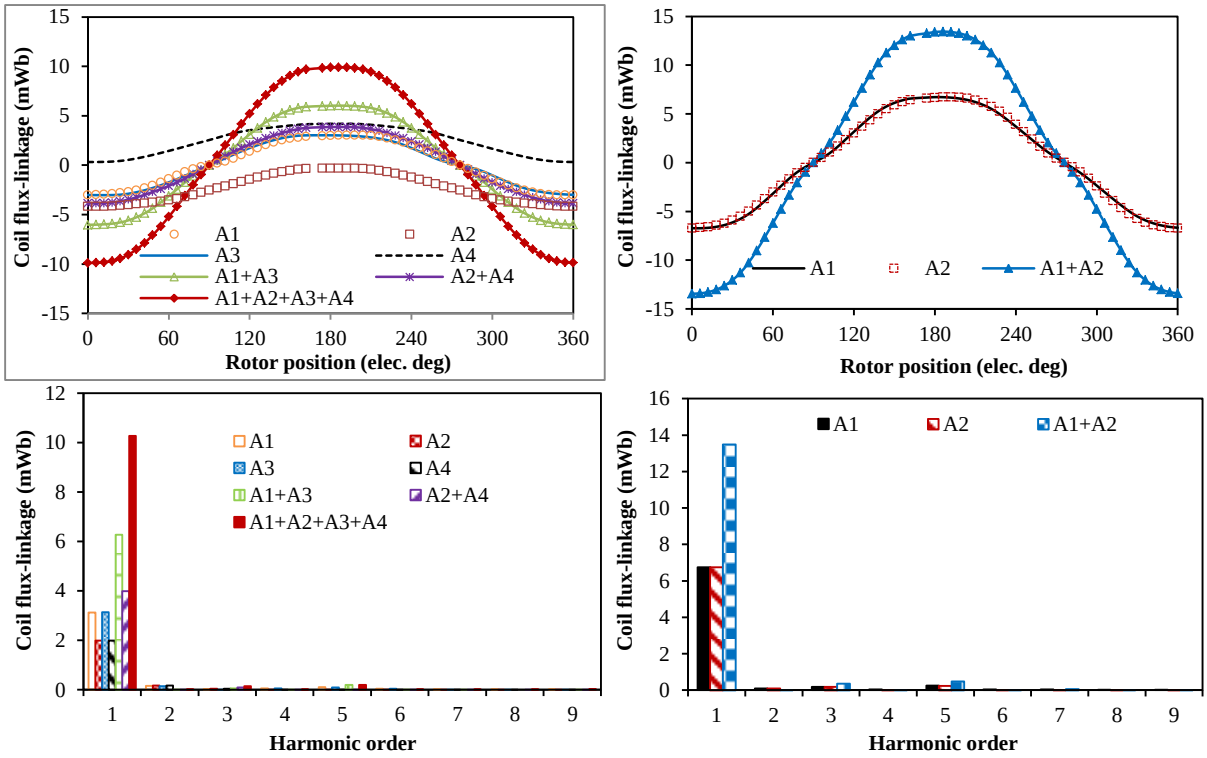

(b) 5-rotor-pole

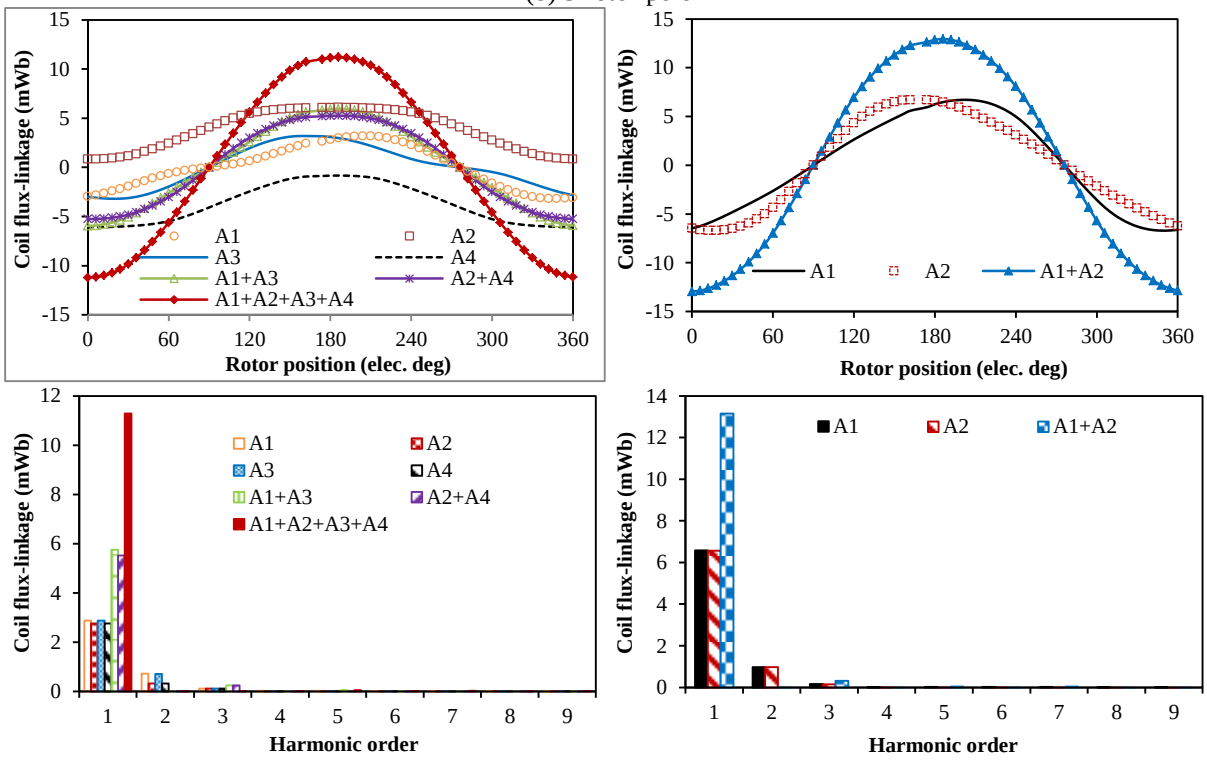

(c) 7-rotor-pole

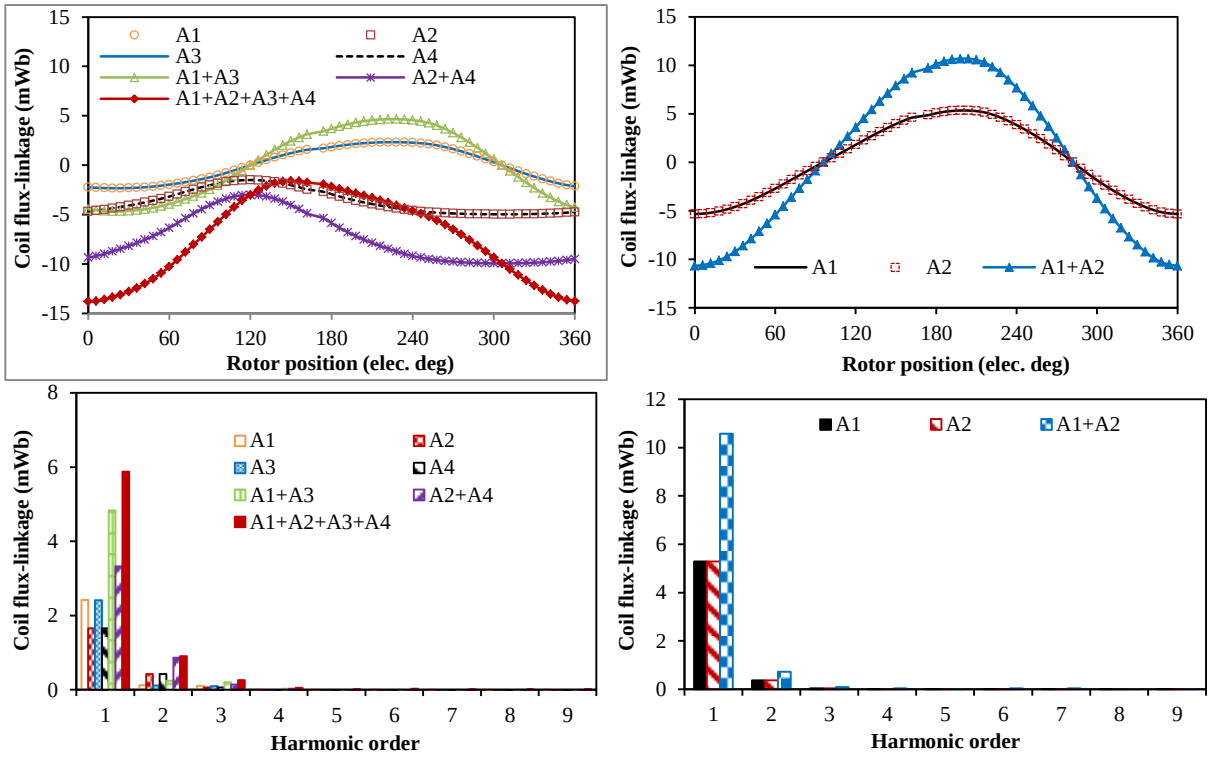

(d) 8-rotor-pole

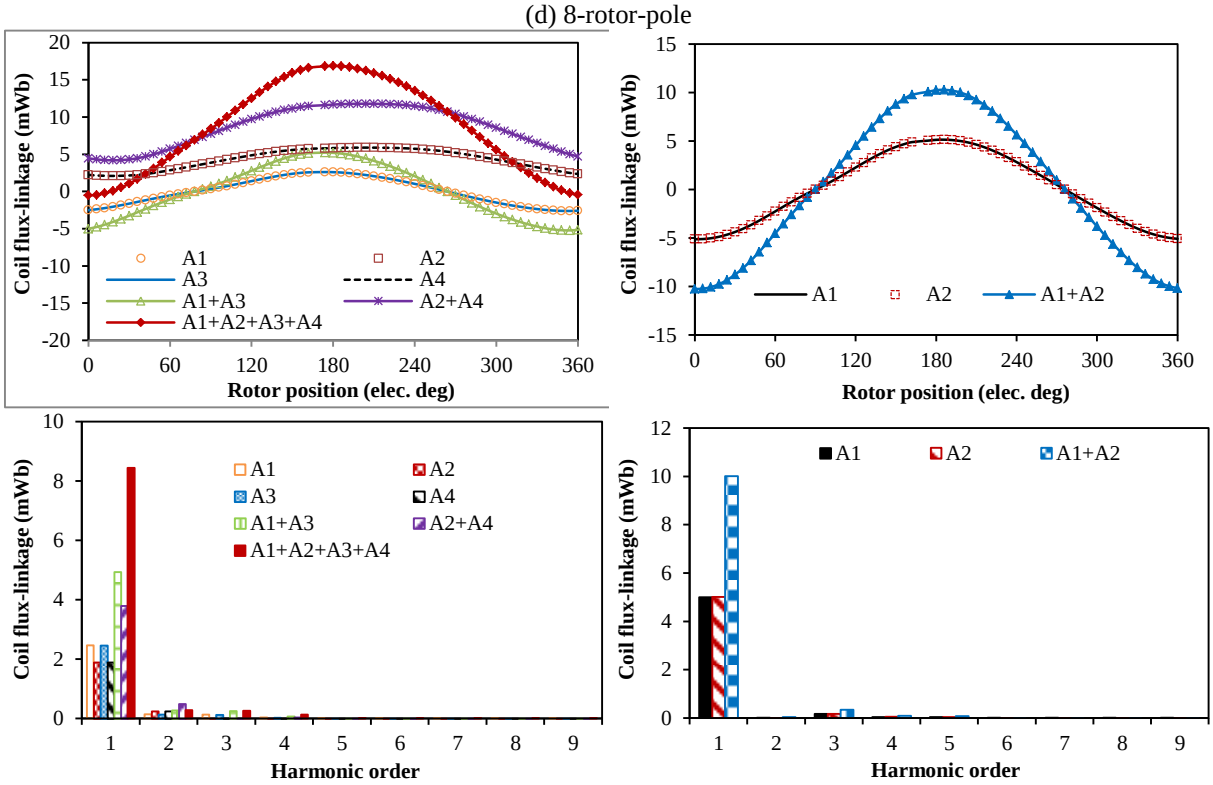

(e) 10-rotor-pole

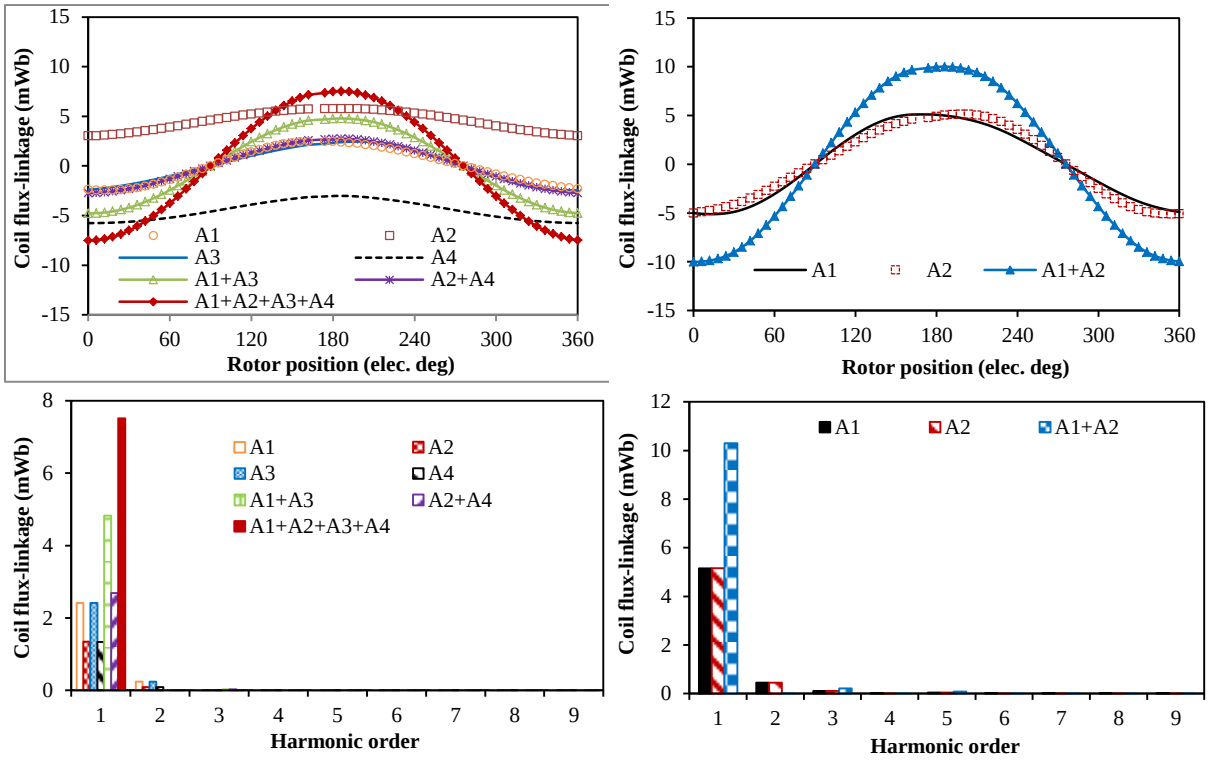

(f) 11-rotor-pole

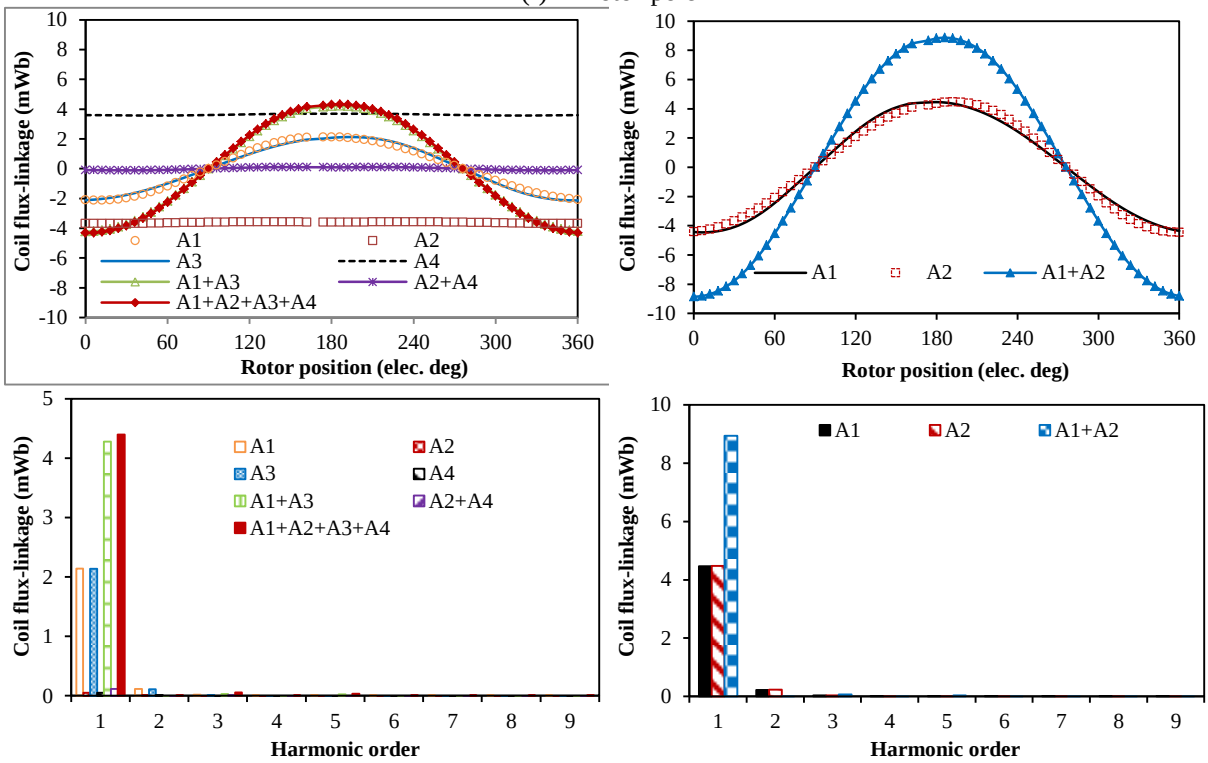

(g) 13-rotor-pole

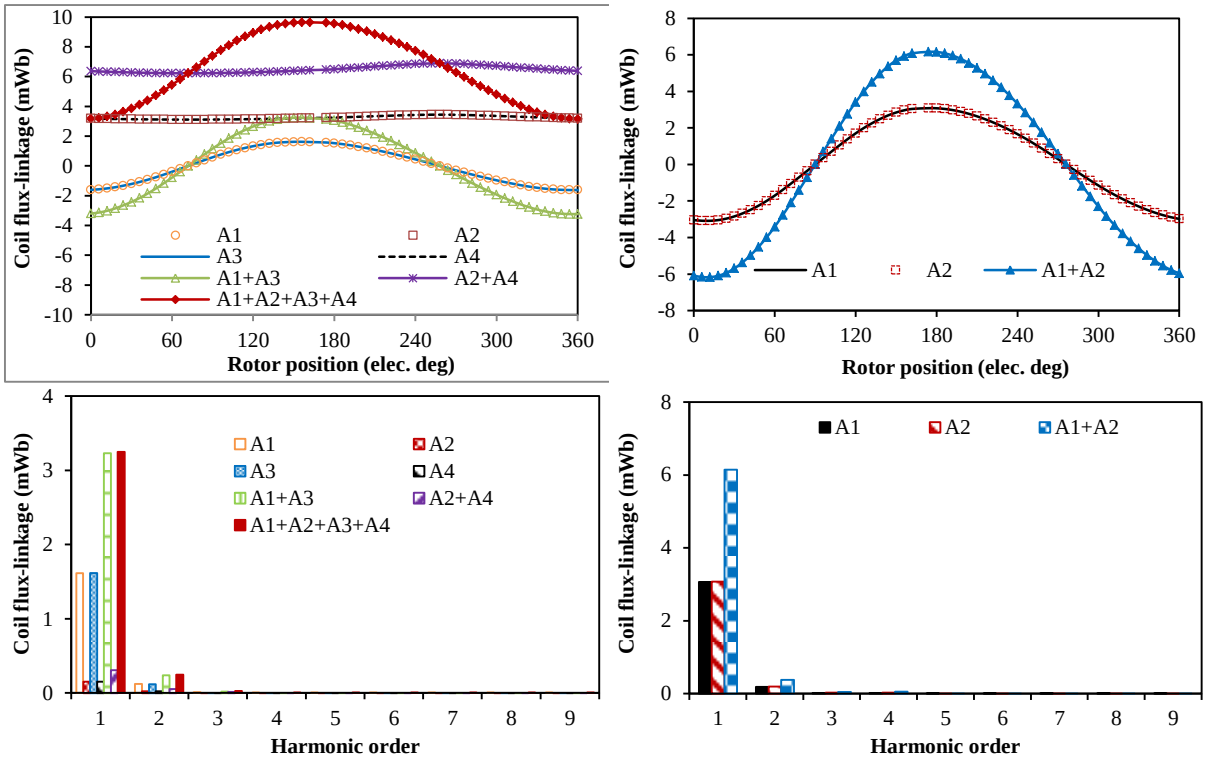

(h) 14-rotor-pole

Fig.4.11 Comparison of open-circuit coil flux linkages in analysed machines having all-pole wound.

Figs.4.12 and 4.13 compares the phase flux-linkage waveforms and spectra of the anayzed all- and alternate-pole-wound machines having different rotor pole numbers. It can be clearly seen that the flux linkage waveforms of the even-rotor pole machines are unipolar while their odd-rotor pole counterparts have bipolar waveforms. Note also that the 5- and 7-pole machines exhibit relatively more sinusoidal and symmetrical waveforms, as well as relatively higher flux-linkage values than the other analysed machines owing to their high flux per pole characteristics. Nevertheless, as said before, the alternate-pole-wound machines exhibits higher peak-to-peak and fundamental flux-linkage values than their all-pole-wound equivalents. It should also be noted that the flux-linkage waveforms of the even rotor pole machines are both non-sinusoidal and asymmetric about the rotor position.

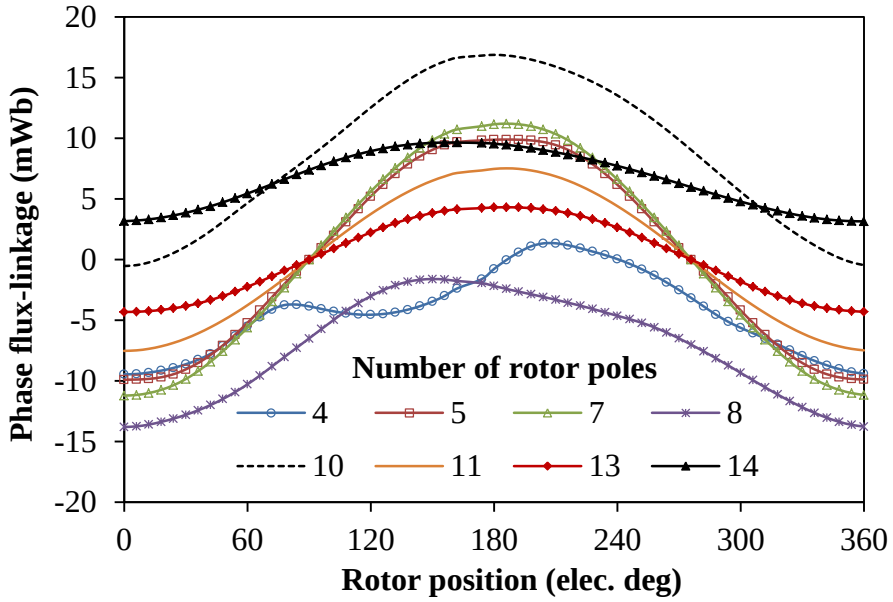

(a) Waveforms

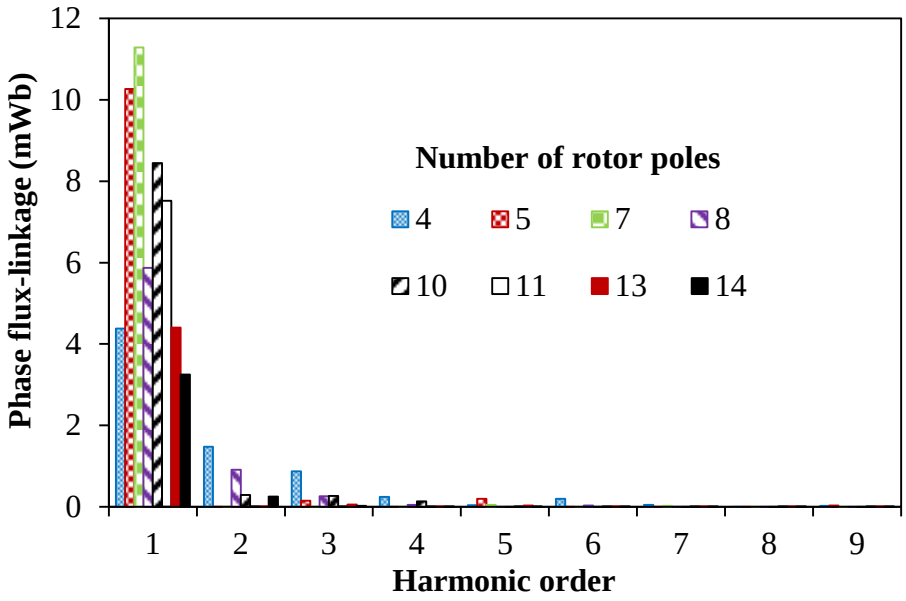

(b) Harmonics

Fig.4.12 Open-circuit flux-linkage variation with rotor position in all-pole wound machines.

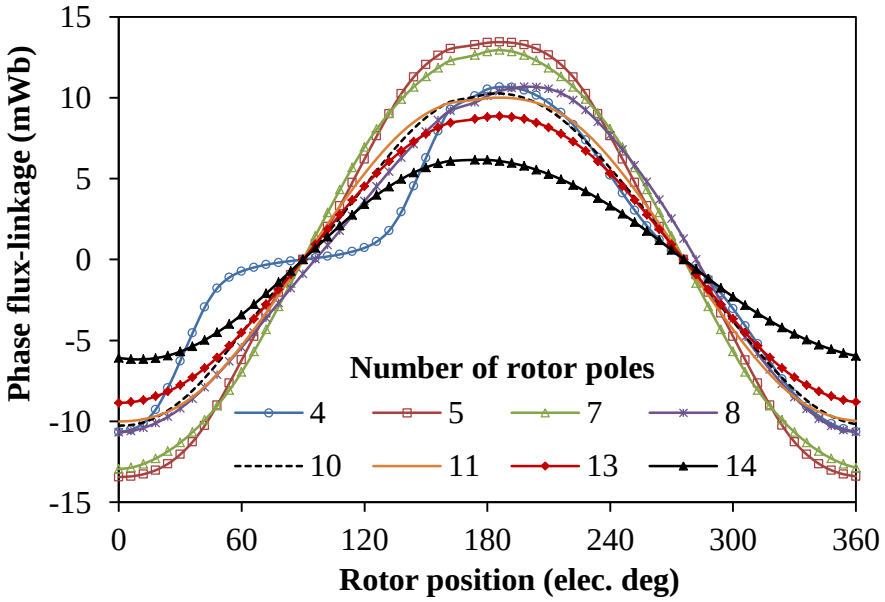

(a) Waveforms

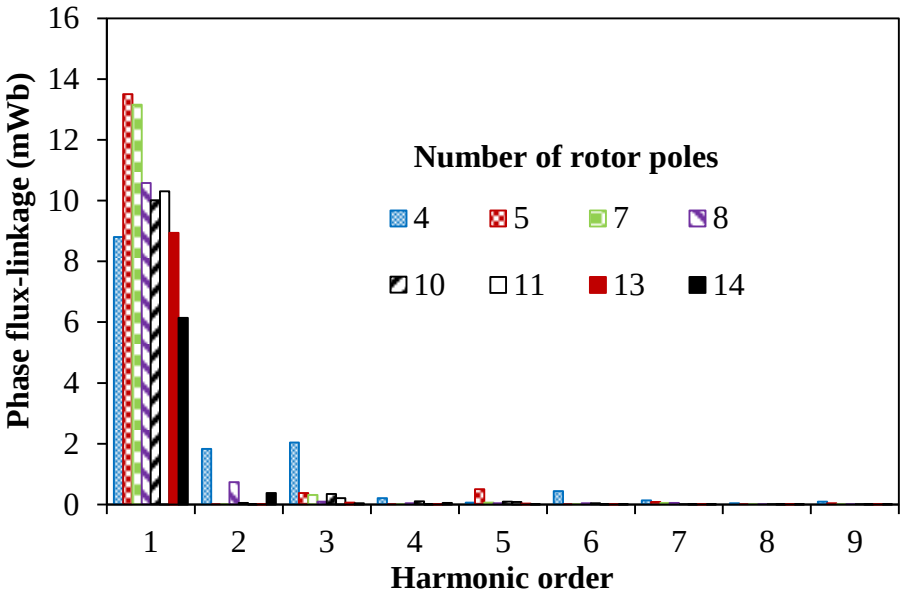

(b) Spectra

Fig.4.13 Open-circuit flux-linkage variation with rotor position in alternate-pole wound machines.

The open-circuit back-EMFs are compared in Fig.4.14 (a) together with the harmonic spectra in Fig.4.14 (b). After adopting alternate-pole-wound topology, the fundamental back-EMF of the analysed machines is much larger than their counterparts having all-pole-wound. Moreover, the largest fundamental back-EMF is obtained in the 10-pole and 13-pole machines having all- and alternate-pole-wound, respectively. The results also reveal that the

even-rotor pole machines are characterized by even order harmonics, which is the root causing asymmetric waveform.

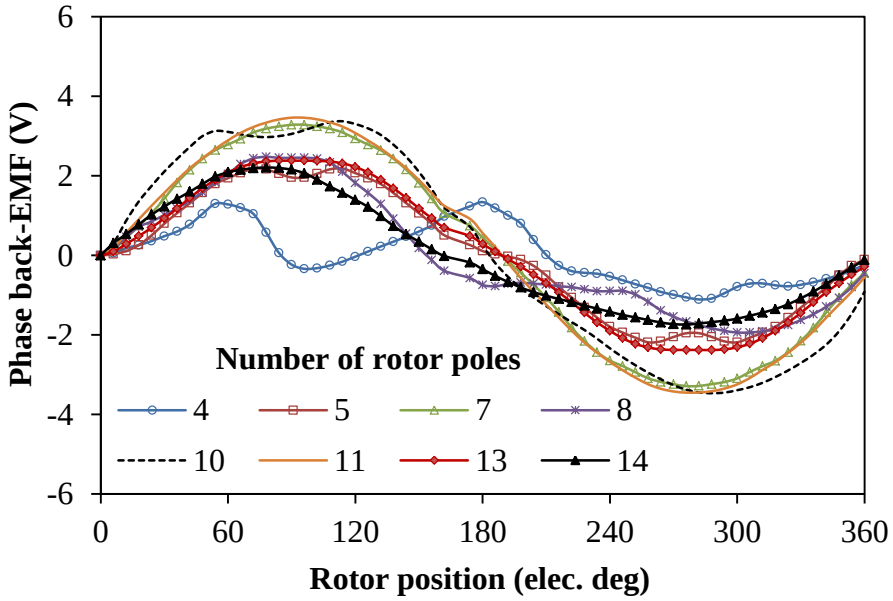

(a) Waveforms

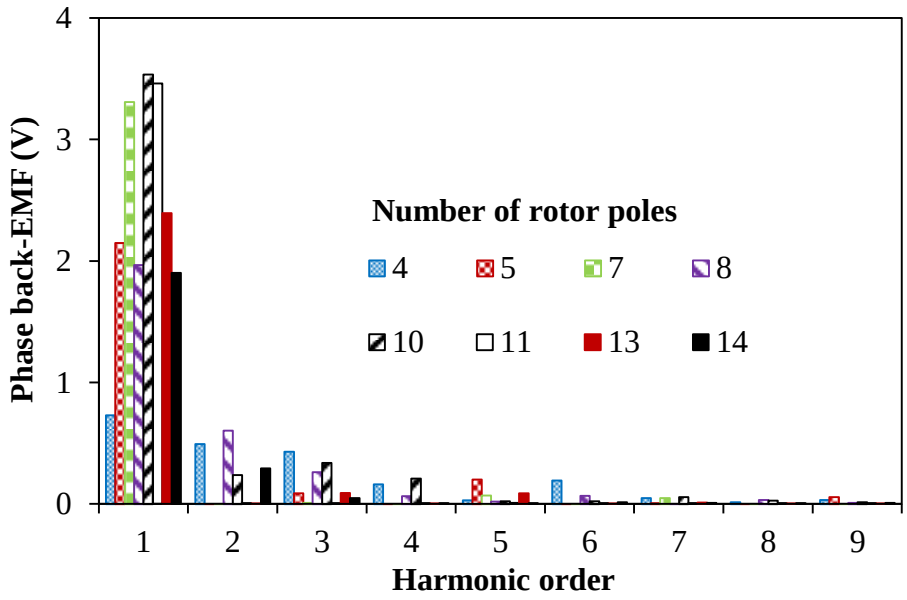

(b) Spectra

Fig.4.14 Comparison of open-circuit phase back-EMF in the analysed machines having all-pole-wound, 400rpm.

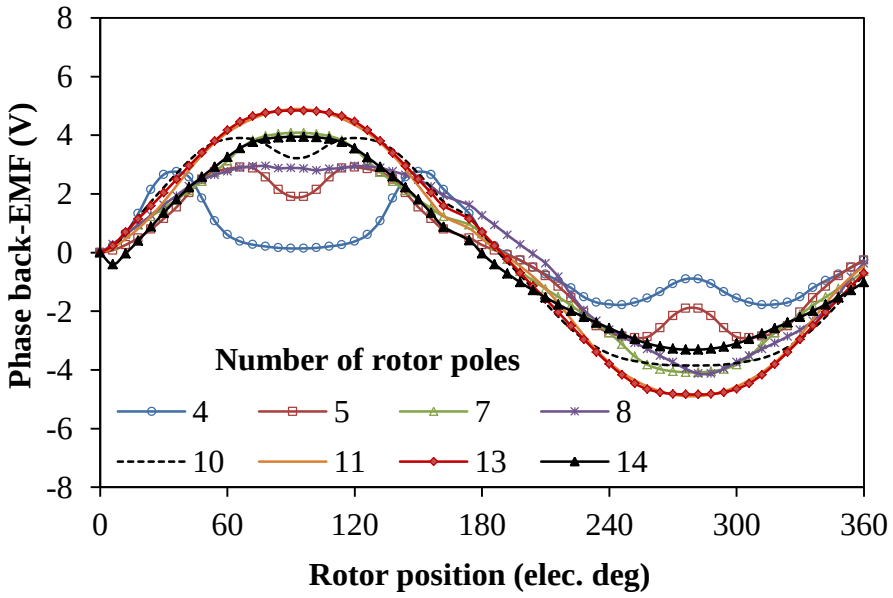

(a) Waveforms

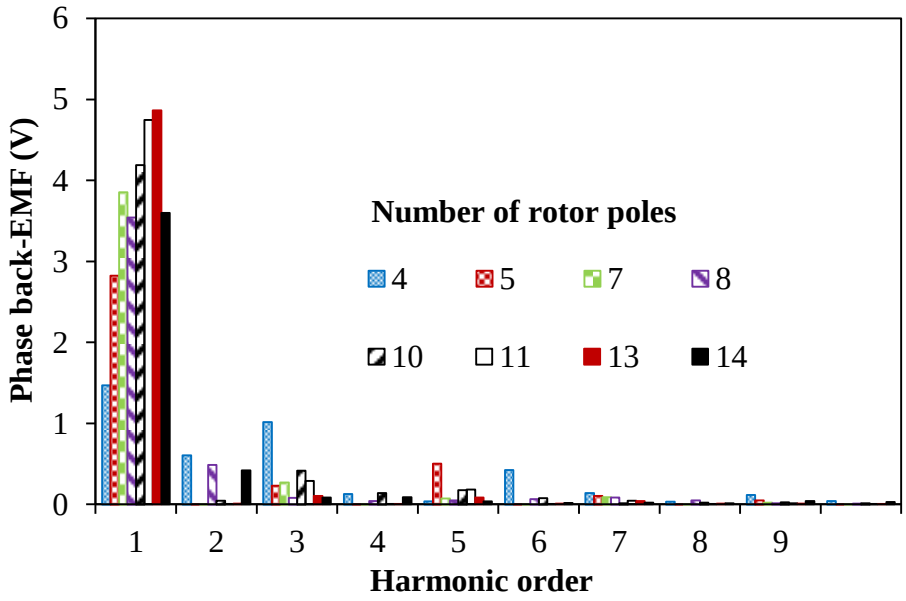

(b) Spectra

Fig.4.15 Comparison of open-circuit phase back-EMF in the analysed machines having alternate-pole-wound, 400rpm.

4.3.2 Torque ripple and total harmonic distortion

The cogging torque occurs as a result of the magnetic interaction between the stator poles and the permanent magnets as the rotor rotates. The order of cogging torque of the proposed machines is given by:

$$Cog.Torq._{order} = \frac{LCM(N_r, N_s)}{N_r} \tag{4.4}$$

where *LCM* is the lowest common multiple of the stator and rotor pole (N_s and N_r) combinations.

The cogging torque waveforms and spectra of the analysed machines are depicted in Fig.4.16. The even-rotor pole machines, especially the 4-pole machine, seem to possess significant amount of cogging torque.

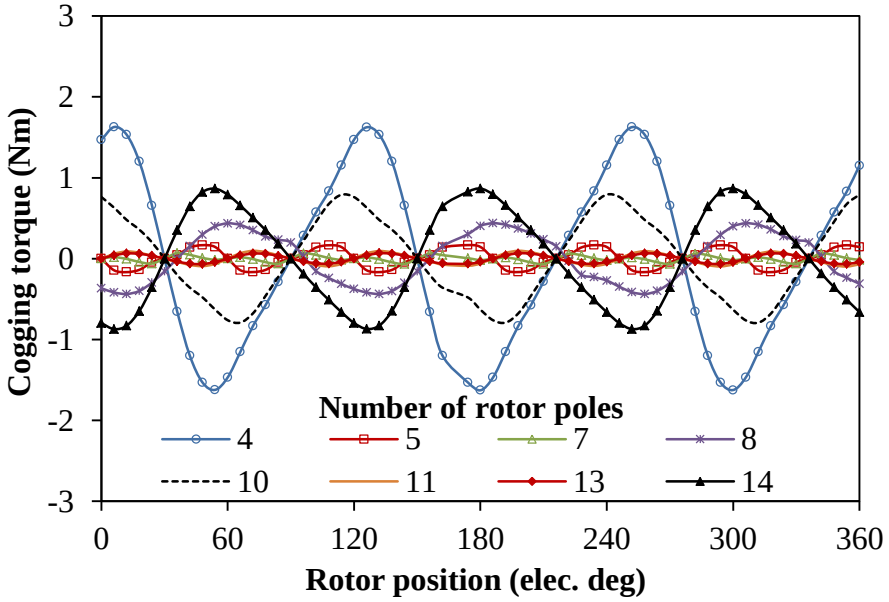

(a) Waveforms

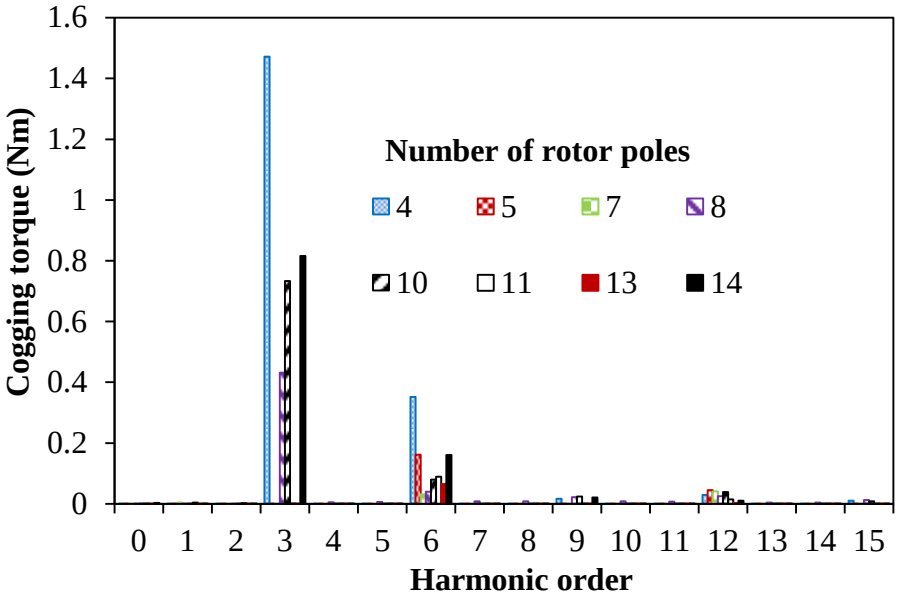

(b) Spectra

Fig.4.16 Comparison of cogging torques in analysed machines.

Torque ripples and total harmonic distortions (THD) at different load conditions (copper loss) are shown in Figs.4.17 and 4.18 respectively. The results in Fig. 4.17 show that the even-rotor pole machines exhibit the large amount of torque ripple at all conditions. The 4-pole machine has the largest torque ripple and THD compared to its counterparts. Thus, similar trend in THD is seen in Fig. 4.18. The machines with low THD indicate that they have more sinusoidal back-EMF waveforms and thus fewer harmonics.

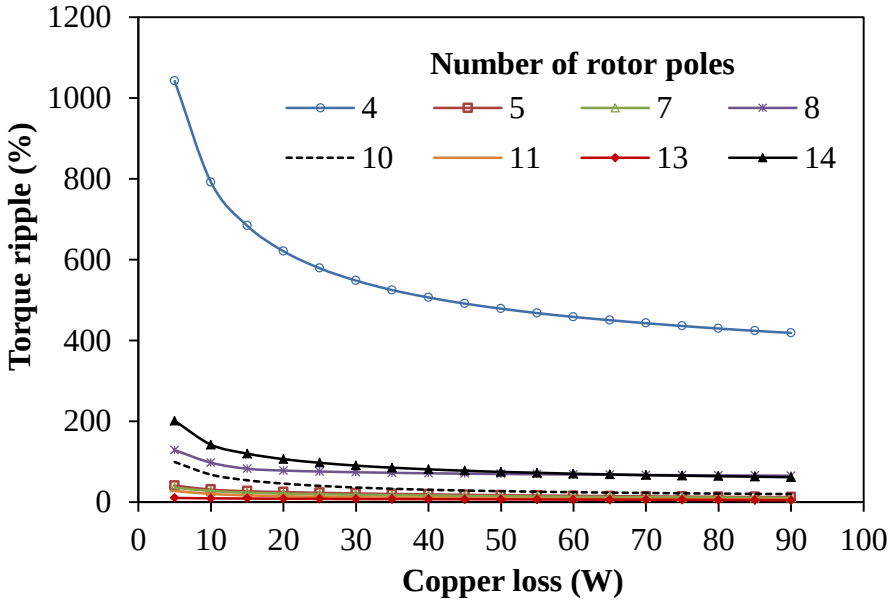

(a) All-pole-wound

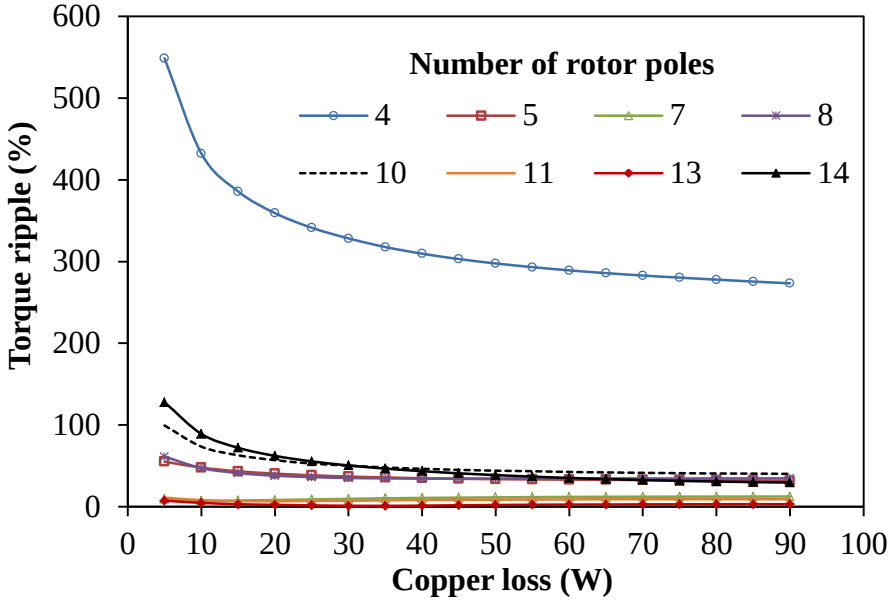

(b) Alternate-pole-wound

Fig.4.17 Variation of torque ripple with q-axis current, i_d=0.

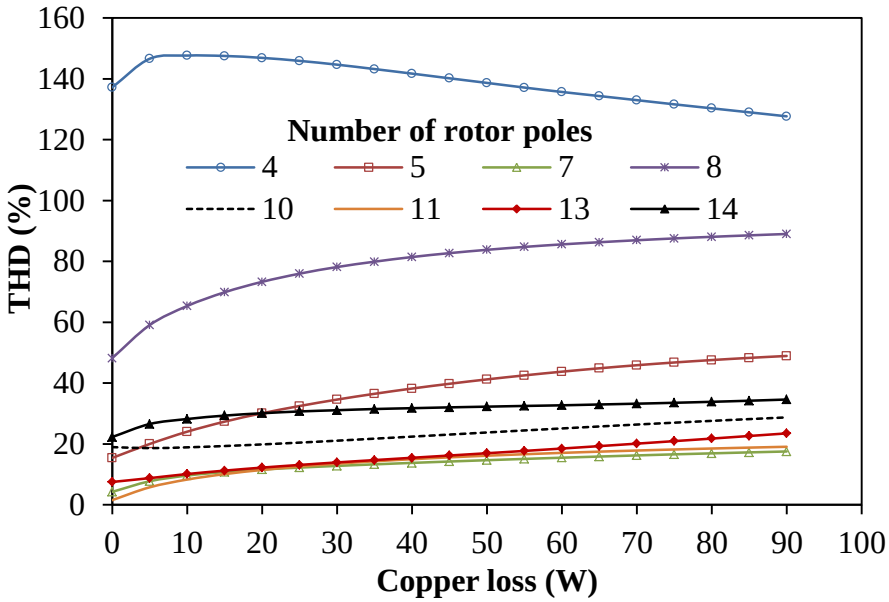

(a) All-pole-wound

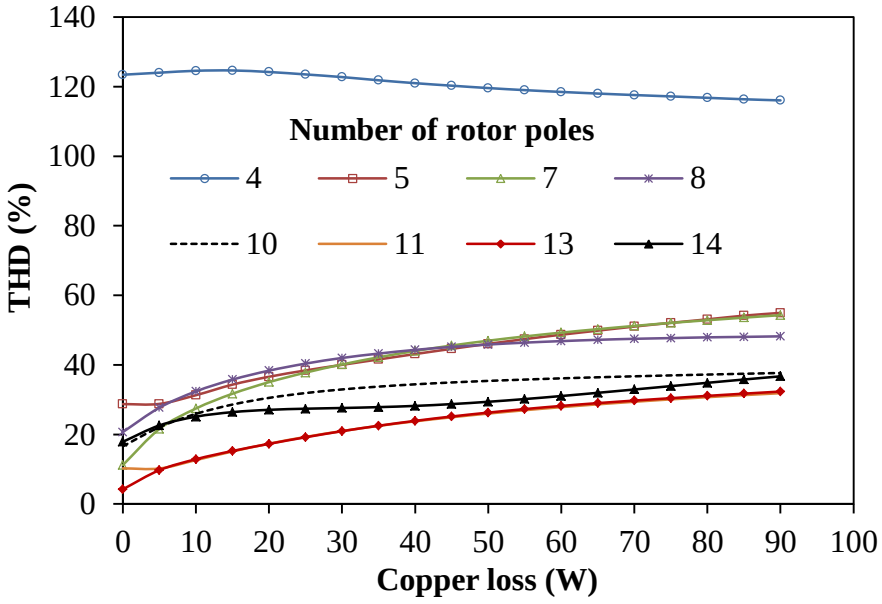

(b) Alternate-pole-wound

Fig.4.18 Variation of total harmonic distortions (THD) with *q*-axis current.

4.3.3. On-load performance

Figs.4.19 and 4.20 compare the torque waveforms of all the analysed machines under copper loss p_{cu}=30W, with zero *d*-axis current control (i_d=0). The i_d=0 control is adopted in this analysis due to negligible reluctance torque in the analysed machines. Similar to the differences in back-EMFs, the average torque of the machines with alternate-pole-wound is

much higher than that of all-pole-wound counterparts, albeit with higher torque ripples in general.

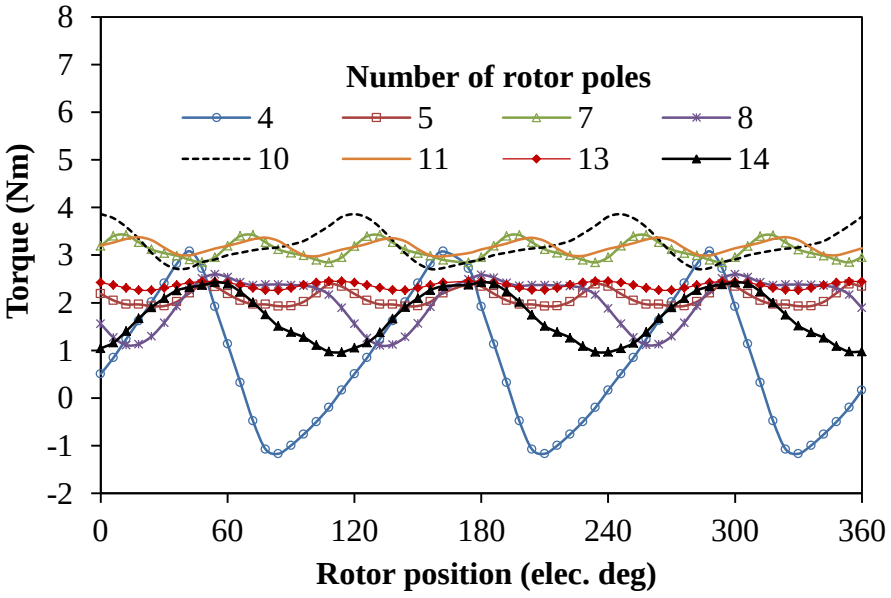

(a) Waveforms

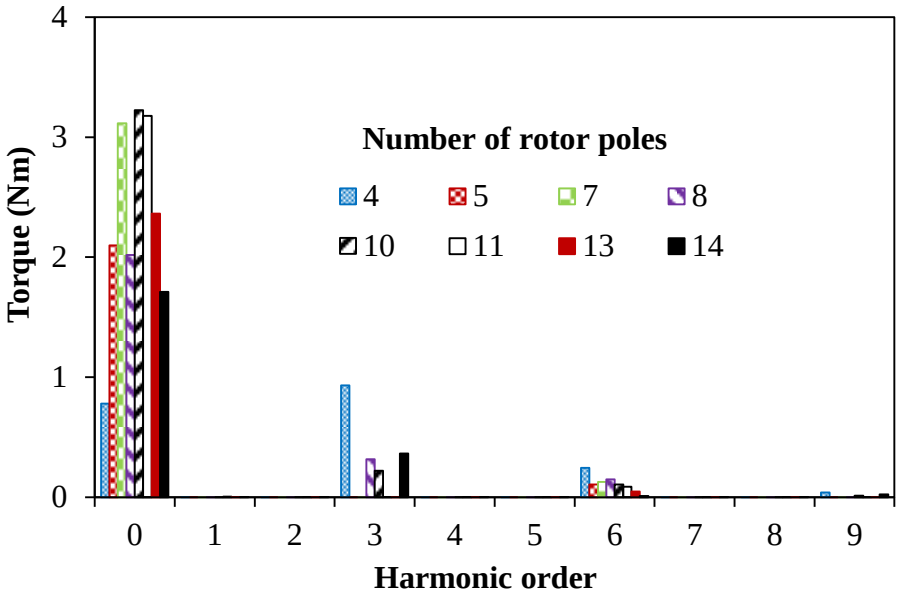

(b) Spectra

Fig.4.19 Comparison of torque waveforms and spectra in all-pole-wound machines, (copper loss = 30W, i_d=0).

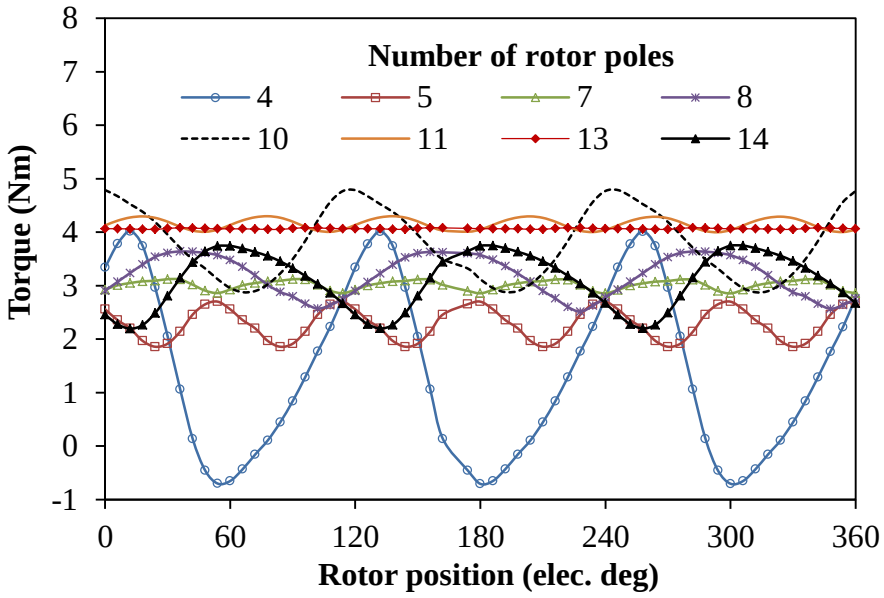

(a) Waveforms

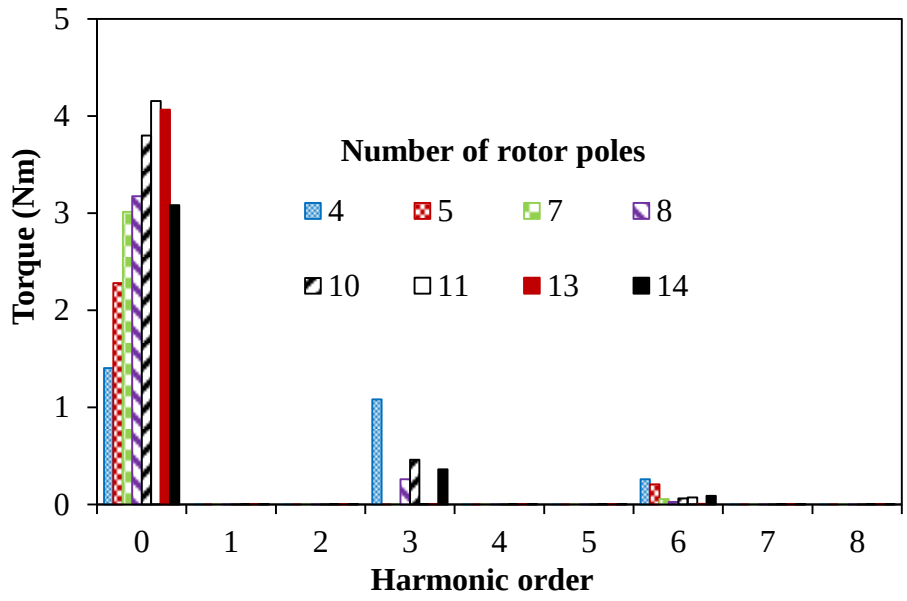

(b) Spectra

Fig.4.20 Comparison of torque waveforms and spectra in alternate-pole-wound machines (copper loss = 30W, i_d=0).

Further, the variations of average torque against current and current density are shown in Figs.4.21 and 4.22. The results reveal that when the magnetic circuit is not severely saturated, the 10-pole and 11-pole machines have the largest torque density in the respective winding topologies, i.e. all- and alternate-pole-wound. The least torque is seen in the 4-pole machines.

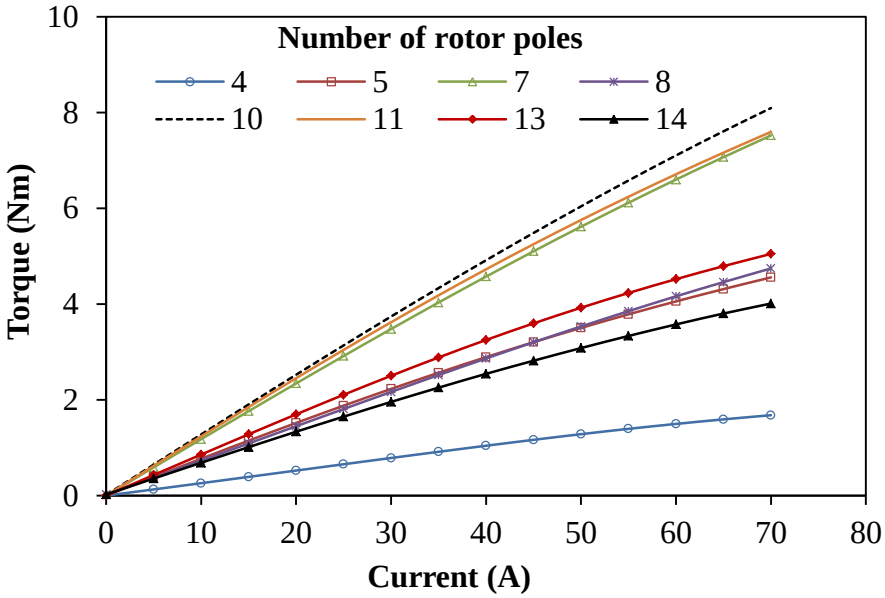

(a) All-pole-wound

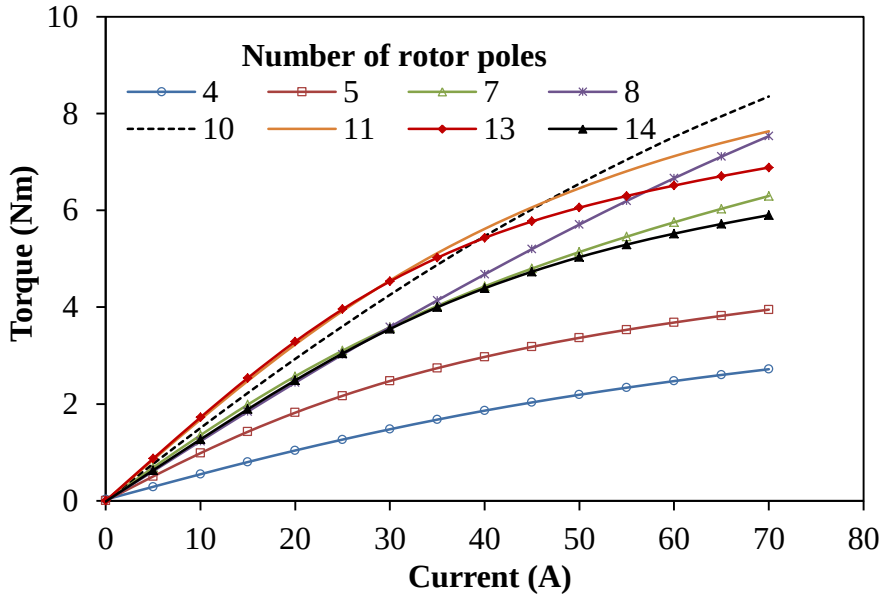

(b) Alternate-pole-wound

Fig.4.21 Comparison of average torque against current, i_d=0.

The saturation curves of the analysed machines are also shown in Figs.4.21 and 4.22 in terms of the torque variation with current density and copper loss, respectively. The 11-pole exhibits larger torque density under rated conditions compared to the other machines, although the 10-pole machines could withstand heavy overload than the rest of other machines, as seen from Figs.4.21, 4.22 and 4.23.

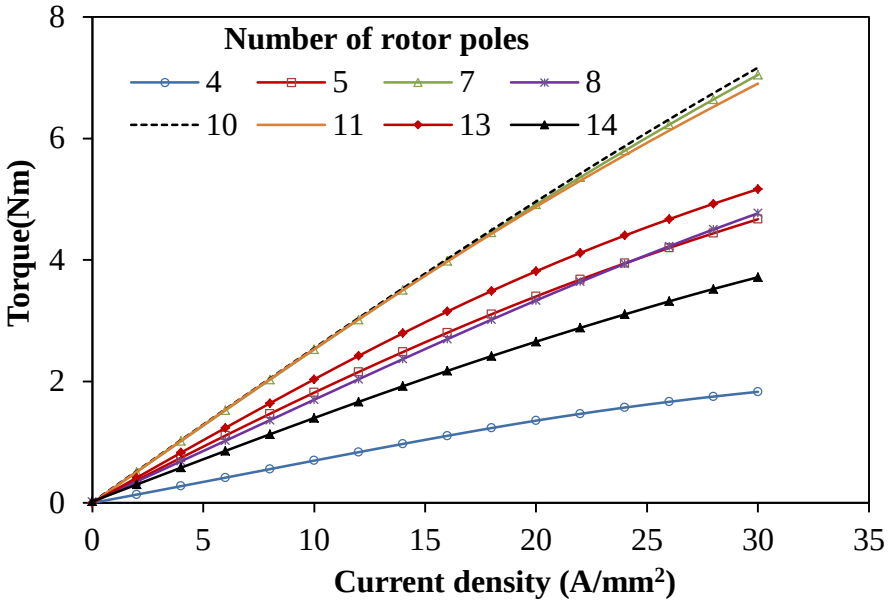

(a) All-pole-wound

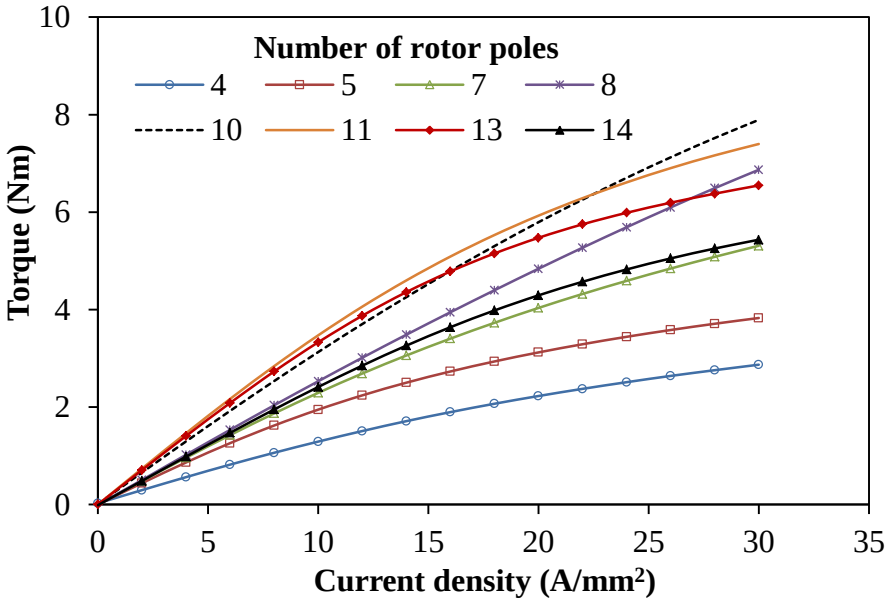

(b) Alternate-pole-wound

Fig.4.22 Comparison of average torque against current density, i_d=0.

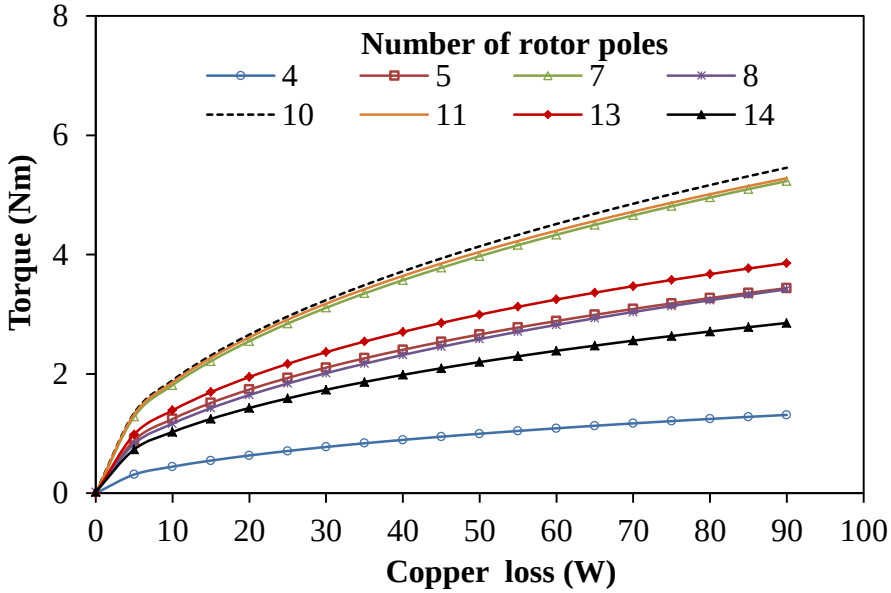

(a) All-pole-wound

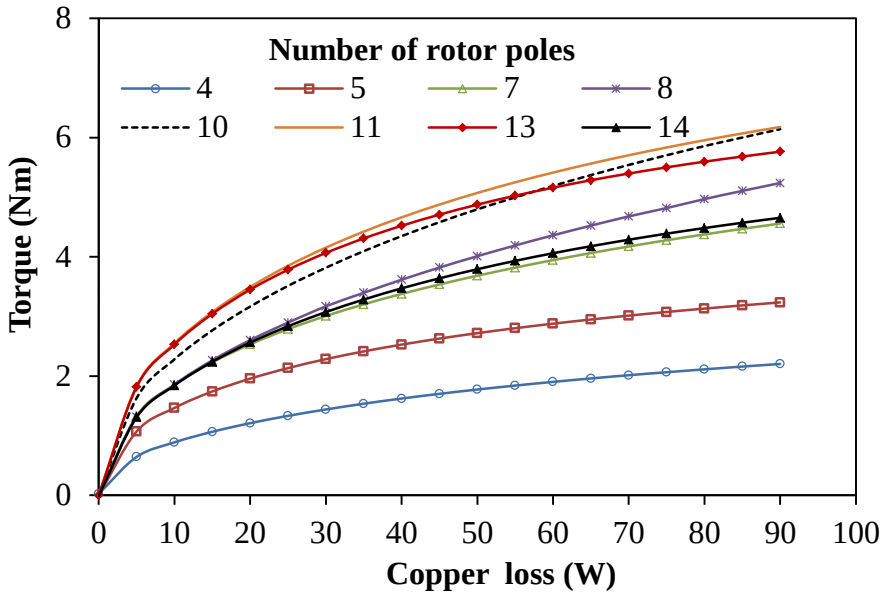

(b) Alternate-pole-wound

Fig.4.23 Comparison of torque against copper loss, i_d=0.

4.3.1 Winding inductances

In this sub-section, the influence of cross-coupling between the *dq*-axis inductances of the analysed machines is accounted for in the calculation. The influence of *dq*-axis currents, i_d and i_q, on the *dq*-axis inductances, L_d and L_q, is shown in Figs.4.24 and 4.25, respectively. For both machines having either all- or alternate-pole-wound, L_d increases with $|i_d|$, although for the machines having all-pole-wound configuration, the influence of $|i_d|$ is very small. The variations of L_d with *q*-axis current i_q in all the analysed machines are negligible. As for L_q, it

generally increases with $|i_d|$ and i_q. However, the influence of i_d and i_q on L_q is insignificant, except for the 14-rotor pole machines whose inductance values are relatively large at very low current. It is worth mentioning that the machines with odd-rotor pole number have higher inductance values than their equivalent even-rotor pole counterparts, as listed in Tables 4.1 and 4.2 and shown in Figs.4.24 and 4.25.

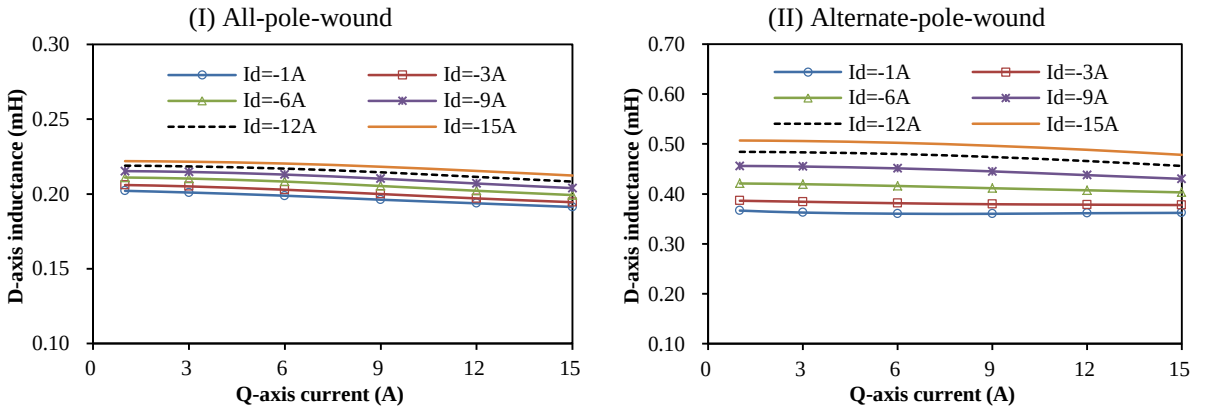

(a) 5-rotor pole

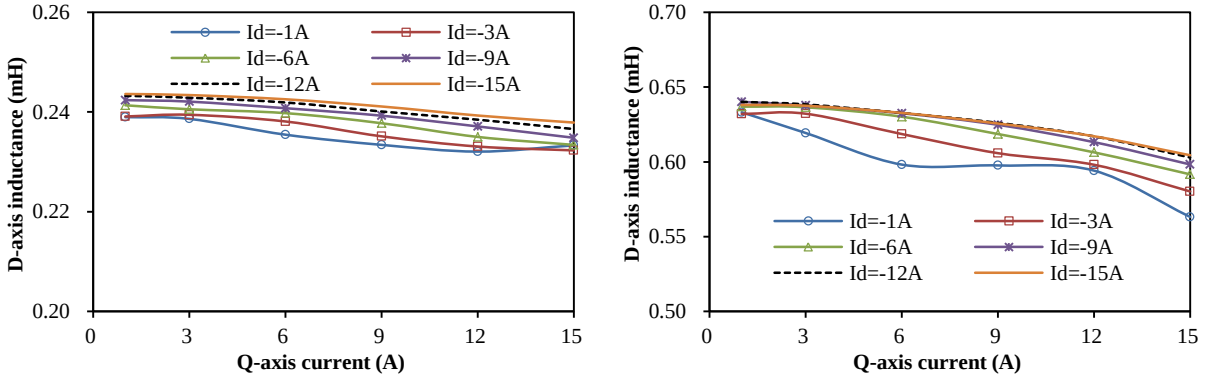

(b) 7-rotor pole

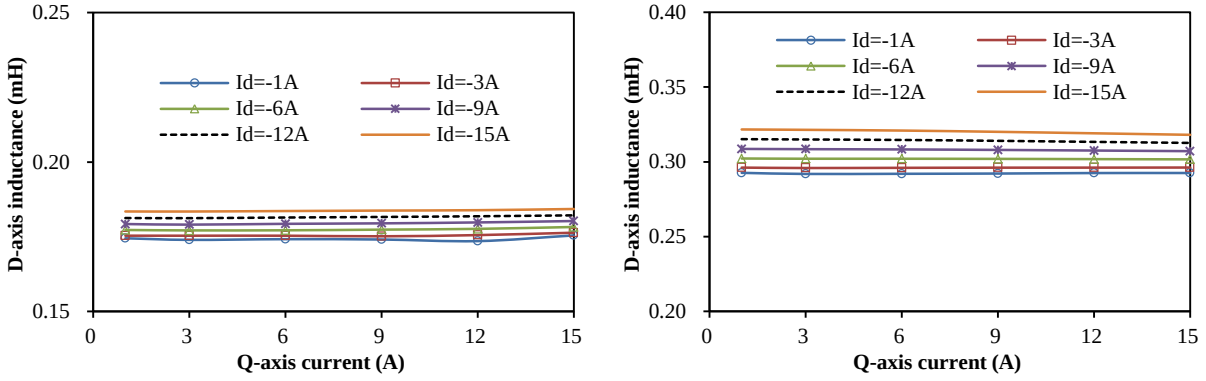

(c) 10-rotor pole

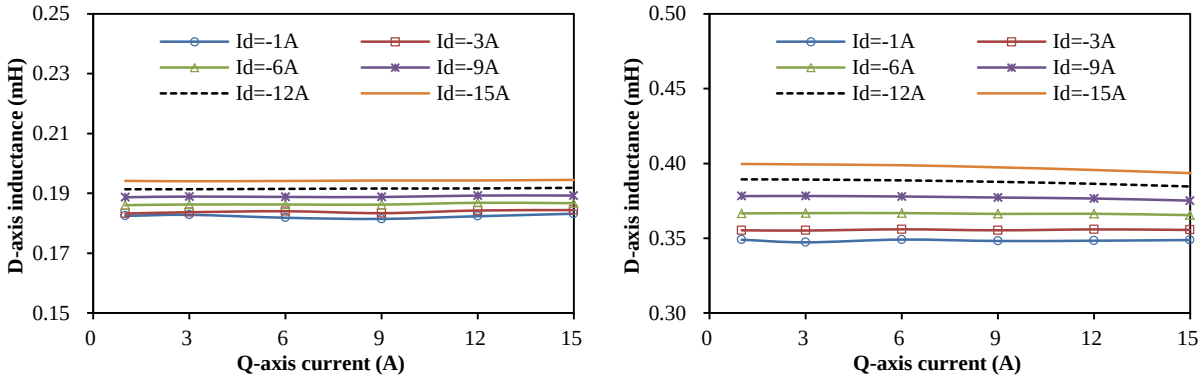

(d) 11-rotor pole

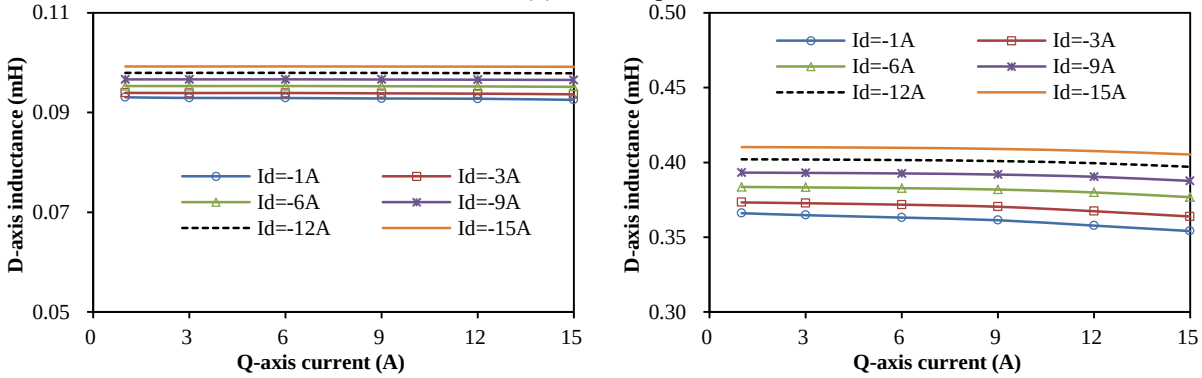

(e) 13-rotor pole

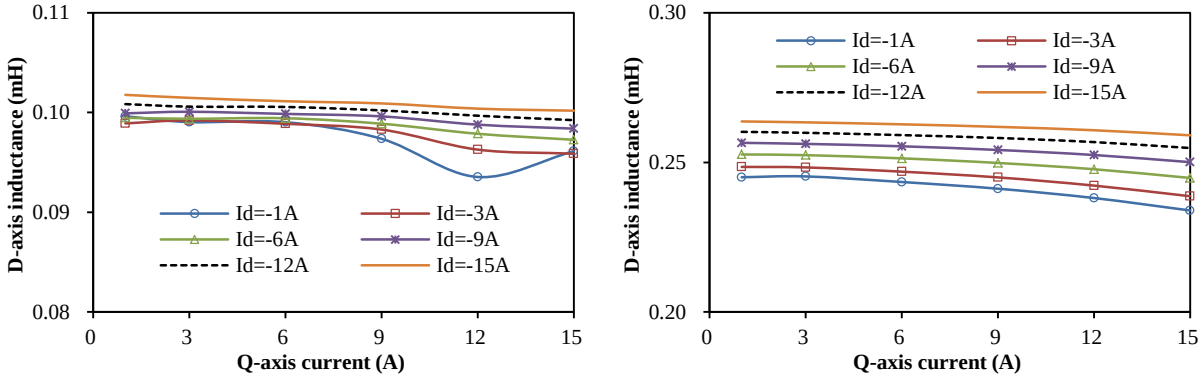

(f) 14-rotor pole

Fig.4.24 Variation of *d*-axis inductance L_d against i_d and i_q.

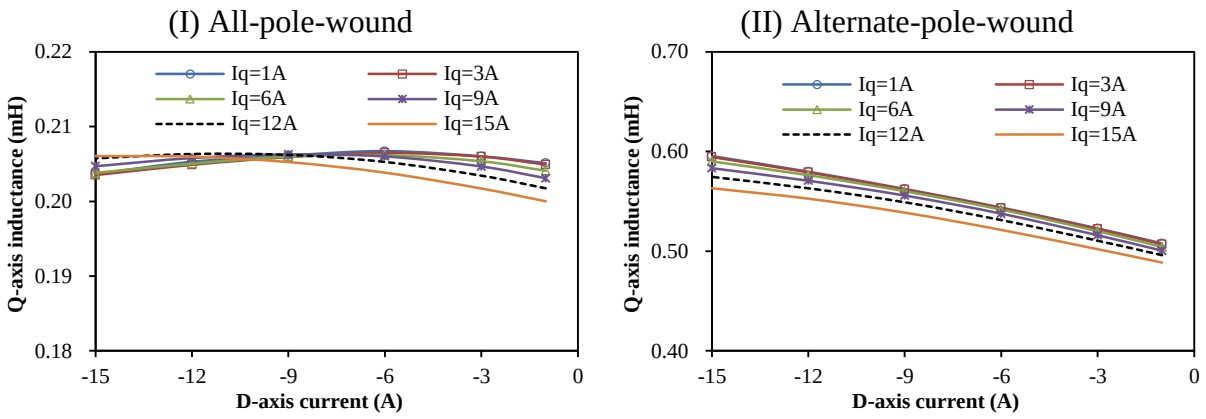

(a) 5-rotor pole

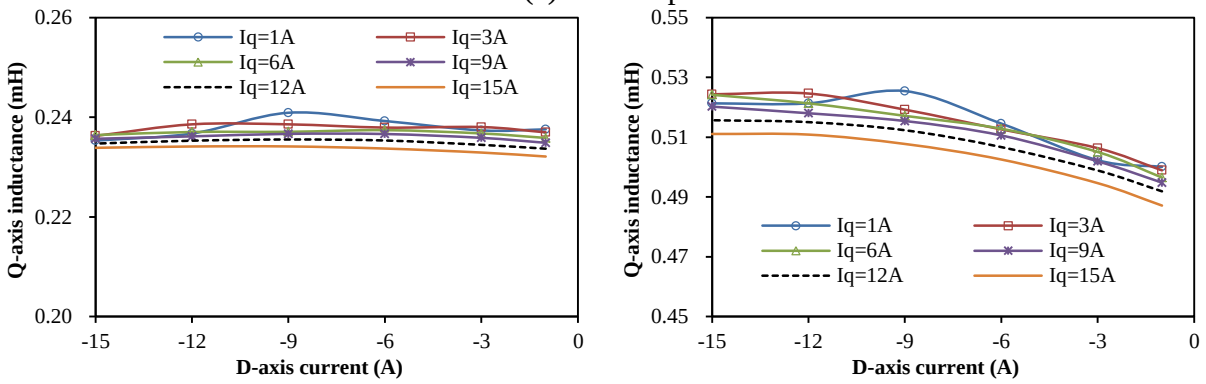

(b) 7-rotor pole

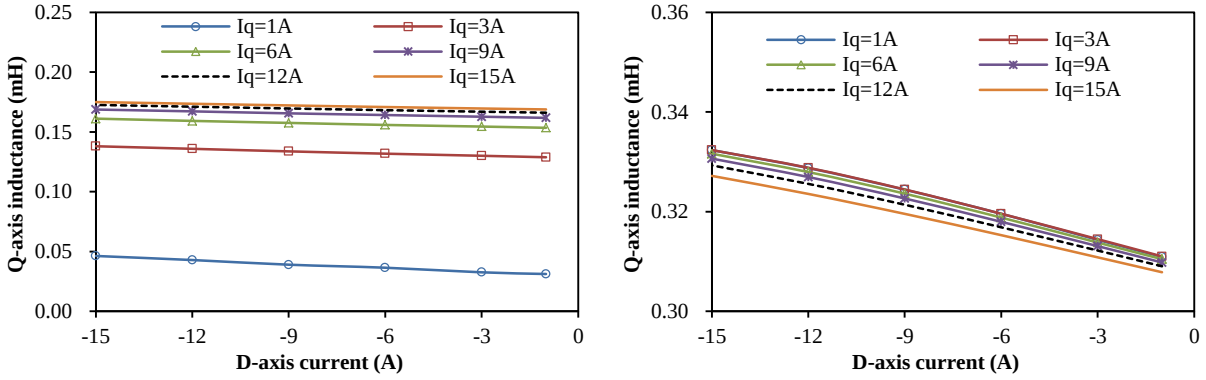

(c) 10-rotor pole

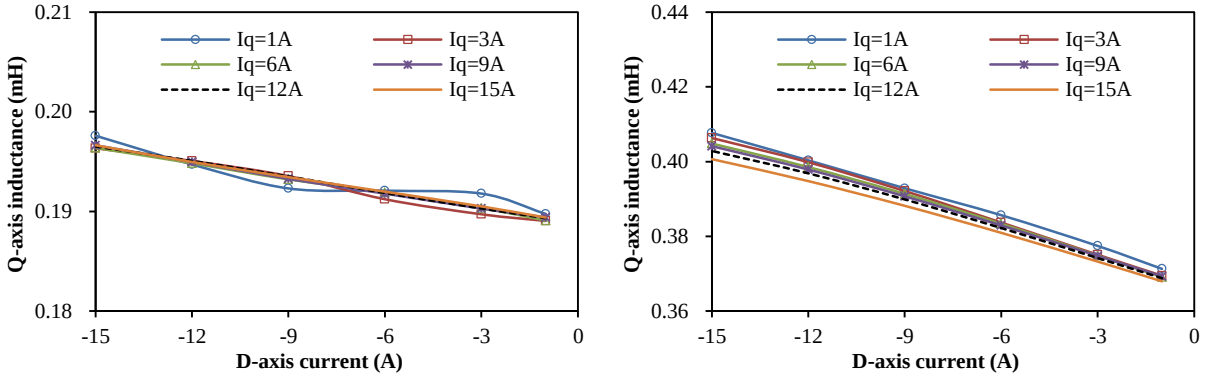

(d) 11-rotor pole

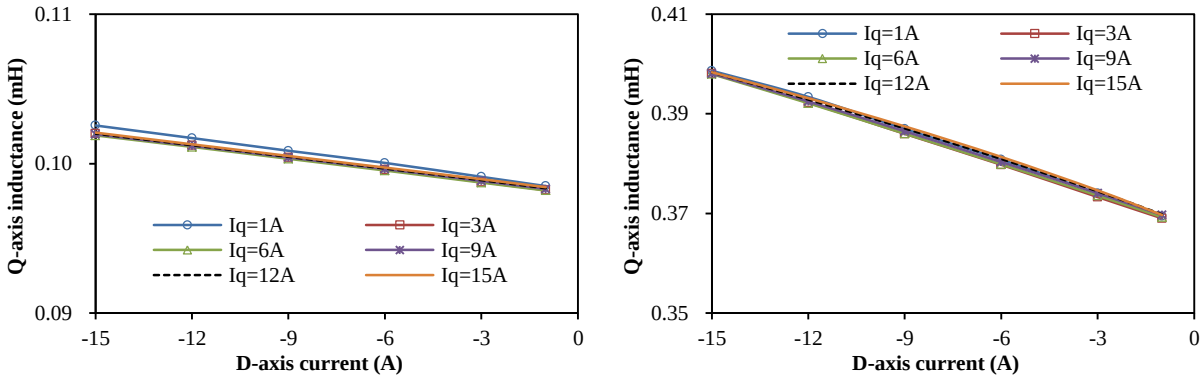

(e) 13-rotor pole

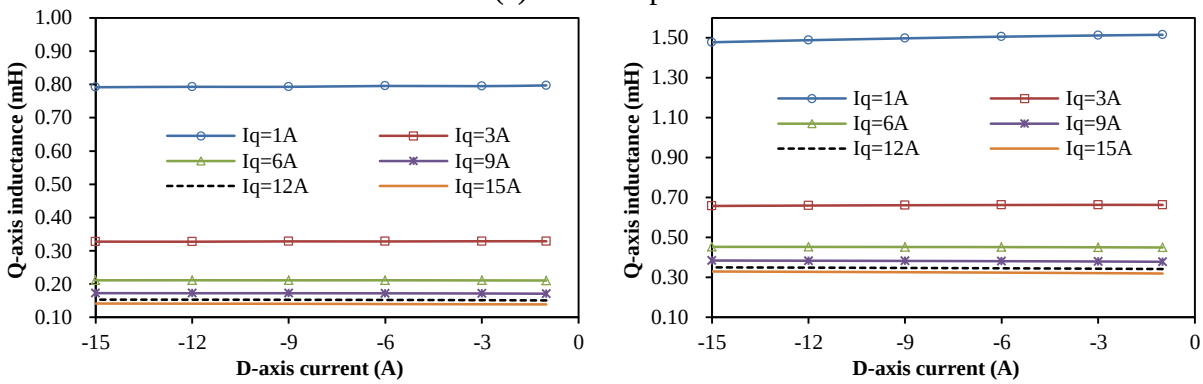

(f) 14-rotor pole

Fig.4.25 Variation of q-axis inductance L_q against i_d and i_q.

4.4 Influence of unbalanced magnetic force on the rotor

When the number of rotor poles is odd, there exists unbalanced magnetic force (UMF). Figs.4.26 and 4.27 compare UMFs in the analysed machines with odd rotor pole numbers at different load conditions. The amount of UMF decreases with increase in current in all the machines except for the 11-pole machine in which the UMF varies directly with the supplied current.

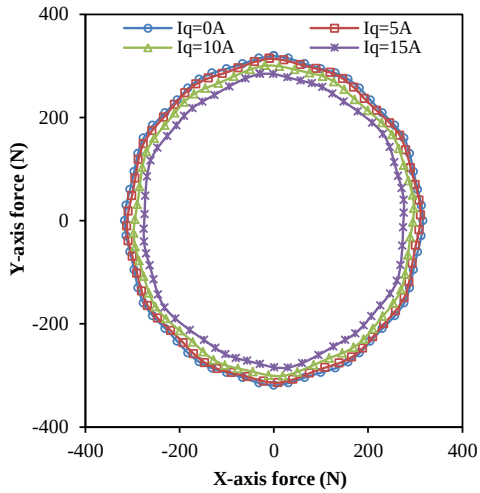

(a) 5-rotor pole

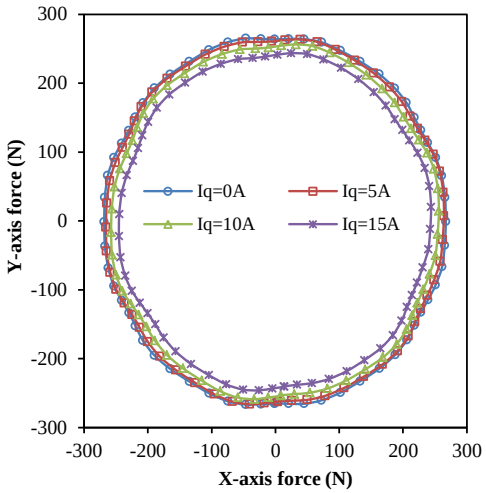

(b) 7-rotor pole

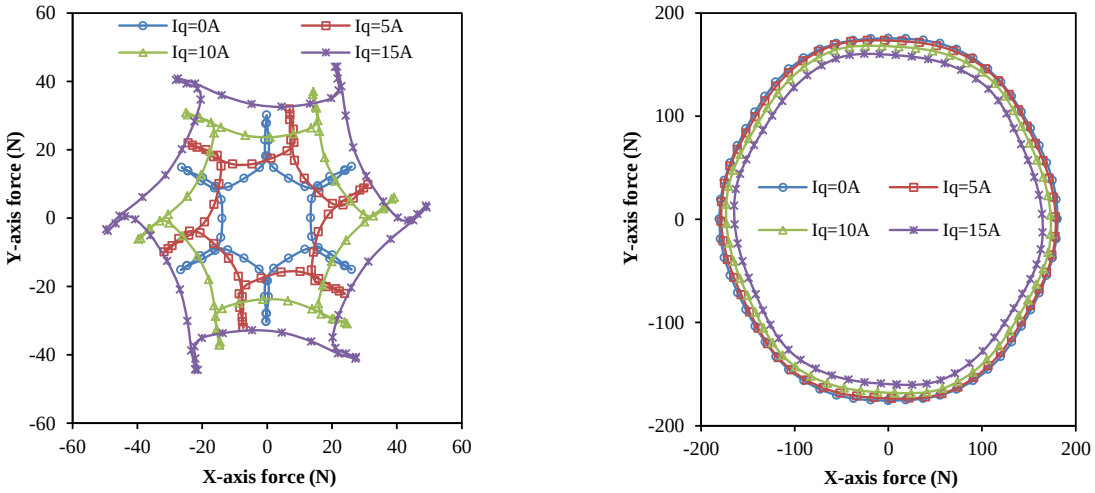

(c) 11-rotor pole (d) 13-rotor pole

Fig.4.26 Comparison of unbalanced magnetic force in analysed machines, i_d=0.

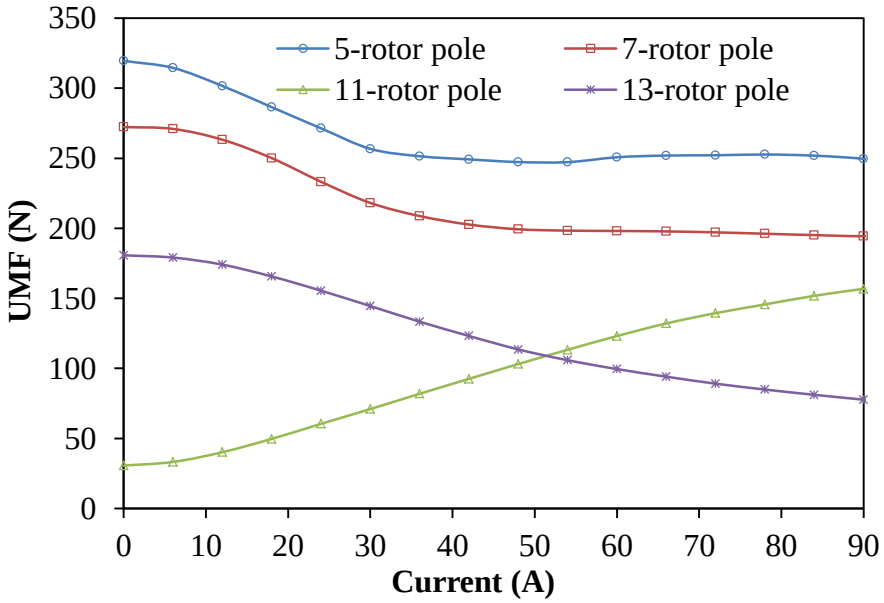

Fig.4.27 Comparison of unbalanced magnetic force in analysed machines, i_d=0.

Similarly, Fig.4.28 compares the variation of UMFs of the analysed machines with rotor position. It is worth noting that the largest amount of UMF occurs in the 5-pole machine, and this is followed by the 7-pole machine. The least amount of the UMF is obtained in the 11-pole machine.

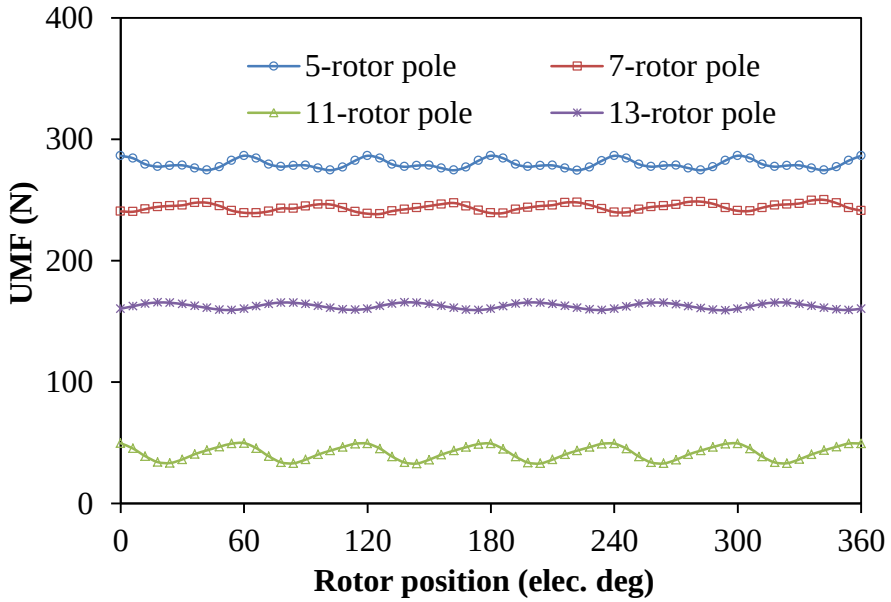

Fig.4.28 Variation of unbalanced magnetic force with rotor position in analysed machines (i_d=0, I=15A).

4.5 Losses and efficiency characteristics

The magnet eddy current losses of the machines are depicted in Fig.4.29. It is clear that the machines with high rotor-pole numbers (13- and 14-pole in particular) exhibit higher magnet eddy current loss, due to higher electrical frequency.

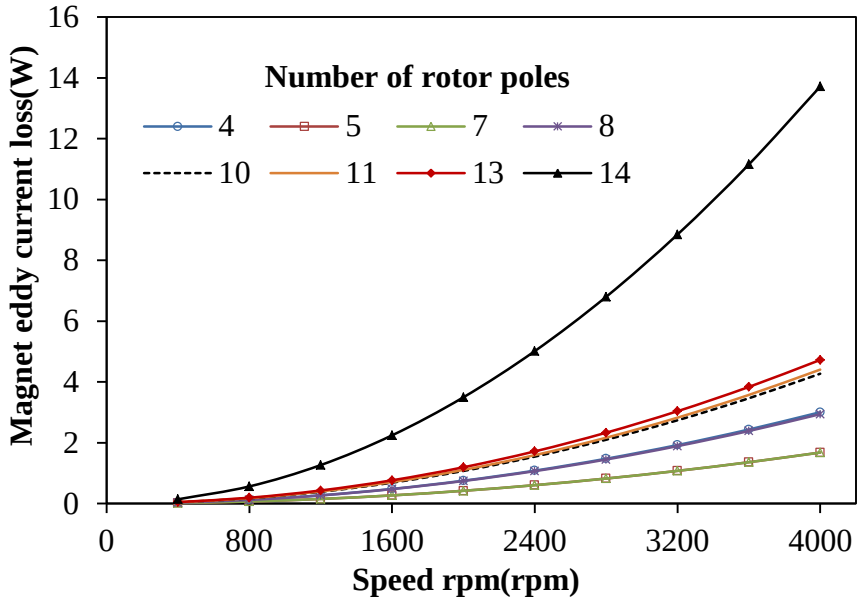

(a) All-pole-wound

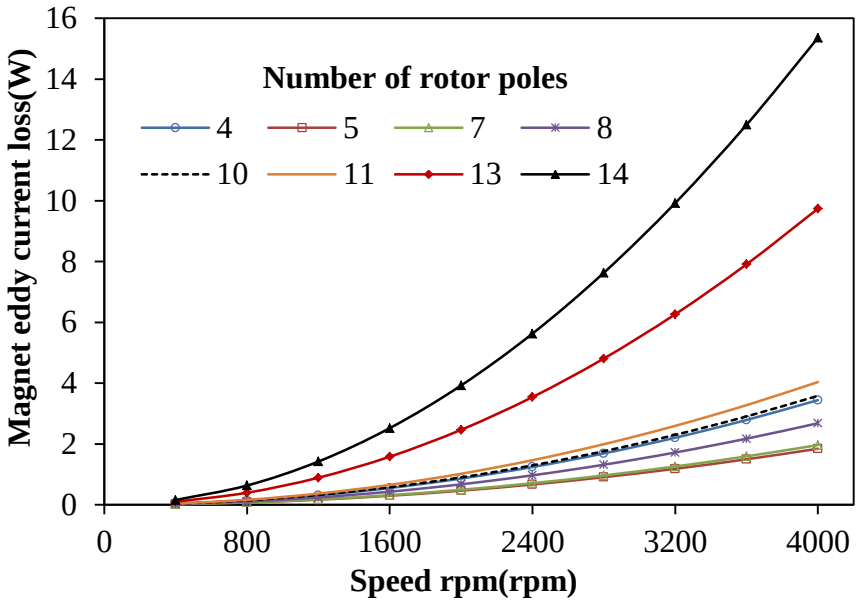

(b) Alternate-pole-wound

Fig.4.29 Variation of PM eddy current loss with speed, *I*=15A.

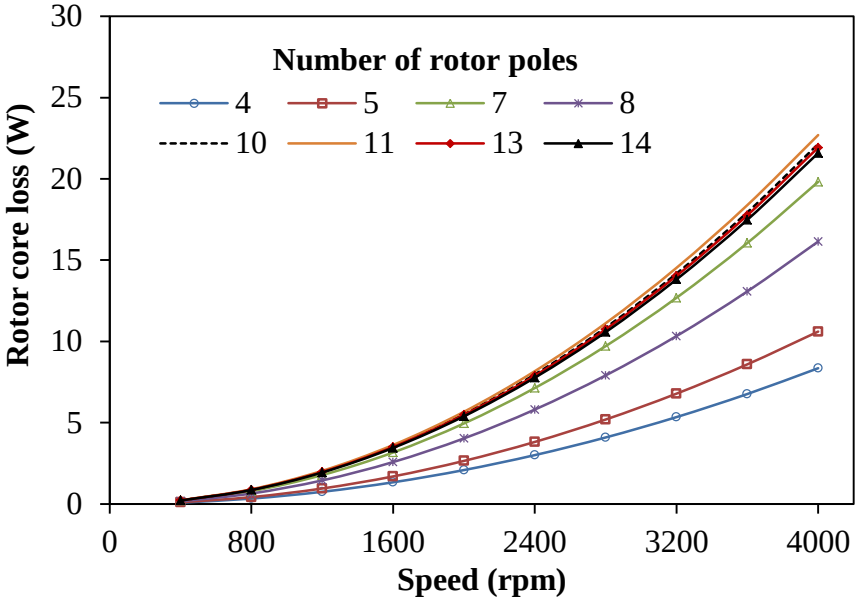

(a) All-pole-wound

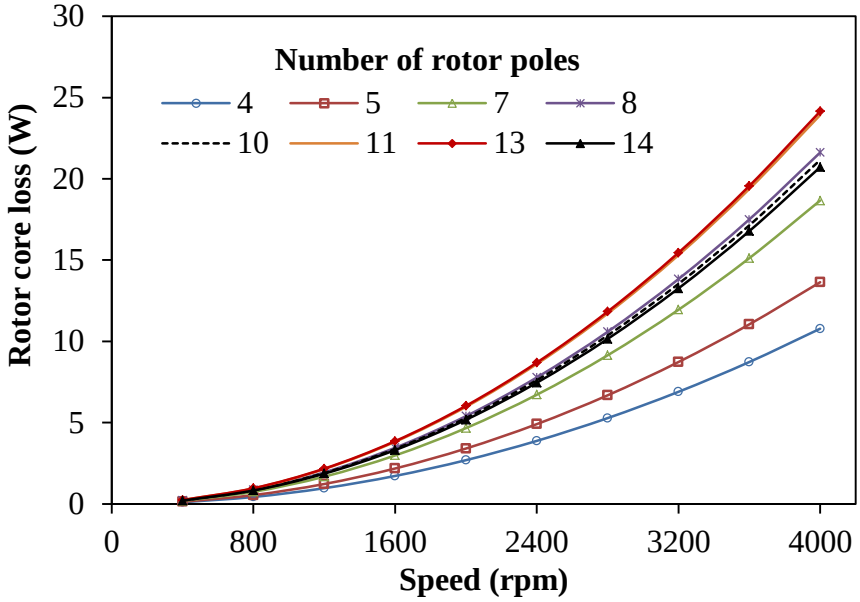

(b) Alternate-pole-wound

Fig.4.30 Variation of rotor core loss with speed, *I*=15A.

The rotor and stator core losses of the analysed machines are given in Figs.4.30 and 4.31 respectively. Moreover, the total core losses of the machines at rated current are shown in Fig.4.32. The analyses show that the 13-pole machine is characterised by the highest core loss, the least core loss is seen in the 4-pole machine. Further, a comparison of the PM eddy current loss, the rotor core loss, the stator core loss and the total core loss of the analysed machines at high speed (4000rpm) are illustrated in Fig.4.33. Note that the values of PM eddy current losses and the core loss at fixed copper loss condition (30W) are listed in Table.4.3.

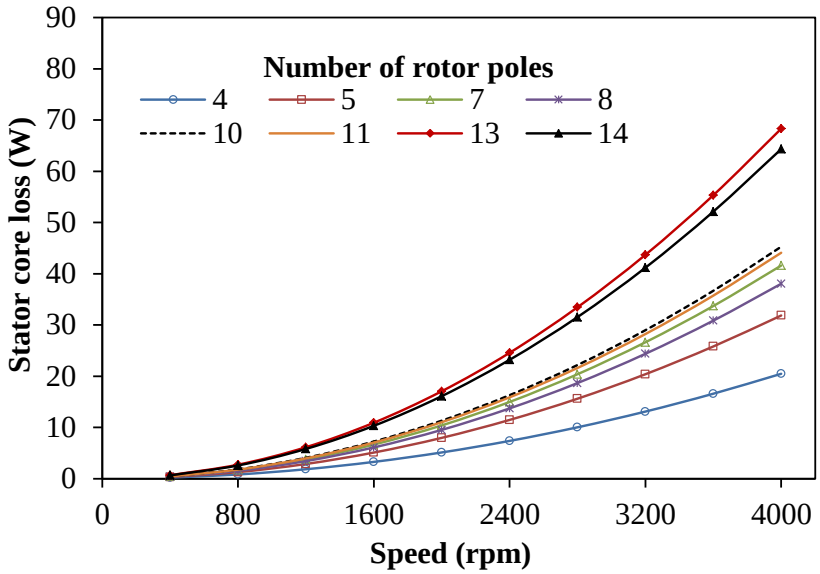

(a) All-pole-wound

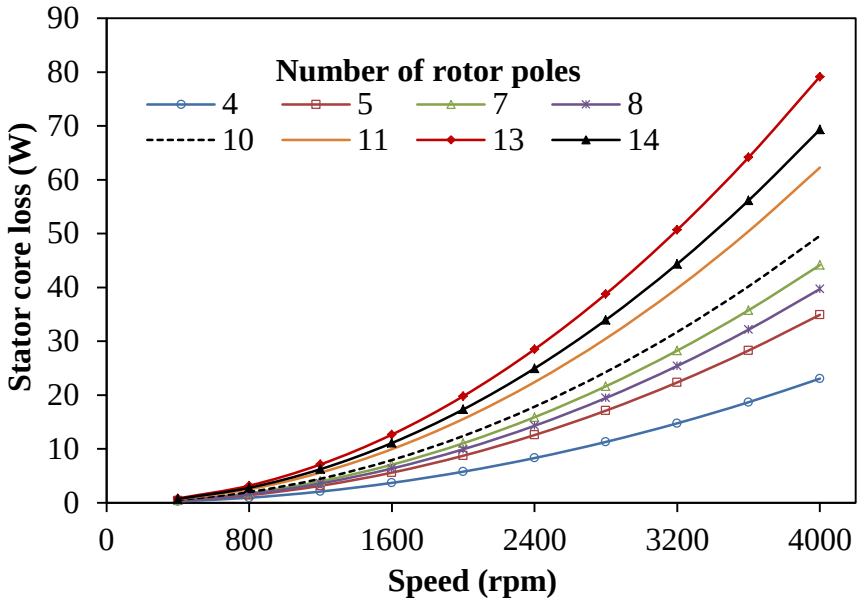

(b) Alternate-pole-wound

Fig.4.31 Variation of stator core loss with speed, *I*=15A.

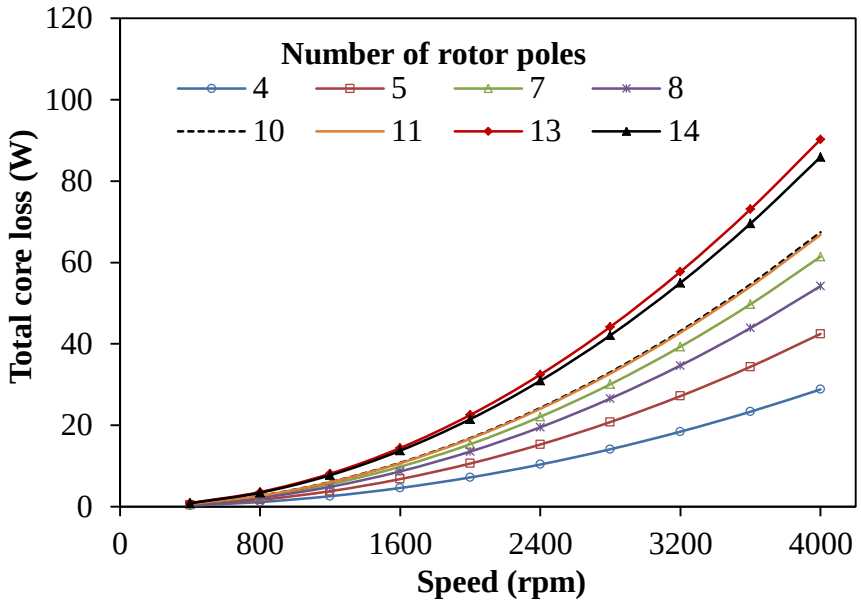

(a) All-pole-wound

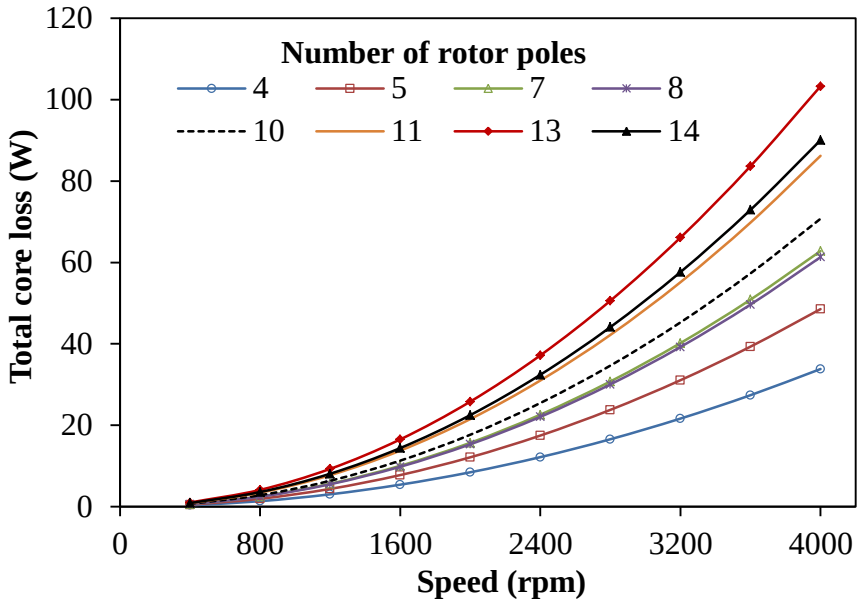

(b) Alternate-pole-wound

Fig.4.32 Variation of total core loss with speed, *I*=15A.

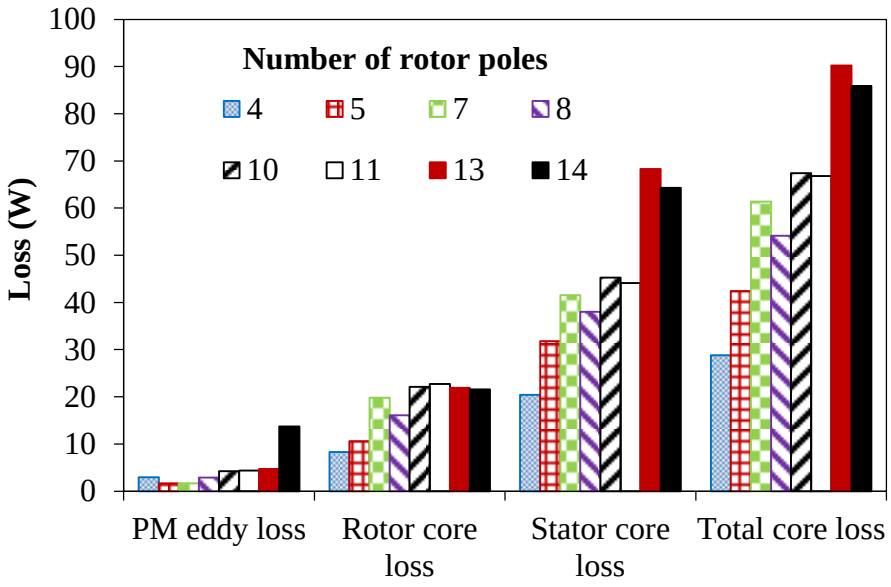

(a) All-pole-wound

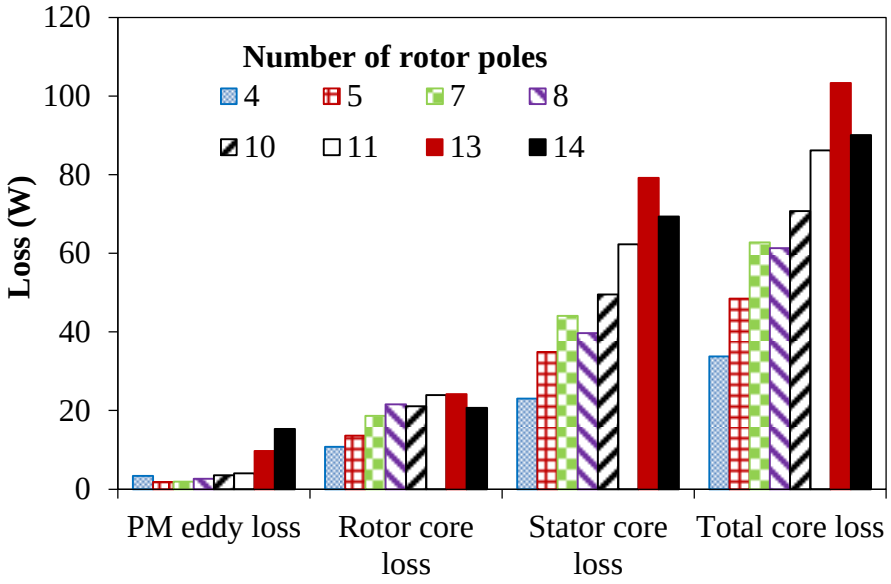

(b) Alternate-pole-wound

Fig.4.33 Comparison of losses (I=15A, 4000rpm).

The efficiency, η, of the machines is calculated by

$$\eta = \frac{P_{out}}{P_{in}} * 100\% = \frac{P_{out}}{P_{out} + \text{losses}} * 100\% \quad (4.5)$$

The efficiencies of the analysed machines at fixed copper loss (30W) are compared in Fig.4.34 and also listed in Table 4.3.

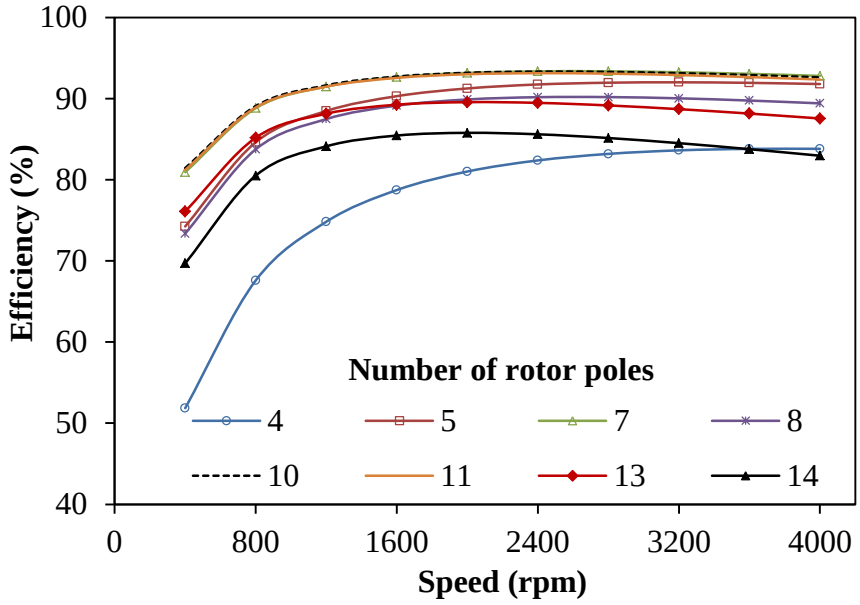

(a) All-pole-wound

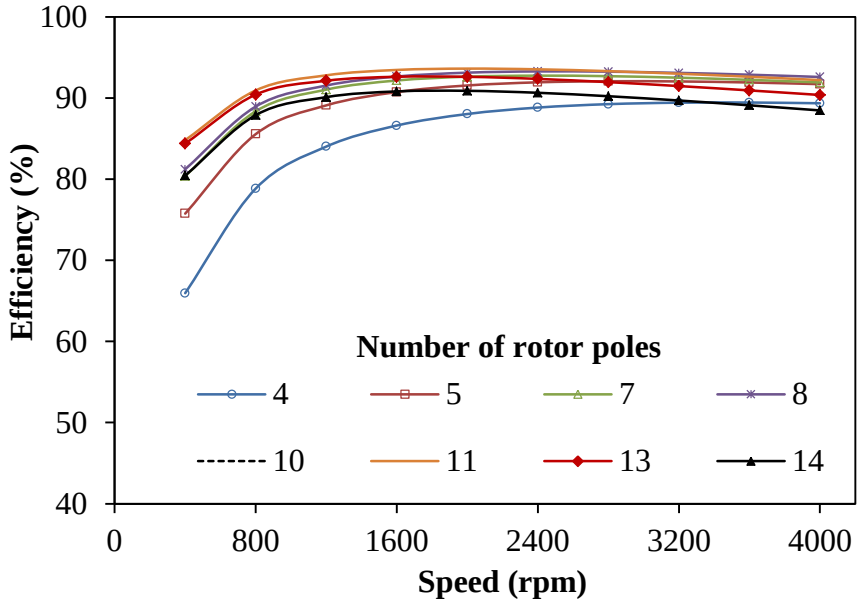

(b) Alternate-pole-wound

Fig.4.34 Comparison of efficiency, copper loss=30W.

TABLE 4.3 LOSSES AND EFFICIENCY OF ANALYSED MACHINES

Winding type	**All-pole-wound**							
Rotor pole No, N_r	**4**	**5**	**7**	**8**	**10**	**11**	**13**	**14**
P_{EM} (W)	326.65	703.17	912.92	591.92	810.12	798.56	494.95	358.56
p_{iron} (W)	29.77	29.84	33.87	33.16	26.22	26.90	25.58	24.71
p_{PM} (W)	3.33	1.25	1.04	1.24	1.73	2.01	2.12	4.73
η (%)	83.81	92.01	93.36	90.19	93.32	93.13	89.56	85.78
Winding type	**Alternate-pole-wound**							
Rotor pole No, N_r	**4**	**5**	**7**	**8**	**10**	**11**	**13**	**14**
P_{EM} (W)	529.97	668.33	757.25	798.13	955.02	870.10	681.11	645.45
p_{iron} (W)	29.63	26.47	28.12	26.13	31.07	27.19	21.53	27.65
p_{PM} (W)	2.93	1.14	1.05	1.41	2.18	2.10	2.76	7.09
η (%)	89.44	92.06	92.75	93.28	93.79	93.62	92.62	90.88

4.6 Torque/power-speed characteristics

The PM flux-linkages of the analysed machines under different *q*-axis currents are displayed in Fig.4.35. It can be seen that in all the analysed machines, the rated on-load PM flux linkages are similar to those under open circuit operation condition. This indicates that these machines have small cross-coupling effect between *d*- and *q*-axes, when the current is small. However, the cross-coupling effect will be stronger with larger current due to heavier saturation.

Under vector control, the phase voltage limitation could be expressed as:

$$V_{max} = \frac{2}{\pi} V_{DC} \tag{4.6}$$

where V_{dc} is DC-link voltage, which is set to 22.9V in the calculation for the analysed machines.

The electromagnetic torque, T, of the analysed PS-SFPM machines is given by

$$T = 1.5N_r[\psi_{PM} I_q + (L_d - L_q) I_d I_q] \tag{4.7}$$

where N_r is the number of rotor poles. ψ_{PM} is the PM flux-linkage. I_d, I_q and L_d, L_q are the *d*- and *q*-axis currents and inductances, respectively.

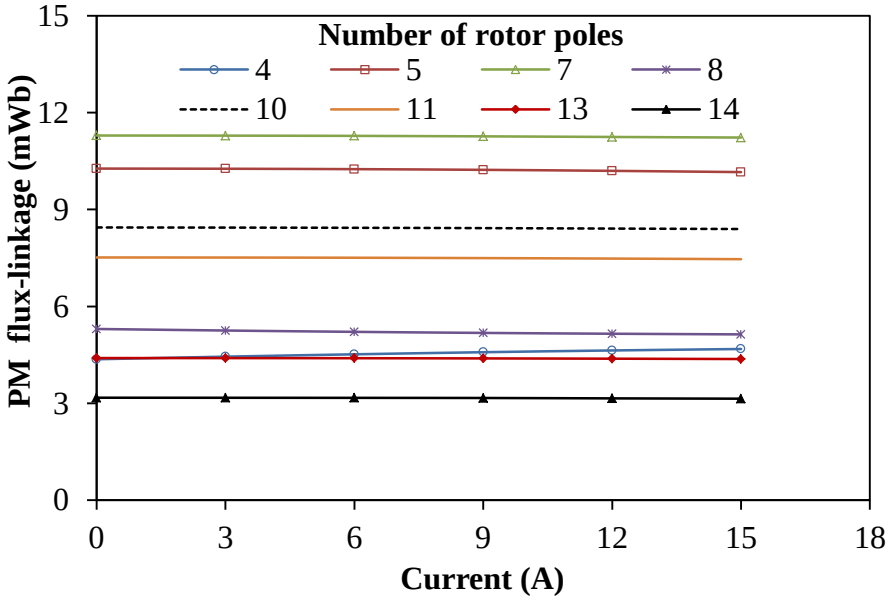

(a) All-pole-wound

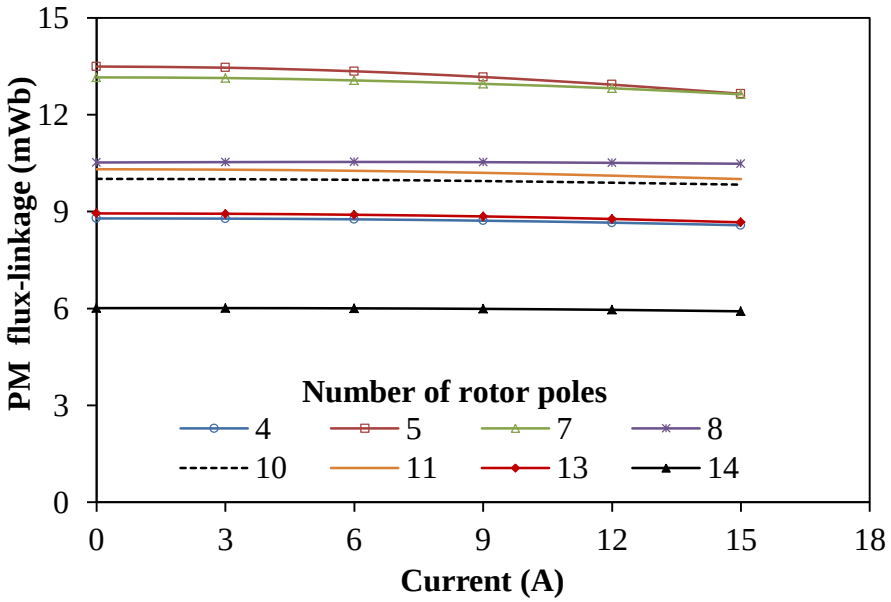

(b) Alternate-pole-wound

Fig.4.35 Variation of PM flux-linkages against *q*-axis current, i_d=0.

Following the aforementioned condition and the method described in [QI09], the torque/power-speed curves for all machines are calculated as shown in Figs.4.36 and 4.37. Considering the torque capability, the alternate-pole-wound machines could be a viable option.

It is worth mentioning that at rated current condition (I=15A) and limited inverter voltage of 15V, the 10- and 13-pole machines exhibit the higher torque profile for the all- and alternate-wound topologies, respectively. Moreover, the cross-coupling effect of the winding inductances is taken into consideration in the calculation. The flux weakening capabilities, maximum torques and powers of the analysed machines are listed in the Table 4.4.

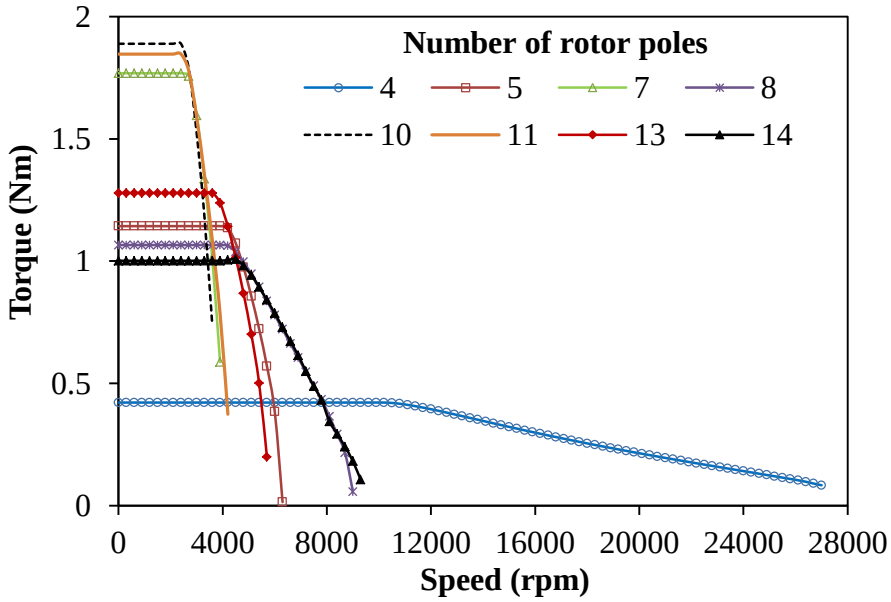

(a) Torque versus speed

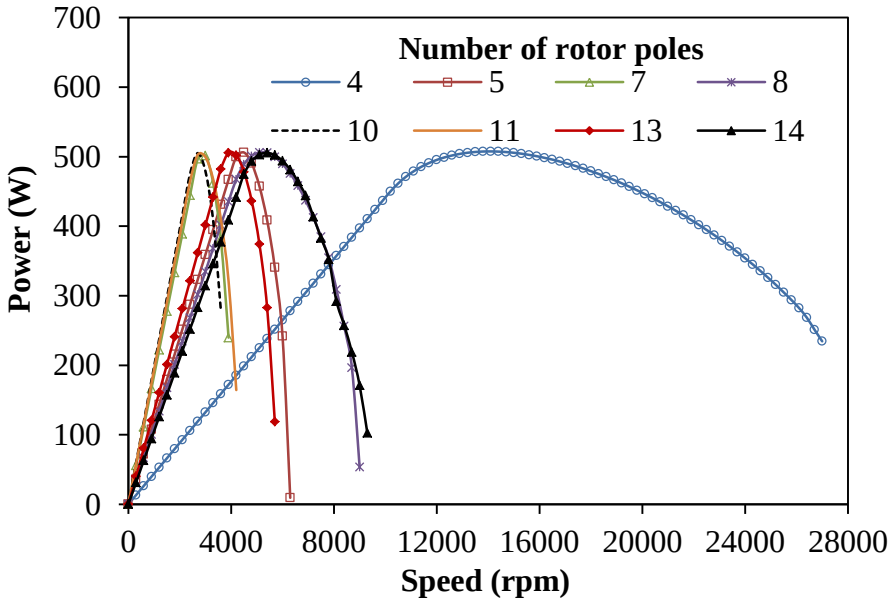

(b) Power versus speed

Fig.4.36 Comparison of torque/power-speed characteristics (I_{max}=15A, V_{dc}=22.9V).

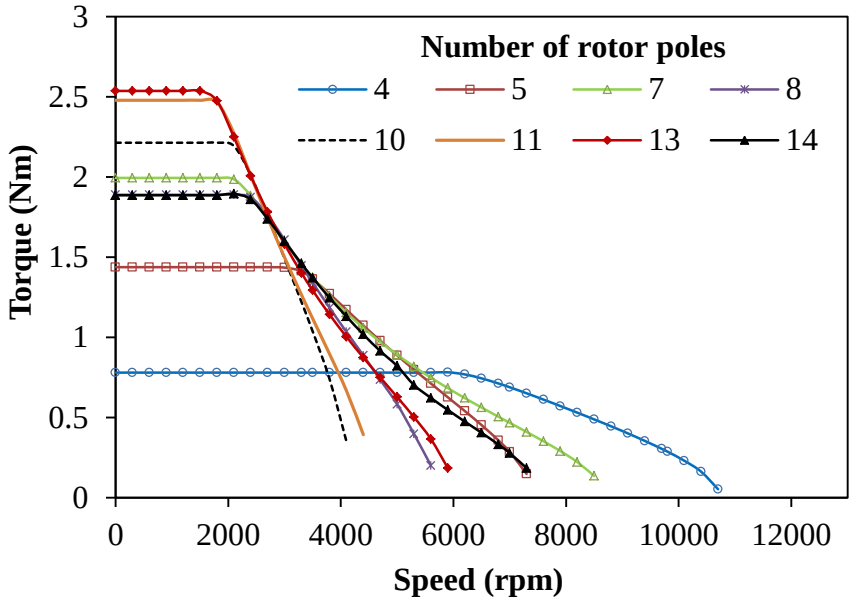

(a) Torque versus speed

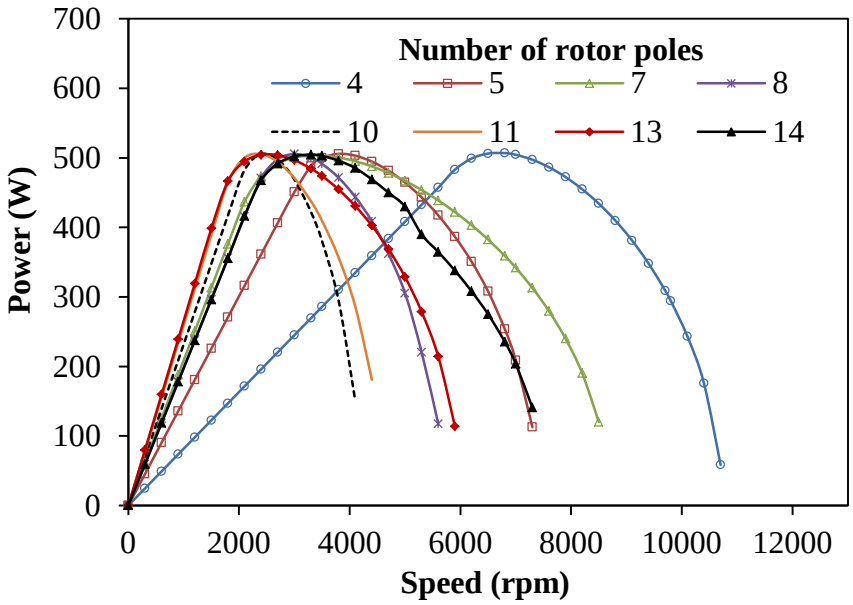

(b) Power versus speed

Fig.4.37 Comparison of torque/power-speed characteristics (I_{max}=15A, V_{dc}=22.9V).

TABLE 4.4 FLUX WEAKENING Capability

Winding type	**All-pole-wound**							
Rotor pole number, N_r	**4**	**5**	**7**	**8**	**10**	**11**	**13**	**14**
D-axis inductance (mH)*	0.17	0.19	0.23	0.19	0.18	0.18	0.10	0.10
Q-axis inductance (mH)*	0.10	0.20	0.23	-0.005	0.17	0.19	0.10	0.139
PM flux (mWb)	4.36	10.27	11.29	5.30	8.45	7.52	4.40	3.17
K_{fw}	0.58	0.28	0.31	0.54	0.32	0.36	0.34	0.47
Base speed (rpm)	10100	4000	2600	4000	2400	2400	3600	4100
Maximum speed (rpm)	27000	6300	4000	9000	3800	4300	5700	9400
Max. speed / base speed	2.67	1.58	1.54	2.25	1.58	1.79	1.58	2.29
Maximum torque (Nm)*	0.421	1.14	1.77	1.07	1.89	1.85	1.28	1.01
Maximum power (W)*	507.56	506.70	505.59	506.50	505.10	505.33	506.79	505.49
Torque density (kNm/m^3)	4.90	13.19	19.57	12.69	20.27	19.98	14.86	10.76
Winding type	**Alternate-pole-wound**							
Rotor pole number, N_r	**4**	**5**	**7**	**8**	**10**	**11**	**13**	**14**
D-axis inductance, $L_{d\,(}$mH)	0.20	0.36	0.56	0.36	0.29	0.35	0.35	0.23
Q-axis inductance, $L_{q\,(}$mH)	0.29	0.49	0.49	0.38	0.31	0.37	0.37	0.32
PM flux (mWb)	8.79	13.50	13.16	10.52	10.01	10.31	8.95	6.01
K_{fw}	0.34	0.4	0.64	0.51	0.43	0.51	0.59	0.57
Base speed (rpm)	5600	2900	2000	2200	1900	1700	1600	2000
Maximum speed (rpm)	10700	7400	8600	5700	4200	4500	6000	7500
Max. speed / base speed	1.91	2.55	4.3	2.59	2.21	2.65	3.75	3.75
Maximum torque (Nm)*	0.78	1.44	1.99	1.89	2.21	2.48	2.54	1.90
Maximum power (W)*	507.25	505.75	503.56	505.40	505.38	505.78	505.15	504.61
Torque density (kNm/m^3)	8.84	14.33	18.94	19.97	23.89	26.12	25.56	19.38

*: At I_{max}=15A, V_{dc}=22.9V.

4.7 Electromagnetic performance comparison of all- and alternate-pole wound machines

In this section, the electromagnetic performances of the proposed machines having different winding configurations and 10- / 11-rotor poles are quantitatively compared. The analyses include both load and open-circuit conditions. The results reveal that the proposed 11-pole machine having alternate-pole-wound stands out the best amongst the crowd of other analysed machines in terms of more sinusoidal back-EMF waveforms/less harmonics, better torque density, and less PM usage. Nevertheless, it seems to saturate quicker during overload when compared to the other machines as will be seen later in this section. Fig.4.38 shows the comparison of open-circuit flux-linkage of the machines with their corresponding spectra. It is worth noting that all the machines exhibit bipolar sinusoidal waveforms except the 10-pole machine with all-pole-wound configuration whose waveform is unipolar. Similarly, the open circuit back-EMF waveforms and their respective harmonic spectra are depicted in Fig.4.39. Note that 11-pole machine with alternate-wound topology has the largest peak-peak values of both back-EMF and flux-linkages. It should also be noted that the compared even-rotor pole machines have inherent asymmetric and non-sinusoidal back-EMF waveforms, which is an undesirable quality.

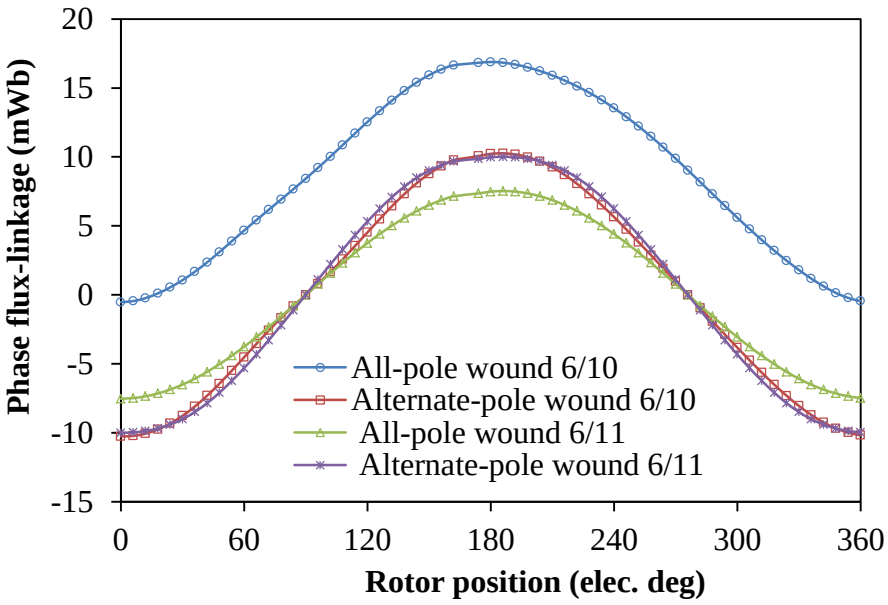

(a) Waveforms

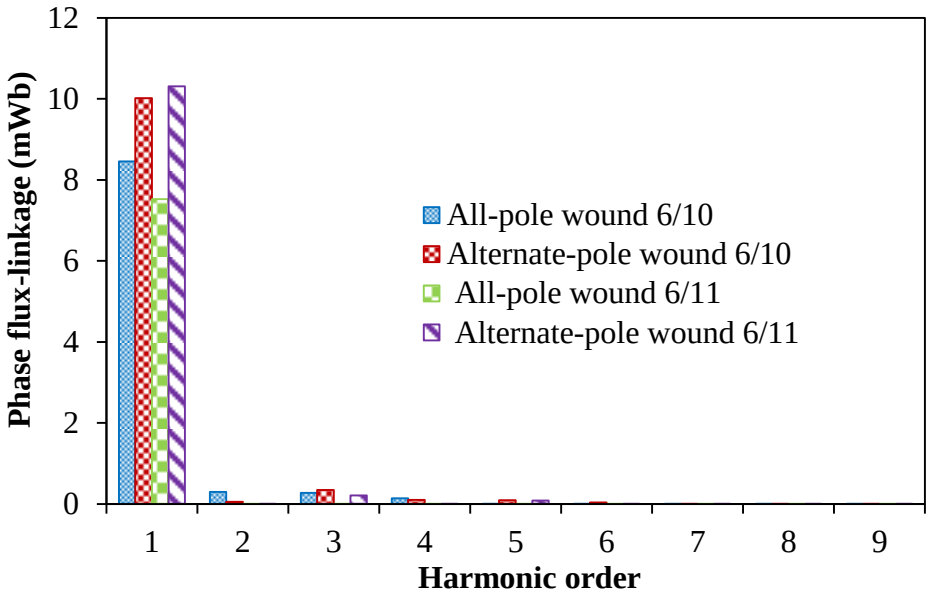

(b) Spectra

Fig.4.38 Open-circuit flux-linkage variation with rotor position in the analysed machines.

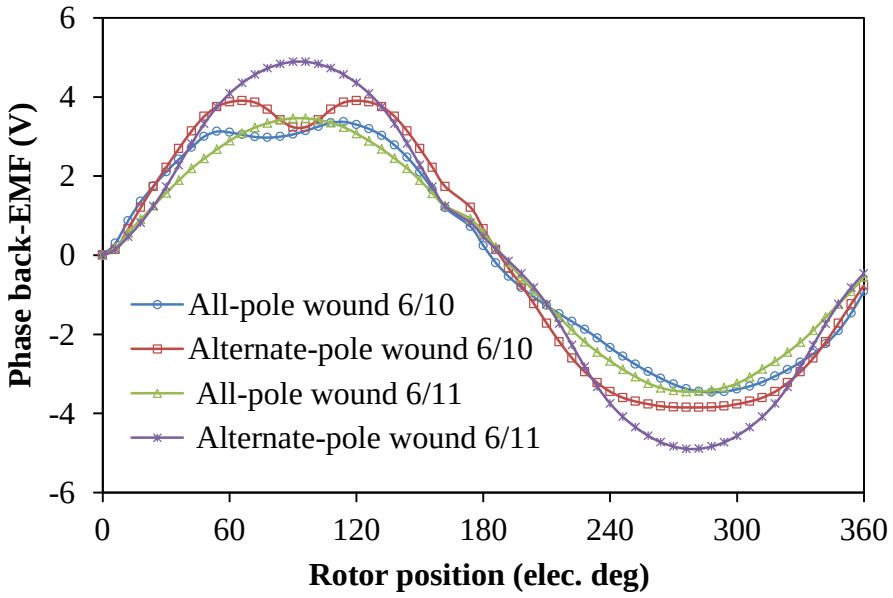

(a) Waveforms

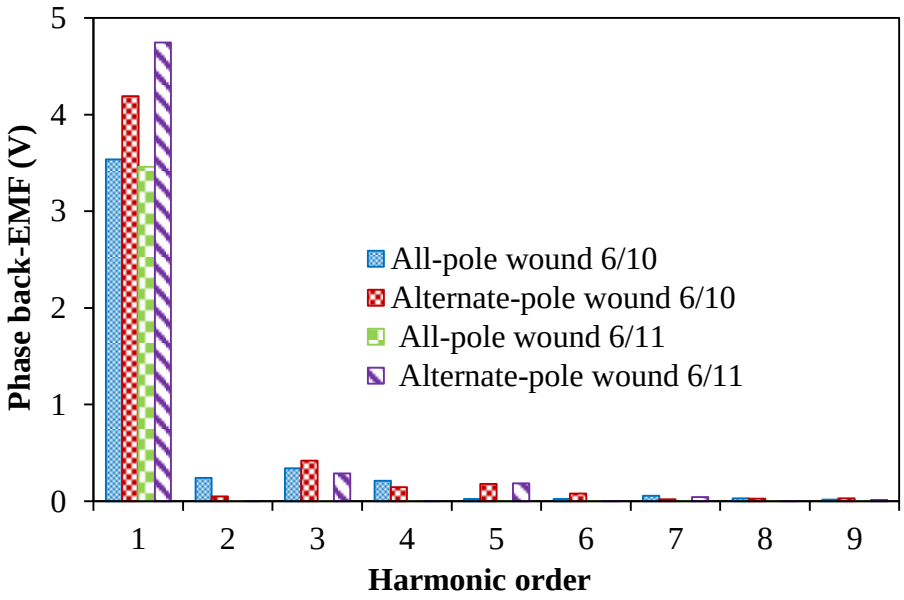

(b) Spectra

Fig.4.39 Comparison of open-circuit phase back-EMFs in the analysed machines having all-pole-wound, 400rpm.

Due to the larger fundamental back-EMF value of the 11-pole machine having alternate-pole-wound, it has the best torque potential amonsgt the compared machines as seen in Fig.4.40. Moreover, the torque versus current/copper loss curves of Figs.4.41 and 4.42 show that the 11-pole machine having all-pole-wound seems to be the best candidate amongst the other machines at fixed copper loss condition in terms of torque capability, although it may be easily saturated at excessive electric loading as seen from Fig. 4.41.

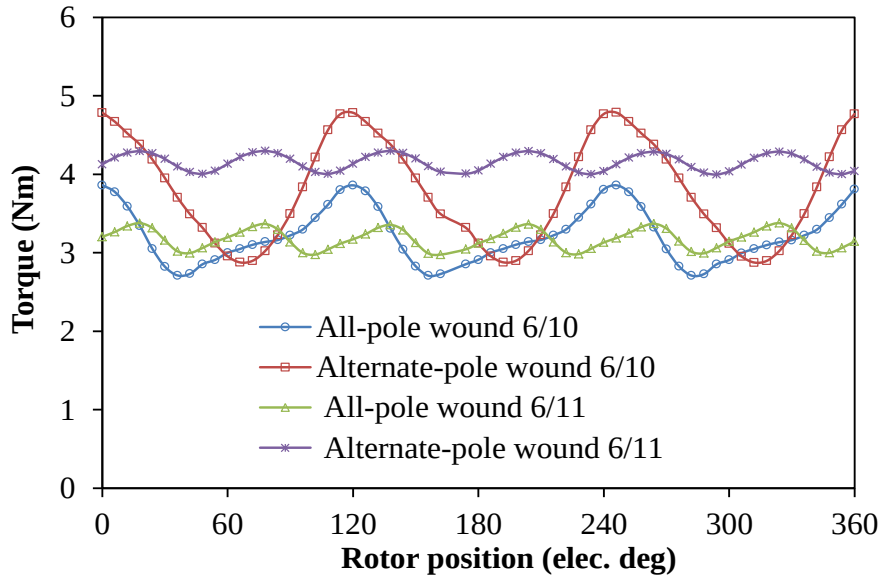

(a) Waveforms

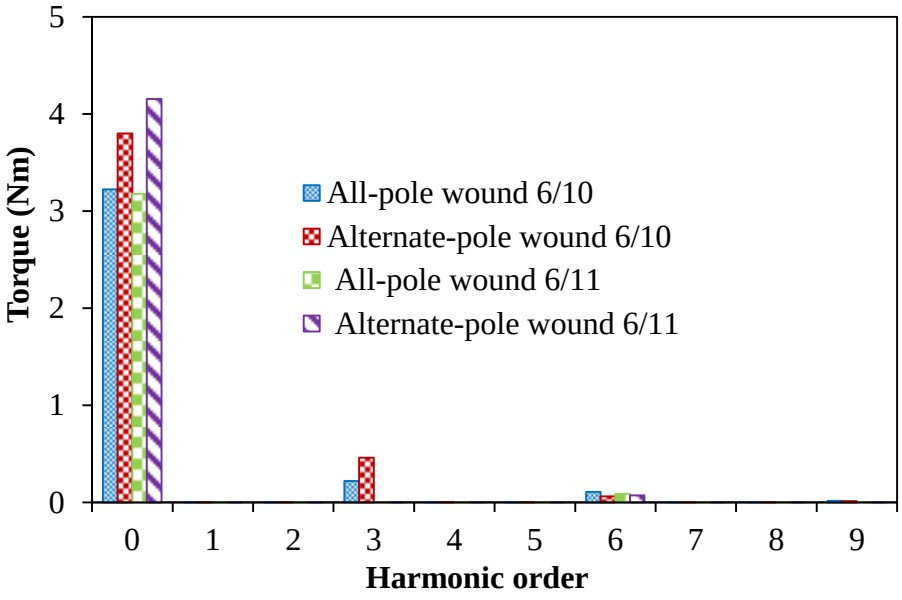

(b) Spectra

Fig.4.40 Comparison of torque waveforms in all-pole-wound machines, (copper loss = 30W, i_d=0).

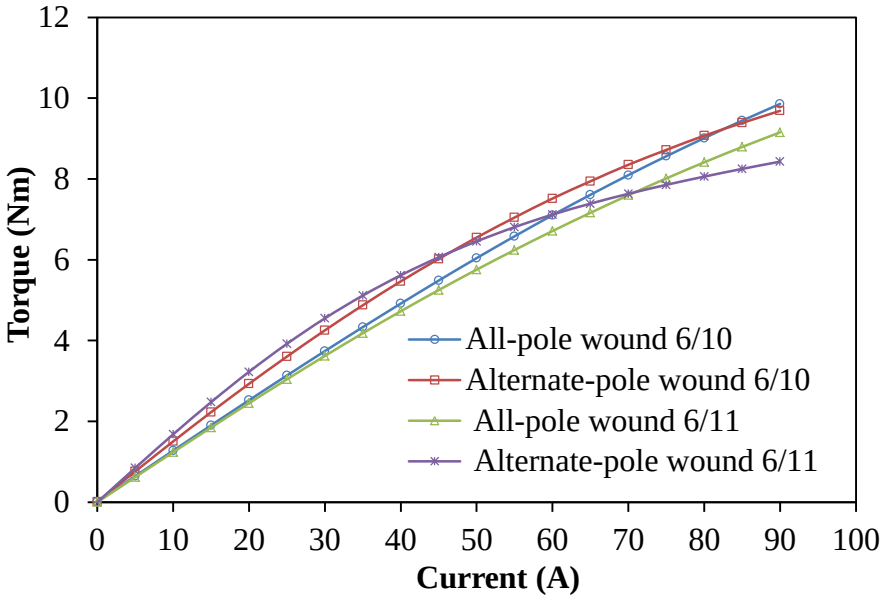

Fig.4.41 Comparison of average torque against current, i_d=0.

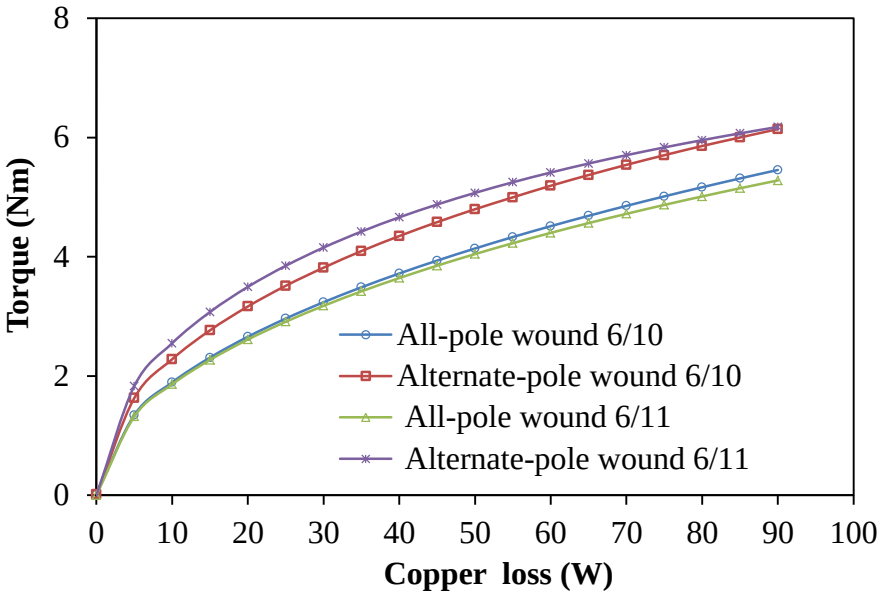

Fig.4.42 Comparison of torque against copper loss, i_d=0.

The torque variation with current phase angle is shown in Fig.4.43. The results reveal that the maximum torque of the machines occurs at zero current angle, *i.e.* when the rotor aligns with the *d*-axis. Clearly, it indicates the negligible reluctance torque in all the analysed machines. Again, the 11-pole machine demonstrates the best torque profile amongst all, under this condition.

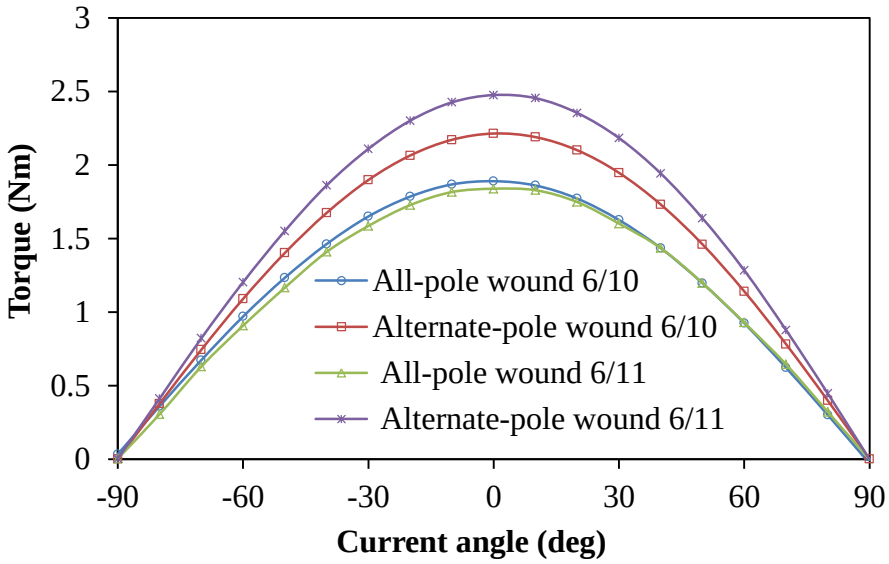

Fig.4.43 Comparison of torque against phase current angle, i_d=0.

In terms of the PM usage, the average torque per PM volume against current is calculated and shown in Fig.4.44. Clearly, the 11-pole machine with alternate-pole-wound has the best PM

usage and the highest ratio of average torque to PM volume, which is important for the cost sensitive applications.

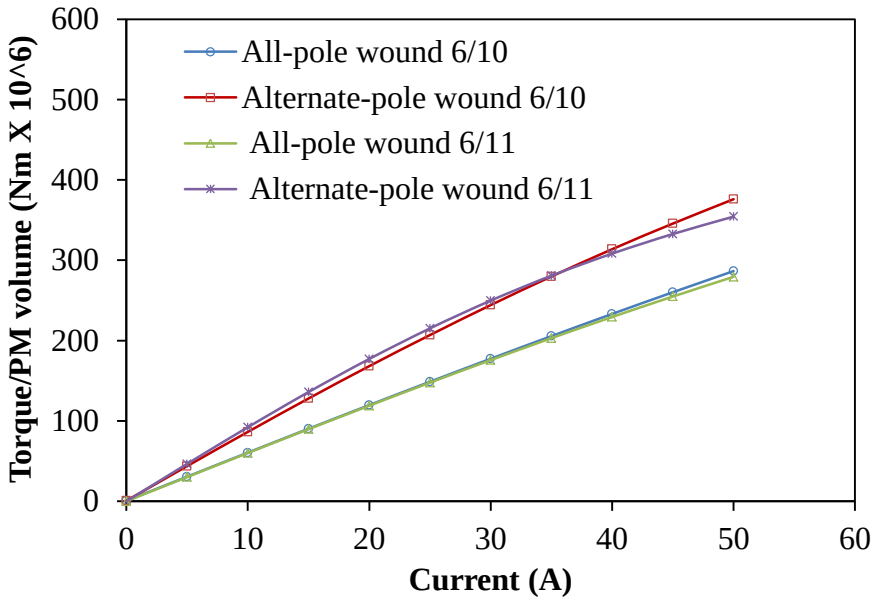

Fig.4.44 Comparison of ratio of average torque to PM volume against current, i_d=0.

4.8 Experimental validation

PS-SFPM machine having alternate-pole-wound topology with E-core outer stator structure which has the same parameters as shown in Table 4.2 has been manufactured and tested to validate the analyses, as shown in Fig.4.45. Fig.4.46. compares the measured and predicted open-circuit back-EMFs at rated speed. Due to end-effect, the 2D predicted result is much larger than the measured one. However, the 3D FEA result agrees very well with the measured result.

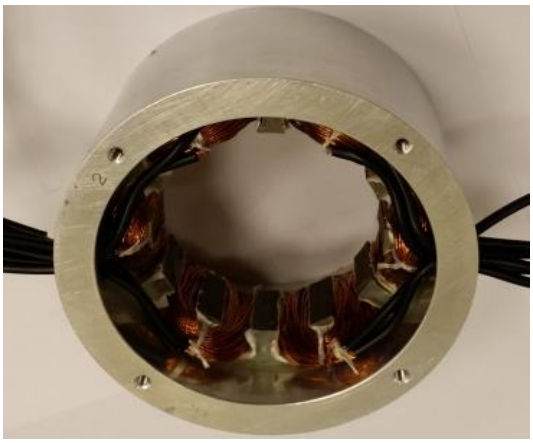

(a) Outer stator

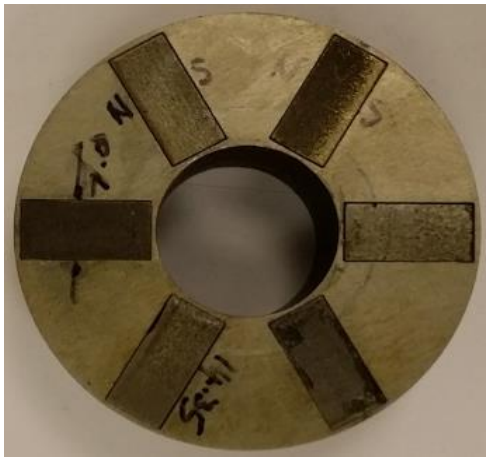

(b) Inner stator

(c) Lamination sheet

(d) Assembled motor

(e) Rotor

Fig.4.45 Manufactured prototype of the proposed machine.

The 3D-mesh and the no load flux density distribution of the analysed machine are depicted in Fig.4.46. Figs.4.47 and 4.48 compare the measured and 3D FEA predicted static torques under different currents. It shows good agreement considering manufacturing tolerances and measuring errors. Overall, the experiments have validated the analyses.

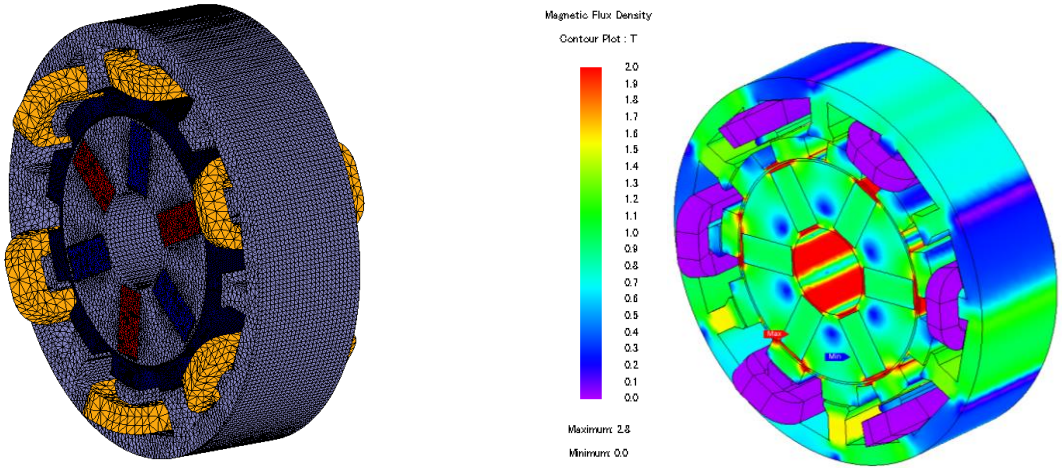

(a) mesh (b) flux density

Fig.4.46 Mesh and flux density distribution, no load.

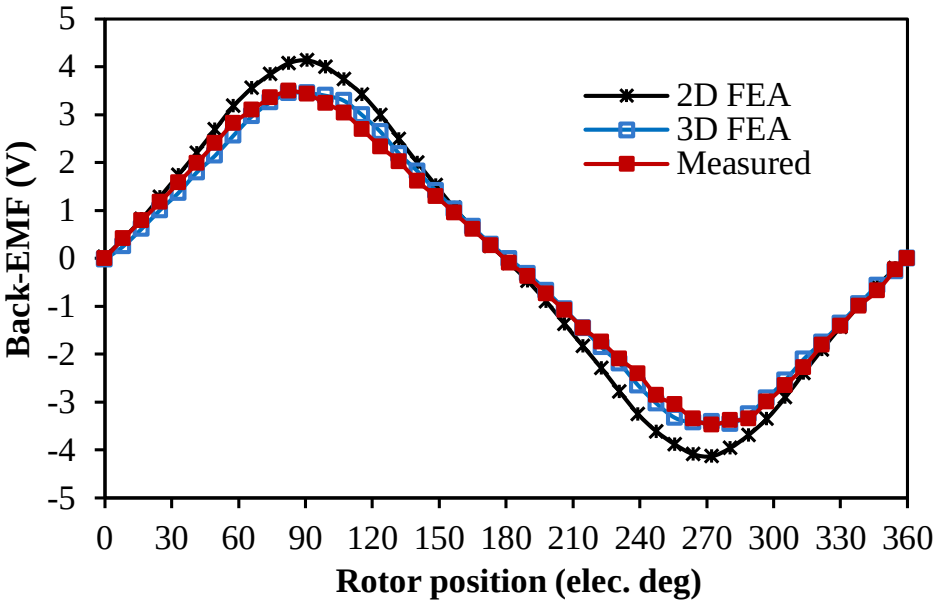

(a) Waveforms

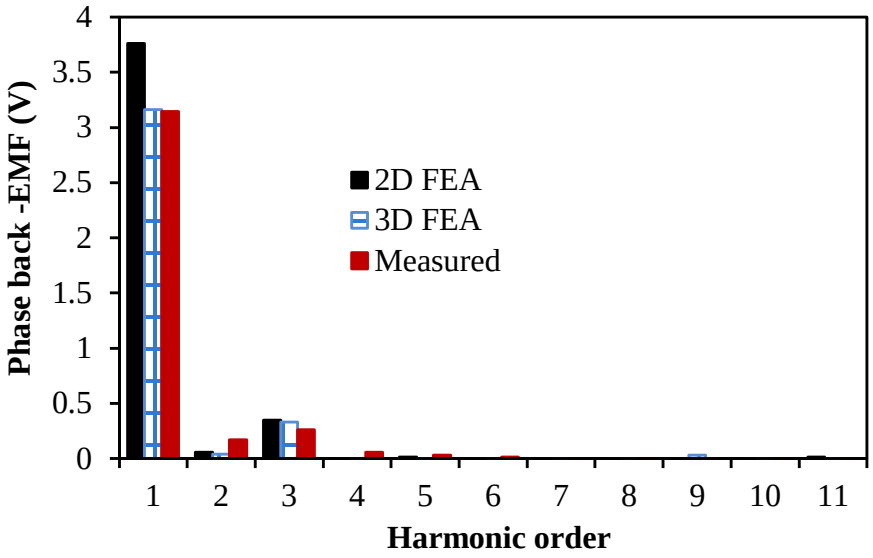

(b) Spectra

Fig.4.47 Comparison of predicted and measured open-circuit back-EMFs, 400rpm.

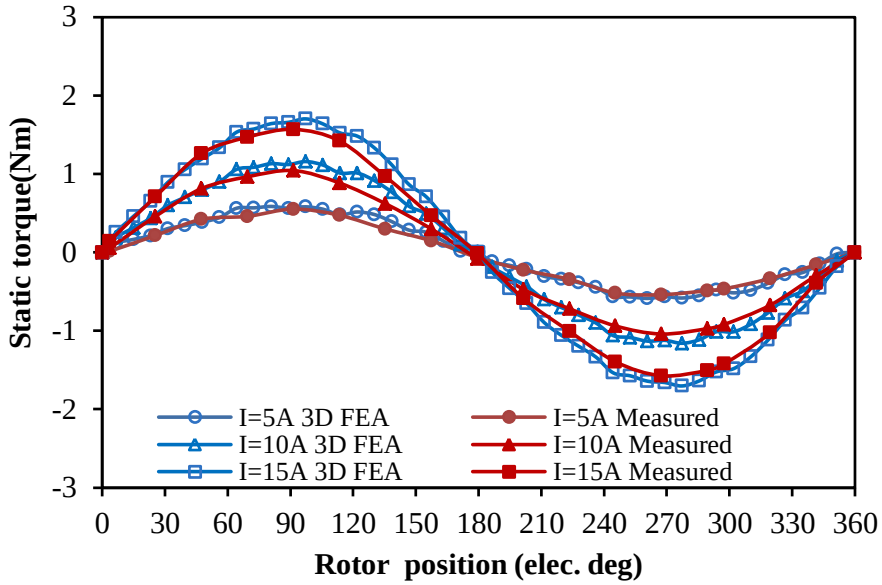

Fig.4.48 Comparison of predicted and measured static torques.

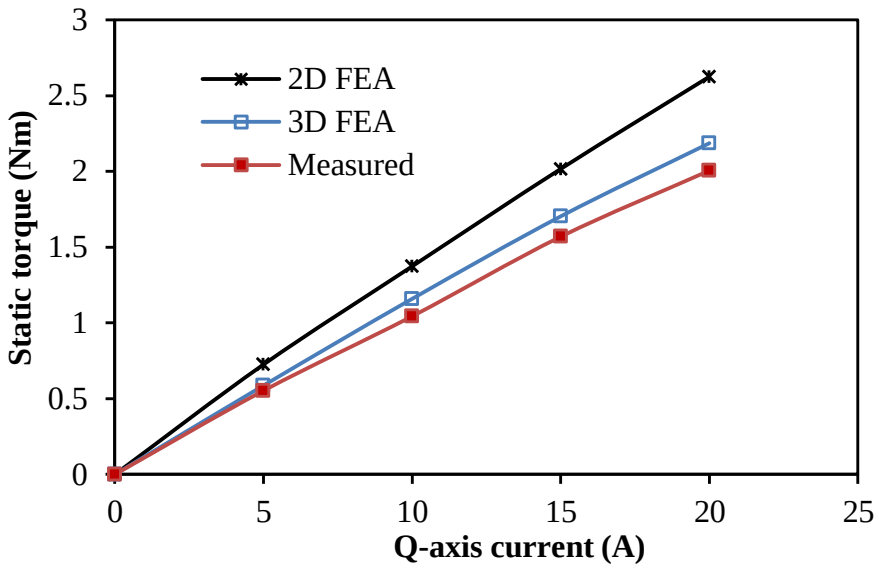

Fig.4.49 Comparison of predicted average torques against i_q (i_d=0A).

Fig.4.50 shows the comparison of predicted and measured self- and mutual-inductances of the prototype machine. It can be observed that the measured and 2D FE predicted self- and mutual-inductances agree well with each other. However, the measured inductances are slightly higher than the 2D FE predicted ones, since 2D FE predicted inductance cannot account for the end winding inductance.

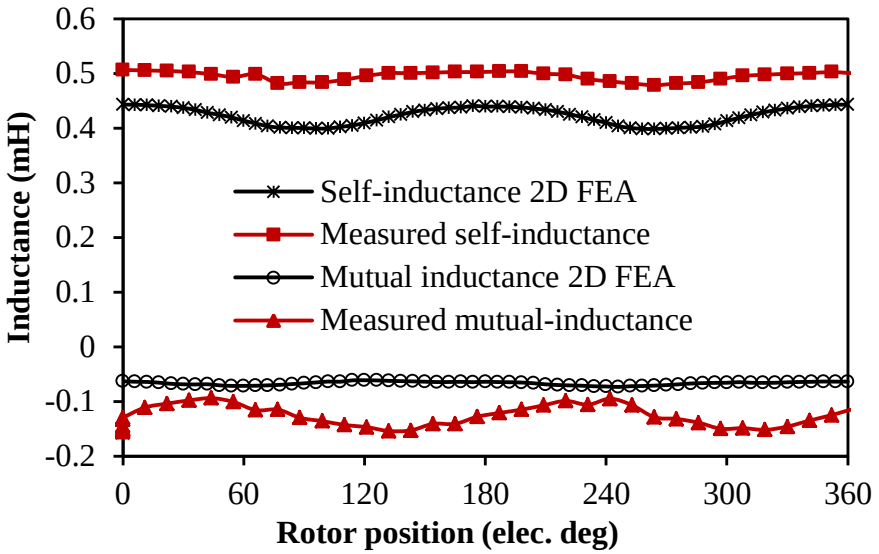

Fig.4.50 Comparison of predicted and measured self- and mutual inductances of the PS-SFPM prototype machine.

Fig.4.51 and Table 4.5 give the phase winding terminal voltage and phase current waveforms of different phase resistance load R_{load}, when the machine operates at generator mode at 400rpm. As shown in Fig.4.51, the distortion of the voltage waveform is stronger when the

load is higher as the resistance is smaller, as may be expected. The measured maximum currents are slightly smaller than those predicted by 2D FEA, due to end effect.

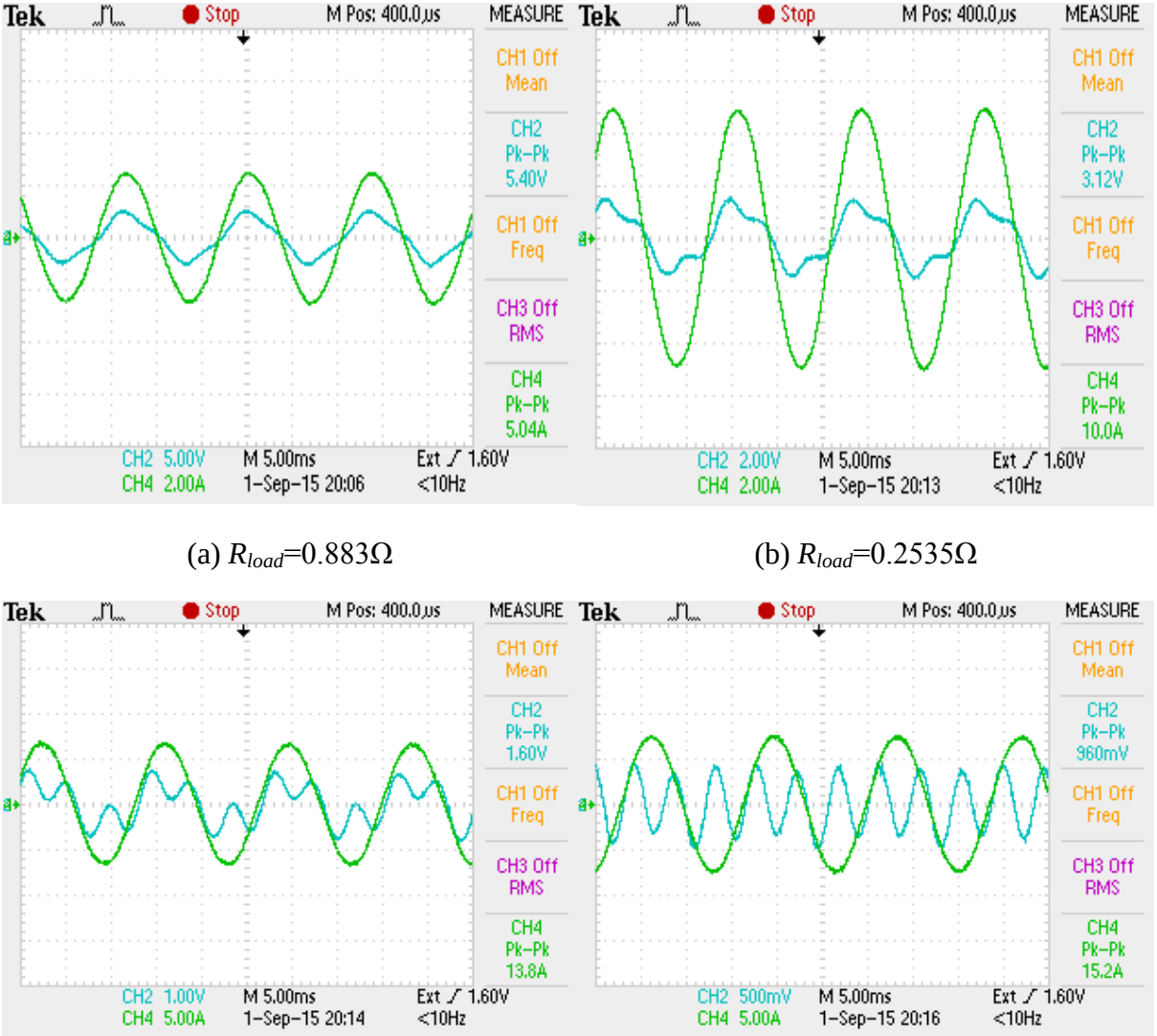

(a) R_{load}=0.883Ω (b) R_{load}=0.2535Ω

(c) R_{load}=0.089Ω (d) R_{load}=0

Fig.4.51 Phase winding terminal voltage (CH2) and phase current (CH4) waveforms of the prototype operating at generator mode at 400rpm.

TABLE 4.5 COMPARISON OF 2D FE PREDICTED AND MEASURED MAXIMUM CURRENTS

R_{load} (Ω)	Measured (A)	2D FEA predicted (A)
0.883	2.5	3.10
0.2535	5	6.15
0.089	6.9	8.12
0	7.6	9.57

Fig.4.52 shows the phase winding PWM voltage (CH2), rotor position (CH3) and current (CH4) waveforms of the prototype operating at motor mode at 400rpm, based on the test rig shown in Fig.4.52. In Fig.4.52, T_{load} is the load torque. The DC voltage and phase current limits are set as 18V and 7.5A, respectively.

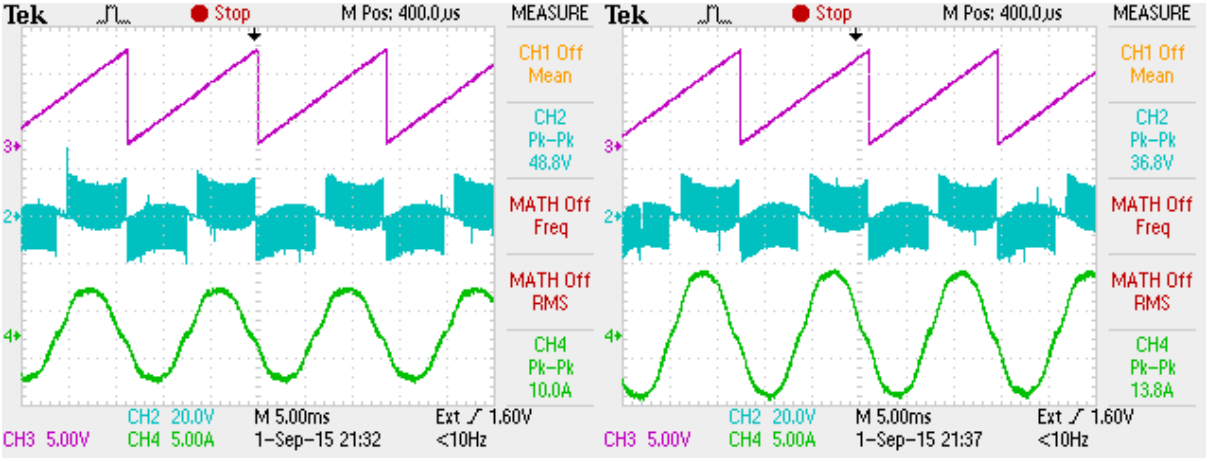

(a) T_{load}=0.22Nm (b) T_{load}=0.4Nm

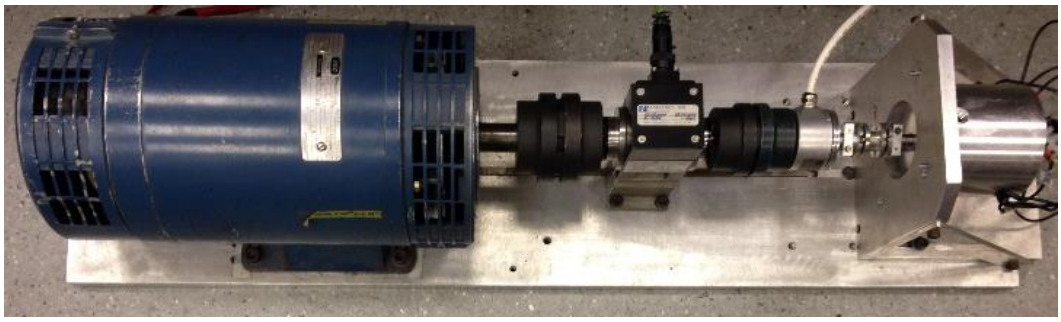

Fig.4.52 Phase winding PWM voltage (CH2), rotor position (CH3) and current (CH4) waveforms of the prototype operating at motor mode at 400rpm and photo of the test rig including DC machine, torque sensor, position sensor and prototype from left to right.

4.8 Summary

A novel type of partitioned stator switched flux permanent magnet (PS-SFPM) machines with either all- or alternate-pole-wound are developed in this chapter. The proposed PS-SFPM machines have two stators which separately accommodate the armature windings and the PMs, and between which is the rotor made of iron pieces, and/or the number of stator poles with PMs equal to half of that with armature windings. The results show that the PS-SFPM machines having alternate-pole-wound exhibit higher average torque than their all-pole-wound counterparts. However, it may easily undergo saturation when subjected to heavy

electric loading. Their electromagnetic performances are compared, such as open-circuit flux-linkages and back-EMFs, cogging torque, static torque waveforms, average torque against current and PM utilization ratio, etc. Amongst all the compared machines, the 11-pole machine having alternate-pole-wound seems to exhibit the best performance since it has more sinusoidal and symmetrical back-EMF waveform, and better torque/power density at fixed copper loss condition, as well as less PM usage. A prototype machine is manufactured and tested to validate the analyses.

CHAPTER 5

SWITCHED FLUX PM MACHINES HAVING TWO SEPARATE STATORS WITH C-CORE OUTER STATOR STRUCTURE

5.1 Introduction

Permanent magnet (PM) machines have been researched extensively due to their merits which include but are not limited to high torque, better efficiency, wide speed range and good flux-weakening capabilities etc. In particular, tremendous investigations are on-going on switched flux (SF) machines. Switched flux (SF) machine was firstly proposed as a single phase generator in the 1950s [RAU55]. Nevertheless, it received little or no attention until its introduction as a three-phase SFPM machine by [HOA97]. This re-emergence could possibly be due to the availability of high energy density PM materials as well as advancement in computer-aided designs and the availability of improved power electronic devices. For about two decades now, SFPM machines have been widely researched [HOA97], [ZHU05], [HUA08], [ILH10], [CHE10b] and [CHE10d]. Compared with conventional rotor-PM machines, SFPM machines have better thermal dissipation capability since the PMs are placed in the stator [ZHU05] and [CHE11]. Meanwhile, due to the flux focusing effect, SFPM machines can deliver higher torque than other types of stator-PM machines, *i.e.* doubly-salient PM [WAN01], [MOR10] and flux reversal PM machines [LIA95], and [WU14], as pointed out in [ZHU07] and [ZHA09]. Some modified topologies are also studied, such as alternate pole winding [OWE10], E-core [CHE11b], and C-core SFPM machines [CHE11c], multiphase and hybrid configurations [THO09], [GAU14], and [WAN12]. In [MCF14], [WU15] and [MCF15], it is found that the operation principle of SFPM machines is based on magnetic gearing effect. There are abundant air gap field harmonics due to the modulation of the salient rotor pole of the PMs and armature reaction fields, which is similar to magnetic gears [ATA01], [ATA04], [RAS05], and [JIA10] and magnetically geared machines [WAN08], [WAN09**]**, [QU11], [EVA15], and [AWA16b]. Indeed, a novel magnetically-geared SFPM machine with separated PMs and armature winding is proposed and analysed in [EVA15], of which the topology is similar to the magnetically-geared machine [WAN08] and [WAN09]. For the magnetically geared SFPM machines having partitioned stators proposed in [EVA15], it has higher machine inner space utilization than the conventional SFPM machines with a single stator [CHE10b]. According to the magnetic gearing effect [MCF15a], [WU15a], and [MCF15b], by separating the PMs

and armature windings in the inner and outer stators, respectively, the total slot area can be increased to improve the torque density.

There are three parts in a magnetic gear, *i.e*. the outer PM component, the inner PM component and the sandwiched iron pieces. The torque can be transferred from one part to the other, making magnetic gear a torque-transmitting device. Various gear ratios can be obtained with two different rotating parts [ATA04]. When one rotating PM component is replaced by an armature winding stator with the same field function as in a magnetic gear with two rotating PM components (the iron pieces remain static), a magnetically geared machine analysed in [WAN08] and [WAN09] can be obtained. From this point of view, magnetically geared SFPM machines proposed and analysed in [EVA15], can be regarded as the machines corresponding to the magnetic gear with rotating outer PM component and iron pieces, whilst the inner PM component is static [RAS05].

As shown in Fig.5.1, the magnetically geared SFPM machines have three parts separated by two air-gaps, *i.e*. the outer stator with armature windings, the inner stator with inserted PMs and the sandwiched rotating rotor with iron pieces. In addition, the outer and the inner stators have the same pole number in the magnetically geared SFPM machines. The schematic diagram of the proposed machine is depicted in Fig.5.1.

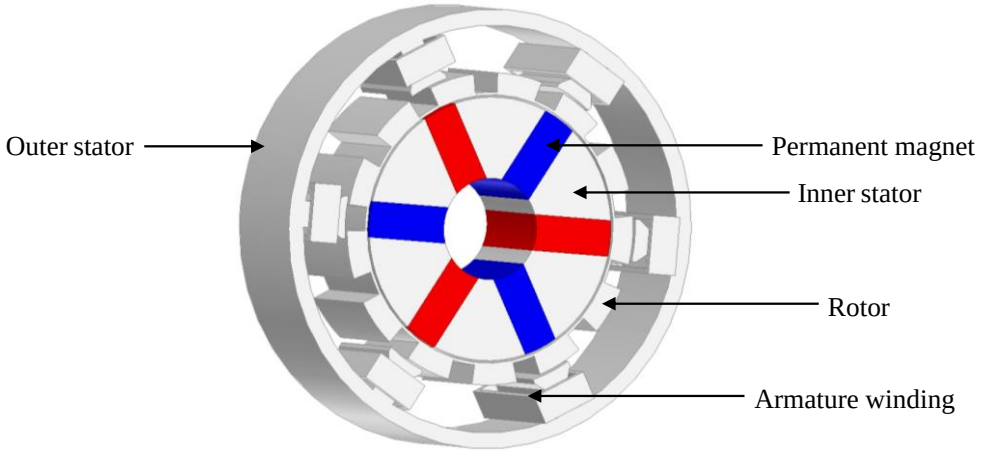

Fig.5.1 Illustration of the proposed magnetically geared SFPM machine.

In this study, a novel type of magnetically geared SFPM machines is proposed, in which the relationship between the stator pole number N_s and the rotor pole number N_r is given by:

$$|2N_s \pm k| = N_r \tag{5.2}$$

where k is an integer.

The proposed machine configuration is different from that with $|N_s \pm k| = N_r$ analysed in [EVA15]. It is worth mentioning that the PM volumes of the proposed machines are smaller than the ones in [EVA15]. Thus, it would be relatively economical to use in terms of torque density per magnet usage. Moreover, the analysed machines are similar to that in [CHE10b] but with PMs relocated to the inner stator.

Further, feasible stator/rotor-pole combinations are analysed using 2-dimensional (FEA) technique. Then, the influence of main design parameters on the average electromagnetic torque is investigated. Finally, a prototype is built and tested for validation of the predicted FEA results.

According to [ATA04], the general expression for the angular velocity of either of the rotor-PMs in a magnetic gear having two rotating parts and a stationary steel piece is given by:

$$\omega_{i,j} = \frac{ip}{ip + jn_s}\omega_r + \frac{jn_s}{ip + jn_s}\omega_s \tag{5.2}$$

where ω_r and ω_s are the rotational velocities of the rotor-PMs and the stationary modulating ring respectively, with corresponding pole pair numbers p and n_s. The maximum torque transmission will occur when i=1 and j=-1.

If we replace the outer rotor-PM with a stator having space harmonics produced by the windings, while rotating the modulating ring; then by analogy, the gear ratio of the proposed magnetically geared SFPM machines can be obtained as:

$$G_{ratio} = \frac{-1 * (j) * N_s}{iN_r} = \frac{N_s}{N_r} \tag{5.3}$$

where N_s and N_r are the stator and rotor pole numbers of the proposed machines.

TABLE 5.1 MAIN DESIGN PARAMETERS OF ANALYSED MAGNETICALLY GEARED SFPM MACHINES

Item	**Magnetically geared SFPM machines**							
Rotor pole number, N_r	**4**	**5**	**7**	**8**	**10**	**11**	**13**	**14**
Stator pole number, N_s	6							
Number of phases, m	3							
Base speed (rpm)	400							
Number of turns/phase	72							
Outer stator diameter (mm)	90							
Active stack length (mm)	25							
Split ratio	0.639	0.66	0.75	0.68	0.71	0.71	0.72	0.73
Rotor radial thickness (mm)	5.89	6.52	3.95	6.27	5.06	5.11	4.48	4.52
Slot opening/pitch ratio	0.585	0.51	0.79	0.61	0.799	0.77	0.75	0.77
Stator back iron thickness (mm)	4.69	3.96	3.44	3.39	3.81	3.15	3.27	3.45
Air gap length (mm)	0.5							
Shaft diameter (mm)	20.8							
Copper loss (W)	30							
Magnet relative permeability	1.05							
Magnet remanence (T)	1.2							
PM volume (k.mm^3)	15.88	16.54	18.00	14.38	15.46	16.26	18.32	19.72
Torque density (kNm/m^3)	14.45	26.41	30.53	6.92	22.55	31.84	31.31	22.30

5.2 Machine optimization and influence of leading design parameters on the average torque

The variation of average torque on the main design parameters of the analysed machines are depicted in Figs.5.2 to 5.7. The varied design parameters include: the split-ratio, the slot opening/tooth pitch, the rotor radial thickness, the rotor pole arc/pole pitch ratio, the stator tooth-width thickness and the stator back-iron thickness.

5.2.1 Split ratio

Initially, there is a direct proportionality between the variations of average torque with the split ratio until such a value when the electromagnetic saturation becomes critical due to smaller space for the armature conductors. Hence, there is an optimum value of split ratio as seen in Fig.5.2.

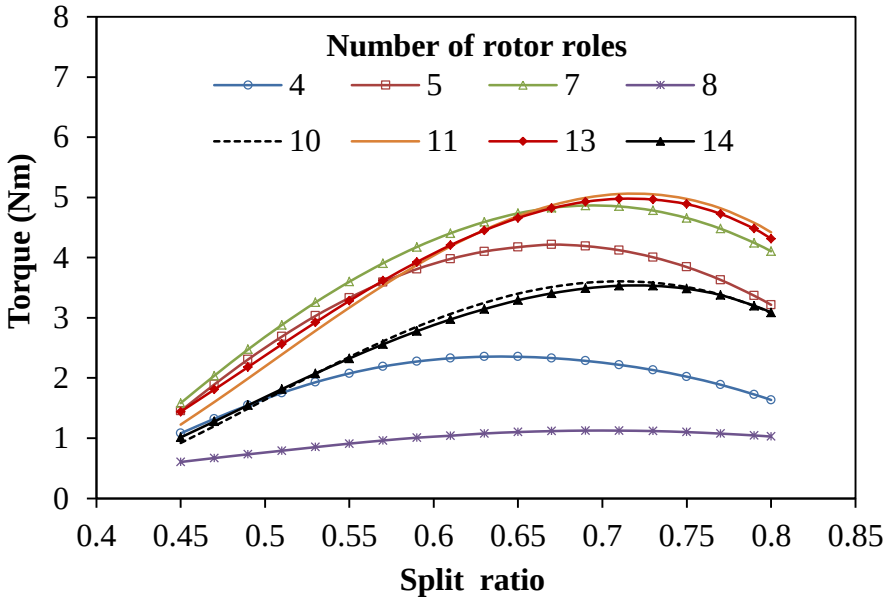

Fig.5.2 Comparison of the influence of split ratio on average torque.

5.2.2 Slot opening

Similarly, there would be an optimum value of slot opening/tooth pitch ratio as illustrated in Fig.5.3, larger slot opening may lead to higher slot area of the armature conductors and hence higher electric load. However, this also causes thinner outer stator teeth and higher electromagnetic saturation [AWA16]. Moreover, the high slot opening/tooth pitch ratio value is related to its large slot area.

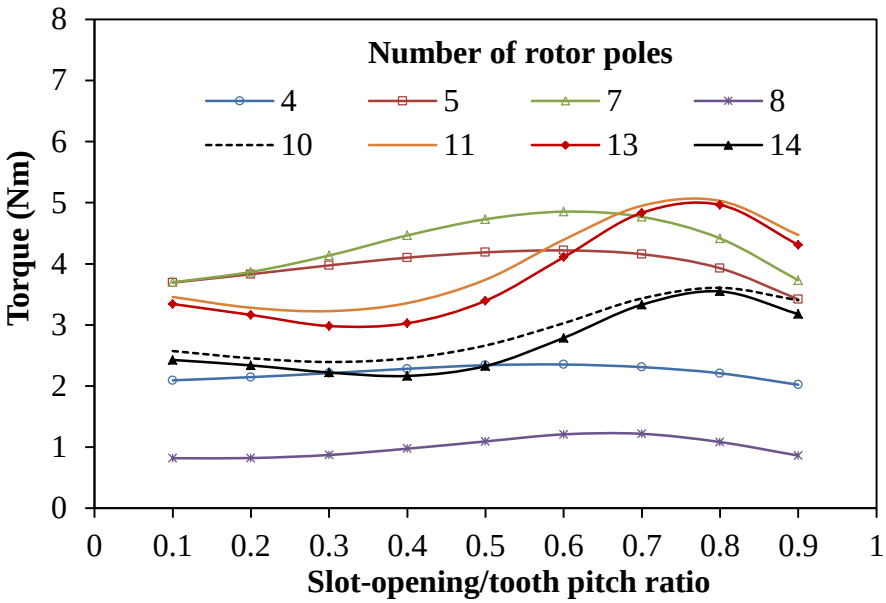

Fig.5.3 Comparison of the influence of slot opening/tooth pitch ratio on average torque.

5.2.3 Rotor radial thickness

Moreover, smaller size of the rotor radial thickness may undergo a quicker saturation, thus resulting in low flux per pole and consequently low average torque; while over enlarged radial thickness may occupy the available spaces for the armature windings, thereby leading to a reduced phase current at a fixed copper loss condition. Thus, an optimum value of the rotor radial thickness would occur in-between these two situations. The variation of average torque with rotor radial thickness is shown in Fig.5.4.

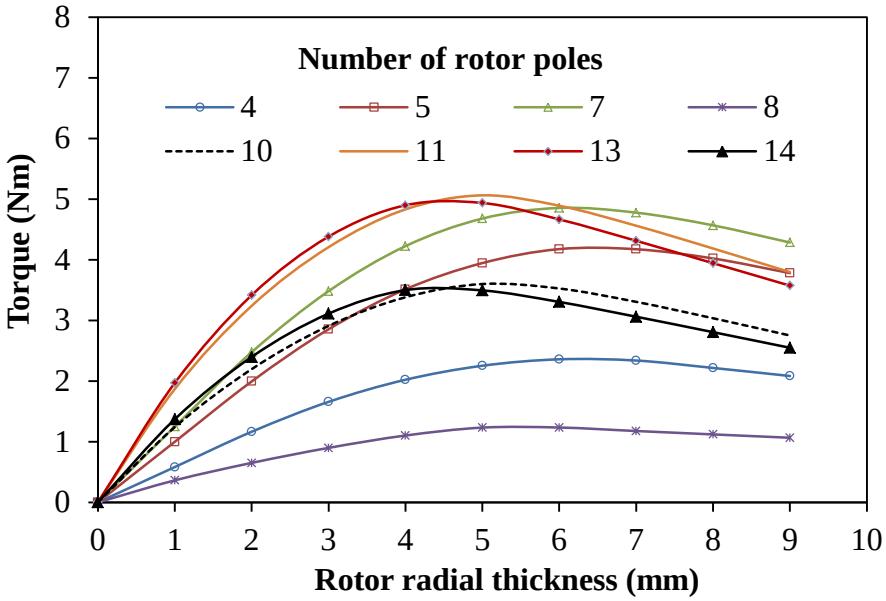

Fig.5.4 Comparison of the influence of rotor radial thickness on average torque.

5.2.4 Rotor iron pole arc/pole pitch

The respective optimum values of the rotor pole arcs are shown in Fig.5.5 and also listed in Table 5.1. It is worth noting that the optimum values of these pole arcs would be dependent on the amount of the resultant magnetic flux surrounding the inner and outer arcs consecutively.

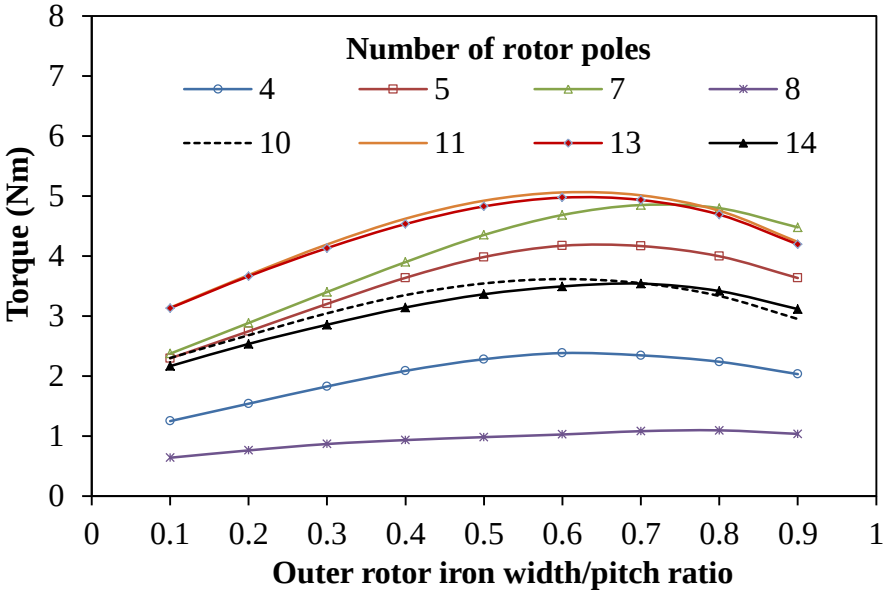

(a) Outer rotor iron pole arc/pitch ratio

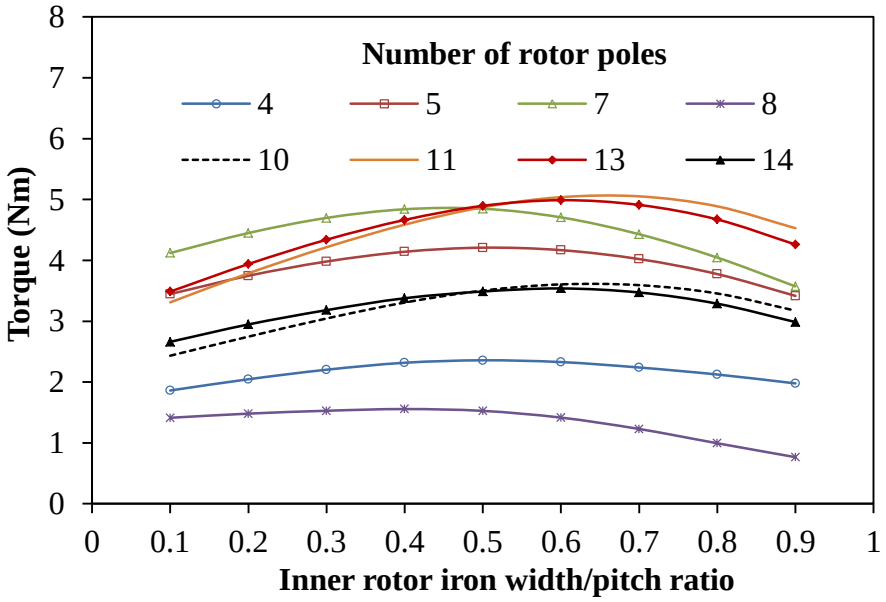

(b) Inner rotor iron pole arc/pitch ratio

Fig.5.5 Comparison of the influence of rotor iron width on average torque.

5.2.5 Stator tooth-width thickness.

Further, as shown in Figs.5.6 and 5.7, the analysed machines would have an initial sharp increase for the average torque variation with the stator back-iron thickness and the stator tooth-width thickness due to the concentration of useful flux on these parts of the machine, and subsequently reduces as their thickness increases above its zenith point due to larger amount of leakage flux as well as reduced slot area.

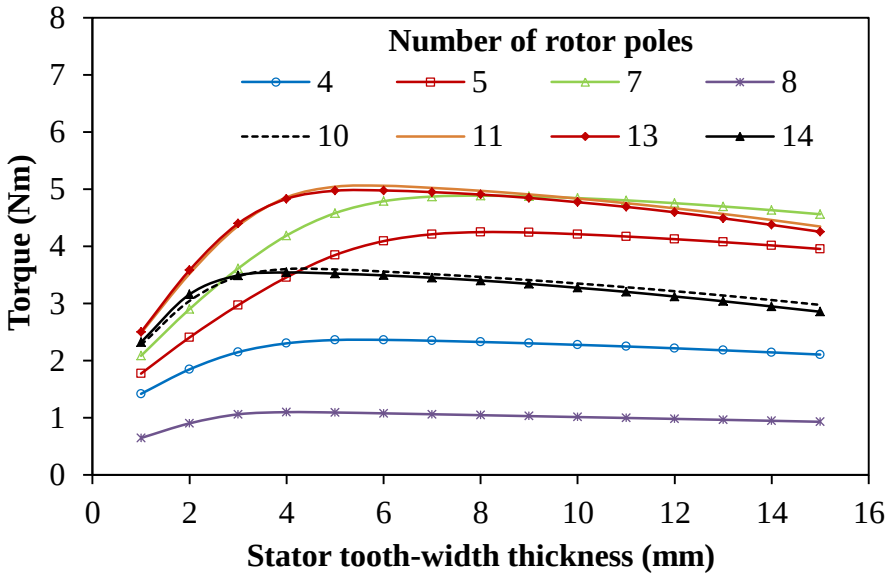

Fig.5.6 Comparison of the influence of outer stator tooth-width thickness on average torque.

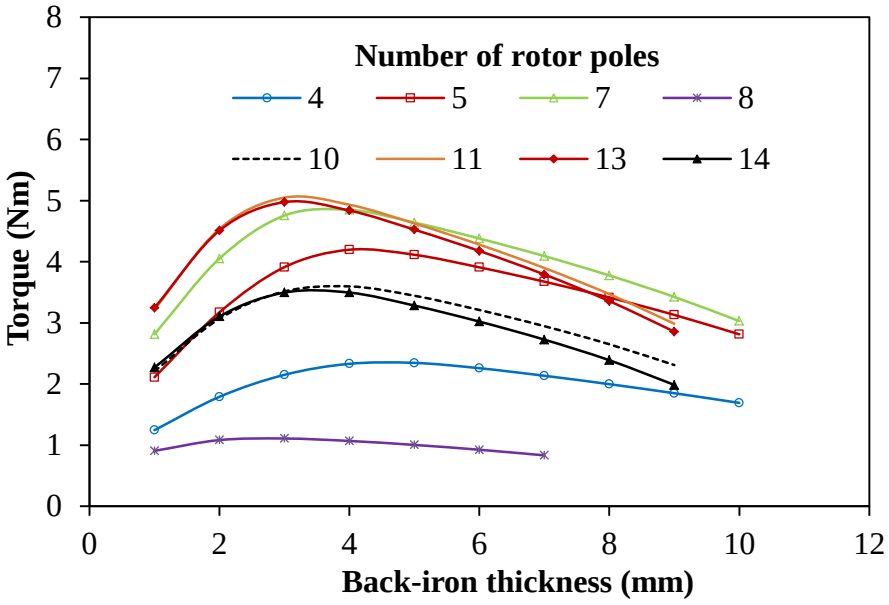

Fig.5.7 Comparison of the influence of outer stator back-iron thickness on average torque.

5.3 Winding configurations and coil-EMF phasors

The coil phasors and winding configuration of the machines are shown in Fig.5.8. Note that the coil phasor *k*' (*k'*=1, 2, 3, 4, 5, 6) is the opposite phasor of *k*. Based on the coil back-EMF phasors, we have analysed all the machines and quantitatively compared their electromagnetic performances in this study.

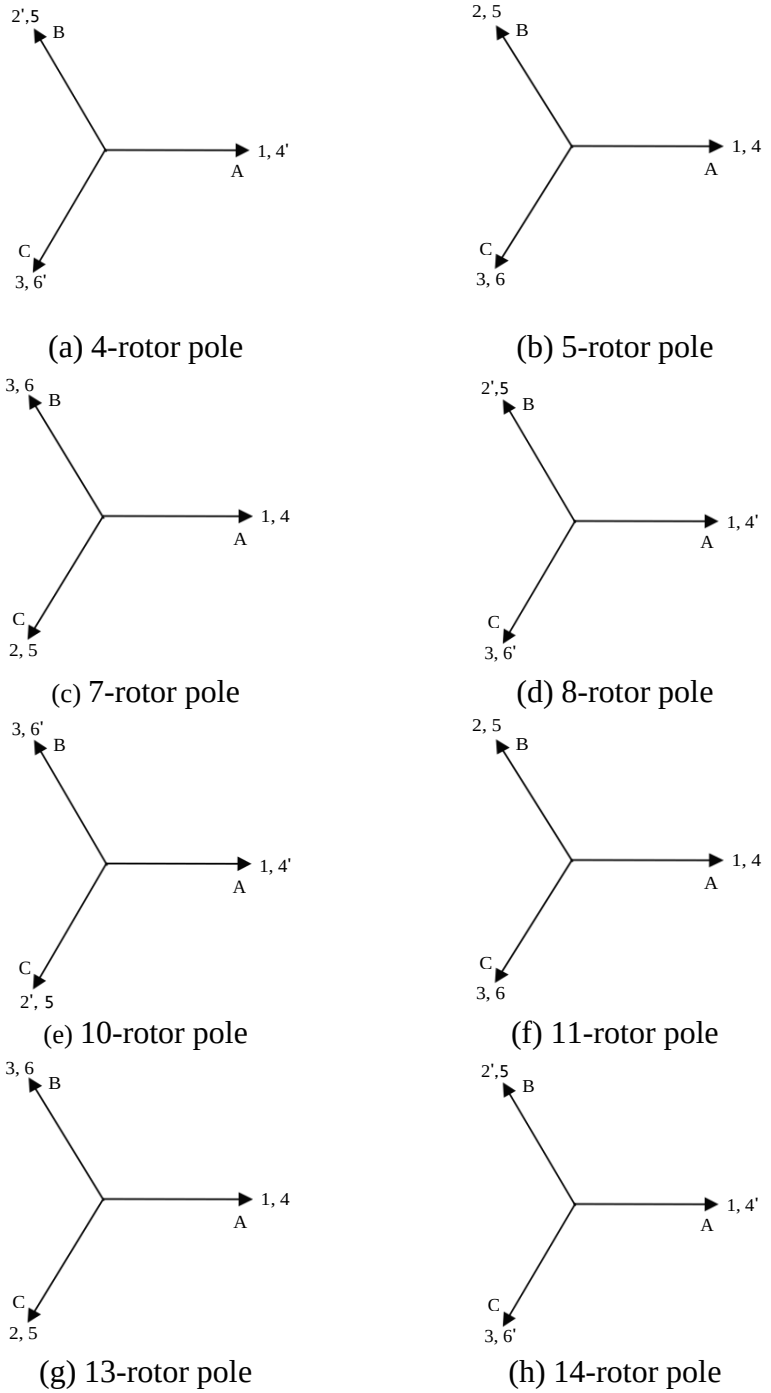

(a) 4-rotor pole (b) 5-rotor pole

(c) 7-rotor pole (d) 8-rotor pole

(e) 10-rotor pole (f) 11-rotor pole

(g) 13-rotor pole (h) 14-rotor pole

Fig.5.8 Coil EMF phasors and winding configurations of analysed machines.

5.3.1 Airgap-field distributions and flux densities.

The open circuit flux densities with their corresponding flux line distributions of the analysed machines are shown in Fig.5.9, evaluated at zero *d*-axis control.

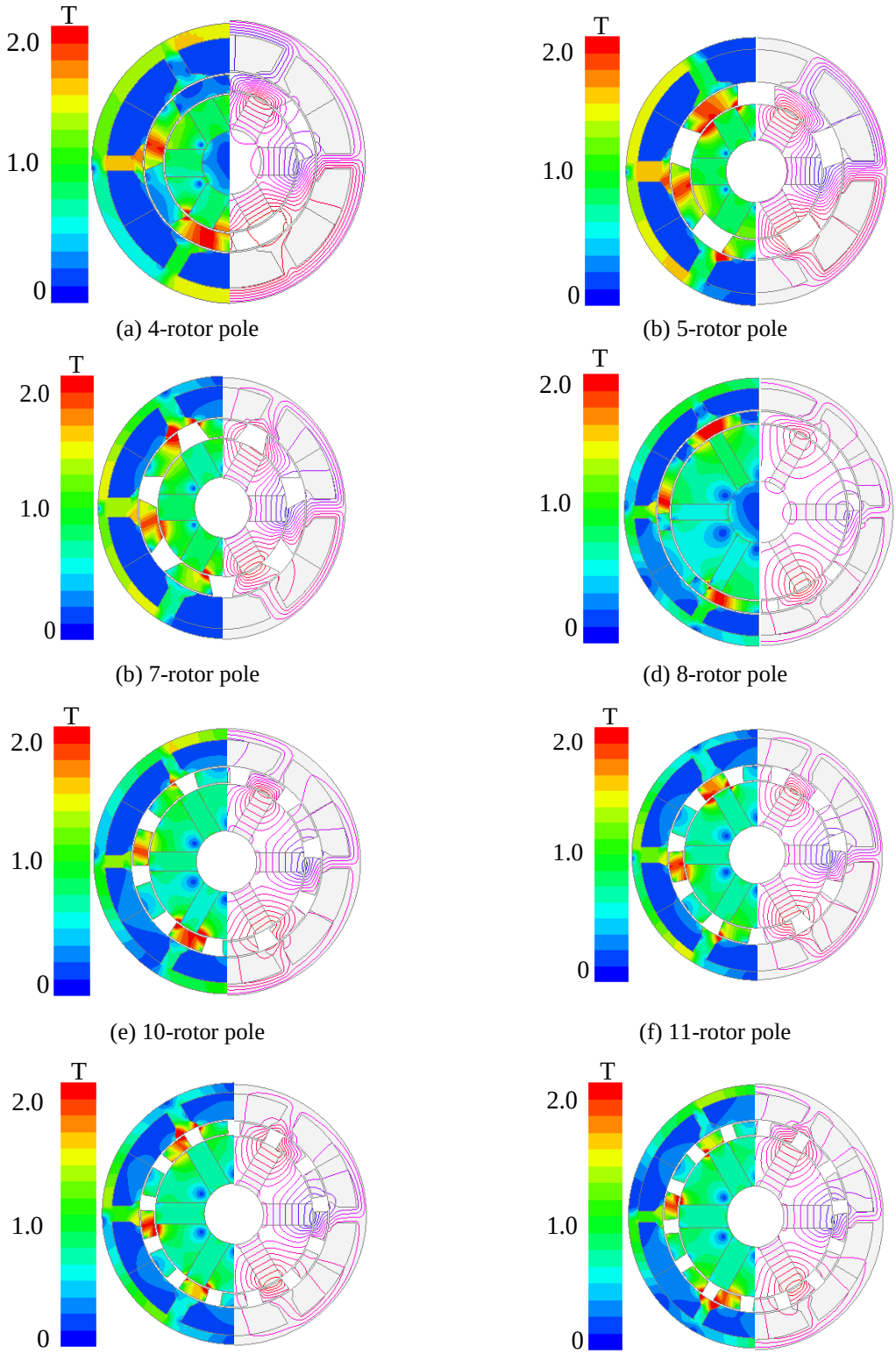

(a) 4-rotor pole (b) 5-rotor pole

(b) 7-rotor pole (d) 8-rotor pole

(e) 10-rotor pole (f) 11-rotor pole

(g) 13-rotor pole (h) 14-rotor pole

Fig.5.9 Open-circuit field and flux distributions of the analysed machines, i_d=0.

5.4 Influence of rotor pole number on the electromagnetic performance

The open-circuit phase flux-linkage waveforms with their corresponding harmonic spectra are shown in Fig.5.10. The fundamental values of the flux-linkage obtained from the Fast Fourier Transforms (FFT) are 13.39mWb, 21.07mWb, 17.04mWb, 4.82mWb, 8.94mWb, 11.51mWb, 9.55mWb and 6.22mWb for the 4- , 5- , 7- , 8- , 10- , 11- , 13- and 14-rotor pole machines, respectively. Further, the back-EMF waveforms of the analysed machines with their respective spectra are depicted in Fig.5.11. It is worth mentioning that the odd-rotor pole machines exhibits more sinusoidal and symmetrical flux-linkage and back-EMF waveforms than their equivalent even rotor pole counterparts because the resultant even order harmonics from the coil waveforms are cancelled in the odd rotor pole SFPM machines. On the contrary, the coil flux-linkage and back-EMF of the analysed even rotor pole machines have identical waveforms, thus the individual coil harmonics will manifest in the resultant phase flux-linkage and back-EMF waveforms/spectra, thereby making the waveforms to be non-sinusoidal and asymmetric. Note also that the maximum flux per pole on the respective machines is dependent on their varying electrical frequencies similar to the conventional SFPM machines [CHE10b]. It is worth noting that the back-EMF waveform of the 11-rotor pole machine is more sinusoidal and symmetrical amongst all the analysed machines. Moreover, the 11-rotor pole machine exhibits the largest fundamental value of the back-EMF and consequently the largest output electromagnetic torque. To obtain symmetrical phase back-EMF waveforms, the stator/rotor-pole combinations should satisfy:

$$\frac{N_s}{HCF(N_s, N_r)} = \ even\ number \tag{5.4}$$

where *HCF* is the highest common factor.

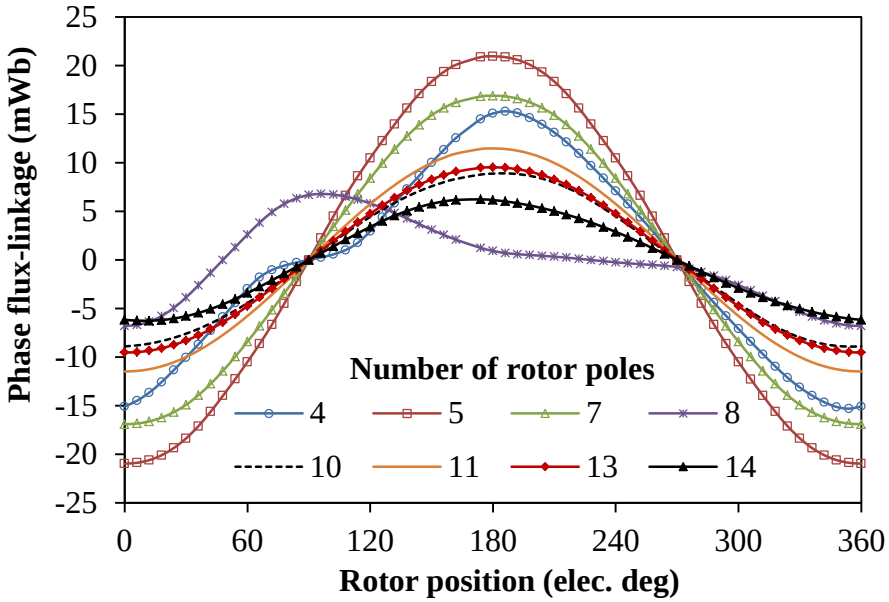

(a) Waveforms

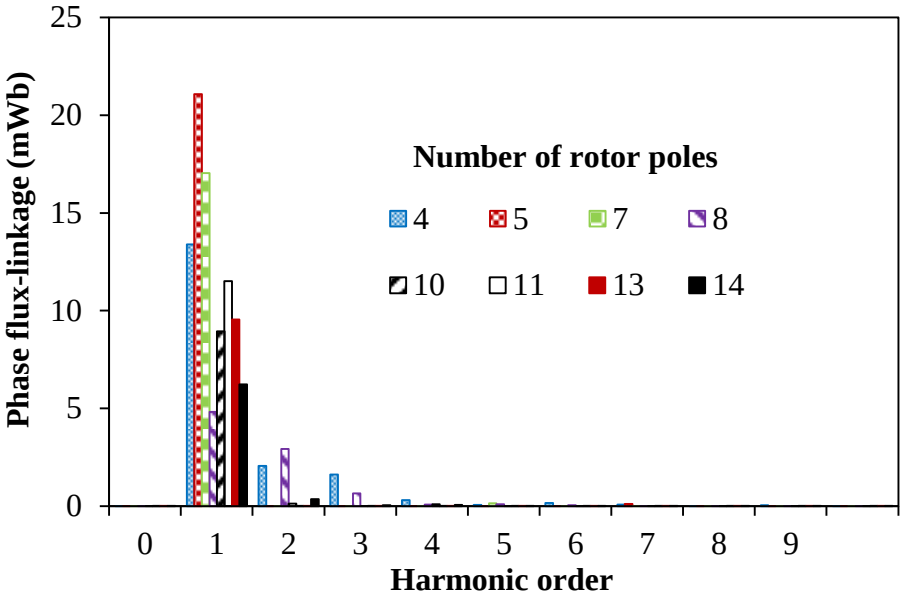

(b) Spectra

Fig.5.10 Comparison of open-circuit phase flux-linkage, i_d=0.

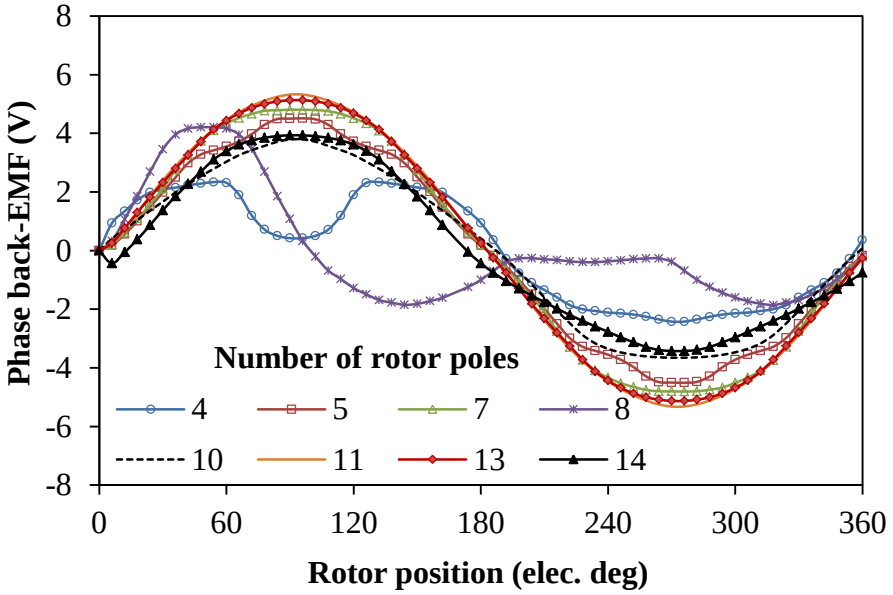

(a) Waveforms

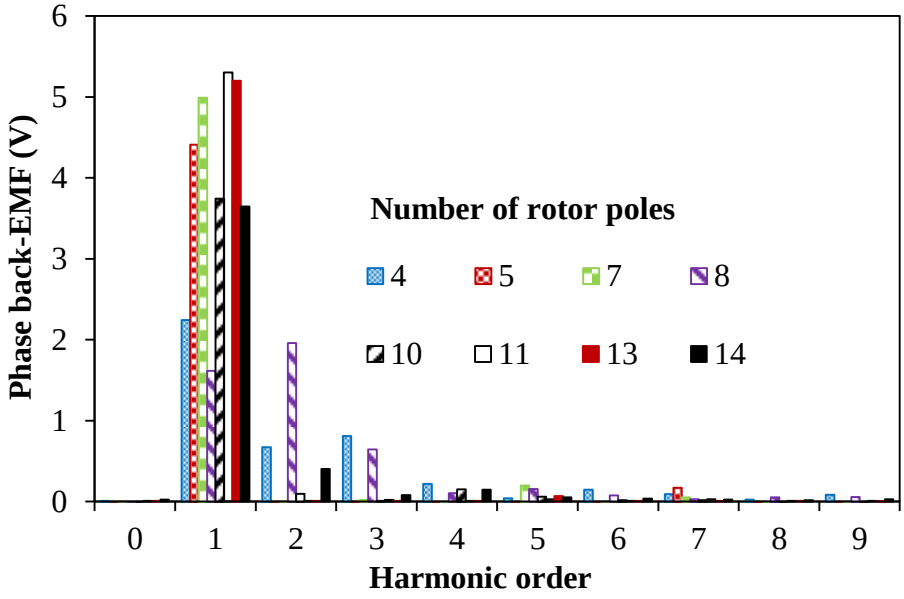

(b) Spectra

Fig.5.11 Variation of phase back-EMF with rotor position, at 400rpm.

Obviously, from the predicted cogging torque results shown in Fig.5.12, the machines with odd numbers of rotor poles, *i.e.* 5, 7, 11 and 13, seem to have lower cogging torque compared with their even numbered counterparts, *i.e.* 4, 8, 10 and 14. The peak-to-peak values of the cogging torque of these machines with 4-, 5-, 7- , 8- , 10- , 11- , 13- , and 14-rotor poles are approximately 2.4Nm, 0.13Nm, 0.3Nm, 1.8Nm, 1.0Nm, 0.05Nm, 0.008 and 0.746Nm, respectively. It is worth noting that the even rotor pole machines, in particular the 4- and 8-rotor pole machines are characterized by high cogging torque, which is caused by the poorer

goodness factor of cogging torque, C_T. The amplitude of the cogging torque is related to the goodness factor C_T, by:

$$C_T = \frac{N_r N_s}{LCM(N_r, N_s)} \tag{5.5}$$

where *LCM* is the least common multiple.

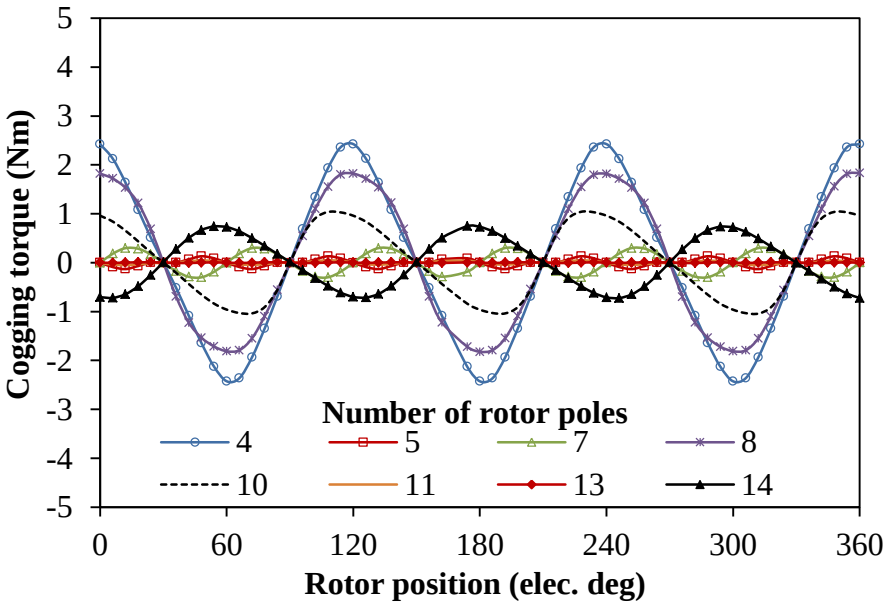

(a) Waveforms

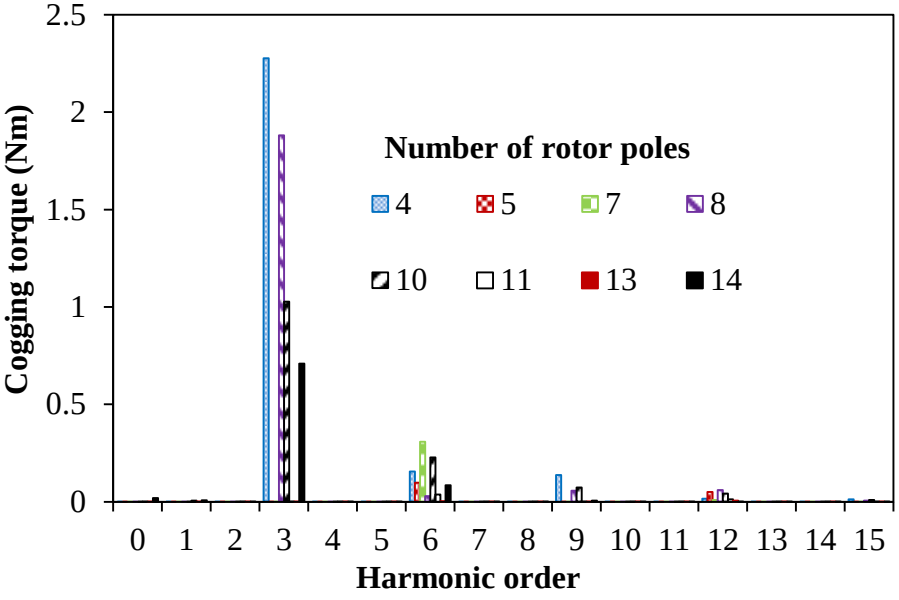

(b) Spectra

Fig.5.12 Comparison of cogging torque in the analysed machines.

Fig.5.12 (b) illustrates the cogging torque harmonics of these analysed machines. The cogging torque spectra show that the magnitudes of the 3rd and the 6th orders of harmonics are

significant in the machines with even number of rotor poles, which causes larger cogging torque.

Fig.5.13 shows the comparison of the electromagnetic torque of the proposed machines. It is observed that the 11-rotor pole machine has the highest torque of ~ 5.06Nm, amongst all the 8 analysed machines, and also a small torque ripple due to smaller back-EMF harmonics and cogging torque. The 13-rotor pole machine has slightly less electromagnetic torque of about 4.98Nm. However, the electromagnetic torque of the 8-rotor pole machine is only 1.1Nm, which is significantly very low compared to other machines. The low values of the output torque seen in the 8- and 4-rotor pole machines are essentially due to their possession of large cogging torque, since the output electromagnetic torque of a given PM machine is equivalent to the product of its phase currents and the respective fundamental back-EMF values. The harmonic spectra of the electromagnetic torque are shown in Fig.5.13 (b). In the machines with odd rotor pole numbers, the harmonics are with $6k$ (k=1, 2, 3…) orders, whilst they are $3k$ (k=1, 2, 3…) in the machines with even rotor pole numbers.

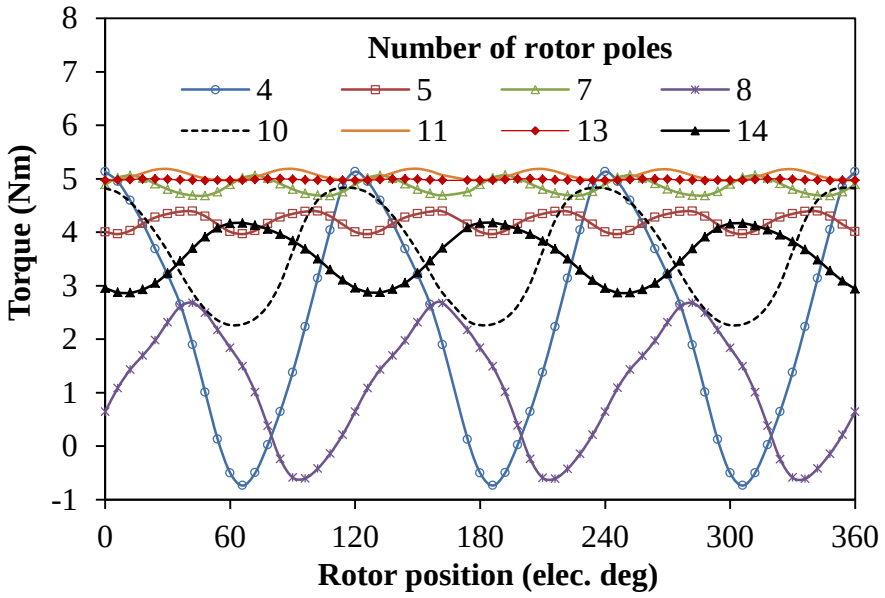

(a) Waveforms

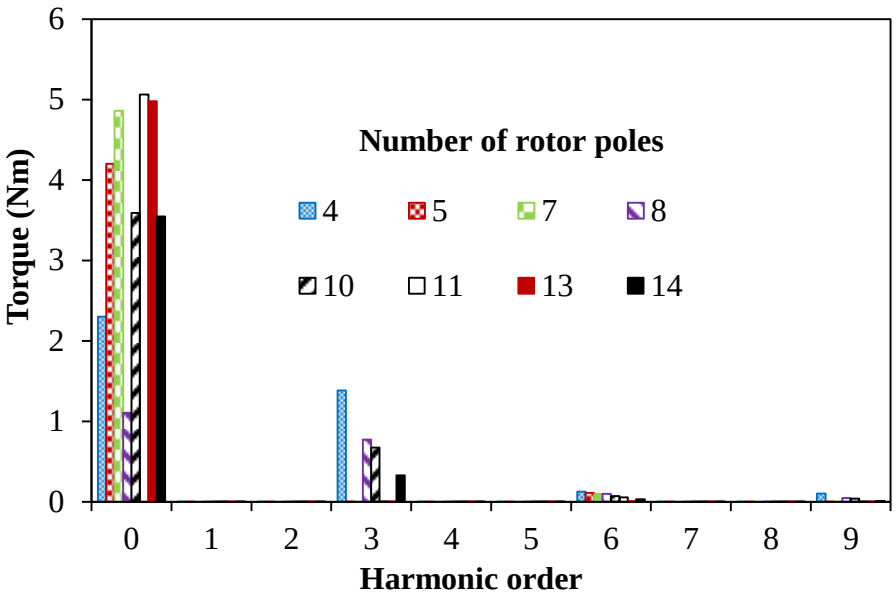

(b) Spectra

Fig.5.13 Comparison of torque characteristics (i_d=0, copper loss=30W).

It is evident from Figs. 5.14 and 5.15 that the 11- and 13-rotor pole machines are potential candidates for high torque density, which is desirable for direct drive applications at low speed. Moreover, the torque-current and torque-copper loss saturation curves of the analysed machines are displayed in Figs.5.14 and 5.15 respectively. Note that the load-withstand capability of the odd rotor pole machines is higher than that of their even rotor pole counterparts. The average torque per PM volume characteristics at different currents of the analysed machines are shown in Fig.5.16. It can be seen that the proposed 11- and 13-pole magnetically geared SFPM machines have higher PM utilization compared to other analysed machines whilst the 8-pole counterpart suffers from the smallest torque per PM volume, followed by the 4-rotor pole machine.

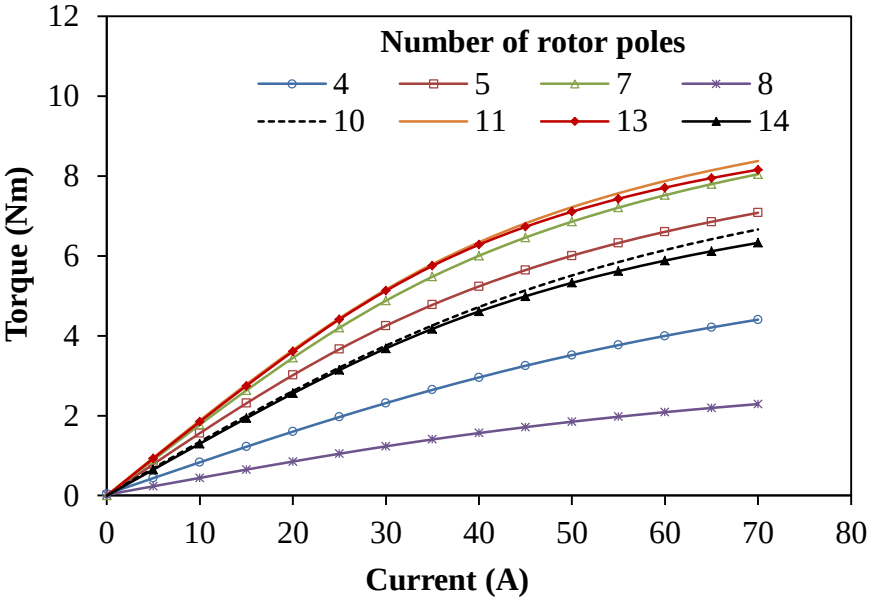

Fig.5.14 Comparison of average torque versus current, i_d=0.

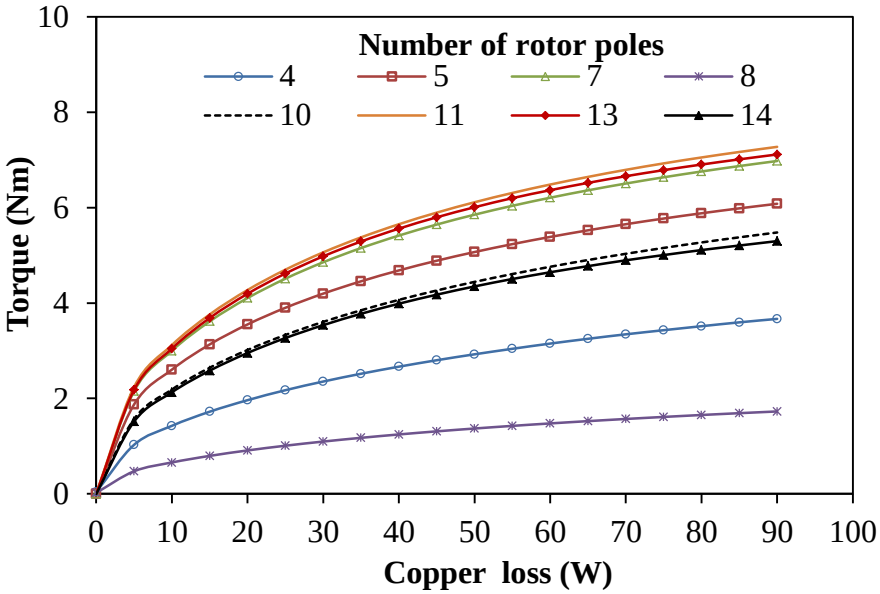

Fig.5.15 Comparison of average torque versus copper loss, i_d=0.

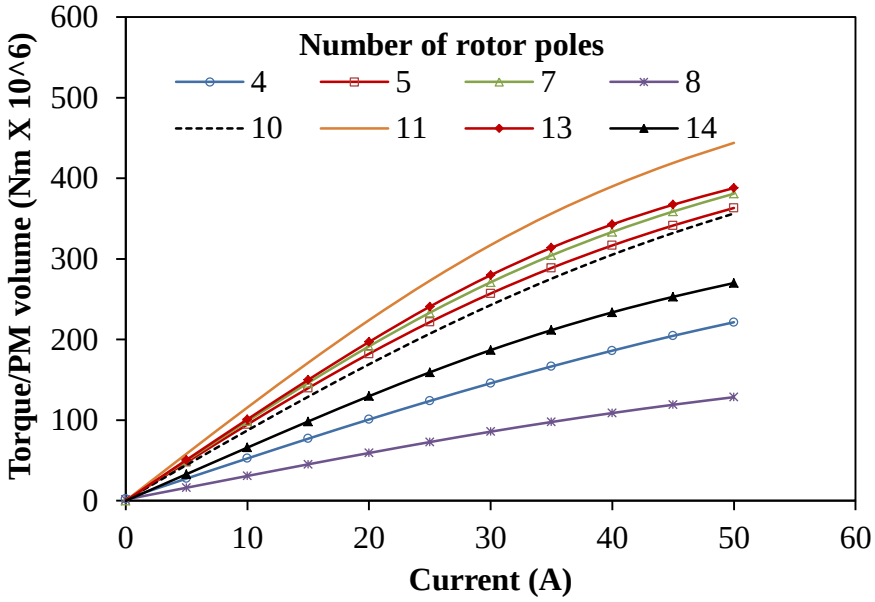

Fig.5.16 Comparison of average torque per PM volume versus q-axis current, i_d=0.

As mentioned earlier, the proposed machines are optimized using the genetic algorithm optimization technique at a fixed copper loss of 30W. During the optimization with fixed copper loss, the following condition must be fulfilled:

$$\frac{I_a^2 N_a^2}{A_a} = constant \tag{5.6}$$

where I_a is the phase RMS current. N_a is the number of turns per phase. A_a is the slot area.

The phase resistance of the machine is given by:

$$R_a = \frac{\rho_{cu} 2nN_t(L_{axial} + L_{end})}{A_a k_{pf} \Big/ N_t} = \frac{2n\rho_{cu} N_t^2 (L_{axial} + L_{end})}{A_a k_{pf}} \tag{5.7}$$

where ρ_{cu} is resistivity of copper. K_{pf} is the winding packing factor. N_t is the number of turns per coil. L_{axial} is the active stack length. N is the number of coils per phase. L_{end} is the end winding length.

With the end winding neglected for simplicity, the copper loss p_{cu} can be obtained by:

$$p_{cu} = 3I_a^2 R_a = \frac{6I_a^2 \rho_{cu} n N_t^2 L_{axial}}{A_a k_{pf}} \tag{5.8}$$

5.5 Influence of unbalanced magnetic forces (UMF) on the rotor

In the foregoing analysis, it is found that the odd-rotor pole magnetically geared SFPM machines can deliver higher torque than the even rotor pole ones. However, it should be noted that the odd rotor pole number rotors will cause unbalanced magnetic force [ZHU07b] on the rotor. As shown in Figs.5.17 and 5.18 the proposed 6-stator teeth/11-pole and 6-stator teeth/13-pole magnetically geared SFPM machines exhibit smaller unbalanced magnetic forces than the 6-stator teeth/5-pole and 6-stator teeth/7-pole machines.

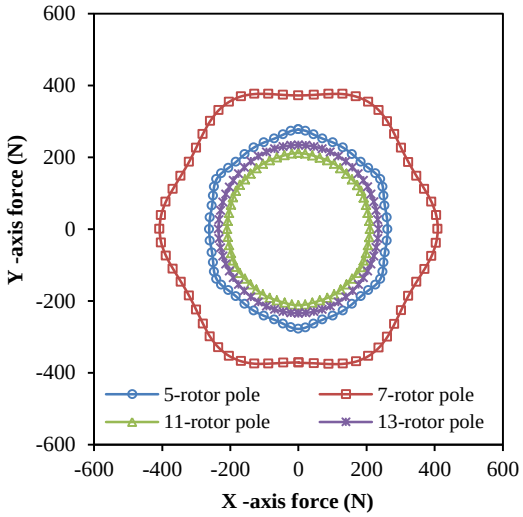

Fig.5.17 Comparison of open-circuit unbalanced magnetic force in analysed machines.

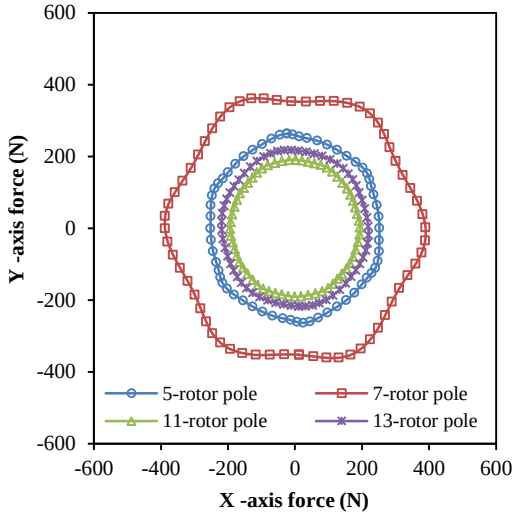

Fig.5.18 Comparison of on-load unbalanced magnetic force in analysed machines (i_d=0, i_q=15A).

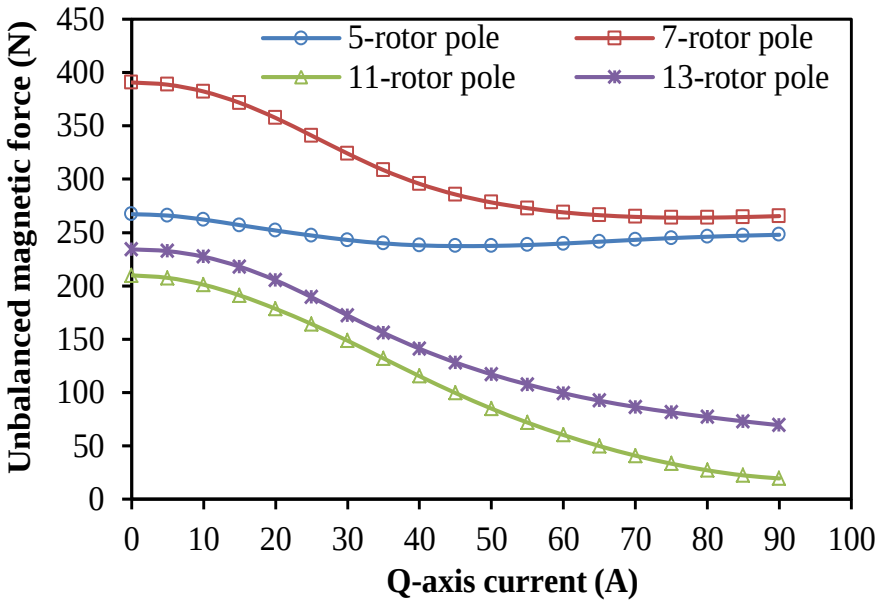

Fig.5.19 Comparison of unbalanced magnetic force versus *q*-axis current, i_d=0.

5.6 Inductance characteristics

The winding inductance profile of the analysed machines is given in Figs.5.20 and 5.21. This includes the *d*- and *q*-axis inductances as well as the machines' self- and mutual-inductances.

5.6.1 D- and Q-axis inductances

Figs.5.20 (a) and (b) show the *d*- axis and *q*-axis inductances of the analysed machines, respectively. The plots reveal that the machines have similar value of the *q*-and *d*-axis inductances, which implies that their saliency ratios would be close to unity. Hence, the machines would essentially have negligible reluctance torque. Moreover, the odd rotor pole machines exhibit the larger value of *q*-axis inductance especially for the 5-rotor pole machine. We have employed the inductance calculation technique detailed in [QI09] in the calculation of the winding inductances, i.e. by transforming the *a*, *b*, *c* currents and flux-linkages to *d* and *q* variables.

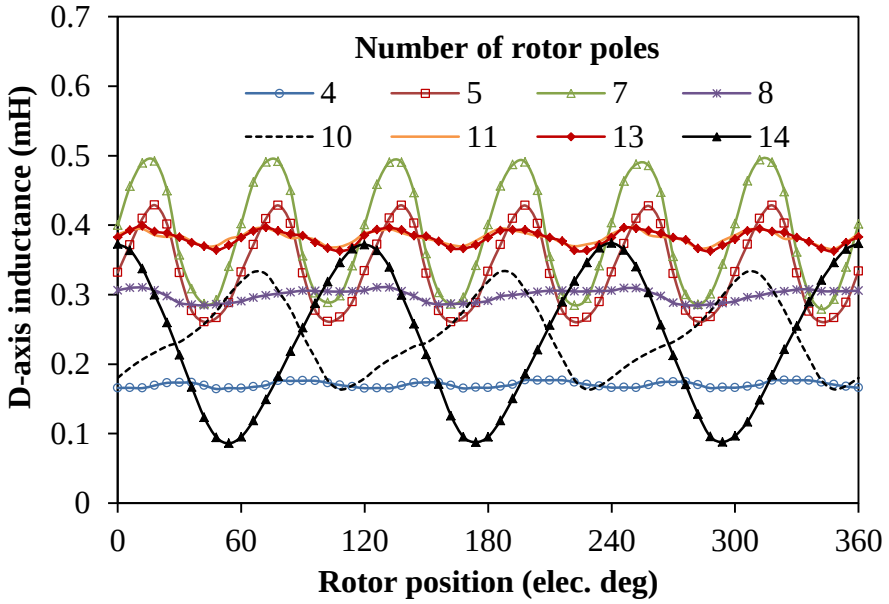

(a)

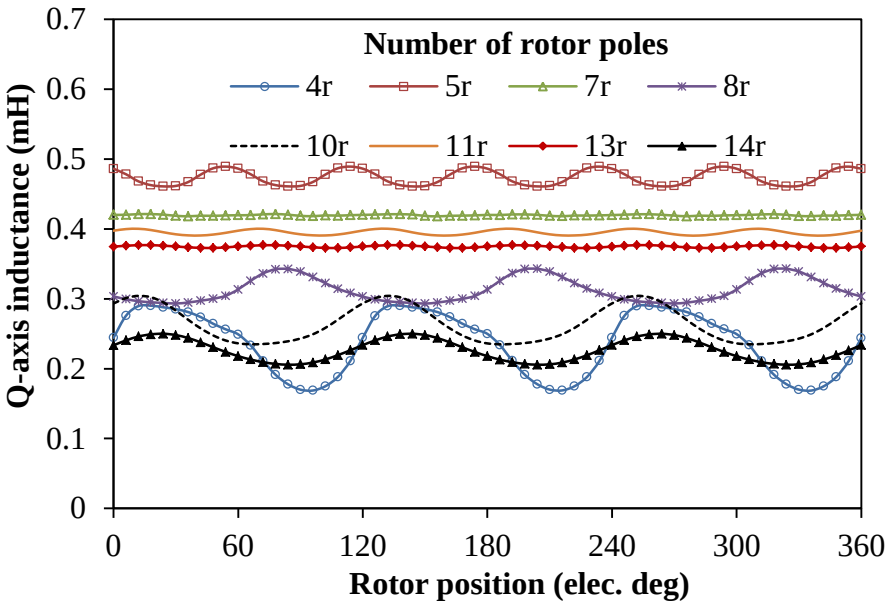

(b)

Fig.5.20 Variation of winding inductances with rotor position, (I_d=-1A or I_q=15A).

5.6.2 Self- and mutual-inductances

The self- and mutual-inductances of the analysed machines are compared in Figs.5.21 (a) and (b), respectively. The machines have relatively similar self-inductance values. It is worth noting that the analysed machines having odd-rotor pole numbers exhibit much lower mutual-inductance values than their equivalent even rotor pole counterparts, which is a good fault-tolerant quality. The respective values of the inductances are given in Table 5.2.

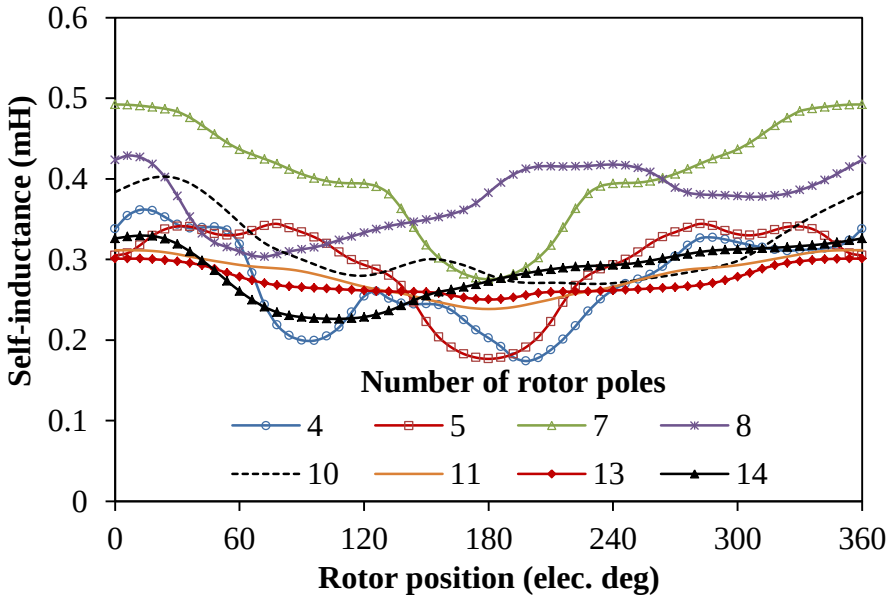

(a) Self-inductances

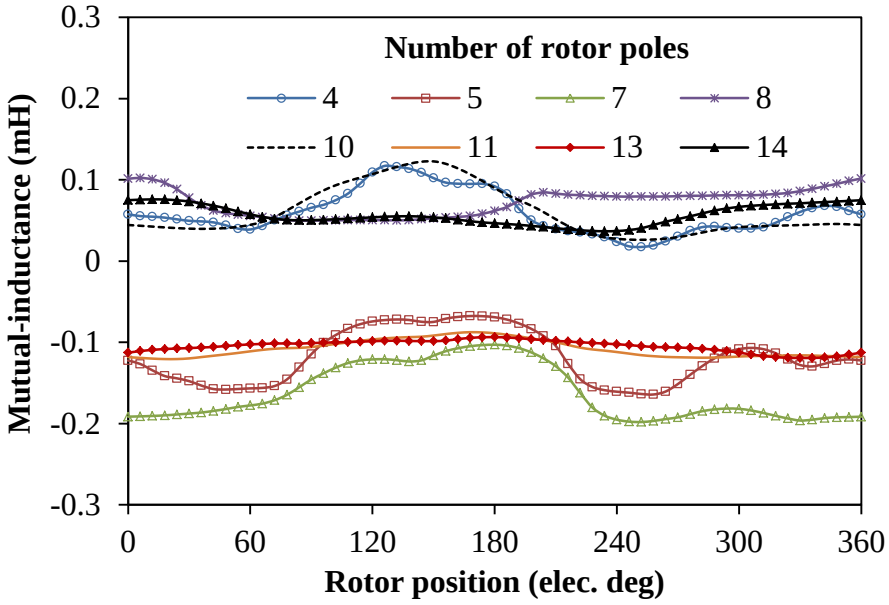

(b) Mutual-inductances

Fig.5.21 Comparison of self- and mutual-inductances, I=15A.

5.7 Torque-speed and flux-weakening capabilities

The torque-speed and power-speed curves of the analysed machines are shown in Fig.5.21. It is observed that the machine with N_r=11exhibits the largest torque amongst the compared machines. This is followed by the machine with N_r=13. The worst value of torque is obtained in the 8-rotor pole machine. Moreover, the 13-rotor pole machine exhibits the best flux-

weakening capability since it has the highest value of maximum speed to base speed ratio. However, all analysed machines have comparable power, *i.e.* almost constant power since they were optimized for maximum output torque. It is worth noting that we considered the cross-coupling effect of the magnetic circuits, at different currents in the calculation of the torque/power-speed characteristics. The flux weakening potentials of the analysed machines is listed in Table 5.2.

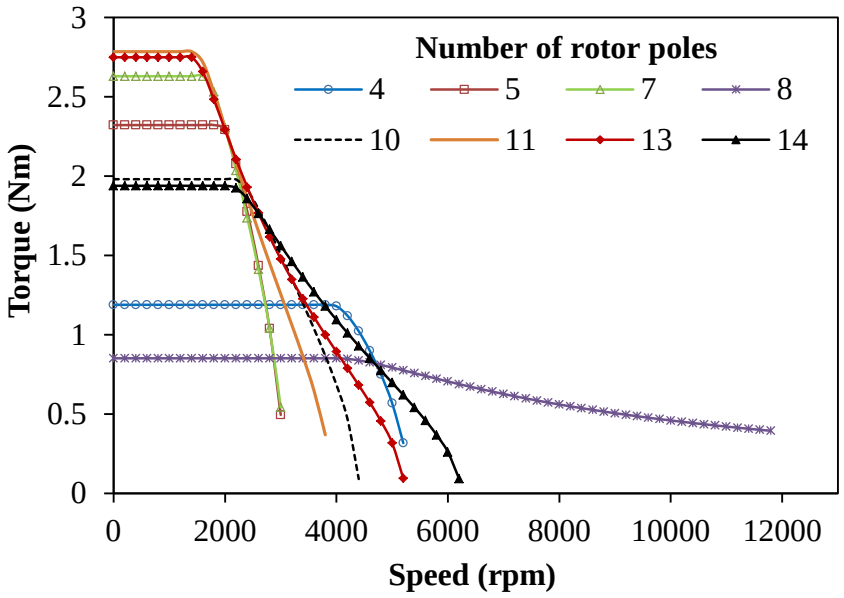

(a) Torque versus speed

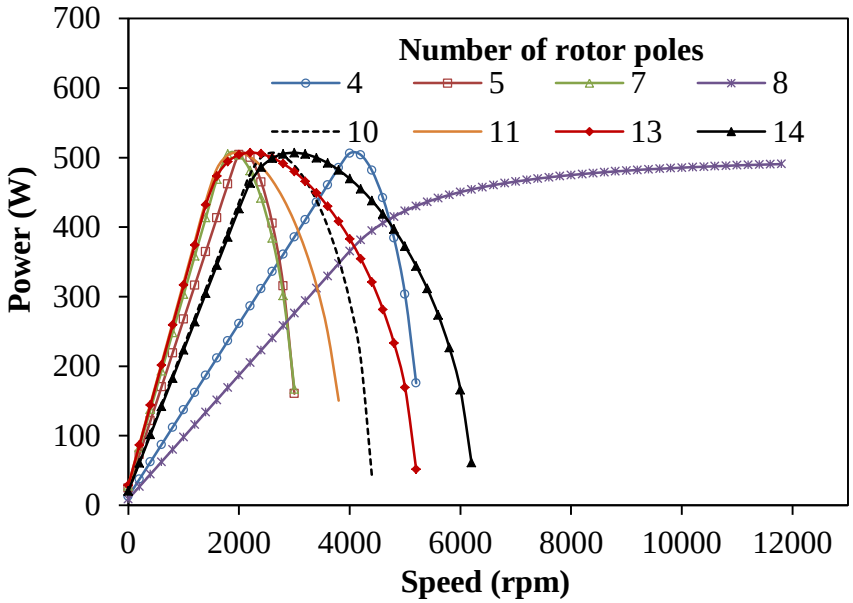

(b) Power versus speed

Fig.5.22 Comparison of torque-speed characteristics, (V_{dc} = 22.9V, I_{max} = 15A).

TABLE 5.2 FLUX WEAKENING CAPABILITY, INDUCTANCES AND SALIENCY RATIOS

Item	Value							
Rotor pole number, N_r	**4**	**5**	**7**	**8**	**10**	**11**	**13**	**14**
D-axis inductance, L_d (mH)	0.218	0.475	0.479	0.325	0.268	0.434	0.431	0.251
Q-axis inductance, L_q (mH)	0.265	0.538	0.459	0.3105	0.279	0.426	0.401	0.235
Saliency ratio, L_q/L_d	1.2	1.1	0.96	0.96	1.03	0.98	0.93	0.94
PM flux (mWb)	13.17	20.5	16.71	4.73	8.79	11.251	9.396	6.155
K_{fw}	0.25	0.35	0.43	1.03	0.46	0.58	0.69	0.61
Base speed (rpm)	3900	2000	1700	4000	2200	1500	1400	2100
Maximum speed (rpm)	5400	3100	3100	12000	4500	4000	5300	6300
Max. speed/base speed	1.38	1.55	1.82	3	2.05	2.67	3.79	3
Maximum torque (Nm)	1.19	2.32	2.63	0.85	1.98	2.785	2.75	1.94
Maximum power (W)	507.87	507.19	507.60	490.99	506.96	507.23	507.12	506.93
Self-inductance, L_{aa} (mH)	0.274	0.295	0.406	0.374	0.314	0.280	0.274	0.285
Mutual-inductance, M_{ab} (mH)	0.059	-0.118	-0.162	0.072	0.0599	-0.108	-0.105	0.057
M_{ab}/L_{aa}	0.215	-0.4	-0.39	0.193	0.191	-0.386	-0.383	0.2
Power factor	0.73	0.75	0.4	0.44	0.82	0.63	0.6	0.9

5.9 Experimental validation

Overall, the electromagnetic performances of the proposed 6-stator pole magnetically geared SFPM machines with different rotor poles have been analysed and quantitatively compared. The results show that the 6-stator tooth/11-pole one has the highest torque density and smallest torque ripple among all the analysed 8 machines. A 6-stator tooth/11-rotor pole prototype of the proposed machine is built and tested to verify the FE analysis, since it seems to exhibit the best quality of high torque capability amongst the other compared machines. Fig.5.23 shows the built prototype consisting of outer and inner stators, 11-pole modulating rotor, and laminated steel sheet, respectively. For ease of manufacturing, a 0.5mm thick of iron rib is added to support the rotor iron pieces adjacent to the inner air-gap. The 3D-FEA mesh plot and the flux density distribution of the prototype at no load condition are shown in Fig.5.24.

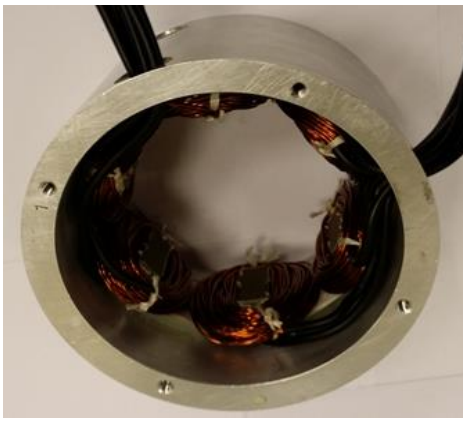

(a) 6-pole outer stator

(b) 6-pole inner stator

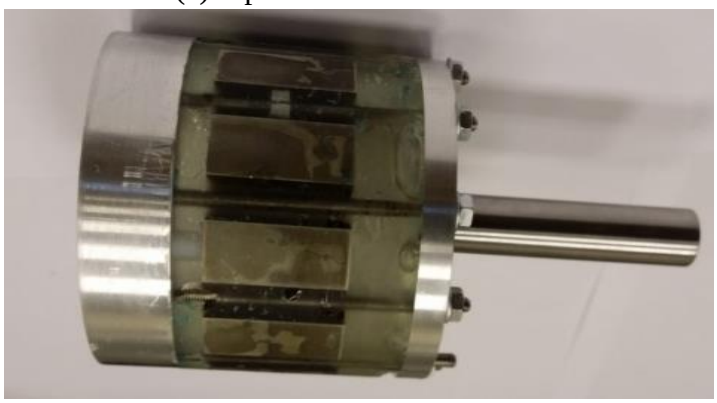

(c) Fabricated rotor

(d) Laminated outer stator steel

Fig.5.23 Manufactured prototype of the proposed 6-stator/11-pole machine

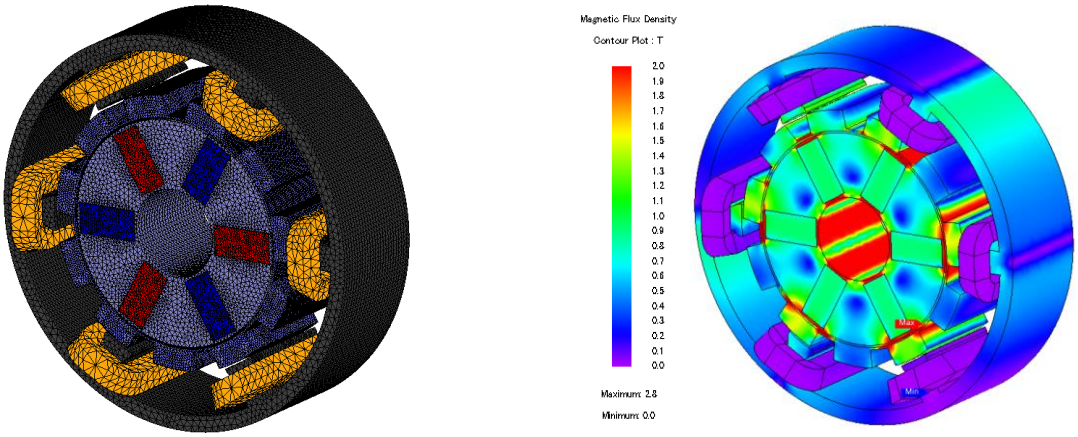

(a) mesh (b) flux density

Fig.5.24 Mesh and flux density distribution, no load.

Fig.5.24 compares the FE predicted and the measured phase back-EMF results, including both waveforms and spectra. There is a discrepancy between the 2D-FE predicted results and the measured values owing to the significant end-effects associated with such machines of small active length, 25mm. The difference between the 3D-FE predicted and measured phase fundamental back-EMFs can be explained by the lamination stacking factor and also the manufacturing tolerances.

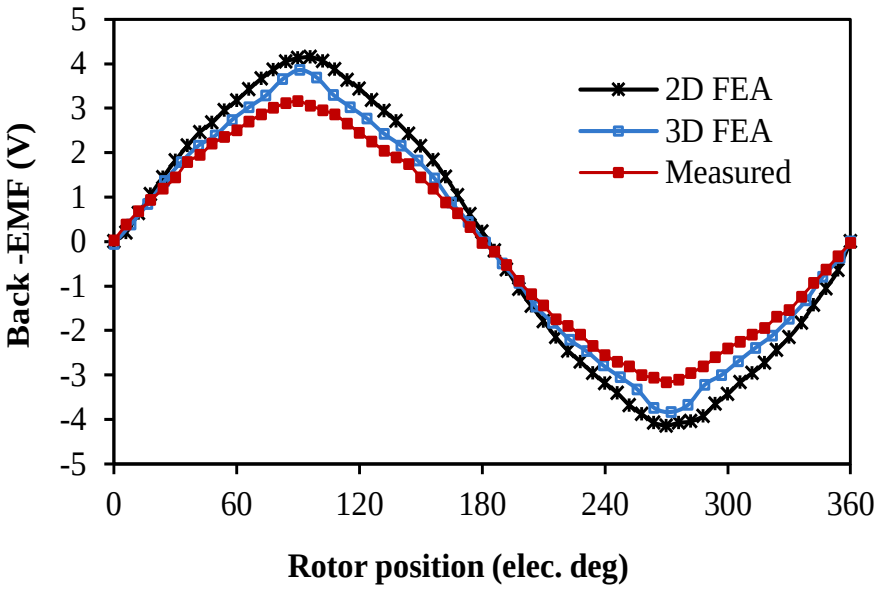

(a) Waveforms

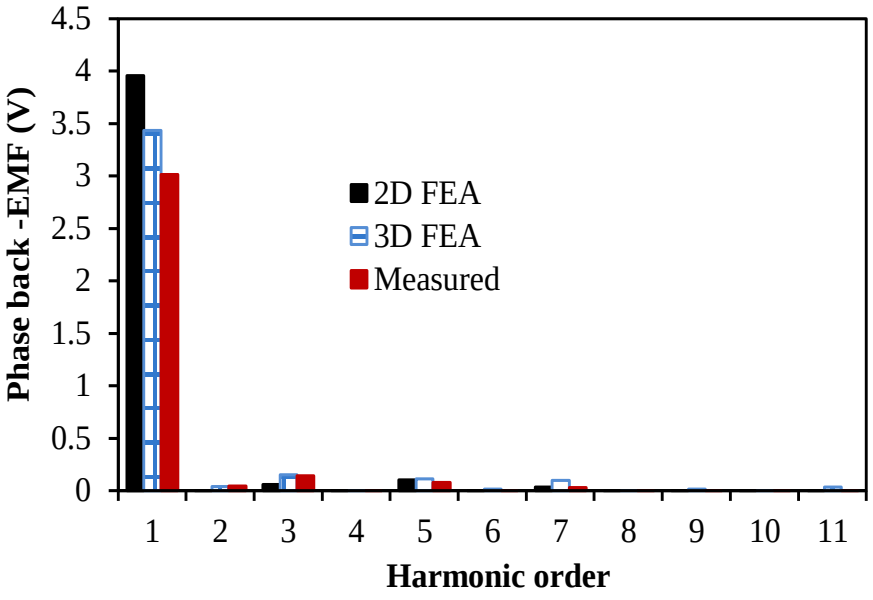

(b) Spectra

Fig.5.25 Comparison of FE predicted and measured phase back-EMFs at 400rpm rotor speed.

The comparison between 3D-FE predicted and measured static torque waveforms with different *q*-axis currents are shown in Fig.5.25. It can be seen that the measured and predicted results match well, although the measured peak static torques are a little smaller than the 3D-FE analyses. The difference between the 3D-FE predicted and measured peak static torques shown in Fig.5.26, is also due to the lamination stacking factor as well as the manufacturing tolerances.

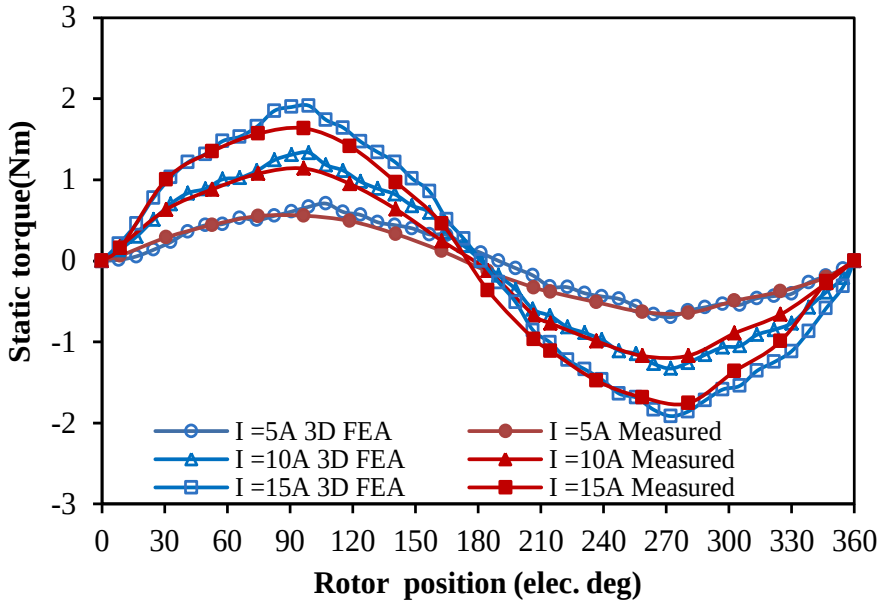

Fig.5.26 Comparison of FE predicted and measured static torque waveforms with different *q*-axis currents.

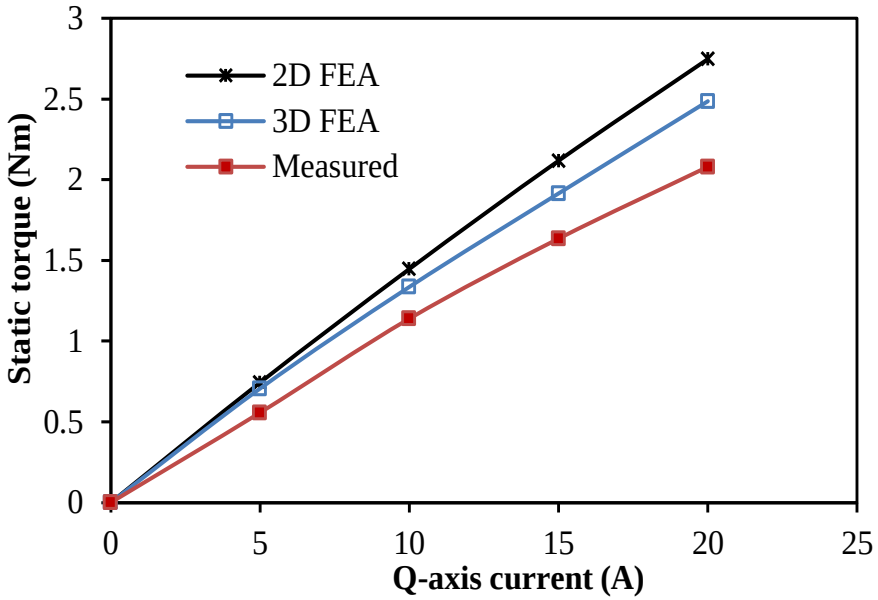

Fig.5.27 Comparison of FE predicted and measured peak static torques with different *q*-axis currents.

5.9 Summary

Firstly, the proposed machines were optimized for maximum torque using genetic algorithm approach. We employed the 2-dimensional finite element (FEA) analysis in the performance prediction of the magnetically geared SFPM machines. It is observed that the electromagnetic performances of the machines are influenced by the design parameters. The selected design parameters include: the split ratio, the slot opening/tooth pitch ratio, the rotor radial thickness, the rotor pole arc/pole pitch, the stator-tooth width thickness, and the back-iron thickness. Further, the influence of stator and rotor pole combinations on the electromagnetic performances is investigated and quantitatively compared. The predicted results reveal that the odd rotor pole machines are potential candidates for high output torque, low torque ripple/cogging torque and minimum PM usage. Moreover, the 11-rotor pole machine seems to be the best candidate amongst all the analysed machines, since it exhibits the highest phase fundamental back-EMF and torque capability, and the smallest phase back-EMF harmonics, cogging torque and torque ripple. The applications of the proposed machines range from wind power generation, aerospace, to propulsion systems. Finally, we have validated the predicted results by experiments with good agreement.

CHAPTER 6
COMPARISON OF SINGLE- /DOUBLE-STATOR AND PARTITIONED STATOR SWITCHED FLUX PM MACHINES

6.1 Introduction

In this chapter, the electromagnetic performance of double-stator SFPM (DS-SFPM) machine, conventional SFPM machines and partitioned stator SFPM (PS-SFPM) machines having C-core and E-core stator structures will be compared quantitatively. The analyses will include the open circuit flux-linkage and back-EMF waveforms and spectra, torque-current and torque-copper loss characteristics, self- and mutual-inductance waveforms, and loss and efficiency maps. Fig.6.1 shows the schematic diagrams of the analysed machines. The parameters and results of the analysed machines are listed in Table 6.1. This includes the machine's size/active length, stator/rotor pole combinations, fundamental flux-linkage and back-EMF amplitudes, average torque, winding inductances and efficiency characteristics etc.

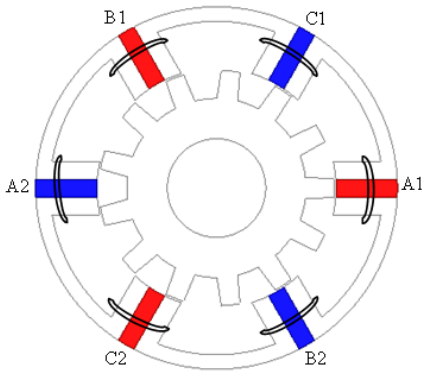

(a) C-core SFPM 6/13

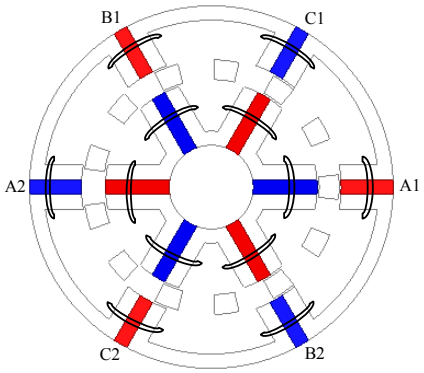

(b) DS-SFPM 6/13

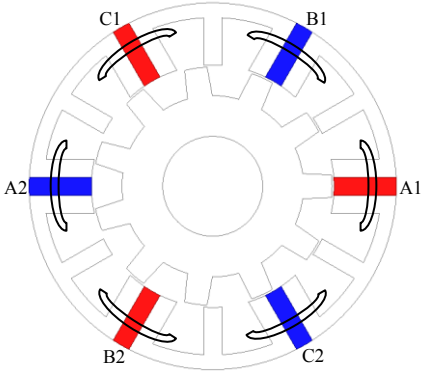

(c) E-core SFPM 6/11

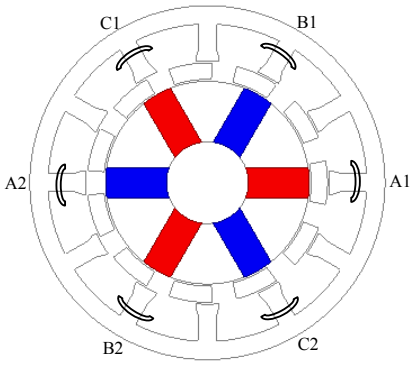

(d) PS-SFPM 6/11 (E-core)

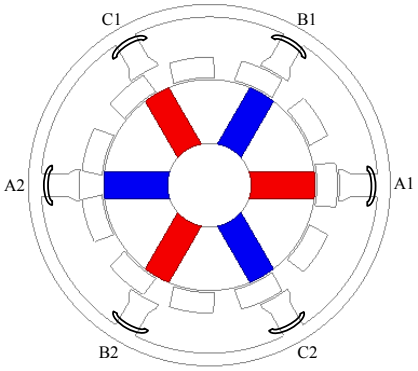

(e) PS-SFPM 6/11 (C-core)

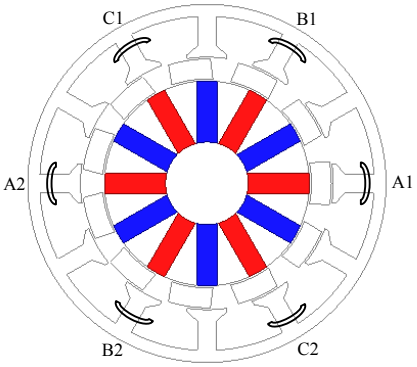

(f) PS-SFPM 12/11

Fig.6.1 Cross-sections of the analysed machines.

TABLE 6.1 PARAMETERS OF THE ANALYSED MACHINES

Item	Value					
Machine topology	C-core SFPM 6/13	DS-SFPM 6/13	E-core SFPM 6/11	PS-SFPM 6/11 (E-core)	PS-SFPM 6/11 (C-core)	PS-SFPM 12/11
Stator pole number, *Ns*	6	6	6	6	6	12
Rotor pole number, *Nr*	13	13	11	11	11	11
Number of turn/phase				72		
Outer stator diameter (mm)				90		
Axial length (mm)				25		
PM remanence (T)				1.2		
Relative permeability				1.05		
Airgap length (mm)				0.5		
Av. Torque (Nm)*	3.75	5.36	3.30	4.15	5.061	5.64
Peak-to-Peak Cogging torque (Nm)	0.028	0.317	0.285	0.097	0.050	0.0215
Total harmonic distortions, THD (%)	2.99	4.70	7.37	10.24	1.72	3.42
Phase flux-linkage (mWb)	10.96	9.45	12.20	10.31	11.51	13.33
Phase back-EMF (V)	5.96	5.14	5.62	4.75	5.30	6.14
Self-inductance, *Laa* (mH)**	0.373	0.220	0.445	0.289	0.280	0.364
Mutual-inductance, *Mab* (mH)**	-0.163	-0.097	-0.110	-0.065	-0.108	0.024
Mab /Laa	-0.439	-0.439	-0.248	-0.226	-0.386	0.067

Ld	0.49	0.30	0.48	0.34	0.38	0.32
Lq	0.57	0.33	0.57	0.37	0.40	0.36
Lq/Ld	1.17	1.11	1.17	1.07	1.03	1.12
Torque density (kNm/m^3)	23.6	33.7	20.7	26.1	31.8	35.5
Efficiency (%)*	91.91	93.94	92.01	93.62	93.62	93.54

*: Copper loss = 30W; **: Current, *I*= 15A.

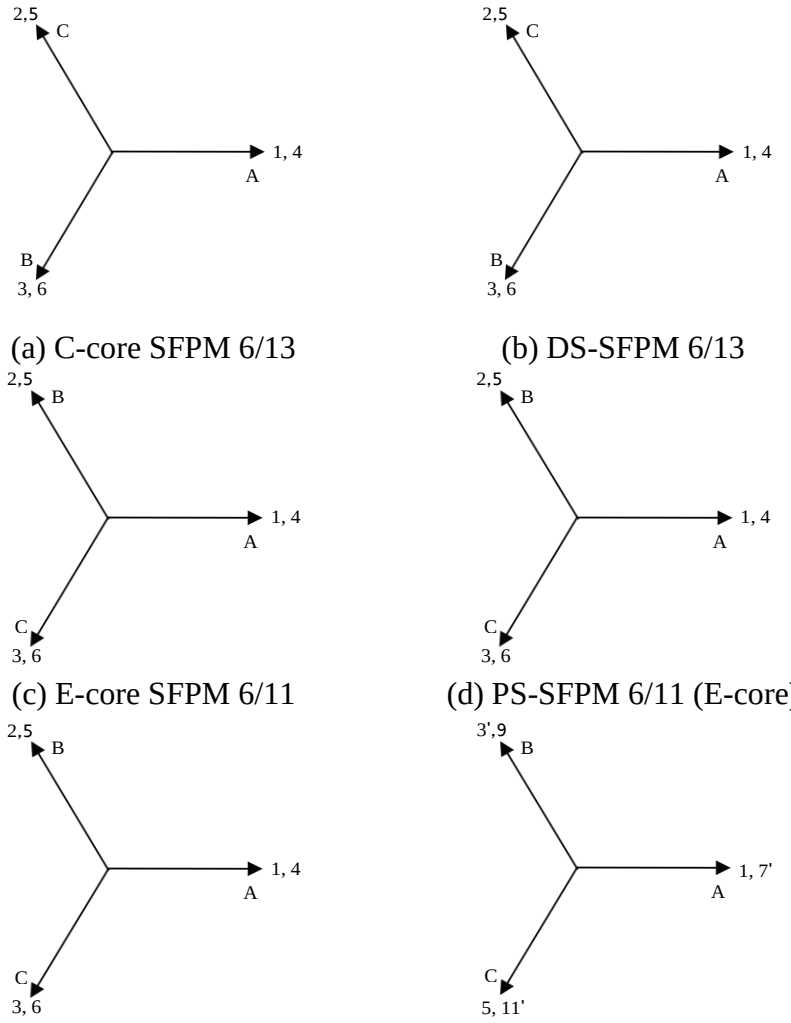

(a) C-core SFPM 6/13 (b) DS-SFPM 6/13

(c) E-core SFPM 6/11 (d) PS-SFPM 6/11 (E-core)

(e) PS-SFPM 6/11 (C-core) (f) PS-SFPM 12/11

Fig.6.2 Coil EMF phasors and winding configurations of analysed machines.

6.2 Comparison of electromagnetic performances

Open-circuit phase flux-linkage waveforms of the analysed machines are shown in Fig.6.3. It can be seen that the waveforms are essentially sinusoidal and symmetrical about the rotor

position. The largest value of the flux-linkage is observed in the PS-SFPM having 12PMs while the least value is seen in the DS-SFPM machine.

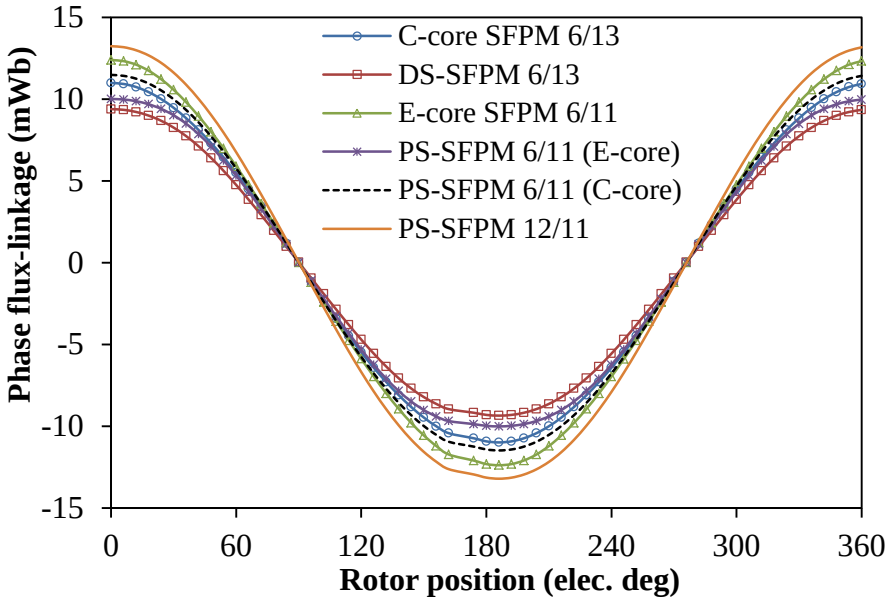

(a) Waveforms

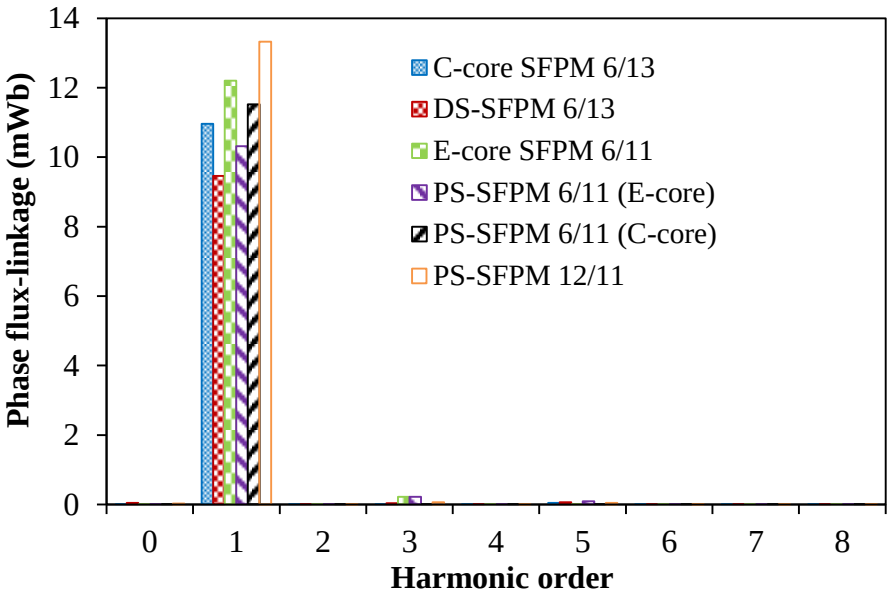

(b) Spectra

Fig.6.3 Open-circuit flux-linkages.

Similarly, the largest fundamental back-EMF amplitude is seen in the PS-SFPM 12/11 while the least value of the back-EMF is observed in the PS-SFPM 6/11(E-core) as shown in Fig.6.4. Although the compared back-EMF waveforms are symmetrical about the rotor position, they are not entirely sinusoidal since they exhibit a bit of 3^{rd} and 5^{th} harmonics.

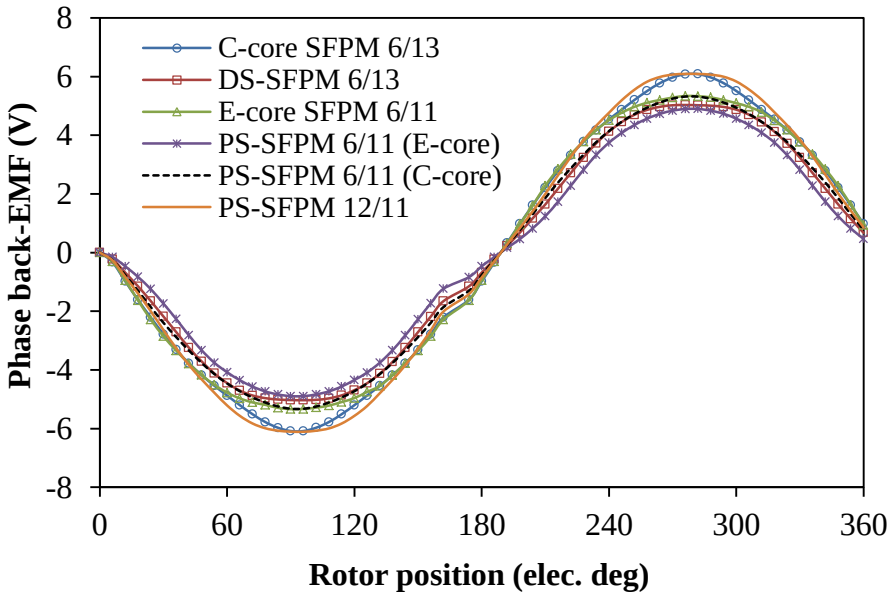

(a) Waveforms

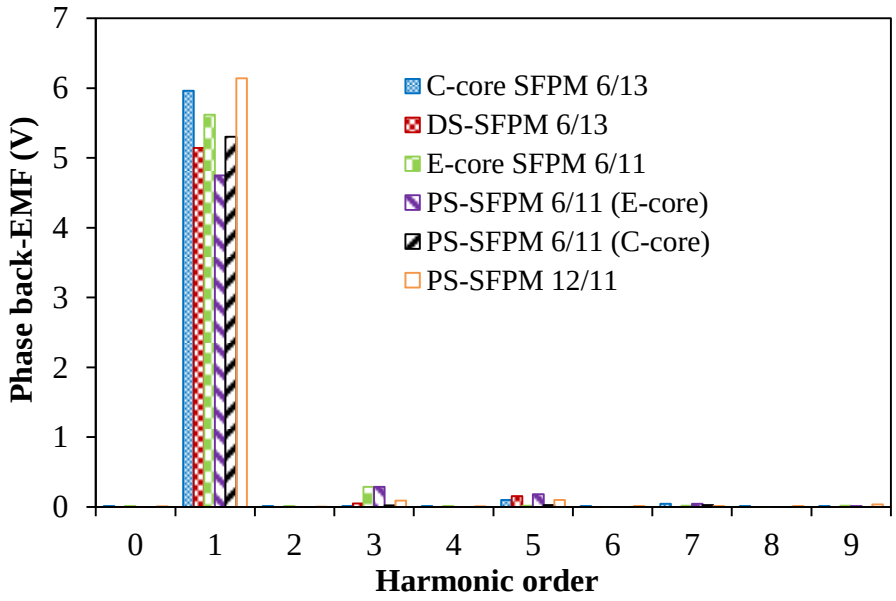

(b) Spectra

Fig.6.4 Comparison of open-circuit phase back-EMFs in analysed machines, 400rpm.

The torque waveforms of the analysed machines with their corresponding spectra at fixed copper loss (30W) is shown in Fig.6.5. The results reveal that the largest output torque of the analysed machines is obtained in the PS-SFPM machine having 12PMs. This is followed by the DS-SFPM mnachine. The least value of the output torque is obtained in the conventional E-core SFPM machine.

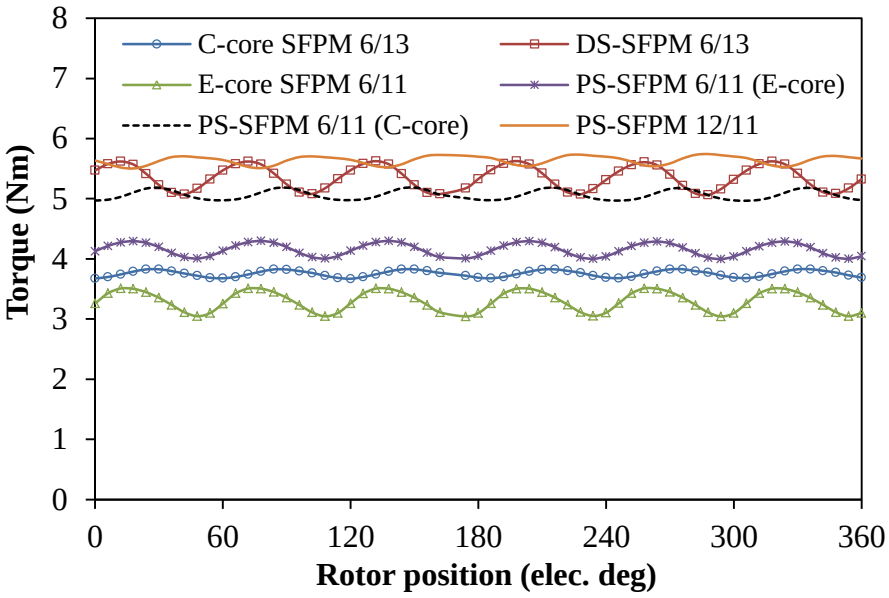

(a) Waveforms

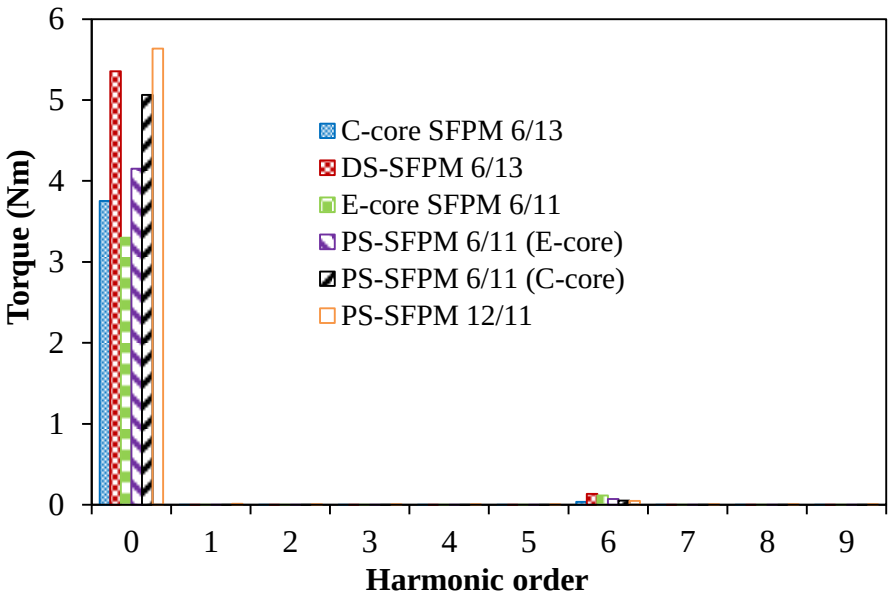

(b) Spectra

Fig.6.5 Comparison of torque waveforms in analysed machines, (copper loss = 30W, i_d=0).

Figs.6.6 to 6.8 show the average torque saturation curves of the analysed machines at different current, current density, and copper loss, respectively. It can be observed that the PS-SFPM machine having 12PMs and the DS-SFPM machine have higher torque capability than the rest of the other compared machines.

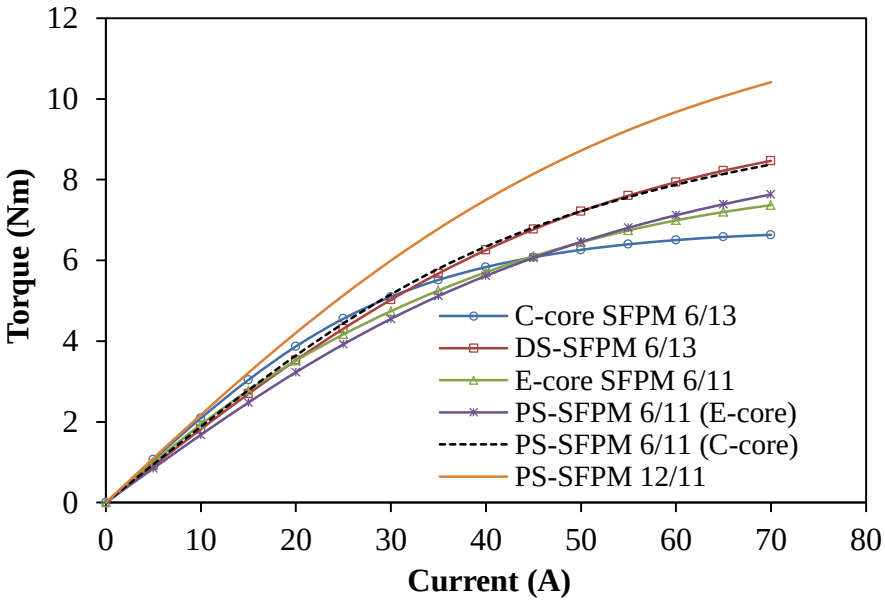

Fig.6.6 Comparison of average torque against current, i_d=0.

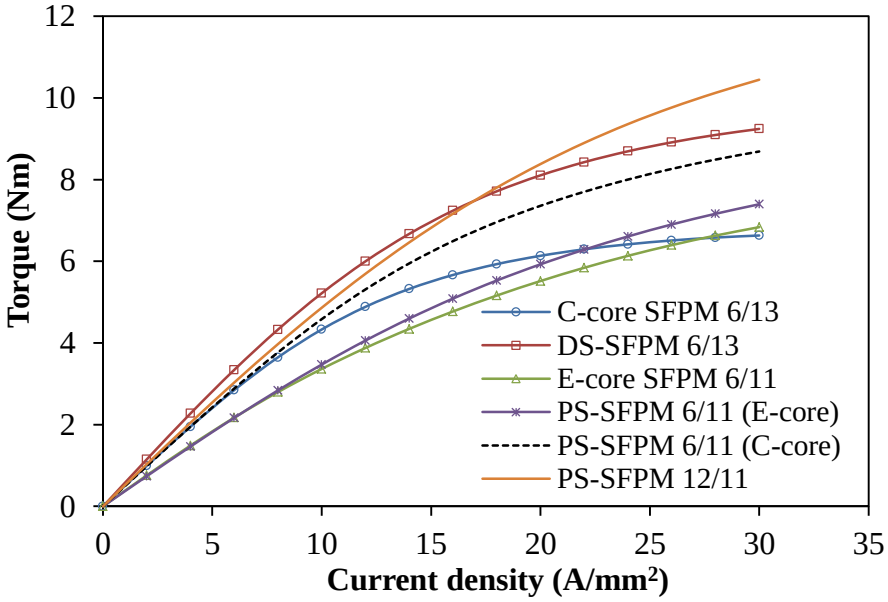

Fig.6.7 Comparison of average torque against current density, i_d=0.

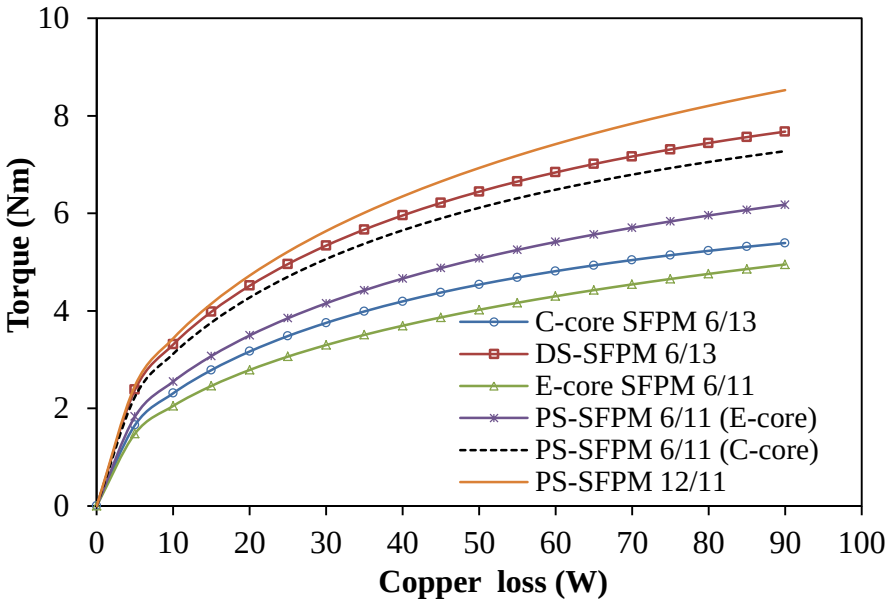

Fig.6.8 Comparison of torque against copper loss, i_d=0.

Further, the PM usages of the analysed machines are shown in Fig.6.9. Although the PS-SFPM machine having 12PMs exhibits the largetst torque capapbility, it has the least ratio of torque to PM usage. Thus, the PS-SFPM 12/11 may not be the ideal canditate when the cost is taken into consideration.

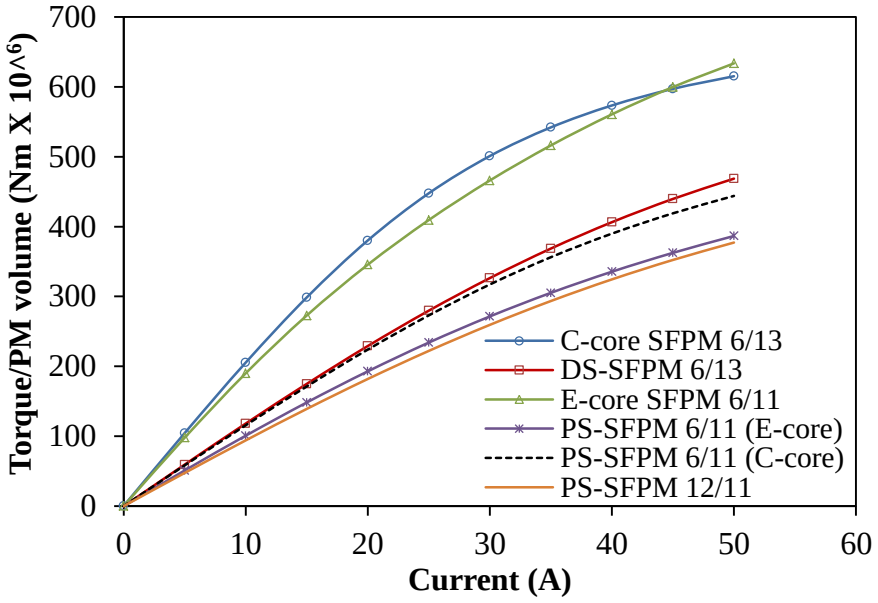

Fig.6.9 Comparison of ratio of average torque to PM volume against current, i_d=0.

6.2.1 Torque ripple and total harmonic distortion

This sub-section investigates the effect of electric loading on torque ripple and total harmonic distortions (THD) of the voltage.

Similarly, the torque ripple of the analysed machines is defined as the ratio of the difference between the maximum and minimum torque to the average torque over one electrical period.

$$T_{ripple} = \frac{T_{max} - T_{min}}{T_{avg}} * 100\% \quad (6.1)$$

where T_{max}, T_{min}, and T_{avg} are the maximum, minimum and average torque respectively.

The open-circuit cogging torque waveforms and spectra of the analysed machines are compared in Fig.6.10. The DS-SFPM and conventional E-core SFPM machines have similar cogging torque values which are relatively higher than those of the other compared machines. Nevertheless, the cogging torques are negligible compared to their overall output torque. Moreover, the torque ripple and voltage total harmonic distortions (THD) of the analysed machines at different load conditions are given in Figs.6.11 and 6.12, respectively. Obviously, the THDs of the analysed machines generally increase with increase of load. Note that the DS-SFPM and conventional E-core SFPM machines have larger torque ripples which are in aligning with their respective cogging torque amplitudes.

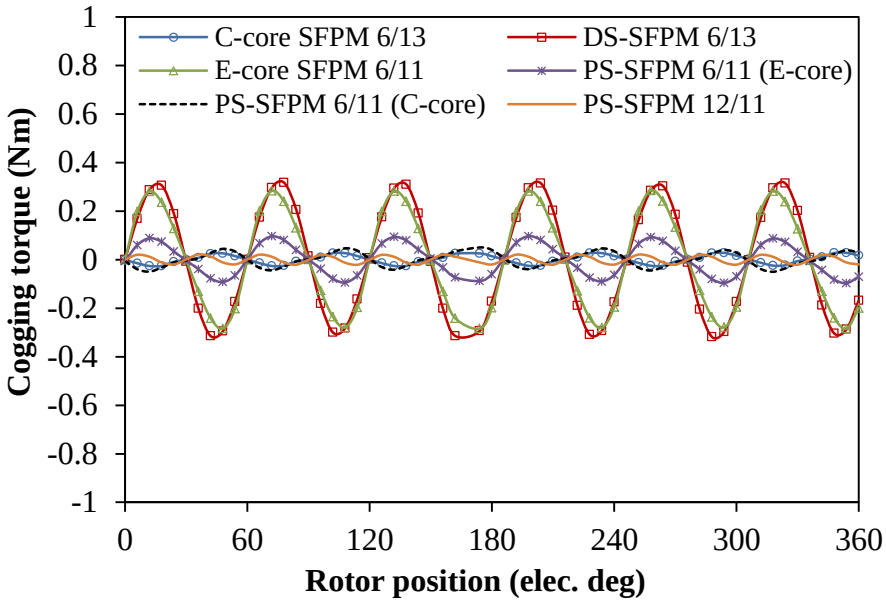

(a) Waveforms

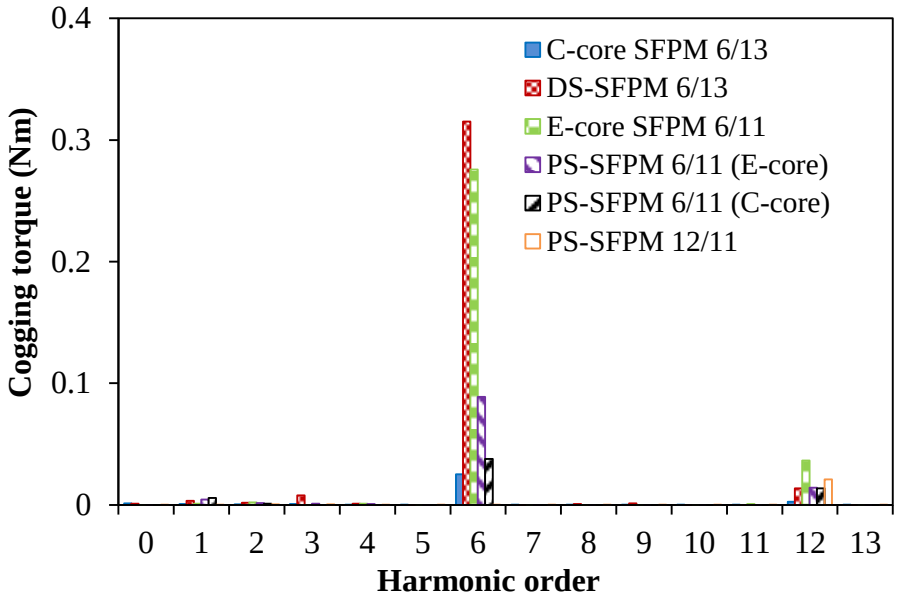

(b) Spectra

Fig.6.10 Comparison of cogging torques in analysed machines.

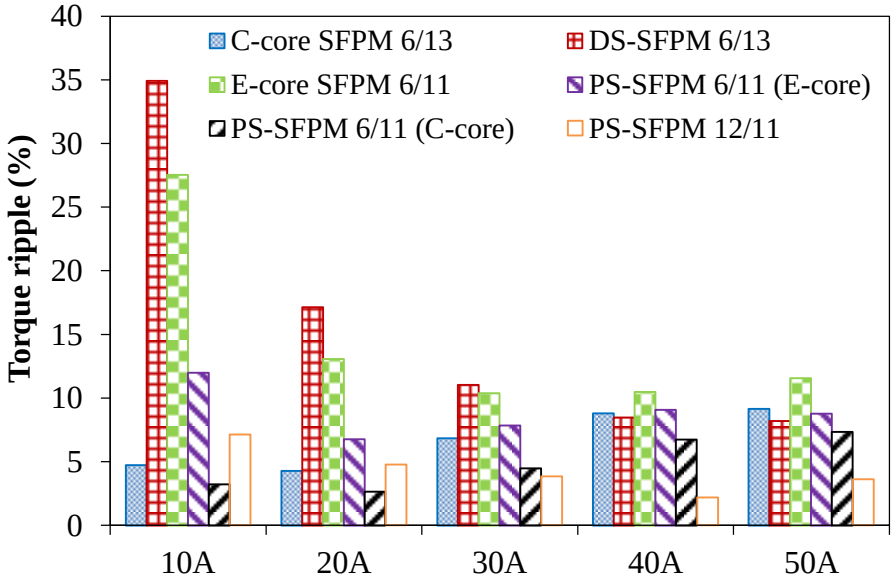

Fig.6.11 Variation of torque ripple with q-axis current, i_d=0.

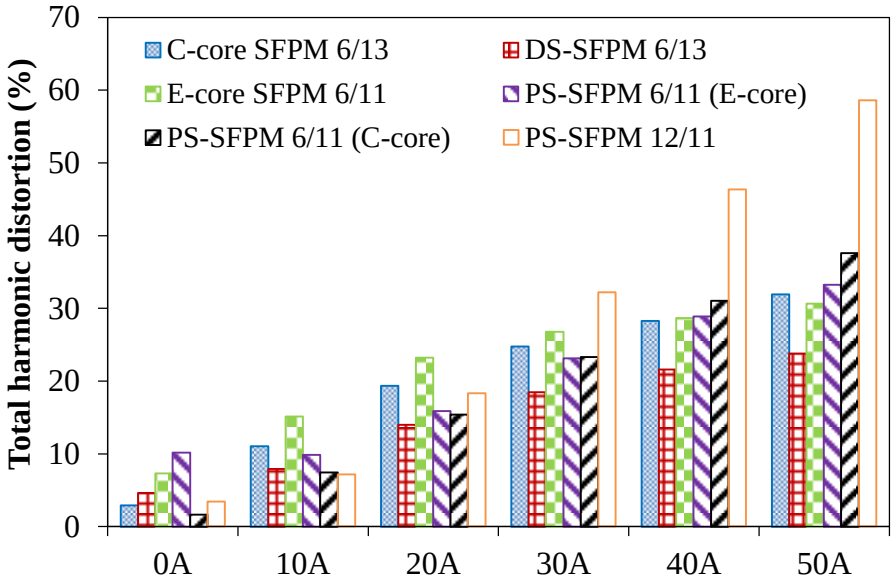

Fig.6.12 Variation of total harmonic distortions (THD) with *q*-axis current.

6.2.2 Inductance characteristics

Figs.6.13 and 6.14 show the self- and mutual-inductance waveforms of the compared machines, respectively. It can be seen that the largest value of self-inductance is obtained in the conventional E-core SFPM machine, which is a good fault-tolerant characteristic. The analysed machines have similar low mutual-inductance values except for that of the PS-SFPM machine having 12PMs whose mutual-inductance value is positive. The mutual inductance of the machine can be either positive or negative since it depends on the polarity of the coil connection of the mutually coupled coils. Thus, the coil phasor diagram of Fig.6.2 clearly shows the reason behind the positive mutual-inductance value of the PS-SFPM12/11 machine. It is worth noting that each of the coil groups in the analysed machines have same polarity except that of the PS-SFPM12/11 whose coil group consist of two coils with different sign orientation. Further, the *d*- and *q*-axis inductance variation with rotor position of the compared machines is depicted in Fig.6.15. It can be observed that the C-core and E-core SFPM machines have similar inductance values which are higher than those of the other compared machines. Also, it should be noted that the least value of the winding inductances occurred in the DS-SFPM machine. It is worth mentioning that the values of the *q*-and *d*-axes inductance of each of the analysed machines are similar. Therefore, their saliency ratios are ~ equal to one as seen in Table 6.1. Hence, it indicates that the analysed machines would have

negligible reluctance torque. Fig.6.16 shows the field distributions of the analysed machines under the excitation of phase A current.

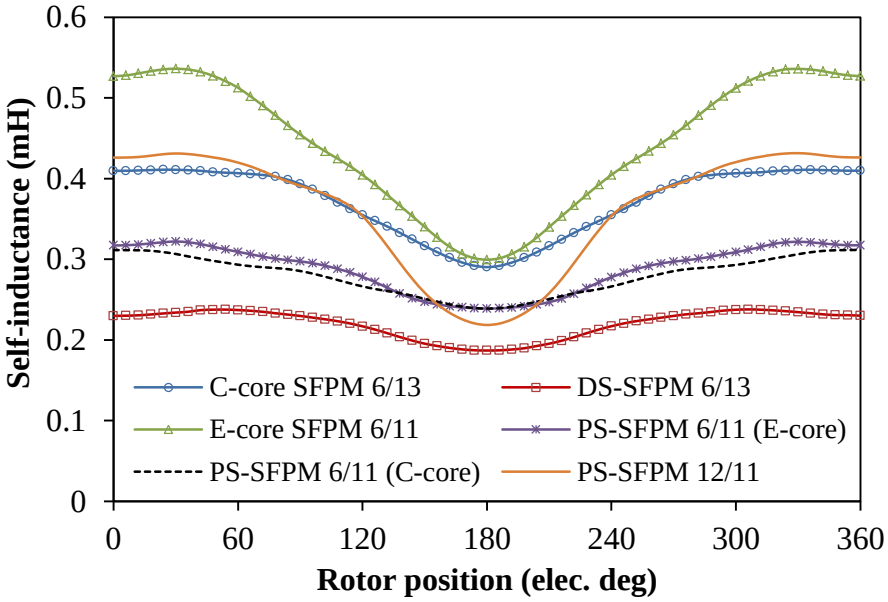

Fig.6.13 Variation of self-inductance with rotor position, *I*=15A.

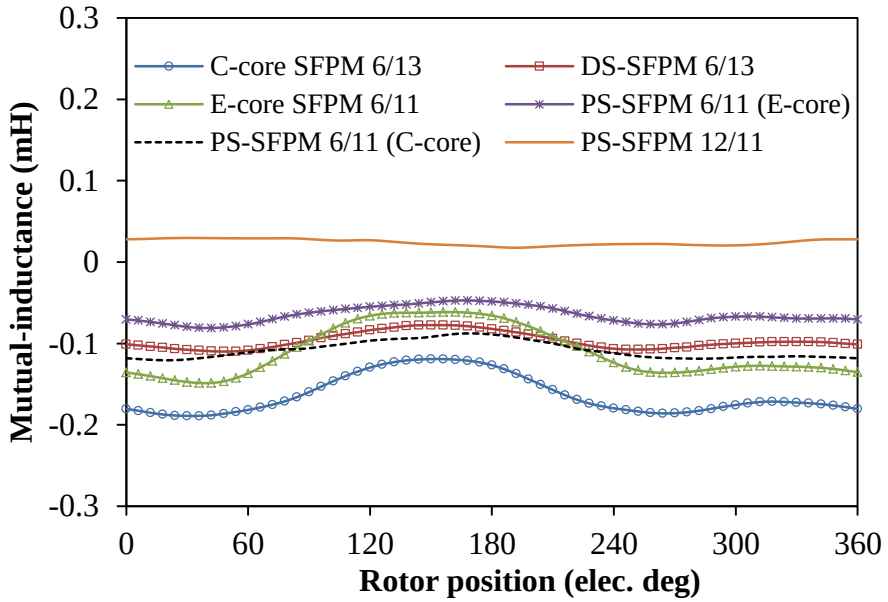

Fig.6.14 Variation of mutual-inductance with rotor position, *I*=15A.

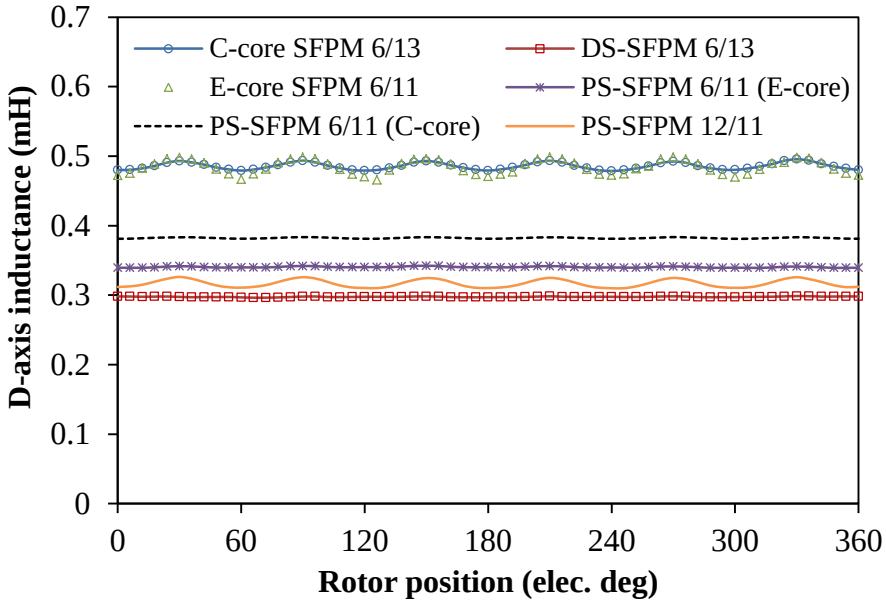

(a) *D*-axis inductance

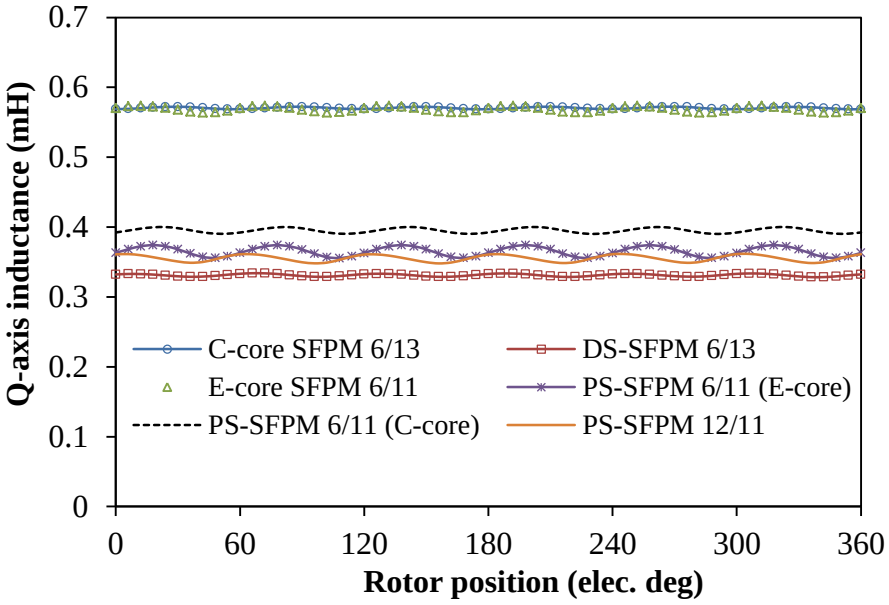

(b) *Q*-axis inductances

Fig.6.15 Variation of winding inductances with rotor position, (I_d=-1A or I_q=15A).

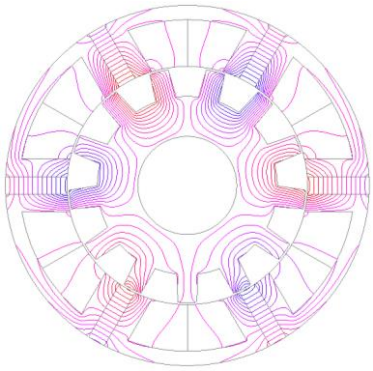

(a) C-core SFPM 6/13

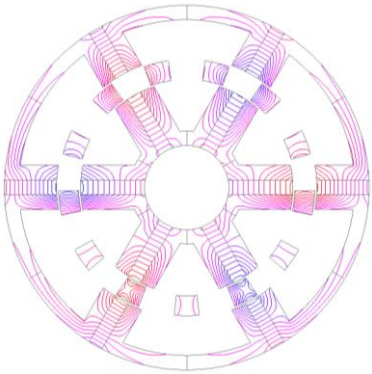

(b) DS-SFPM 6/13

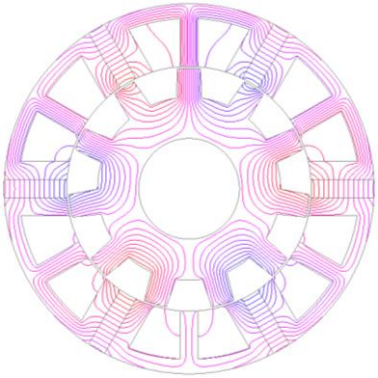

(c) E-core SFPM 6/11

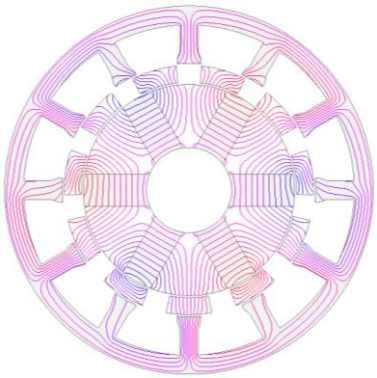

(d) PS-SFPM 6/11 (E-core)

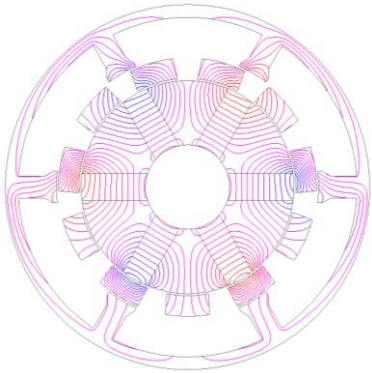

(e) PS-SFPM 6/11 (C-core)

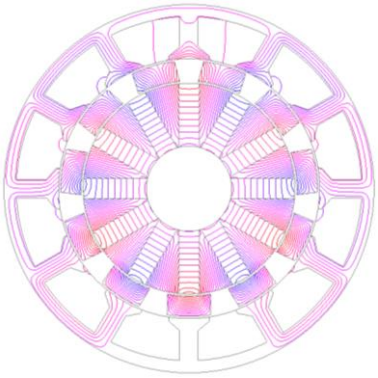

(f) PS-SFPM 12/11

Fig.6.16 Field distributions of analysed machines (I_a=15A, I_b=I_c=0A).

6.2.3 Losses and efficiency profiles

The estimation of losses in the design and analysis of electrical machines is very crucial since the overall efficiency of the machines largely depends on it. Also, the thermal effect (temperature distribution) of the machine is dependent on losses. Reduction of iron losses in PM machines by optimization of the machine geometry are given in [MI05], [YAM13] [LEE08] and [FUK12]. Nevertheless, it should be noted that the average torque may be compromised a bit. Also, [OKA16] has shown that the use of appropriate material could reduce the iron loss of a given synchronous machine significantly. Similarly, the permanent

magnet eddy current loss on the analysed machines can be minimized by several techniques such PM segmentation [THO14], [CHO11] and [YAM09]. The classical loss equation given in (6.3) is adopted in this analysis.

$$P_{loss} = K_h B_m^2 f + K_e (B_m f)^{1.5} + K_c (B_m f)^2 \quad (6.2)$$

where B_m is the maximum value of the magnetic flux density, f is the frequency; K_h, K_e, and K_c are the loss coefficients for hysteresis, excess and eddy current losses respectively.

The permanent magnet eddy current and total core losses of the analysed machines are depicted in Figs.6.17 and 6.18, respectively. It is obvious that the largest eddy current loss is obtained in the DS-SFPM machine. Similarly, the highest amount of total core loss is seen in the PS-SFPM machine having 12PMs. The analysed E-core machines have lower loss values than their compared counterparts. Moreover, the DS-SFPM machine and the PS-SFPM machines have comparable efficiency values as shown in Fig.6.19, which is relatively higher than those of the conventional E-core and C-core SFPM machines. The values of their efficiency are listed in Table 6.1.

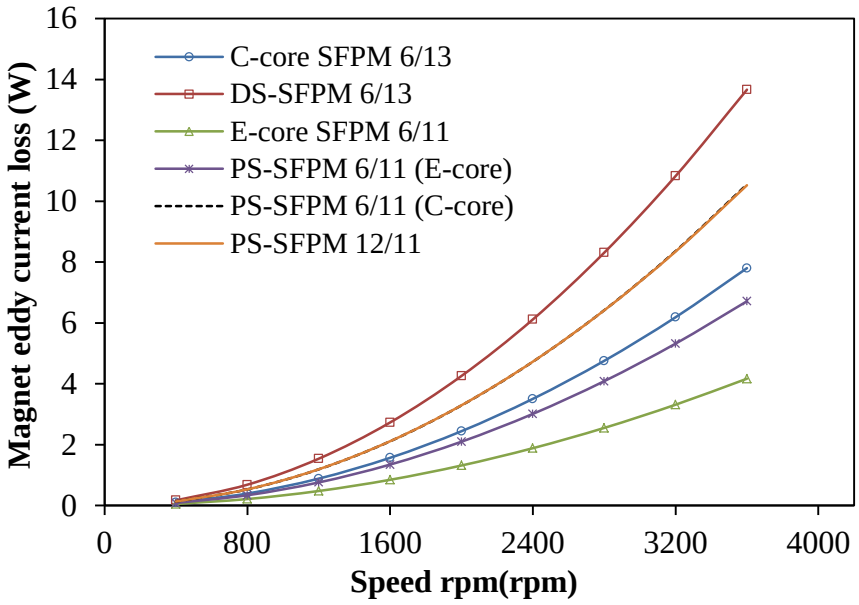

Fig.6.17 Variation of PM eddy current loss with speed, copper loss = 30W.

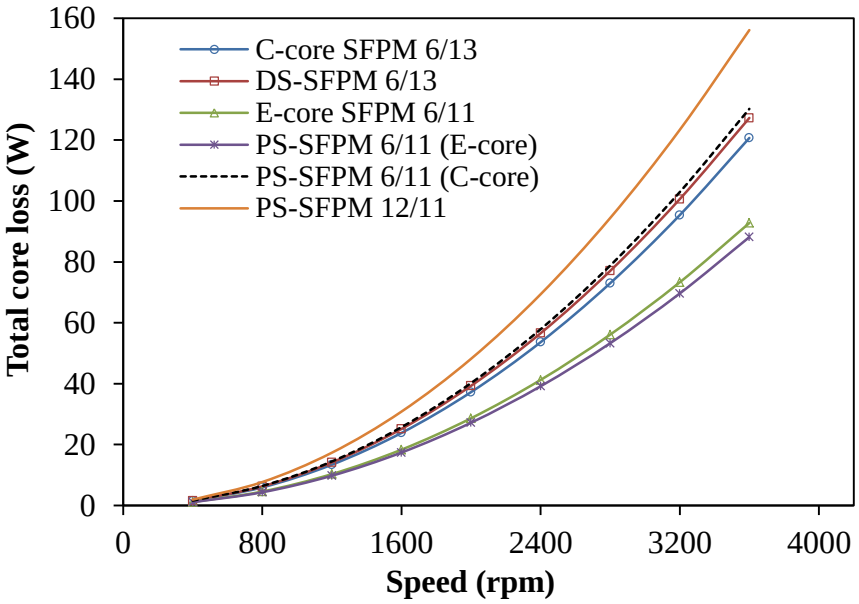

Fig.6.18 Variation of total core loss with speed, coper loss =30W.

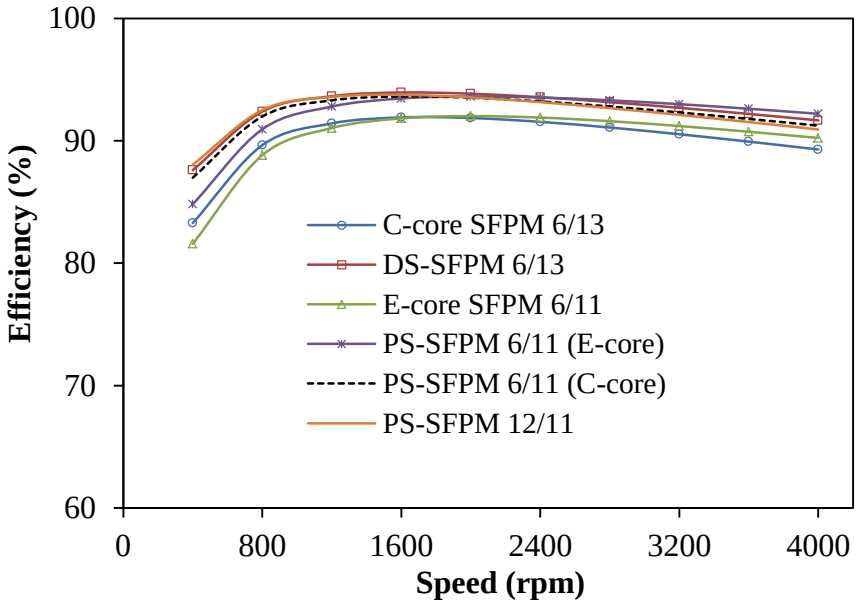

(a) Efficiency versus speed

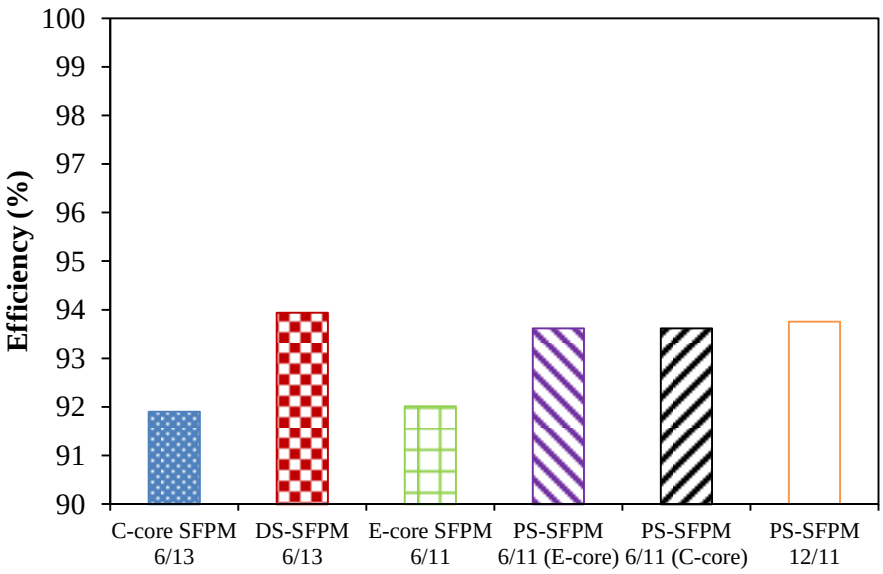

(b) Maximum efficiency, 1600rpm

Fig.6.19 Comparison of efficiency, copper loss=30W.

6.3 Summary

A comparative study of different machine topologies is presented in this chapter. From the analysed results, although the PS-SFPM having 12PMs has the largest torque density amongst the other compared machines due to its high utilization of the inner space with PMs, it suffers from poor ratio of torque to PM volume. This implies that it would be more expensive to produce such a machine when compared to the other analysed machines. Moreover, the PS-SFPM 12/11 has very large amount of total core loss, which would eventually reduce the overall efficiency of the machine.

CHAPTER 7
GENERAL CONCLUSIONS

7.1 Summary of different machine configurations

In this study, different novel SFPM machine topologies having non-overlapping concentrated windings have been designed, analysed and quantitatively compared. Firstly, an overview of different PM machines and magnetically-geared machines are presented. Further, the electromagnetic performances of the proposed machines are presented.

TABLE 7.1 SUMMARY/COMPARISON OF THE PROPOSED MACHINES

Item	**Value**			
Machine topology	DS-SFPM 6/13	PS-SFPM 6/10 (E-core) All-pole wound	PS-SFPM 6/11 (E-core) Alternate-pole wound	PS-SFPM 6/11 (C-core)
Stator pole number, N_s	6			
Rotor pole number, N_r	13	10	11	11
Average torque (Nm)*	5.36	3.23	4.15	5.061
Peak-to-Peak Cogging torque (Nm)	0.317	0.71	0.097	0.050
Total harmonic distortions, *THD* (%)	4.70	137	10.24	1.72
Phase flux-linkage (mWb)	9.45	17.06	10.31	11.51
Phase back-EMF (V)	5.14	3.54	4.75	5.30
Self-inductance, L_{aa} (mH)	0.220	0.16	0.289	0.280
Mutual-inductance, M_{ab} (mH)	-0.097	-0.01	-0.065	-0.108
M_{ab}/L_{aa}	-0.439	-0.06	-0.226	-0.386
D-axis inductance, L_d (mH)	0.3482	0.18	0.35	0.434
Q-axis inductance, L_q mH)	0.3552	0.17	0.37	0.426
Saliency ratio, L_q/L_d	1.02	0.94	1.06	0.98
Base speed (rpm)**	1500	2400	1700	1500
Maximum speed (rpm)**	3900	3800	4500	4000
Max. Speed/base speed	2.6	1.58	2.65	2.67
Maximum power (W)**	508.73	505.10	505.78	507.23
Flux-weakening factor, k_{fw}	0.55	0.32	0.51	0.58
PM eddy current loss (W)*	2.73	1.73	2.10	2.11
Total core loss (W)*	25.14	26.22	27.19	25.73
Torque density (kNm/m^3)	33.67	20.27	26.12	31.84
Efficiency (%)*	93.94	93.32	93.62	93.62

*: Copper loss = 30W; **: Current, I_{max}= 15A, V_{dc}=22.9V.

7.2 Conclusions

The comparison of the electromagnetic performances of the proposed machines is summarized in Table 7.1. All the analysed machines are optimized using genetic algorithm technique with the goal to achieve maximum average torque at fixed copper loss (30W) condition. It is worth mentioning that the series turns per phase of these machines as well as the size of their outer diameter are kept same in the analysis for fair comparison. Similarly, since the physical geometry of the machine influences their electromagnetic performances, the effect of design parameters on the average torque of the proposed machines is detailed in this study. Further, the influence of stator/rotor pole combination on the electromagnetic performances of the proposed machines is also investigated. The predicted results reveal that the machines having odd rotor pole number are potential candidates for high output torque, low torque ripple/cogging torque and minimum PM usage when compared with their even rotor pole counterparts, albeit with high unbalanced magnetic force (UMF). The impact of winding configuration, i.e. all- and alternate-pole-wound topologies, on the overall machine performance is also given in this study. In general, it is observed that the alternate-pole-wound machines exhibit larger torque/power density than their all-pole-wound counterparts. A detailed account of losses and efficiency profile of the analysed machines are also presented in this work. The flux-weakening capabilities of the analysed machines are also presented.

Amongst the proposed machines, it can be seen that the DS-SFPM machine seems to be the most promising candidate since it exhibits the largest torque density at fixed copper loss condition. This is followed by the PS-SFPM machine having C-core outer-stator structure. It should be noted that the developed DS-SFPM machines have good efficiency, albeit with high cogging torque. However, it has the highest value of PM eddy current loss due to its high utilization of PMs. It also suffers from poor ratio of torque to PM volume. The least output torque is seen in the PS-SFPM machine having E-core outer-stator structure. The analyses also show that the developed machines could deliver higher electromagnetic torque than their equivalent single-stator counterparts.

It is worth mentioning that the phase flux-linkage waveforms of all the developed machines are essentially sinusoidal. Similarly, it is worth noting that the proposed E-core machines having all-pole-wound topology exhibit unipolar phase flux-linkage waveforms which are different from the other proposed machines whose flux-linkage waveforms are bipolar.

Moreover, the back-EMF waveforms of these machines are essentially sinusoidal. Above all, the investigations are validated by experiments with good agreement. The developed machines could have wide range of applications including automotive, aerospace, and wind power generation.

In summary:

- Novel topologies of SFPM machines having two separate stators have been developed and their electromagnetic performance is presented.
- The effect of machine geometries on the average torque of the analysed machines is investigated.
- The influence of winding configuration as well as stator/rotor pole combinations on the overall performance of the analysed machines is also given.
- The investigated double airgap SFPM machines are capable of producing larger torque/power density their single-stator counterparts.
- High performance dual-airgap SFPM machines with reduced magnet volume are realized.
- Good agreements are achieved between the predicted FEA results and the experiments.

7.3 Future work

The following proposals on the analysed machines could yield good feasible results:

- The thermal modelling and analyses of the proposed machines could be investigated in order to obtain the temperature effect on different parts of the machines.
- Also the analytical modelling of the proposed machines is worth exploring.
- Moreover, permanent magnet eddy current loss reduction as well as mitigation of torque ripple/cogging torque on the machines could be investigated.
- Further, a research on the use of both DC and AC sources, i.e. hybrid, could be a viable option.
- Furthermore, analysis of vibration and noise of the proposed machines may be a worthwhile adventure.

REFERENCES

[ABB10] M. Abbasian, M. Moallem, B. Fahimi, "Double-stator switched reluctance machines (DSSRM): fundamentals and magnetic force analysis," *IEEE Trans. Energy Convers.*, vol. 25, no. 3, pp. 589-597, Dec. 2010.

[ASH11] M. Ashabani and Y.A.I. Mohamed, "Multiobjective shape optimization of segmented pole permanent-magnet synchronous machines with improved torque characteristics," *IEEE Trans. Magn.*, vol. 47, no. 4, pp. 795-804, April 2011.

[ATA01] K. Atallah, and D. Howe, "A novel high-performance magnetic gear," *IEEE Trans. Magn.*, vol. 37, no. 4, pp. 2844-2846, Jul. 2001.

[ATA04] K. Atallah, S.D. Calverley and D. Howe, "Design, analysis and realisation of a high performance magnetic gear," *IEE Proc.-Electr. Power Appl.*, vol. 151, no. 2, pp. 135-143, Mar. 2004.

[ATA08] K. Atallah, J. Rens, S. Mezani, and D. Howe, "A Novel "Pseudo" direct-drive brushless permanent magnet machine," *IEEE Trans. Magn.*, vol. 44, no. 11, pp. 4349-4352, Nov. 2008.

[AWA15] C.C. Awah, Z.Q. Zhu, Z, Wu, and D. Wu, "High torque density magnetically-geared switched flux permanent magnet machines*", in Proc. Int. Conf. Ecological Vehicles and Renewable Energies,* Monaco, Mar. 2015, pp.1-6.

[AWA16a] C. C. Awah, Z. Q. Zhu, Z. Z. Wu, H. L. Zhan, J. T. Shi, D. Wu, and X. Ge, "Comparison of partitioned stator switched flux permanent magnet machines having single- or double-layer windings," *IEEE Trans. on Magn.*, vol. 52, no. 1, pp. 1-10, Art. ID 9500310, Jan. 2016.

[AWA16b] C.C. Awah, Z.Q. Zhu, Z.Z. Wu, D. Wu and X. Ge, "Electromagnetic performance of switched flux PM machines with two separate stators," *Computation and Mathematics in Electrical and Electronics Engineering,* vol. 35, no. 2, pp. 1-15, 2016.

[BEL10] A. Belahcen, A. Arkkio, "Permanent magnets models and losses in 2D FEM simulation of electrical machines," *in Proc. Int. Conf. Electr. Mach. Dri.,* Rome, Italy, 2010, pp. 1-6.

[BIA06] N. Bianchi, S. Bolognani, M. D. Pre, and G. Grezzani, "Design considerations

for fractional-slot winding configurations of synchronous machines," *IEEE Trans. Ind. Appl.*, vol. 42, no. 4, pp. 997-1006, Jul./Aug. 2006.

[BIA08] N. Bianchi, S. Bolognani, and M.D. Pre, "Magnetic loading of fractional-slot three-phase PM motors with nonoverlapped Coils," *IEEE Trans. Ind. Appl.*, vol. 44, no. 5, pp. 1513-1521, Sept./Oct. 2008.

[BOL01] I. Boldea, J. Zhang, and S.A. Nasar, "Characterization of flux reversal machine (FRM) in low speed (direct) servo drives-the pole-PM configuration," *in Proc. Int. Conf. Electr. Mach. Dri.*, 2001, pp. 664-671.

[BOL14] I. Boldea, L.N. Tutela, L. Parsa, D. Dorrell, "Automative electric propulsion systems with reduced or no permanent magnets: an overview," *IEEE Trans. Ind. Electron.*, vol. 61, no. 10, pp. 5696-5711, Oct. 2014.

[CHA07] J. Chang, J. Lee, J. Kim, S. Chung, D. Kang and H. Weh, "Development of rotating type transverse flux machine," *in Proc. Int. Conf. Electr. Mach. Dri*., 2007, pp. 1090-1095.

[CHA07] F. Chai, S. Cui, and S. Cheng, "Performance analysis of double-stator starter generator for the hybrid electric vehicle," *IEEE Trans. Magn*., vol.41, no.1, pp. 484-487, Jun. 2007.

[CHA09] F. Chai, J. Xia, B. Guo, S. Cheng, and J. Zhang, "Double-stator permanent magnet synchronous in-wheel motor for hybrid electric drive system," *IEEE Trans. Magn.*, vol. 45, no. 1, pp. 278-281, Jan. 2009.

[CHE01] M. Cheng, K.T. Chau, and C.C. Chan, "Design and analysis of a new doubly salient permanent magnet motor," *IEEE Trans. Magn.*, vol. 37, no. 4, pp. 3012-3020, Jul. 2001.

[CHE08] L. Chen, B. Li, C. Liu, R. Tang, "Design and study of novel transverse flux permanent magnet synchronous motor," in Proc. Int. Conf. Electr. Mach. Syst., 2008, pp. 3554-3558.

[CHE10a] J.T. Chen, and Z.Q. Zhu, "Comparison of all and alternate poles wound flux-switching PM machines having different stator and rotor pole numbers," *IEEE Trans. Ind. Appl.*, vol. 46, no. 4, pp. 1406-1415, Jul./Aug. 2010.

[CHE10b] J. T. Chen, and Z. Q. Zhu, "Winding configurations and optimal stator and rotor pole combination of flux switching PM brushless AC machines," *IEEE Trans. Energy Convers.*, vol. 25, no. 2, pp. 293-302, Jun. 2010.

[CHE10c] J.T. Chen, Z.Q. Zhu, S. Iwasaki and R. Deodhar, "Comparison of losses and efficiency in alternate flux-switching permanent magnet machines", *in Proc. Int. Conf. Electr. Mach. (ICEM)*, Rome, Italy, 2010, pp.1-6.

[CHE10d] J. T. Chen, and Z. Q. Zhu, "Influence of the rotor pole number on optimal parameters in flux-switching PM brushless ac machines by the lumped-parameter magnetic circuit model," *IEEE Trans. Ind. Appl.*, vol. 46, no. 4, pp. 1381-1388, Jul./Aug. 2010.

[CHE11c] J. T. Chen, Z. Q. Zhu, S. Iwasaki, and R. P. Deodhar, "Influence of slot opening on optimal stator and rotor pole combination and electromagnetic performance of switched-flux PM brushless AC machines," *IEEE Trans. Ind. Appl.*, vol. 47, no. 4, pp. 1681-1691, Jul./Aug. 2011.

[CHE11] M. Cheng, W. Hua, J. Zhang, and W. Zhao, "Overview of stator-permanent magnet brushless machines," *IEEE Trans. Ind. Electron.*, vol. 58, no. 11, pp. 5087-5101, Nov. 2011.

[CHE11a] J.T. Chen, Z.Q. Zhu, S. Iwasaki, and R.P. Deodhar, "A novel hybrid-excited switched-flux brushless AC machine for EV/HEV applications," *IEEE Trans. Magn.*, vol. 60, no. 4, pp. 1365-1373, May 2011.

[CHE11b] J.T. Chen, Z.Q. Zhu, S. Iwasaki, and R.P. Deodhar, "A novel E-core switched flux PM brushless AC machine," *IEEE Trans. Ind. Appl.*, vol. 47, no. 3, pp. 1273-1282, May/Jun. 2011.

[CHE14] H. Chen, R. Qu, J. Li, and B. Zhao, Comparison of interior and surface permanent magnet machines with fractional slot concentrated windings for direct-drive wind generators," *in Proc. Int. Conf. Electr. Mach. Syst.*, Hangzhou, China, 2014, pp. 2612-2617.

[CHO06] H.W. Cho, S.M. Jang, and S.K. Choi, "A design approach to reduce rotor losses in high-speed permanent magnet machine for turbo-compressor," *IEEE Trans. Magn.*, vol. 42, no. 10, pp. 3521-3523, Oct. 2006.

[CHO11] L. Chong, R. Dutta, M.F. Rahman, and H. Lovatt, "Experimental verification of core and magnet losses in a concentrated wound IPM machine with V-Shaped magnets used in field weakening applications," *in Proc. Int. Conf. Electr. Mach. and Dri. (IEMDC)*, 2011, pp. 977-982.

[CUI08] S. Cui, Y. Yuan and T. Wang, "Research on switched reluctance double-rotor motor used for hybrid electric vehicle," *in Proc Int. Conf. Electr. Mach. Syst.*, 2008, pp. 3393-3396,

[DEO97] R.P. Deodhar, S. Anderson, I. Boldea, and T. J.E. Miller, "The flux reversal machine: A new brushless doubly-salient permanent-magnet machine," *IEEE Trans. Ind. Appli.*, vol. 33, No. 4, pp. 925-934, Jul./Aug. 1997.

[ELR08] A.M. El-Refaie and T.M. Jahns," Impact of winding layer number and magnet type on synchronous surface PM machines designed for wide constant-power speed range operation," *IEEE Trans. Energy Convers.*, vol. 23, no. 1, pp.53-60, Mar. 2008.

[ELR10] A. M. El-Refaie, "Fractional-slot concentrated-windings synchronous permanent magnet machines: opportunities and challenges," *IEEE Trans. Ind. Electron.*, vol. 57, no. 1, pp. 107-121, Jan. 2010.

[ELR14] A.M. EL-Refaie, J.P. Alexander, S. Galioto, P.B. Reddy, K.K. Huh, P. D. Bock, and X. Shen, "Advanced high-power-density interior permanent magnet motor for traction applications," *IEEE Trans. Ind. Appl.*, vol. 50, no. 5, pp. 3235-3248, Sept./Oct. 2014.

[EVA11] D. J. Evans and Z. Q. Zhu, "Influence of design parameters on magnetic gear's torque capability," *in Proc. Int. Conf. Electr. Mach. and Dri. (IEMDC)*, 2011, pp. 1403-1408.

[EVA15] D. J. Evans, and Z. Q. Zhu, "Novel partitioned stator switched flux permanent magnet machines," *IEEE Trans. Magn.*, vol. 51, no. 1, Art. ID 8100114, Jan. 2015.

[FAS14] A. Fasolo, L. Alberti, and N. Bianchi, "Performance comparison between switching-flux and IPM machines with rare-earth and ferrite PMs," *IEEE*

Trans. Ind. Appl., vol. 50, no. 6, pp. 3708-3716, Nov./Dec. 2014.

[FEI12] W. Fei, P.C.K. Luk, J.X. Shen, Y. Wang, and M. Jin, "A novel permanent-magnet flux switching machine with an outer-rotor configuration for in-wheel light traction applications," *IEEE Trans. Ind. Appli.,* vol. 48, no. 5, pp. 1496-1506, Sept./Oct. 2012.

[FRA11] N.W. Frank, and H.A. Toliyat, "Analysis of the concentric planetary magnetic gear with strengthened stator and interior permanent magnet inner rotor," *IEEE Trans. Ind. Appli.*, vol. 47, no. 4, pp.1652-1660, Jul./Aug. 2011.

[FUK12] T. Fukami, H. Aoki, and K. Shima, "Assessment of core losses in a flux-modulating synchronous machine," *IEEE Trans. Ind. Appl.*, vol. 48, no. 2, pp. 603-611, Mar./Apr. 2012.

[GAL13] M. Galea, T. Hamiti, C. Gerada, "Torque density improvements for high performance machines," *in Proc. Int. Conf. Electr. Mach. Dri*., pp. 1066-1073,

[GAO14] Y. Gao, R. Qu, J. Li, Z. Zhu and D. Li," HTS vernier machine for direct drive wind power generation," *IEEE Trans. Appl. Supercond.*, vol. 24, no. 5, pp. 5202905, May 2014.

[GAU14] B. Gaussens, E. Hoang, M. Lécrivain, P. Manfe, and M. Gabsi , "A hybrid-excited flux-switching machine for high-speed DC-alternator applications," *IEEE Trans. Ind. Electron.*, vol. 61, no. 6, pp. 2976-2989, Jun. 2014.

[GER12] A. D. Gerlando, G.M. Foglia, M.F. Iacchetti, and R. Perini, "Evaluation of manufacturing dissymmetry effects in axial flux permanent-magnet machines: analysis method based on field functions," *IEEE Trans. Magn.*, vol. 48, no. 6, pp. 1995-2008, Jun. 2012.

[GER15a] S. Gerber, and R. Wang, "Evaluation of movement facilitating techniques for finite element analysis of magnetically geared electrical machines," *IEEE Trans. Magn.*, vol. 51, no. 2, pp.1-5, Feb. 2015.

[GER15b] S. Gerber, and R. Wang, "Design and evaluation of a magnetically geared PM machine," *IEEE Trans. on Magn.*, vol. 51, no. 8, pp. 1-10, Art. ID 8107010,

Aug. 2015.

[GOS13] J. Goss, D. Staton, R. Wrobel, P. Mellor, “Brushless AC interior-permanent magnet motor design: comparison of slot/pole combinations and distributed vs. concentrated windings,” *in Proc. Int. Conf. Energy Convers. Congress. Exp.*, 2013, pp.1213-1219.

[GRI13] Y. Gritli, A. Tani, M. Mengoni, L. Zarri, G. Serra, F. Filippetti, and D. Casadei, “Rotor demagnetization diagnosis in five-phase surface–mounted permanent magnet generators under time–varying conditions,” *in Proc. Int. Conf. Clean Electr. Power.,* 2013, pp. 603-609.

[HAO12] L. Hao, M. Lin, W. Li, H. Luo, X. Fu, and P. Jin, “Novel dual-rotor axial field flux-switching permanent magnet machine,” *IEEE Trans. Magn.,* vol. 48, no. 11, pp. 4232-4235, Nov. 2012

[HAO14] L. Hao, M. Lin, D. Xu, and W. Zhang, “Cogging torque reduction of axial field flux-switching permanent magnet machine by adding magnetic bridge in stator tooth,” *IEEE Trans. Supercond.,* vol. 24, no. 3, pp. 0503405 , Jun. 2014.

[HOA07] E. Hoang, M. Lecrivain, and M. Gabsi, “A new structure of flux synchronous polyphased machine with hybrid excitation,” *in Proc. Eur. Power Electron.,* Aalborg, Denmark, 2007, pp.1-8.

[HOA97] E. Hoang, A. H. Ben Ahmed, and J. Lucidarme, “Switching flux permanent magnet polyphased synchronous machines,” *in Proc. Eur. Power Electron. Conf.,* Trondheim, Norway, 1997, vol. 3, pp. 903-908.

[HOA97] E. Hoang, A. H. Ben-Ahmed and J. Lucidarme, “Switching flux permanent magnet polyphased synchronous machines,” *7th European Conf. on Power Electronics and Applications,* pp.903-908, 1997.

[HUA08] W. Hua, M. Cheng, Z. Q. Zhu, and D. Howe, “Analysis and optimization of back-EMF waveform of a novel flux-switching PM motor,” *IEEE Trans. Energy Convers.*, vol. 23, no. 3, pp. 727-733, Sep. 2008.

[HUA09] W. Hua, M. Cheng, and G. Zhang, ”A novel hybrid excitation flux-switching motor for hybrid vehicles,” *IEEE Trans. Magn*., vol. 45, no. 10, pp. 4728-4731, Oct. 2009.

[HUA98] S. Huang, J. Luo, F. Leonardi, and T. Lipo, "A general approach to sizing and power density equations for comparison of electrical machines," *IEEE Trans. Ind. Appl.*, vol. 34, no. 1, pp. 92-97, Jan. 1998.

[ILH10] E. Ilhan, B. L. J. Gysen, J. J. H. Paulides, and E. A. Lomonova, "Analytical hybrid model for flux switching permanent magnet machines," *IEEE Trans. Magn.*, vol. 46, no. 6, pp. 1762-1765, Nov. 2010.

[ISH06] D. Ishak, Z.Q. Zhu, and D. Howe, "Comparison of PM brushless motors, with either all teeth or alternate teeth wound*," IEEE Trans. Energy Convers*., vol. 21, no. 1, pp. 95-103, Mar. 2006.

[JAC96] A.G. Jack, B.C. Mecrow, and J.A. Haylock, "A comparative study of permanent magnet and switched reluctance motors for high-performance fault-tolerant applications," *IEEE Trans. Ind. Appl.*, vol. 32, no. 4, pp. 889-895, Jul./Aug. 1996.

[JAH86] T. M. Jahns, G. B. Kliman, T. W. Neumann, "Interior permanent-magnet synchronous motors for adjustable-speed drives," *IEEE Trans. Ind. Appl.*, vol. 22, no. 4, pp. 738-747, Jul. 1986.

[JAN14] D.K. Jang and J.H. Chang, "Design of a vernier machine with PM on both sides of rotor and stator," *IEEE Trans. Magn*., vol. 50, no. 2, pp. 7021704, Feb. 2014.

[JIA09] L. Jian, K.T. Chau, Y. Gong, J.Z. Jiang, C. Yu, and W. Li, "Comparison of coaxial magnetic gears with different topologies," *IEEE Trans. Magn*., vol. 45, no. 10, pp. 4526-4529, Oct. 2009.

[JIA10] L. Jian, and K. T. Chau, "A coaxial magnetic gear with Halbach permanent-magnet arrays," *IEEE Trans. Energy Convers.*, vol. 25, no. 2, pp. 319-328, Jun. 2010.

[JIN10] M.J. Jin, Y. Wang, J.X. Shen, P.C.K. Luk, W.Z. Fei, and C.F. Wang, "Cogging torque suppression in a permanent flux-switching integrated-starter generator," *IET. Electr. Power Appl.*, vol.4, no.8, pp.647-656, 2010.

[KIM04] T.H. Kim, J. Lee, "A study of the design for the flux reversal machine," *IEEE Trans. Magn.*, vol. 40, no. 4, pp. 2053-2055, Jul. 2004.

[KIM05] T.H. Kim, K.B. Jang, Y.D. Chun, and J. Lee, "Comparison of the characteristics of a flux reversal machine under the different driving methods," *IEEE Trans. Magn.*, vol. 41, no. 5, pp. 1916-1919, May 2005.

[KIM07] K.C. Kim, D.H. Koo, J.P. Hong, and J. Lee, "A Study on the characteristics due to pole-arc to pole-pitch ratio and saliency to improve torque performance of IPMSM," *IEEE Trans. Magn.*, vol.43, no.6, pp. 2516-2518, Jun.2007.

[KIM09] T. H. Kim, "A Study on the design of an inset-permanent-magnet-type flux-reversal machine, *IEEE Trans. Magn.*, vol. 45, no. 6, pp. 2859- Jun. 2009.

[KIM13] S.I. Kim, J. Cho, S. Park, T. Park, and S. Lim, "Characteristics comparison of a conventional and modified spoke-type ferrite magnet motor for traction drives of low-speed electric vehicles," *IEEE Trans. Ind. Appl.*, vol. 49, no. 6, pp. 2516-2523, Nov./Dec. 2013.

[KIM16] D. Kim, H. Hwang, S. Bae and C. Lee, " Analysis and design of double-stator flux-switching permanent magnet machine using ferrite magnet in hybrid electric vehicles," *IEEE Trans. Magn.*, vol. 52, no. 7, pp. 8106604, Jul. 2016.

[LEE08] S.J. Lee, S.I. Kim, J.P. Hong, "Investigation on core loss according to stator shape in interior permanent magnet synchronous motor", *Proceedings of International Conference on Electrical Machines and Systems, ICEMS2008,* pp. 3158-3161.

[LEE14] C.H.T. Lee, K.T. Chau, C. Liu, and C. Qiu, "Design and analysis of a new multitoothed magnetless doubly salient machine," *IEEE Trans. Appl. Supercond.*, vol. 24, no. 3, pp. 5200804, Jun. 2014.

[LEI15] G. Lei, C. Liu, Y. Guo, and J. Zhu, "Multidisciplinary design analysis and optimization of a PM transverse flux machine with soft magnetic composite core," *IEEE Trans. Magn.*, vol. 51, no. 11, pp. 8109704 , Nov. 2015.

[LI11] G.J. Li J. Ojeda, E. Hoang and M. Gabsi, "Thermal-electromagnetic analysis of a fault-tolerant dual-star flux-switching permanent magnet motor for critical

applications," *IET Electr. Power Appl*., vol. 5, no. 6, pp. 503-513, 2011.

[LI11] Jiangui Li, Student Member, and K. T. Chau, A Novel HTS PM Vernier Motor for Direct-Drive Propulsion," *IEEE Trans. Appli. Supercond.*, vol. 21, no. 3, pp. 1175-1179, Jun. 2011.

[LI14] D. Li, R. Qu, and T.A. Lipo, "High-power-factor vernier permanent-magnet machines," *IEEE Trans. Ind. Appli.*, vol. 50, no. 6, pp. 3664-3674, Nov./Dec. 2014.

[LI15] Y. Li, D. Bobba, and B. Sarlioglu, "Design and performance characterization of a novel low-pole dual-stator flux switching permanent magnet machine," *in Proc. Energy Convers. Congress. Exp.,* 2015, pp. 5586-5592.

[LI15] S. Li, Y. Li, and B. Sarlioglu, "Partial irreversible demagnetization assessment of flux switching permanent magnet machine using ferrite permanent magnet material," *IEEE Trans. Magn.,* vol. 51, no. 7, Art. ID 8106209, Jul.2015.

[LIA95] Y. Liao, F. Liang, and T. A. Lipo, "A novel permanent magnet motor with doubly salient structure," *IEEE Trans. Ind. Appl.*, vol. 31, pp. 1069–1078, Sep./Oct. 1995.

[LIU08] C. Liu, K.T. Chau, J.Z. Jiang, "Comparison of stator-permanent-magnet brushless machines," *IEEE Trans. Magn*., vol. 44, no. 11, pp. 4405-4408, Nov. 2008.

[LIU09] X. Liu, K. T. Chau, J. Z. Jiang, and Chuang Yu, "Design and analysis of interior-magnet outer-rotor concentric magnetic gears," *Journal of Appli. Phy*., vol. 105, pp. 07F101, 2009.

[LIU12a] C. Liu, K.T. Chau, J. Zhong and F. Li, "Quantitative comparison of double-stator permanent magnet vernier machines with and without HTS bulks," *IEEE Trans. Appli.*, Supercond., vol. 22, no. 3, pp. Jun. 2012.

[LIU12b] C. Liu, K.T. Chau, and Z. Zhang, "Novel design of double-stator single-rotor magnetic-geared machines," *IEEE Trans. Magn*., vol. 11, no. 48, pp.4180-4183, Nov. 2012.

[LIU13] X. Liu and Z.Q. Zhu, "Comparative study of novel variable flux reluctance machines with doubly fed doubly salient machines," *IEEE Trans. Magn*., vol. 49, no. 7, pp. 3838-3841, Jul. 2013

[LIU14] C. Liu, K.T. Chau, and Q. Chun, "Design and analysis of a new magnetic-geared memory machine," *IEEE Trans. Appl. Supercond.*, vol. 24, no. 3, pp. 0503005, 2015.

[LIU14] X. Liu, D. Wu, Z.Q. Zhu, A. Pride, R.P. Deodhar, and T. Sasaki, "Efficiency improvement of switched flux PM memory machine over interior PM Machine for EV/HEV applications," *IEEE Trans. Magn*., vol. 50, no. 11, pp. Nov. 2014.

[LIU14] C.T. Liu, H.Y. Chung, and C.C. Hwang, "Design assessments of a magnetic-geared double-rotor permanent magnet generator," *IEEE Trans. Magn*., vol. 50, no. 1, pp. 4001004, Jan. 2014.

[LIU14] C. Liu, K. T. Chau, and C. Qiu, "Design and analysis of a new magnetic-geared memory machine," *IEEE Trans. Appl. Supercond*., vol. 24, no. 3, Art. ID 0503005, Jun. 2014.

[LOP08] D.A.G. Lopez, J.A. Tapia, R. Wallace, and A. Valenzuela, "Design and test of an axial flux permanent-magnet machine with field control capability," *IEEE Trans. Magn.*, vol. 44, no. 9, pp. 2168-21, Sept. 2008.

[MAG04] F. Magnussen, P. Thelin, and C. Sadarangani, "Performance evaluation of permanent magnet synchronous machines with concentrated and distributed windings including the effect of field-weakening," *in Proc. Int. Conf. Power. Electro. Mach. Dri*., pp. 2004, 679-685.

[MAG07] F. Magnussen and H. Lendenmann, "Parasitic effects in PM machines with concentrated windings," *IEEE Trans. Ind. Appli*., no. 43, no. 5, pp. 1223-1232, Sept./Oct. 2007.

[MCF14] J. D. McFarland, T. M. Jahns, and A. M. EL-Refaie, "Analysis of the torque production mechanism for flux-switching permanent magnet machines," in

Proc. IEEE Eng. Con. Congr. Exp., Pittsburgh, USA, 2014, pp. 310-317.

[MCF15] J. D. McFarland, T. M. Jahns, and A. M. EL-Refaie, "Analysis of the torque production mechanism for flux-switching permanent magnet machines," *IEEE Trans. Ind. Appl.*, vol. 51, no. 4, pp.3041-3049, Jul./Aug.2015.

[MEZ15] S. Mezani1, T. Hamiti, L. Belguerras, T. Lubin, M. Rashed, and C. Gerada, "Magnetically Geared induction machines," *IEEE Trans. Magn.*, vol. 51, no. 11, pp. 8111404, Nov. 2015.

[MI05] C.C. Mi, G.R. Slemon, and R. Bonert, "Minimization of iron losses of permanent magnet synchronous machines," *IEEE Trans. Energy Convers.*, vol. 20, no. 1, pp. 121-127, Mar. 2005.

[MOR10] D. S. More, and B. G. Fernandes, "Analysis of flux-reversal machine based on fictitious electrical gear," *IEEE Trans. Energy Convers.*, vol. 25, no. 4, pp. 940-947, Dec. 2010.

[MUN08] A.R. Muñoz, F. Liang, and M.W. Degner, "Evaluation of interior PM and surface PM synchronous machines with distributed and concentrated windings," *in IEEE Proc. Power. Electro.*, 2008, pp. 1189-1193.

[NIG12] N. Niguchi, K. Hirata, A. Zaini, S. Nagai, "Proposal of an axial-type magnetic-geared motor," *in Proc. Int. Conf. Electr. Mach.*, 2012, pp. 738-743.

[NIU07] S. Niu, K.T. Chau, J.Z. Jiang and C. Liu, " Design and control of a new double-stator cup-rotor permanent-magnet machine for wind power generation," *IEEE Trans. Magn.*, vol. 43, no. 6, pp. 2501-2503, Jun. 2007.

[NIU08] S. Niu, K. T. Chau, and J. Jiang, "Analysis of eddy-current loss in a double-stator cup-rotor PM machine," *IEEE Trans. Magn.*, vol. 44, no. 11, pp. 4401-4404, Nov. 2008.

[NIU11] S. Niu, S.L. Ho, and W.N. Fu, "Performance analysis of a novel magnetic-geared tubular linear permanent magnet machine," *IEEE Trans. Magn.*, vol. 47, no. 10, Oct. 2011.

[OKA16] S. Okamoto, N. Denis, Y. Kato, M. Ieki and K. Fujisaki , "Core Loss Reduction of an Interior Permanent-Magnet Synchronous Motor Using

Amorphous Stator Core," *IEEE Trans. Ind. Appl.*, vol. 52, no. 3, pp. 2261-2268, May/Jun. 2016.

[OST03] V. Ostovic, "Memory motors," *IEEE Ind. Appl*., vol. 9. no. 1, pp. 52-61, 2003.

[OWE10] R. Owen, Z.Q. Zhu, A. Thomas, G.W. Jewell and D. Howe, "Alternate poles wound flux switching permanent magnet machines brushless AC machines," *IEEE Trans. Ind. Appl*., vol. 46, no. 2, pp. 790-797, Mar./Apr. 2010.

[PAR05] L. Parsa, and H. A. Toliyat, "Five-phase permanent-magnet motor drives," *IEEE Trans. Ind. Appl.*, vol. 41. No. 1, pp. 30-37, Jan./Feb. 2005.

[PEL12] G. Pellegrino, A. Vagati, B. Boazzo, and P. Gulielmi, "Comparison of induction and PM synchronous motor drives for EV application including design examples," *IEEE Trans. Ind. Appl*., vol.48, no. 6, pp. 2322-2332, Nov./Dec. 1994.

[POP13] A.A. Pop, H. Balan, M. Radulescu, H. Kanchev, "Electromagnetic torque capabilities of axial-flux and radial-flux permanent-magnet machines," *in proc. Int. Symp. Electr. Electro. Engrg*., 2013, pp. 1-4.

[PYR12] J. Pyrhönen, H. Jussila, Y. Alexandrova, P. Rafajdus, and J. Nerg, "Harmonic loss calculation in rotor surface permanent magnets—new analytic approach," *IEEE Trans. Magn.*, vol. 48, no. 8, pp. 2358-2366, Aug. 2012.

[QI09] G. Qi, J.T. Chen, Z.Q. Zhu, D. Howe, L.B. Zhou and C.L. Gu, "Influence of skew and cross-coupling on d- and q-axis inductances and flux-weakening performance of PM brushless AC machines", *IEEE Trans. Magn*., vol. 45, no. 5, pp. 2110-2117, May 2009.

[QU11] R. Qu, D. Li, and J. Wang, "Relationship between magnetic gears and vernier machines," in *Proc. Int. Conf. Electr. Mach. Syst.*, Beijing, China, 2011, pp. 1-6.

[RAM11] T. Raminosoa, C. Gerada, and M. Galea, "Design considerations for a fault-tolerant flux-switching permanent-magnet machine," *IEEE Trans. Ind. Electro.*, vol. 58, no.7, pp. 2818-2825, Jul. 2011.

[RAS05] P.O. Rasmussen, T.O. Anderson, F.T. Jorgensen, and O. Nielsen,

"Development of a high-performance magnetic gear," *IEEE Trans. Ind. Appl*., vol. 41, no. 3, pp. 764-770, May/Jun. 2005.

[RAU55] S. E. Rauch, and L. J. Johnson, "Design principles of the flux-switch alternators," *AIEE Trans*., vol. 74, no. 3, pp. 1261-1268, Jan. 1955.

[RED12] P.B. Reddy, A.M. El-Refaie, H. Kum-Kang, J.K. Tangudu and T.M. Jahns, "Comparison of interior and surface PM machines equipped with fractional-slot concentrated windings for hybrid traction applications," *IEEE Trans. Energy Convers.*, vol. 27, no. 3, pp. 593-602, Sep. 2012.

[SAR94] B. Sarlioglu Y. Zhao T.A. Lipo, "Novel Doubly Salient Single Phase Permanent Magnet Generator," *in Proc. IEEE Ind. Appl*., pp. 9-15, vol.1, 1994.

[SED15] E.B. Sedrine, J. Ojeda, M. Gabsi, I.S. Belkhodja, "Fault-tolerant control using the GA optimization considering the reluctance torque of a five-phase flux switching machine," *IEEE Trans. Energy Convers.*, vol. 30, no. 3, pp. 927-938, 2015.

[SIA08] M. Siatkowski, B. Orlik, "Flux linkage in transverse flux machines with flux concentration," *in Proc. Int. Conf. Optimiz. Electr. Electro. Equip*., 2008, pp. 21-26.

[SIT01] K. Sitapati and R. Krishnan, "Performance comparisons of radial and axial field, permanent-magnet, brushless machines," *IEEE Trans. Ind. Appli*., vol. 37, no. 5, pp. 1219-1226, Sept./Oct. 2001.

[SIZ13] G.Y. Sizov, P. Zhang, D.M. Ionel, N.A.O. Demerdash, and M. Rosu, "Automated multi-objective design optimization of PM AC machines using computationally efficient FEA and differential evolution," *IEEE Trans. Ind. Appl.*, vol. 49, no. 5, pp. 2086-2096, Sept./Oct. 2013.

[SOO94] W. Soong, T.J.E. Miller, "Field Weakening Performance of Brushless Synchronous AC Motor Drives," *IEE Electr. Power Appli*., vol. 141, no. 6, Nov.1994, pp. 331-340.

[SPO03] E. Spooner and L. Hardock, "Vernier hybrid machines," *IEE Electr. Power Appli*., vol. 150, no.6, pp. 655-662, Nov. 2003

[STE12] R.D. Stefano and F. Marignetti, "Electromagnetic analysis of axial-flux permanent magnet synchronous machines with fractional windings with experimental validation," *IEEE Trans. Magn.*, vol. 59, no.6, pp. 2573-2582, Jun. 2012.

[SUL11] E. Sulaiman, T. Kosaka, and N. Matsui, "A new structure of 12 slot-10 pole field-excitation flux switching synchronous machine for hybrid electric vehicles," *Proc. 14th Eur. Conf. Pow. Electron. Appli.*, Birmingham, UK, 2011, pp. 1-10.

[THO09] A.S. Thomas, Z.Q. Zhu, R.L. Owen, G.W. Jewell, and D. Howe, "Multiphase flux-switching permanent-magnet brushless machine for aerospace applications," *IEEE Trans. Ind. Appli*., vol. 45, no. 6, pp. 1971-1981, Nov./Dec. 2009.

[THO14] A.S. Thomas, Z.Q. Zhu and G.J. Li, "Electromagnetic loss investigation and mitigation in switched flux permanent magnet machines", *in Proc. Int. Conf. Electr. Mach. (ICEM)*, 2014, pp. 1146 - 1152.

[TLA16] P. M. Tlali, S. Gerber, and R.J. Wang, "Optimal design of an outer-stator magnetically geared permanent magnet machine," *IEEE Trans. Magn*., vol. 52, no. 1, pp. 8100610, Jan. 2014.

[TOB99] A. Toba, and T. A. Lipo, "Novel dual-excitation permanent magnet Vernier machine," *in Proc. IEEE IAS Annu. Conf.*, Phoenix, USA, 1999, vol. 4, pp. 2539-2544.

[TOD04] H. Toda, Z. Xia, J. Wang, K. Atallah, and D. Howe, "Rotor eddy-current loss in permanent magnet brushless machines, *IEEE Trans. Magn*., vol. 40, no. 4, pp. 2104-2106, Jul. 2004.

[UKA14] H. Ukaji, K. Hirata, and N. Niguchi, "Claw pole magnetic-geared generator for hub dynamos," *in Proc. Int. Conf. Electr. Mach*., 2014, pp. 416-421.

[VAL15] M. Valavi, A. Nysveen, and R. Nilssen, "Effects of loading and slot harmonic on radial magnetic forces in low-speed permanent magnet machine with

concentrated windings, *IEEE Trans. Magn.*, vol. 51, no. 6, pp. 8105310, Jun. 2015.

[WAL13] C.S. Walter, H. Polinder, and J.A. Ferreira, "High-torque-density high-efficiency flux-switching PM machine for aerospace applications," *IEEE Journ. Emerg. Select. Topics. Power. Electro.*, vol. 1, no. 4, pp. 327-336, Dec. 2015.

[WAN01] C. X. Wang, I. Boldea, and S. A. Nasar, "Characterization of three phase flux reversal machine as an automotive generator," *IEEE Trans. Energy Convers.*, vol. 16, no. 1, pp. 74-80, Mar. 2001.

[WAN08] L. Wang, J. Shen, Y. Wang, and K. Wang, "A novel magnetic-geared outer-rotor permanent-magnet brushless motor," in *Proc. of Power Electro. Mach. and Dri.*, Yoke, UK, 2008. pp. 33-36.

[WAN09] L.L. Wang, J.X. Shen, P.C.K. Luk, W.Z. Fei , C.F. Wang, and H. Hao, "Development of a magnetic-geared permanent-magnet brushless motor," *IEEE Trans. Magn.*, vol. 45, no.10, pp. 4578-4581, Oct. 2009.

[WAN11a] Y. Wang, M. Cheng, M. Chen, Y. Du and K.T. Chau, "Comparative study of the electromagnetic performance of switched flux permanent magnet machines," *IET Electr. Power Appl.*, vol. 5, Iss. 3, pp. 317-323, 2011.

[WAN11b] Y. Wang, M. Cheng, Y. Du, and K. T. Chau, "Design of high-torque-density double-stator permanent magnet brushless motors," *IET Electr. Power Appl.*, vol. 5, no. 3, pp. 317-323, Mar. 2011.

[WAN12] Y. Wang and Z.Q. Deng, "Comparison of hybrid excitation topologies for flux-switching machines," *IEEE Trans. Magn.*, vol. 48, no. 9, pp. 2518-2527, Sept. 2012.

[WAN13] Y. Wang, J. Sun, Z. Zou, Z. Wang and K.T. Chau, "Design and analysis of a HTS flux-switching machine for wind energy conversion," *IEEE Trans. Appl. Supercond.*, vol. 23, no. 3, pp. 5000904, Jun. 2013.

[WAN14] A. Wang, C. Wang, W.L. Soong, "Design and optimization of interior PM machines with distributed and fractional-slot concentrated-windings for hybrid electric vehicles," *in Proc. IEEE Conf. Trans. Electr. Asia. Pacific.*, pp. 1-5,

2014.

[WAN15] Y. Wang, R. Qu, and J. Li, "Multilayer windings effect on interior PM machines for EV applications," *IEEE Trans. Ind. Appli*., vol. 51, no. 3, pp. 2208-2214, May/Jun. 2015.

[WAN15] Z. Wan, A. Ahmed and I. Husain, and E. Muljadi, "A Novel transverse flux machine for vehicle traction applications," *in Proc. IEEE Energy. Power. Soc. Meeting.*, 2015, pp. 1-5.

[WAN15] W. Wang, M. Luo, E. Cosoroaba, B. Fahimi and M. Kiani, "Rotor shape investigation and optimization of double stator switched reluctance machine", *IEEE Trans. Magn.*, vol. 51, no.53, Art.ID 8103304, Mar. 2015.

[WAN99] C. Wang, S.A. Nasar, and I. Boldea, "Three-phase flux reversal machine (FRM)," *IEE Proc-Electr. Power Appl.*, vol. 146, no. 2, pp. 139-146, Mar. 1999.

[WU14] D. Wu, J. T. Shi, Z. Q. Zhu, and X. Liu, "Electromagnetic performance of novel synchronous machines with permanent magnets in stator yoke," *IEEE Trans. Magn.*, vol. 50, no. 9, Art. ID 8102009, Sep. 2014.

[WU15] D. Wu, X. Liu, Z.Q. Zhu, A. pride, R. Deodhar and T. Sasaki, "Switched flux hybrid magnet memory machine," *IET Elect Power Appl*., vol. 9, no. 2, pp 160-170, 2015.

[WU15a] Z. Z. Wu, and Z. Q. Zhu, "Analysis of air gap field modulation and magnetic gearing effects in switched flux permanent magnet machines," *IEEE Trans. Magn.*, vol. 51, no. 5, Art. ID 8105012, May 2015.

[WU15b] Z. Z. Wu, Z. Q. Zhu, and J. T. Shi, "Novel doubly salient permanent magnet machines with partitioned stator and iron pieces rotor," *IEEE Trans. Magn.*, vol. 51, no. 5, pp. 1-12, May 2015.

[XUA13] H.V. Xuan, D. Lahaye , H. Polinder , and J.A. Ferreira, "Influence of stator slotting on the performance of permanent-magnet machines with concentrated windings," *IEEE Trans. Magn.*, vol. 49, no. 2, pp. 929-938, Feb. 2013.

[XUE13] X. Xue, W. Zhao, J. Zhu, G. Liu, X. Zhu and M. Cheng, "Design of five-phase modular flux-switching permanent-magnet machines for high reliability applications," IEEE Trans. Magn., vol. 49, no. 7, pp. 3941-3944, Jul. 2013.

[YAM09] K. Yamazaki, M. Shina, Y. Kanou, M. Miwa, and J. Hagiwara, "Effect of Eddy Current Loss Reduction by Segmentation of Magnets in Synchronous Motors: Difference Between Interior and Surface Types," *IEEE Trans. Magn.*, vol.45, no.10, pp. 4756-4759, Oct. 2009.

[YAM13] K. Yamazaki, M. Kumagai, T. Ikemi and S. Ohki, "A novel rotor design of interior permanent magnet synchronous motors to cope with both maximum torque and iron-loss reduction," *IEEE Trans. Ind. Appl.*, vol. 49, no. 6, pp. 2478-2486, Nov./Dec. 2013.

[YEH12] Y.H. Yeh, M.F. Hsieh and D.G. Dorrell, "Different arrangements for dual-rotor dual output radial-flux motors," *IEEE Trans. Ind. Appl.*, vol.48, no. 2, pp. 612-622, Mar./Apr. 2012.

[ZAI14] Z. Zaiyun, Q. Li and X. Zixuan, "Comparison of double-stator flux-switching permanent magnet machine and double-stator permanent synchronous machine for electric vehicle applications", *in Proc. Int. Conf. Electr. Mach. Syst.*, Hangzhou, China, 2014, pp.234-239.

[ZHA09] J. Zhang, M. Cheng, Z. Chen, and W. Hua, "Comparison of stator-mounted permanent-magnet machines based on a general power equation," *IEEE Trans. Energy Convers.*, vol. 24, no. 4, pp. 826-834, Dec. 2009.

[ZHA13] W. Zhang and M. Lin, "Influence of rotor pole number on optimal parameters in E-core axial field flux-switching permanent magnet machine," *in the proc. Int. Conf. Electr. Mach. Syst.*, Busan, Korea, 2013, pp. 1217-1221.

[ZHA13] X. Zhang, R. Qu, H. Chen, and J. Luo, "Analysis of d- and q-axis inductances and saliency ratios in interior permanent magnet machines with fractional-slot concentrated-windings considering harmonic effects," in *Proc. Int. Conf. Electr. Mach. Sys.*, Busan, Korea, 2013, pp. 1080-1085.

[ZHA14] F. Zhao, T.A. Lipo, B.I. Kwon, "Dual-stator interior permanent magnet vernier

machine having torque density and power factor improvement," *Journal of Electr. Power Comp. Syst.*, vol. 42, no. 15, pp. 1717-1726, 2014.

[ZHA14] W. Zhao, T.A. Lipo and B.I. Kwon, "Comparative study on novel dual stator radial flux and axial flux permanent magnet motors with ferrite magnets for traction application," *IEEE Trans. Magn.*, vol. 50, no. 11, pp. 8104404 , Nov. 2014.

[ZHA15] N. Zhao and W. Liu, "Loss calculation and thermal analysis of surface-mounted PM motor and interior PM motor," *IEEE Trans. Magn*., vol. 51, no. 11, pp. 8112604, Nov. 2015.

[ZHU05] Z. Q. Zhu, Y. Pang, D. Howe, S. Iwasaki, R. Deodhar, and A. Pride, "Analysis of electromagnetic performance of switched flux switching permanent magnet machines by non-linear adaptive lumped parameter magnetic circuit model," *IEEE Trans. Magn.*, vol. 41, no. 11, pp. 4277-4287, Nov. 2005.

[ZHU07a] Z. Q. Zhu, and D. Howe, "Electrical machines and drives for electric, hybrid and fuel cell vehicles," *Proc. IEEE*, vol. 95, no. 4, pp. 746-765, Apr. 2007.

[ZHU07b] Z. Q. Zhu, D. Ishak, D. Howe, and J. T. Chen, "Unbalanced magnetic force in permanent-magnet brushless machines with diametrically asymmetric phase winding," *IEEE Trans. Ind. Appl*., vol. 43, no. 6, pp. 1544-1553, Nov./Dec. 2007.

[ZHU08a] Z.Q. Zhu, J.T. Chen, Y. Pang, D. Howe, S. Iwasaki, and R. Deodhar, "Analysis of a novel multi-tooth flux-switching PM brushless AC machine for high torque direct-drive applications," *IEEE Trans. Magn.*, vol. 44, no. 11, pp. 4313-4316, Nov. 2008.

[ZHU08b] Z.Q. Zhu, *et al*, "Analysis and reduction of magnet eddy current loss in flux-switching permanent magnet machines", *in Proc. of Power Electro. Mach. and Dri. (PEMD), 2008, pp.120-124.*

[ZHU09] Z.Q. Zhu, "A simple method for measuring cogging torque in permanent magnet machines," *in IEEE Proc. Power and Energy Society General Meeting*, 2009, pp.1-4.

[ZHU10] Z.Q. Zhu and J.T. Chen, "Advanced flux-switching permanent magnet brushless machines," *IEEE Trans. Magn.*, vol. 46, no. 6, pp.1447-1453, Jun. 2010

[ZHU11] X. Zhu, L. Quan, D. Chen, M. Cheng, Z. Wang, and W. Li, "Design and analysis of a new flux memory doubly salient machine capable of online flux control," *IEEE Trans. Magn*., vol. 47, no. 10, pp. 3220-3223, Oct. 2011.

[ZHU11] Z. Q. Zhu, "Switched flux permanent magnet machines – innovation continues", *Proceedings of International Conference on Electrical Machines and Systems, ICEMS2011*, 20-23 August, 2011, Beijing, paper Keynote Speech-06.

[ZHU14] Z. Q. Zhu, and D. Evans, "Overview of recent advances in innovative electrical machines - with particular reference to magnetically geared switched flux machines," *the 17th International Conference on Electrical Machines and Systems 2014, ICEMS2014*, October, 2014, pp.1-10.

[ZHU15a] Z.Q. Zhu and X. Liu, "Novel stator electrical field excited synchronous machines without rare-earth magnet," *IEEE Trans. Magn*., vol. 51, no. 4, pp. 8103609, Apr. 2015.

[ZHU15b] Z.Q. Zhu, M. Al-Ani, B. Lee and X. Liu, "Comparative study of the electromagnetic performance of switched flux permanent magnet machines," *IET Electr. Power Appl*., vol. 9, Iss. 4, pp. 297–306, 2015.

[ZHU15c] Z. Q. Zhu, Z. Z. Wu, D. J. Evans, and W. Q. Chu, "Novel electrical machines having separate PM excitation stator," *IEEE Trans. Magn.*, vol.51, no. 4, pp. 1-9, Apr. 2015.

[ZHU15d] Z. Q. Zhu, H. Hua, D. Wu, J. T. Shi, and Z. Z. Wu, "Comparison of partitioned stator machines with different PM excitation stator topologies," *in Int. Conf. Ecological Vehicle Renewable Energies*, Monaco, Mar. 2015, pp. 1-7.

[ZUL12] A. Zulu, B.C. Mecrow, and M. Armstrong, "Permanent-magnet flux-switching synchronous motor employing a segmental rotor," *IEEE Trans. Ind. Appl*., vol. 48, no. 6, pp. 2259-2267, Nov./Dec. 2012.

APPENDICES

Appendix A Test rigs for open-circuit, cogging/static and load torque measurements

In order to measure the cogging torque of the prototype machine, the initial value of a load on the beam balance is determined by the digital weight scale. Then the rotor is rotated at different mechanical degrees for a complete cycle. At each new rotor position, the weight on the digital scale will be recorded. After all, the cogging torque will be computed using the relation between distance and force (mass and acceleration due to gravity, g). Thus, Torque = F (N) x distance (m) (measured from the centre of the shaft to the centre of the digital weight scale)]. More detailed procedure is given in [ZHU09]. Similarly, the static torque of the machine is obtained by using the same process as in cogging torque, but with the input phase currents such that the following relation will be satisfied: $I_a=I$; $I_b= I_c=-0.5I$. It is worth mentioning that in order to perform the locked-rotor test; firstly, current will be injected into the machine so as to align the rotor with *d*-axis position. Subsequently, the torque will be obtained at different input current values. Further, the open-circuit back-EMF waveform of the machines is measured from the oscilloscope by driving the machine at a constant speed of 400rpm.

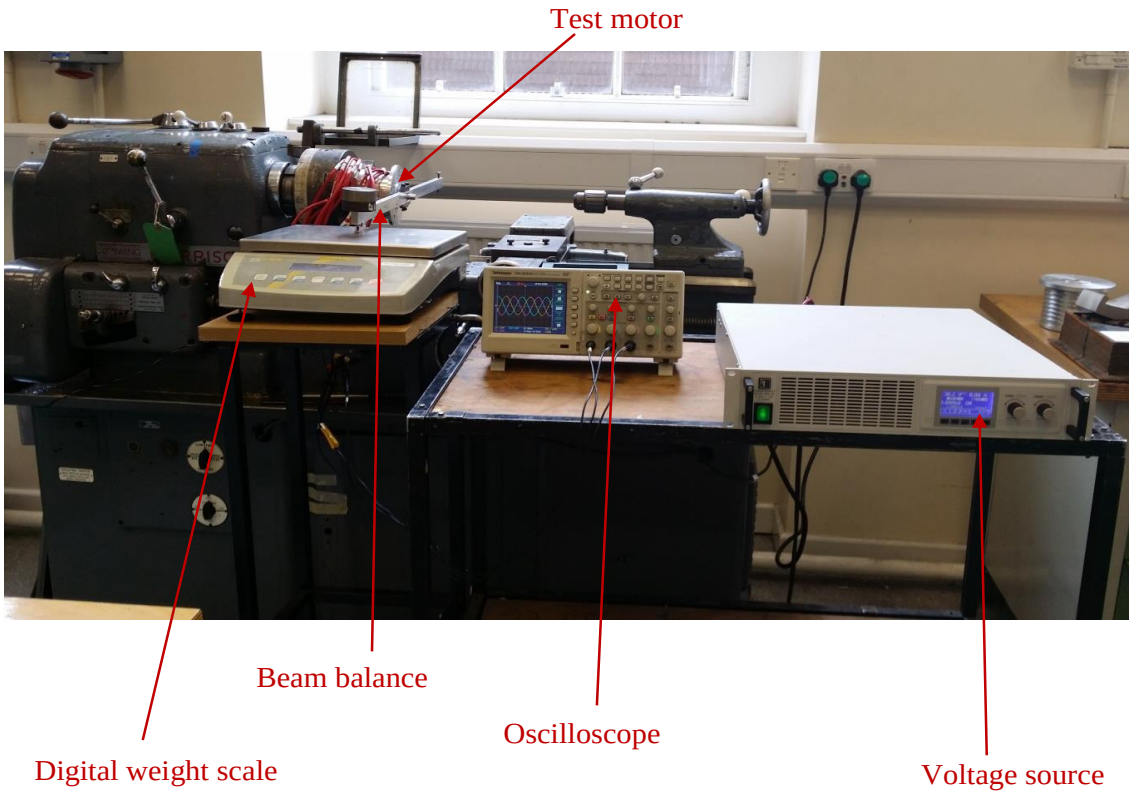

Fig.A1 Experimental set-up for the static test measurements.

Appendix B Publications from the PhD research study

1. C.C. Awah, Z.Q. Zhu, Z.Z. Wu, H.L. Zhan, J.T. Shi, D. Wu, and X. Ge, "Comparison of partitioned stator switched flux permanent magnet machines having single- or double-layer windings," *IEEE Trans. on Magnetics*, vol. 52, no. 1, pp. 1-10, Art. ID 9500310, Jan.2016.
2. C.C. Awah, Z.Q. Zhu, Z.Z. Wu, D. Wu and X. Ge, "Electromagnetic performance of switched flux PM machines with two separate stators," *Journal of Computation and Mathematics in Electrical and Electronics Engineering*, vol. 35, no. 2, pp. 1-15, 2016.
3. C.C. Awah, Z.Q. Zhu, Z.Z. Wu, and D. Wu, "High torque density magnetically-geared switched flux permanent magnet machines*," in Proc. Int. Conf. Ecological Vehicles and Renewable Energies*, Monaco, Mar. 2015, pp.1-6.
4. C.C. Awah; Z.Q. Zhu, Z.Z. Wu, J.T. Shi, D. Wu, "Comparison of partitioned stator switched flux permanent magnet machines having single- and double-layer windings*," in Proc. Int. Conf. Ecological Vehicles and Renewable Energies,* Monaco, Mar. 2015, pp.1-5. (Recommended for IEEE Trans. on Magnetics)
5. C.C. Awah and Z.Q. Zhu, "Influence of rotor pole number on electromagnetic performance of double-stator switched flux PM machines," to be presented at The 13th IEEE Vehicle Power and Propulsion Conference (VPPC2016), Zhejiang University, Hangzhou, China, on Oct. 17-20, 2016.
6. C.C. Awah and Z.Q. Zhu, "Comparative study of high performance double-stator switched flux permanent magnet machines," to be presented at The 13th IEEE Vehicle Power and Propulsion Conference (VPPC2016), Zhejiang University, Hangzhou, China, on Oct. 17-20, 2016.